THE SIGNIFICANCE OF NEGATIVE BENDING MOMENTS IN THE SEISMIC PERFORMANCE OF HOLLOW-CORE FLOORING

A Thesis
submitted in partial fulfilment
of the requirements for the Degree
of
Master of Engineering
at the
University of Canterbury
by
Lisa Joy Woods

University of Canterbury
Christchurch, New Zealand
2008

Blank

Abstract

Hollow-core flooring units are designed as simply supported members. However, frequently in construction, continuity is established between the units and supporting structure by the addition of insitu topping concrete and steel reinforcement. This change in structural form can result in negative bending moments and axial forces being induced in the floor by seismic and other structural actions. Significant negative moments are induced by load combinations that include the effects of seismic forces due to vertical ground motion. The focus of this research was two failure mechanisms possible under these loading conditions, a flexural failure and a shear failure. Both failure mechanisms were investigated analytically and experimentally.

A brittle flexural failure was observed experimentally in a sub-assembly test that contained starter bars and mesh reinforcement in the insitu topping concrete. The failure occurred at loads lower than those predicted using standard flexural theory. It appears that, due to the prestressing and low reinforcement ratio of the topping concrete, the assumption that plane sections remain plane is not appropriate for this situation. It is proposed that a strain concentration factor be introduced to account for the effects of tension stiffening. This factor improves the correlation between observed and predicted flexural strength.

The second failure mode investigated was a flexure-shear failure in a negative moment zone. Flexural cracks reduce the shear strength of a reinforced concrete member. Analytical predictions suggest that some hollow-core floor details could be prone to this type of brittle failure. A flexure-shear failure was not observed experimentally; however, this does not eliminate the possibility of this failure mode.

A summary of other failure mechanisms possible in hollow-core flooring is also presented. All failure modes should to be considered as part of establishing a hierarchy of failure in the design or retrofit of hollow-core floors.

Blank

Acknowledgements

The research reported in this thesis was completed under the supervision and guidance of Professor Des Bull, Professor Richard Fenwick and Dr Stefano Pampanin in the Department of Civil and Natural Resources Engineering at the University of Canterbury, Christchurch, New Zealand. I wish to thank these three men for their time and advice during this project, especially Richard who always made time to explain concepts and ideas to me even when he should have been spending time enjoying his “retirement”.

I have been very fortunate with the financial assistance I have received over the duration of my Masters, both for living costs and towards the experimental component of this project. I wish to thank the following people and organisations for their generosity. Dick and Mary Earle, the Kate Sheppard Memorial Trust, the Todd Foundation, the New Zealand Federation of Graduate Women, the Foundation of Research Science and Technology (FRST) and Stresscrete.

I would like to thank the technical staff at the Civil Engineering Department, especially Tim Perigo, for the assistance and advice during the experimental stage of this research. I also wish to thank the many people who have been happy to answer my questions during this research. These include past researchers; James Jensen, Renee Brook and Dr Jeff Matthews, as well as people involved in the New Zealand hollow-core industry, such as John Marshal and Len McSaveney.

The support and friendship of my colleges, family and friends has been unwavering during this time and has made completing my Masters degree enjoyable.

Blank

Table of Contents

List of Figures

List of Tables

Notation

Notations used regularly throughout this thesis are given here. This is not a complete list, as notations used only once or twice are accompanied by definitions within the text.

d	Distance between extreme compression fibre and centroid of flexural tension reinforcement
D12	Indicates steel reinforcement is comprised of 12 mm diameter deformed bars of Grade 300 steel
f'_c	Compressive strength of concrete
Grade 300	Refers to the steel reinforcement. Signifies that the steel has a fifth percentile characteristic yield strength of 300 MPa
Grade 430	Refers to the steel reinforcement. Signifies that the steel has a fifth percentile characteristic yield strength of 430 MPa. This Grade was commonly used prior to 2001
Grade 500	Refers to the steel reinforcement. Signifies that the steel has a fifth percentile characteristic yield strength of 500 MPa
HD12	Indicates steel reinforcement is comprised of 12 mm diameter deformed bars of Grade 500 steel
HR12	Indicates steel reinforcement is comprised of 12 mm diameter round bars of Grade 500 steel
M_t	The bending moment induced in the specimen during testing, calculated from the specimens' weight and loads applied
M_t/M_y	Normalised bending moment induced in test specimen used to illustrate how close the section being considered is to its theoretical yield capacity
M_y	The bending moment that will theoretically cause the steel reinforcement in the topping concrete of a section of hollow-core floor to yield (calculated from measured material properties)
R12	Indicates steel reinforcement is comprised of 12 mm diameter round bars of Grade 300 steel

1 Introduction and Background

Prestressed hollow-core floor units are a precast concrete component commonly used in New Zealand. Precast concrete construction is popular because of the ease and speed of construction, its thermal and acoustic insulation, as well as its off-site production, which allows factory-like controls. Hollow-core units are a common precast flooring type, as they can achieve long spans at optimum economy. The structural collapse of buildings constructed with precast elements in recent earthquake events overseas has shown the vulnerability of these buildings and highlighted the need for research into this area. A number of issues regarding the seismic performance of existing hollow-core floors are of concern.

Engineers need to be able to assess new and existing hollow-core systems to predict failure modes and detail to avoid these. There is a need for a deeper understanding of how hollow-core floors perform in earthquakes so that a hierarchy of strength can be assessed and used in capacity design of new buildings and in retrofits. Research performed in New Zealand into the seismic performance of hollow-core flooring over the last 15 years has increased awareness of its potential vulnerability and has led to revisions in the way hollow-core flooring is installed. However, much of this is empirical and the actual mechanics of how hollow-core floors behave is still not fully understood.

The research undertaken in this Masters programme adds to current knowledge by compiling a suite of possible failure mechanisms common to hollow-core floors. Some of these have been identified and observed in past experimental research, while others have been predicted from analytical work. Two of the failure mechanisms, possible when hollow-core floors are exposed to negative bending moments, are examined in detail. Analytical and experimental investigations have been undertaken of these mechanisms providing information on their likelihoods and ways to check for them. The two modes are a negative flexural failure and a flexure-shear failure. Both of these failure mechanisms are caused by negative bending moments induced in the floor. Often continuity is established between hollow units and supporting structure by the addition of insitu topping concrete and steel reinforcement. This can result in negative moments and axial forces being induced in the floor by seismic and other structural actions. Vertical seismic accelerations in combinations with other loading can create significant negative moments that are generally not currently considered in the design of hollow-core floors.

1.1 Objectives of this Research

The objectives of this research are:

- To identify issues that affect the performance of hollow-core floors
- To present a suite of possible failure modes in hollow-core floors induced by seismic loading. This will assist designers in identifying a hierarchy of failure when using capacity design for the assessment of hollow-core floors
- To analytically investigate the potential of two failure modes possible when negative bending moments are induced in hollow-core flooring
- To experimentally test two sub-assembly hollow-core floor specimens for failure modes, which were assessed analytically, to allow validation and calibration of analytical procedures
- To discuss the potential of two failure mechanisms possible when floors are exposed to negative bending moments and provide recommendations as to how these may be assessed.

1.2 Outline of Thesis

The basic structure of this thesis follows that of a standard scientific report; however, in some cases these sections are covered by more than one chapter, as shown below:

- Literature review; presented in Chapters 2,3 and 4
- Analytical investigation and experimental predictions; presented in Chapters 5 and 6
- Experimental set-up; presented in Chapter 7
- Experimental results; presented in Chapters 8 and 9
- Discussion; presented in Chapters 10 and 11
- Conclusions; presented in Chapter 12.

The reason some of these sections are described in more than one chapter is the nature of this research. The literature review contains three major components; the history of hollow-core floors and understanding of its performance in New Zealand, factors which affect the performance of hollow-core flooring and then an outline of potential failure modes. The analytical investigation, experimental results and discussion chapters are split into two, as two different failure modes are considered.

2 Literature Review

Concern over the seismic performance of hollow-core floors is not new; since the early 1980s, when pretensioned flooring systems became a dominant construction type, it was noted that existing codes did not fully cover seismic actions. Further guidelines were produced (Charleson et al. 1991), but performance of hollow-core floors in seismic events overseas and the subsequent failure of the Matthews test (Matthews 2004) at the University of Canterbury showed that a large number of New Zealand buildings could be at risk. The ever-evolving understanding of earthquakes and how structures perform has resulted in previously accepted solutions needing to be reassessed. Assessing hollow-core construction in New Zealand is not an easy task. There are many variations on how hollow-core units can be connected into buildings and recommended connection details have changed overtime with updates to standards and guidelines. Different dimensions and material properties of hollow-core units have also been used, leading to a large number of variables that need to be considered. There are currently no clear guidelines for the assessment of hollow-core floors in New Zealand. To create a more resilient community, infrastructure needs to be able to withstand possible natural disasters; by improving the assessment of hollow-core floors under seismic actions, better design and retrofit solutions can be devised.

This chapter contains a description of hollow-core flooring and describes the guidelines that have been employed for its use in New Zealand. Past research in New Zealand is briefly outlined. Specific aspects of past research are considered in greater detail in subsequent sections dealing with potential failure mechanisms.

In this document, the term “hollow-core unit” is used to describe the precast element. “Hollow-core floor”, “floor unit” and “floor system” are used to describe a composite floor installed in a structure comprising of hollow-core units with an insitu reinforced concrete topping. “Test unit” or “test specimen” refers to a section of hollow-core floor built and tested in a laboratory.

2.1 Hollow-core Floor use in New Zealand

Hollow-core units are a type of precast, prestressed member. In New Zealand typical units contain prestressing strands in the bottom of each web and no shear reinforcement. Units are

typically 1200 mm wide and depths range from 150 to 400 mm deep. Hollow-core units are used predominantly in New Zealand as suspended floors, with a 50 to 75 mm deep insitu concrete topping containing passive steel reinforcement. The deeper units can be used to achieve floor spans of up to 18 m. Hollow-core units are manufactured by purpose built extruding machines from low slump concrete. Long lengths of hollow-core are extruded along special beds and then cut to the required lengths once the concrete has gained sufficient strength. The dimensions of these units and the material properties have varied over the years as technology has changed. As a result, there are a wide range of different hollow-core sections found in existing New Zealand buildings. A current common hollow-core floor cross-section is shown in Figure 2-1. In addition to the hollow-core units themselves changing over the time, the way they are used and connected into buildings has also evolved.

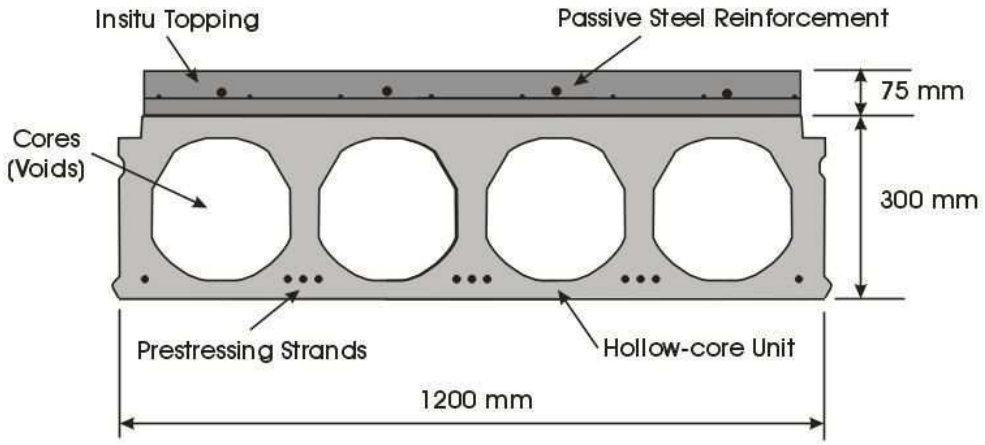

Figure 2-1 Typical hollow-core cross section

Precast construction is popular in New Zealand because of its ease of construction, rapid erection times, the appeal of off-site construction and the factory-like controls. Hollow-core flooring in particular offers advantages over other precast flooring systems because it has a flat soffit, requires little or no propping and provides a safe and stable working platform while still achieving long spans at optimum economy. Variations of hollow-core flooring are also used overseas. Often hollow-core units in non-seismic regions are installed without a structural topping. Other differences include hollow-core units containing prestressing strands at the top of the webs as well as at the bottom and even deeper sections. The diverse types of hollow-core sections and ways which they are installed means that not all research performed on hollow-core internationally can be applied to hollow-core use in New Zealand.

2.2 History of Hollow-core Manufacture: Specifically in New Zealand

The concept of a pretensioned floor slab was first developed in Germany in the mid 1930's. Pretensioning was used in Germany during the second world war period in the construction of submarine bases along the Atlantic and North Sea coasts. Pretensioning became a commercial success in the 1950s in the United States with the development of the seven-wire stress relieved prestressing strand by the John A. Roebling & Sons Corporation. The first extruded hollow-core flooring produced in the United States was around 1954, but it was not until the 1960s that extruded hollow-core flooring products were developed to their potential (Herlihy 1999).

The development of pretensioned concrete in New Zealand was strongly influenced by its use in North America. By the mid 1960s, its use in New Zealand included most of the standardised sections that had originated in North America. In the late 1960s there were some non-extruded hollow-core units produced in New Zealand using cardboard or rubber tubes to form the circular voids by Stresscrete and B&B Concrete Ltd. By the mid 1970s Stresscrete were also using urea formaldehyde or polystyrene foam to form rectangular cores where the foam was left in place. Extruded hollow-core flooring did not appear in New Zealand until 1974 when B&B Concrete Ltd. introduced the first extruding machine (McSaveney 2007). During the 1980s there was a major building boom in New Zealand. This resulted in a tendency towards multi-storey buildings constructed from precast concrete frame elements. Hollow-core flooring became the preferred precast flooring system for spans in the 6 to 12 metre range. The use of precast concrete in flooring rapidly became commonplace, leaving cast-in-place floor construction less common and uncompetitive. Other types of hollow-core extruding machines and slip-formers were introduced in the mid 1980s and the available slab depth increased (McSaveney 2007). Because of the seismic design requirements in New Zealand, manufacturers have opted for machines that produce precast units of minimum weight that require a structural insitu concrete topping. It is common in other countries for hollow-core flooring to be used without a structural topping.

The most commonly used sizes of hollow-core units in existing New Zealand buildings are 200 mm and 300 mm deep. Units have been produced as shallow as 150 mm and since 1996, 400 mm deep units have been available (Herlihy 1999). Hollow-core floor systems are commonly used today in both traditional monolithic reinforced concrete construction and in

the more recent jointed ductile systems (Priestley et al. 1999), suggesting that their use will not diminish in the near future.

2.3 History of Guidelines for Hollow-core use in New Zealand

New Zealand guidelines predominantly followed North American practice because the language and units used North American code requirements were immediately comprehensible to New Zealand engineers. The American Concrete Institute (ACI) 318 codes became standard documents for concrete design in New Zealand in the 1960s. Details used, such as a nominal seating length of 50 mm followed North American practice. By 1968 the Standards Association of New Zealand had produced a Standard Recommendation for Prestressed Concrete, NZSR 32:1968; this document was not superseded until the New Zealand Concrete Structures Standard, "Code of Practice for the Design of Concrete Structures" NZS 3101:1982 parts 1 and 2, was produced. This standard was more specific than its predecessor and contained comprehensive provisions for the seismic design of cast-in-place concrete construction. However, it did not contain provisions covering all aspects of precast concrete structures. Because of the lack of guidance on the use of precast concrete elements as functional parts of seismic resistant structures, a joint study group was appointed by the New Zealand Concrete Society (NZCS) and the New Zealand National Society of Earthquake Engineering (NZSEE). This study group produced a set of guidelines for precast concrete construction (Charleson et al. 1991), commonly referred to as the "Grey Book". A revised New Zealand concrete standard was published in 1995 (Standards New Zealand. 1995) which included standard requirements that were relevant to precast concrete construction. The guidelines for use of structural precast concrete in buildings were reproduced in 1999 (New Zealand Concrete Society. Study Group. et al. 1999) to incorporate relevant research undertaken during the first half of the 1990s and to bring some of the technical aspects in to line with the 1995 revision of the New Zealand Concrete Structures Standard (Standards New Zealand. 1995). Research into hollow-core flooring continued, as with the increase in use of precast concrete construction, came a concern that some of the design solutions being used should be more fully researched. In 2004, Amendment No. 3 to the 1995 New Zealand Concrete Structures Standard was published (Standards New Zealand. 2004). This amendment gave specific guidelines on the installation of hollow-core floors with greater tolerances than previously recommended. A practice advisory was released by the Department of Building and Housing (Department of Building and Housing 2005) to increase

awareness of the latest guidelines for hollow-core support connections. The recommendations from the 2004 Amendment (Standards New Zealand. 2004) have since been incorporated into the latest New Zealand Concrete Structures Standard (Standards New Zealand. 2006). This Standard states:

> "Research into the seismic performance of hollow-core flooring systems is ongoing. The details described in this clause are considered probable best practice, based upon the information on hand in the preparation of the Standard. Modification of the requirements may occur as more research data becomes available."

Research is ongoing and additional guidelines to assist engineers with the design and assessment of hollow-core floors are currently being produced by the Department of Building and Housing. Manufacturers of hollow-core units have also provided their own guidelines.

2.4 Development of Understanding Hollow-core Floor Performance in New Zealand

Early research undertaken into the performance of hollow-core flooring in New Zealand looked at the shear strength of hollow-core units under gravity loads (Blades et al. 1990; Yap 1985). It was later recognised that seismic actions could have a negative effect on the floors, with beam elongation potentially "pulling" the floors off their vertical supports. Research was undertaken into connection details that provided a secondary load path should bearing be lost. This initial research considered gravity loads and the "pull off" effect of parallel reinforced concrete beam elongation (Herlihy 1999; Mejia-McMaster 1994; Oliver 1998). This research was followed by Matthews (2004), who performed a three-dimensional super-assembly test. This work highlighted the effects of relative rotation between the floor units and their supports and incompatible displacements between floors and frame beams. The Matthews research prompted further projects into the effects of relative rotation between support beams and floors (Bull and Matthews 2003; Liew 2004) and into new connection details (Lindsay 2004; MacPherson 2005). Recent work has looked at the effects of both relative rotation and parallel beam elongation on existing hollow-core flooring connections, as well as potential retrofits (Jensen 2006).

2.4.1 Shear under Gravity Loads

When hollow-core was first introduced in New Zealand, the interaction between the units and their supports was not considered. Floors were designed as simply-supported spans; therefore, the critical parameters were the positive moment capacity at the centre span and the shear capacity near the supports. The connection details relied on the bearing length to provide vertical support. The hollow-core units had sufficient positive moment capacity because of the prestressing strands positioned near the bottom of the section. However, the lack of shear reinforcement raised concerns over the shear capacity. Two reports produced by the Ministry of Works and Development Central Laboratories (Blades et al. 1990; Yap 1985) looked into the shear strength of hollow-core floors and the effect that bearing length had on this. These reports stated that a bearing length as small as 5 mm did not reduce the shear strength.

2.4.2 Effects of "Pull Off" from Beam Elongation

In 1991, guidelines for precast construction were produced by a study group appointed by the New Zealand Concrete Society (NZCS) and the New Zealand National Society of Earthquake Engineering (NZNSEE) (Charleson et al. 1991). This document is commonly referred to as the "Grey Book", it contains a comprehensive section on floor unit support and continuity, including information specific to the installation of hollow-core floors. It was stressed that vertical support of precast units was one of the most basic requirements of a safe structure. It was recognised in the Grey Book that actions from seismic loading may effect hollow-core floors. Several connection details were presented to provide alternative load paths if bearing was lost. Research was commenced at the University of Canterbury (Mejia-McMaster 1994) investigating the performance of such connections.

The Grey Book (Charleson et al. 1991) discussed factors that must be considered when determining an appropriate seating length. Including:

- Construction tolerances
- Volume changes due to creep and shrinkage
- Hogging due to thermal effects
- Spalling of supports
- Seismic effects, including both loss of cover concrete in plastic hinge regions of support beams and elongation of moment resisting frame beams.

Although the effects of seismic loading had been recognised, the magnitude of its effect on hollow-core flooring was yet to be researched. The guidelines gave suggestions for seismic detailing but stated that research was urgently required in this area. The guidelines suggested that when seismic loading was considered a load factor for gravity loads of not less than 1.1 should be used. Where necessary seating lengths could not be achieved, alternatives, such as catenary action of topping reinforcement (if tied adequately into the floor) or other special reinforcement, were recommended. Special reinforcement was to provide an alternative load path by kinking (see Figure 2-2) if bearing of the floor unit could be lost. The use of special reinforcement, such as "Hairpin" shaped bars cast into the voids of hollow-core unit, was also suggested for use as a remedial measure if negative seating occurred on site due to construction tolerances. The details shown in Figure 2-3 were illustrated in the guidelines for situations where end seating was inadequate. At the time these details were untested.

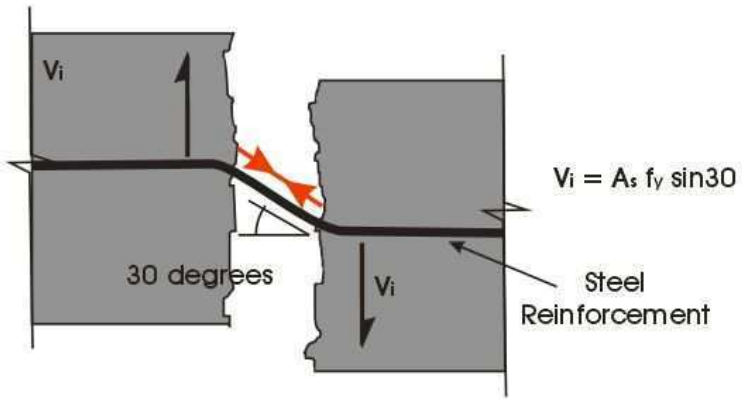

Figure 2-2 Kinking of special reinforcement to provide vertical support if bearing is lost (Adapted from Charleson et al. 1991)

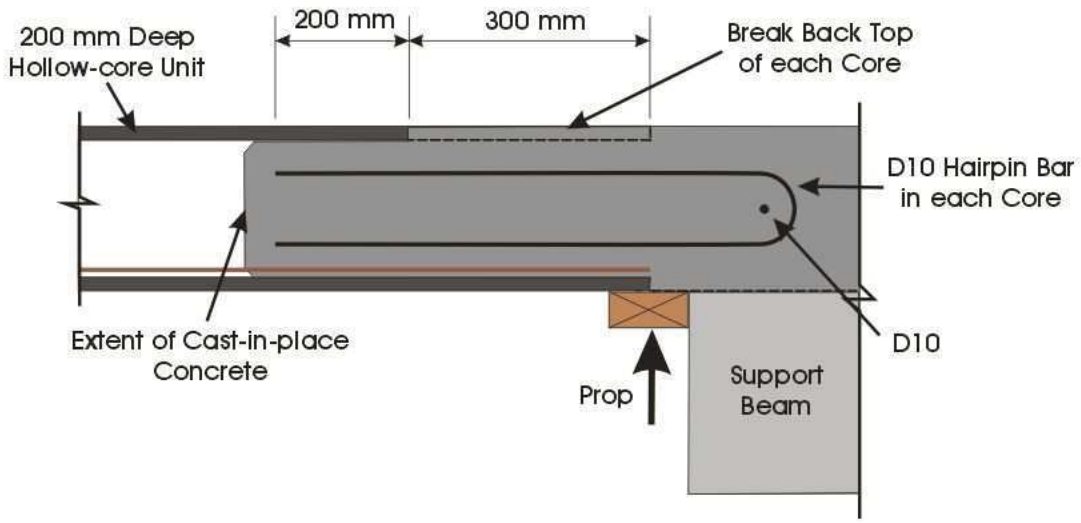

(a) When only lower half of support beam is precast

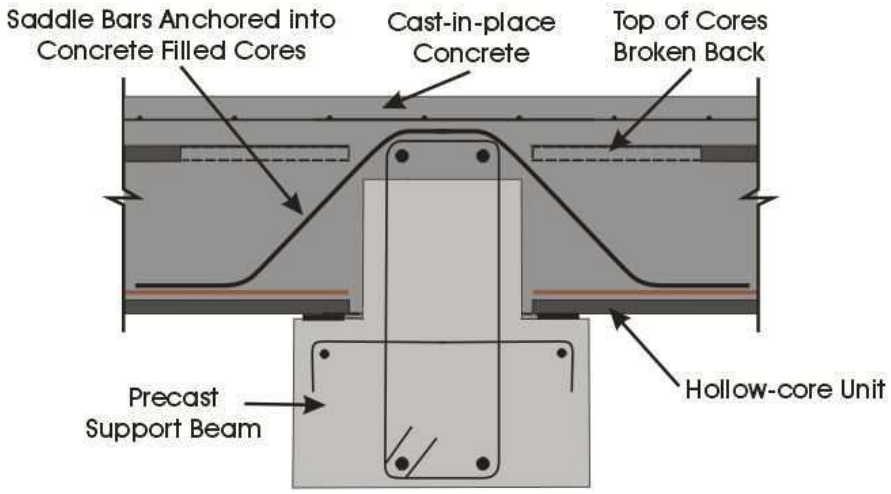

(b) When majority of support beam is precast

Figure 2-3 End support detail suggested in the Grey Book if seating was inadequate (Adapted from Charleson et al. 1991)

Mejia-McMaster (1994) investigated three different hollow-core to support beam connections which met the requirements outlined by the Grey Book. The shear capacity of the connections was assessed under two conditions in sub-assembly tests. Firstly, when the unit had zero seating length and then when the unit was pulled horizontally off its support (to represent the actions induced by elongation of beams parallel to the floor span). Mejia-McMaster concluded that when no axial load is applied the shear capacity at the support could be calculated from the shear friction across the crack and the vertical component of force in the

tie bars. When the floor units were pulled horizontally and bearing was lost, vertical support could be maintained by kinking of the plain round reinforcement. The detail recommended in the Grey Book (shown in Figure 2-3 (b)) failed during testing due to stresses induced by the large angle change in the reinforcement and was therefore not recommended for use in structures which may experience seismic loading.

2.4.3 Northridge Earthquake

Concerns about the effect of seismic loading on hollow-core flooring were renewed in 1994 following an earthquake in Northridge, California, where some precast concrete floor systems did not perform satisfactorily. Observations of damage caused by this earthquake by Iverson and Hawkins (2004) noted that inadequate ties between precast floor elements and lateral load resisting systems could have lead to collapse. Precast building practices in New Zealand were similar to those used in California. This prompted further ways of tying hollow-core floors into buildings being investigated. Oliver (1998) and Herlihy (1999) both further investigated the effect of "pull off" effect possible under seismic loading. The test setup and loading processes were similar to that used by Mejia-McMaster (1994) but incorporated cyclic loading.

Herlihy (1999) commenced his investigation by looking at a "typical" starter bar detail of the time, as illustrated in Figure 2-4 (a). This type of connection is referred to as the typical existing connection detail. From three experimental tests, it was concluded that this detail can not prevent floor collapse in the event of loss of bearing, as the starter bars do not perform as a ductile tie between flooring units and support members. Connection details containing steel reinforcement cast into the voids of the hollow-core floors were then investigated. These showed improved ductility, especially when round bars were used. Investigation into new connection details designed to provide support to hollow-core seating when seating was lost was continued by Oliver (1998). Oliver looked at three different connection details using combinations of fibre reinforced concrete and a "paper-clip" of steel reinforcement in the filled cores (see Figure 2-4 (b)). However, although these details performed better than the "typical" starter bar details tested by Herlihy (1999), they did not have sufficient deformation capacity to sustain the horizontal displacements possible due to beam elongation if a hollow-core floor spanned two bays of a lateral load resisting perimeter frame.

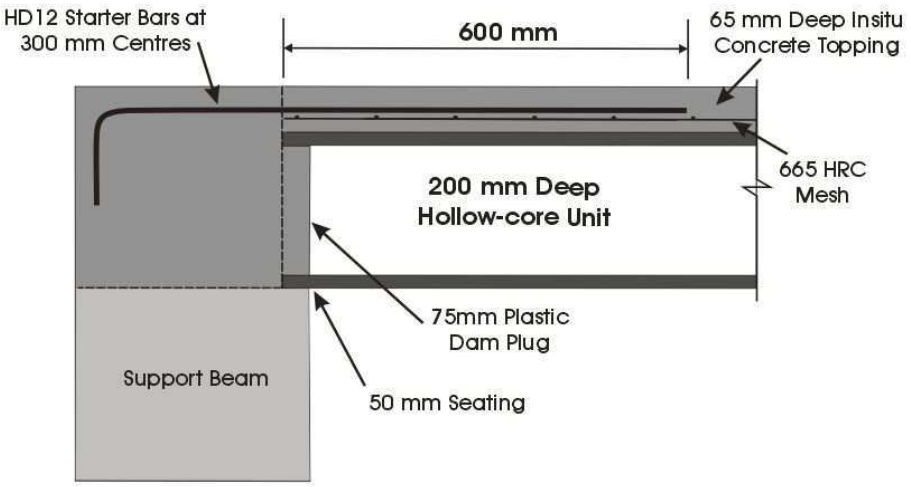

(a) Connection tested by Herlihy (1999)

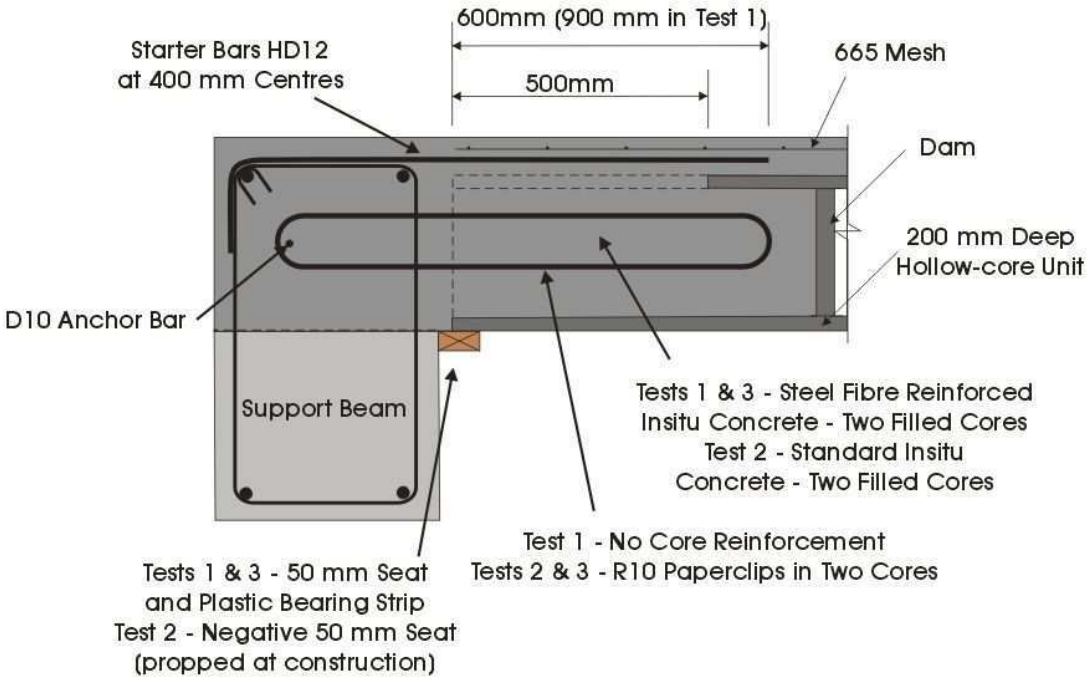

(b) Connection tested by Oliver (1998)

Figure 2-4 Connection details tested for shear capacity after loss of bearing support

In 1999 a second edition of the Grey Book (New Zealand Concrete Society. et al.) was published, this contained similar information to the first edition (Charleson et al. 1991). However, findings from Mejia-McMaster, Oliver and Herlihy were incorporated. These amendments included changing the recommendations for special reinforcement, used as a secondary load path when bearing support is lost. The change was to recommend round bars

for the special reinforcement, instead of deformed, and an increased length of these into the floor units. The study group was not satisfied that the problem of performance of connections between hollow-core floors and their support beams was understood and recommended further research be undertaken.

2.4.4 'Canterbury' Precast Floor and Frame Super-Assembly

A full-scale super-assembly test, of a segment of reinforced concrete frame building, was undertaken by Matthews (2004). The aim of this test was to investigate the buildings overall seismic performance, including three-dimensional effects,. This test and research is referred to as the "Matthews test". Particular emphasis was placed on how the hollow-core flooring within the test specimen performed. Figure 2-5 shows the super-assembly tested by Matthews and the portion of building the test was designed to represent. The super-assembly used in the Matthews test was intended to emulate existing construction practice. The two-way moment resisting frames performed well, however the floor performed poorly. The precast hollow-core units began cracking at an equivalent interstorey drift of just 0.3 %. Failure began at an interstorey drift of 1.9 % and complete collapse occurred at 2.5 %. The performance of the test highlighted deficiencies, raised many questions and prompted further experimental and analytical research into the performance of hollow-core floors by multiple researchers (Bull and Matthews 2003; Fenwick et al. 2004; Jensen 2006; Liew 2004; Lindsay 2004; MacPherson 2005). The test also prompted the Building Industry Authority (now the Department of Building and Housing) to review the use of hollow-core floor systems in New Zealand (Stannard et al. 2007).

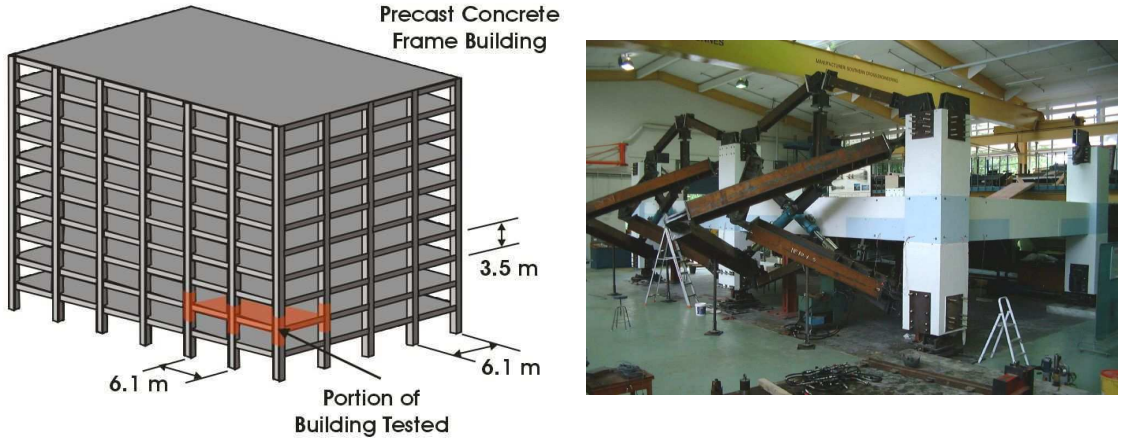

(a) Portion of building tested **(b) Matthews test rig**

Figure 2-5 Super-assembly tested by Matthews (2004)

There were three principle damage modes observed in the Matthews test, these are illustrated in Figure 2-6. A large tear was created in the floor due to the central column, which the hollow-core floor spanned past, being pushed away from the floor due to elongation of the beam plastic hinge zones (see Figure 2-6 (a)). Incompatible displacements between the exterior hollow-core unit and the parallel frame beam caused extensive longitudinal web cracking in these units (see Figure 2-6 (b)). The ends of some hollow-core units became "trapped" at the support, resulting in high positive moments and flexural cracking (see Figure 2-6 (c)).

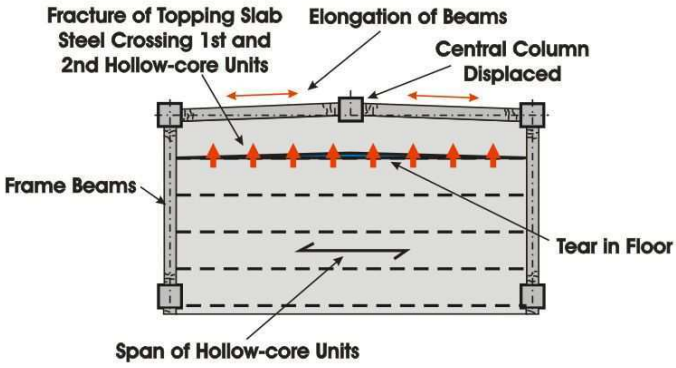

(a) Plan of test unit showing tear caused by movement of central column (Adapted from Jensen 2006)

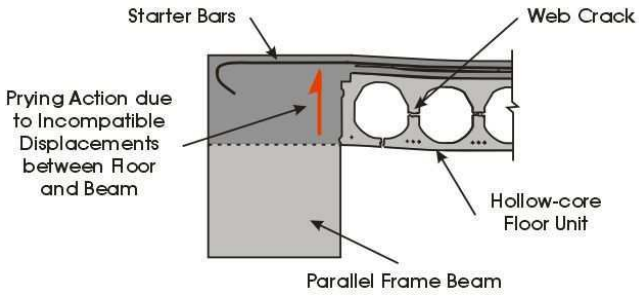

(b) Web cracking caused by incompatible displacement between parallel frame beam and floor

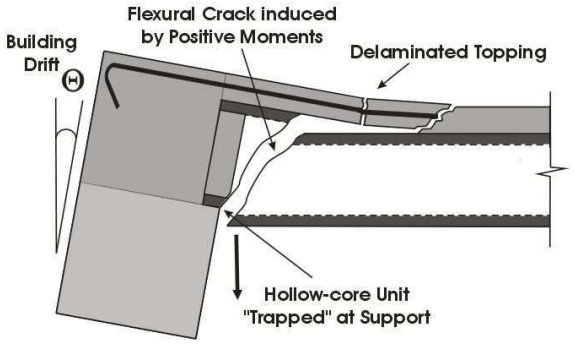

(c) Flexural cracking caused under positive moments (Adapted from Jensen 2006)

Figure 2-6 Principle damage modes observed in the Matthews test

It was observed in the Matthews test that the primary damage causing mechanisms to the seating connection was the relative rotation between the hollow-core floor and its supporting beam due to inter-storey drift. This mechanism had not been considered in the assessment of beam to floor connections by previous researchers (Mejia-McMaster (1994), Herlihy (1999) and Oliver (1998)). To investigate further connection details, Bull and Matthews (2003) proposed using a sub-assembly test set-up which was rotation focused. This set-up was then used by Bull and Matthews (2003) and Liew (2004) to further investigate the performance of existing connections and trial new connection details recommended by a Technical Advisory Group (TAG), which was formed to discuss the implications on the Matthews test for New Zealand.

Two specimens, typical of existing connections, were tested by Bull and Matthews (2003) and are shown in Figure 2-7 (a). One contained a 200 mm deep hollow-core unit and the other a 300 mm deep hollow-core unit. Both specimens experienced flexural cracking starting at the soffit of the units near the support under positive moments, similar to the damage mode observed in the Matthews test illustrated in Figure 2-6 (c). Figure 2-7 (b) and (c) show the connection details proposed by TAG tested by Bull and Matthews. It was concluded that connection performance was improved by these connections, especially by the one that included a compressible backing pad and low friction bearing strip (see Figure 2-7 (b)). However, it was recommended that super-assembly tests be performed to validate viable solutions for new connection details before they were implemented in practice.

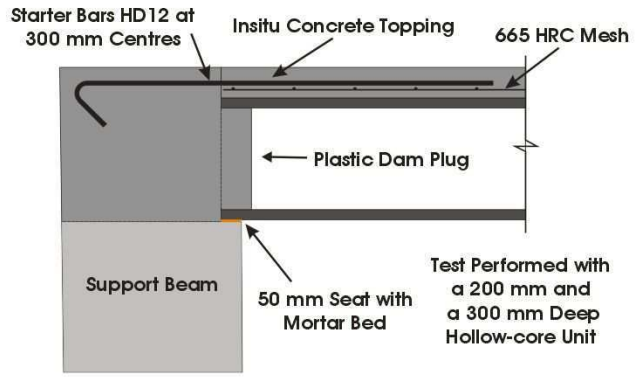

(a) Existing detail

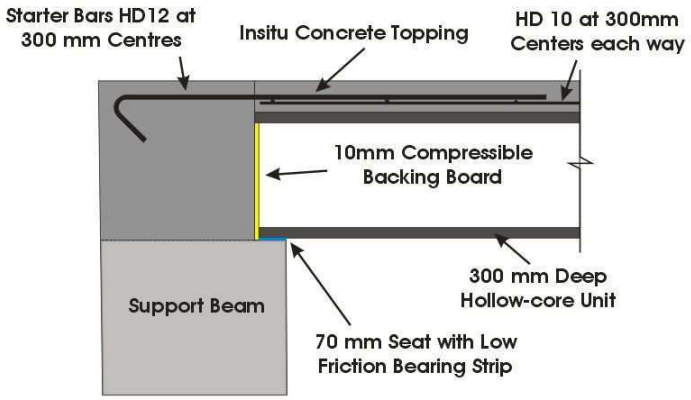

(b) "Pinned" detail

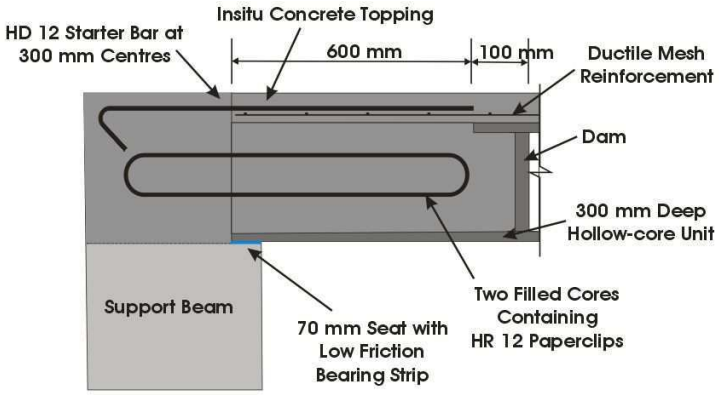

(c) "Fixed" detail

Figure 2-7 Connection details tested by Bull and Matthews (2003) (Adapted from Jensen 2006)

Liew's investigation (2004) concentrated on existing connections with filled cores and also a potential retrofit. The details with filled cores both experienced a failure initiated by a flexural

crack forming at the end of the filled section under a negative bending moment. The amount of steel reinforcement contained in the filled cores was more than required and it was suggested that this was detrimental to the connections performance. The performance of these specimens is discussed further in Section 5.1. The retrofit detail was applied to a connection similar to that shown in Figure 2-7 (a). This involved placing a steel angle beneath the hollow-core unit, increasing the length on which the hollow-core unit was seated. Although the steel angle delayed the loss of support, it also restrained the beam to floor connection causing higher moments to be transferred into the hollow-core section. This resulted in a flexural crack forming at the end of the starter bars under negative moments. It was recommended that this retrofit solution not be used without further investigation.

Fenwick et al. (2004) analytically considered stress conditions in hollow-core units which could lead to failure under seismic actions. Aspects were taken into account that had not been considered prior to the Matthews test (Matthews 2004). The paper investigated a range of actions that could arise in a hollow-core floor diaphragm and provided simple calculations to assess the magnitude of these actions where possible. The paper provided recommendations on how to detail hollow-core floor systems to improve seismic performance and indicated areas where further research was required. Several failure modes predicted in this paper had not been observed experimentally.

The Matthews test rig was reused by Lindsay (2004) and MacPherson (2005), who tested hollow-core floor systems with details improved to better cope with displacement incompatibilities. The aim was to verify that the details performed satisfactorily when the three-dimensional effects, unable to be represented by the sub-assembly tests, were implemented. Lindsay employed the seating connection first tested by Bull and Matthews (2003) that utilised a compressible backing board, a low friction bearing strip and increased seating (see Figure 2-7 (b)). The connection was designed to slide on the bearing strip, effectively performing as a “pinned” connection, reducing the actions transferred from the supporting beam into the hollow-core floor. Lindsay also used a 750 mm infill slab between the first unit and the frame beam parallel to it (similar to that shown in Figure 2-8) and tied the central column into the floor diaphragm with additional steel reinforcement in the insitu topping concrete. The hollow-core floor system used by Lindsay performed well, sustaining equivalent interstorey drifts of 5.0 % without collapse of the floor. Lindsay measured relative

rotation between the floor and support beam and noted that it was affected by the torsion of seating beam due to eccentric loading of hollow-core floors.

Lindsay made several recommendations for future detailing of hollow-core floors based on findings from this research. These included the implementation of an infill slab between hollow-core units and parallel frame beams, not to sit hollow-core units on potential plastic hinge zones of the support beams and to use ductile bars of steel reinforcement in the insitu topping concrete rather than mesh. Figure 2-8 shows these recommendations.

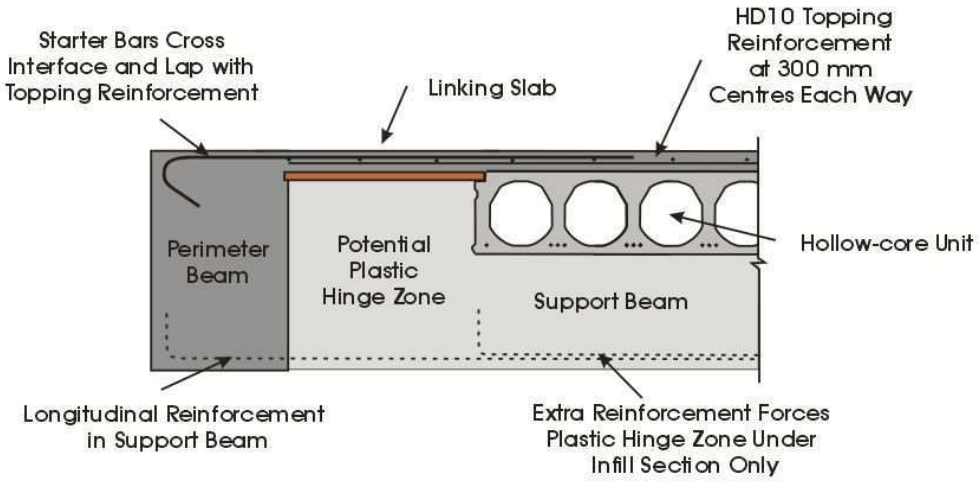

Figure 2-8 Infill slab recommended by Lindsay (Adapted from Lindsay 2004)

The findings from the Lindsay (2004) test were implemented in an amendment to the New Zealand Concrete Structures Standard (Standards New Zealand. 2004). Figure 2-9 shows two connection details recommended in the amendment as "acceptable solutions". The second connection shown was designed using capacity design, ensuring the "critical section" was located at the beam-floor interface and that yielding of the top and bottom steel could accommodate anticipated rotation. MacPherson (2005) used the Matthews test rig to validate this solution, along with other detailing improvements.

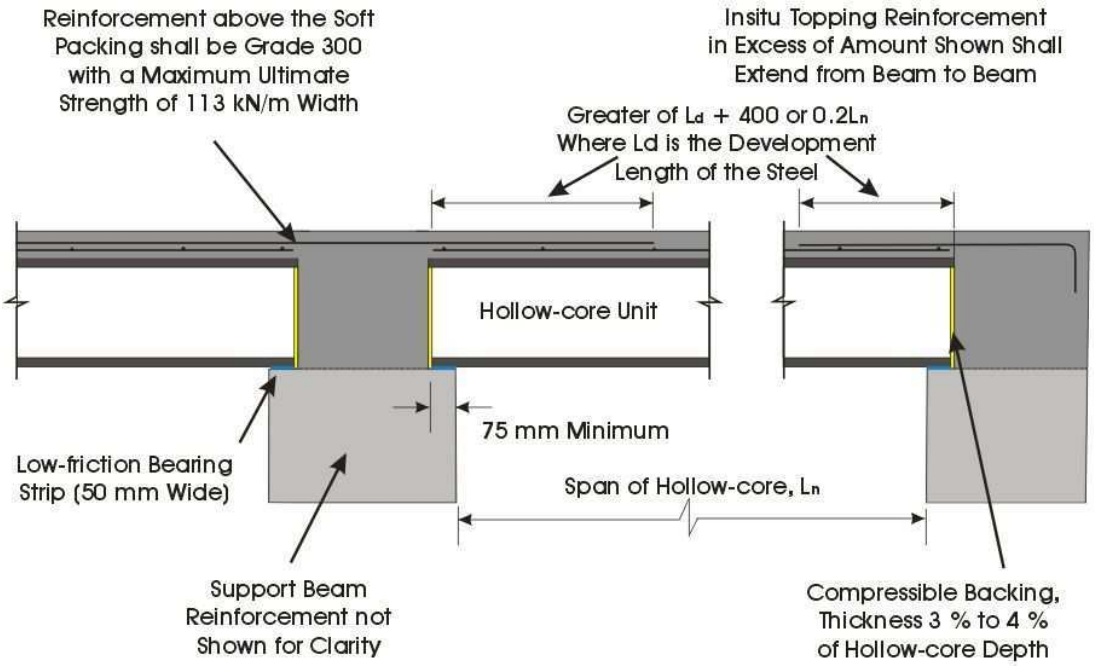

(a) Hollow-core connection with compressible backing and seated on low friction bearing strips

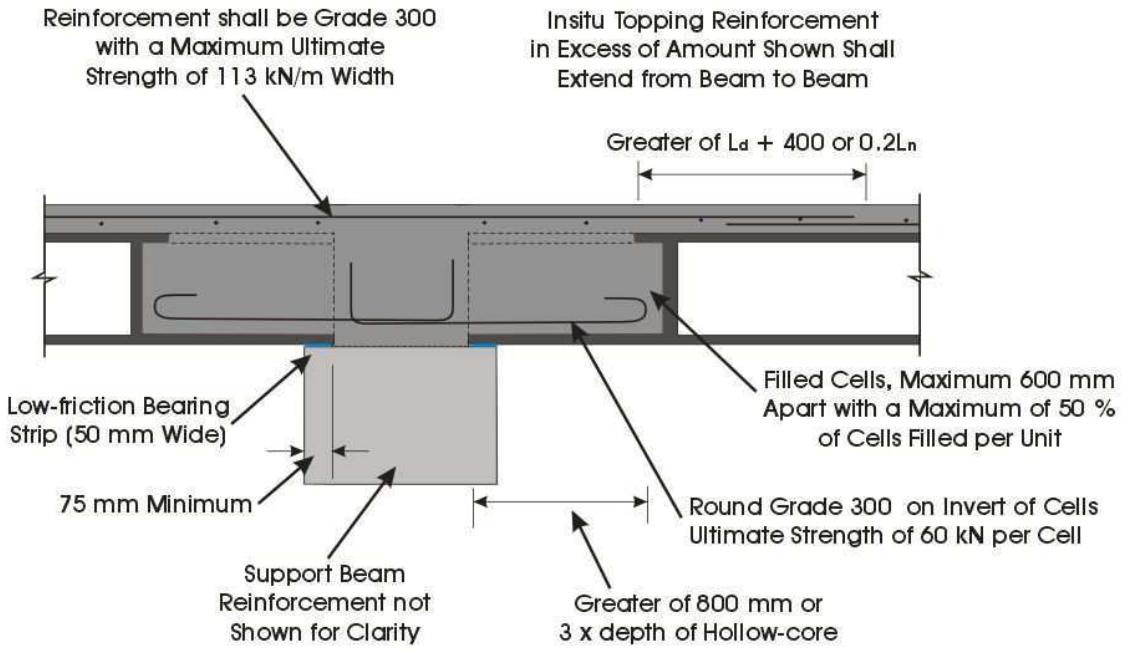

(b) Hollow-core connection with 2 – 2 leg R16 Hairpins in filled cores, seated on low friction bearing strips

Figure 2-9 Hollow-core floor to support beam connection details recommended by the amendment to the New Zealand Concrete Structures Standard (Adapted from Standards New Zealand. 2004)

MacPherson (2005) found that the second connection detail recommended in the amendment to the New Zealand Concrete Structures Standard performed well. The connection behaved

according to how it was designed, with the critical section forming at the beam floor interface. The floor system sustained only minor damage up to drift levels of ± 5 %. MacPherson also performed several sub-assembly tests which incorporated the effects of both beam elongation and relative rotation between the support beam and floor. He concluded, although they had limitations, these provided an accurate representation of the main actions achieved in the super-assembly test. Hence, this type of test could be used to further investigate hollow-core floor to beam connections.

The improved details for hollow-core flooring mean hopefully new buildings containing hollow-core floors will have superior performance in the event of an earthquake. Jensen (2006) looked at the effect that seating length in existing hollow-core floor to beam connections has and how connections with insufficient seating could be retrofitted. The sub-assembly test set-up first used in research by MacPherson (2005), which allowed the effects of elongation and rotation to be assessed, was used. The work carried out by Jensen was predominantly concerned with a loss of vertical support failure and is discussed further in Section 4.2. He clarified aspects of a beam to floor connection that contributed to the likelihood of a loss of support failure.

The review of hollow-core floor systems in New Zealand by the Department of Building and Housing commenced in 2003 and an overview report of outcomes to date was released in March 2007 (Department of Building and Housing 2007). The aim of the review was to determine the number of buildings that may be at risk to damage, and the extent of this damage, in a major New Zealand earthquake. The review was undertaken in three steps; reviewing the performance of buildings containing hollow-core in overseas earthquake events, surveying usage of hollow-core in New Zealand and then thirdly using the information from both these investigations to assess the likely performance of New Zealand buildings in a major earthquake event. Surveys were performed examining the building consent drawings for hollow-core buildings in Christchurch and then Wellington. No survey was completed for Auckland because of its location in a lower seismic region. The performance of hollow-core buildings was assessed by comparing the likely inter-storey displacement (lateral displacement between one floor and the next) in a major earthquake with the ultimate-limit-state inter-storey drift reasonably providing life safety. This value was taken as the peak inter-storey drift (not the ultimate) providing life safety identified by the Technical Advisory Group of Precast Flooring Systems (TAG) by interpreting the Matthews test

(Technical Advisory Group of Precast Flooring Systems 2002). The conclusions and implications drawn from this research presented in a paper at the New Zealand Society for Earthquake Engineering in Palmerston North, March 2007 by Stannard el al (2007) have been questioned (Fenwick 2007). There is concern that the paper is misleading and could cause structural engineers to make unconservative analyses when assessing the safety of buildings containing hollow-core units.

The overview report (Department of Building and Housing 2007) indicated that further investigation would be sensible as 9 % of the buildings surveyed in Wellington and 16 % of buildings in Christchurch could not be considered safe under the criteria considered (Department of Building and Housing 2007). However, as mentioned in the previous paragraph, the method used to calculate these figures has been questioned and they might be even higher. The report also recognised that the performance of hollow-core flooring is dependent on local displacements and actions as well as the exact details used, not simply the projected inter-storey drift. The Department of Building and Housing acknowledged that there was a need for a document providing guidance on the assessment, design and retrofit of existing and new hollow-core floor buildings. The current research is part of an initiative to create such a document. This research aims to improve the understanding of hollow-core floor system performance.

2.5 References

Blades, P. S., Jacks, D. H., Beattie, G. J., and Central Laboratories (N.Z.). (1990). *Investigation of the influence of the end support condition on the shear strength of prestressed voided slabs*, Central Laboratories, Lower Hutt, N.Z.

Bull, D., and Matthews, J. (2003). "Proof of Concept Tests for Hollowcore Floor Unit Connections." *Research Report 2003-1*, Department of Civil Engineering, University of Canterbury, Christchurch, New Zealand.

Charleson, A. (ed), New Zealand Concrete Society. Study Group., New Zealand National Society for Earthquake Engineering., and Centre for Advanced Engineering. (1991). *Guidelines for the use of structural precast concrete in buildings : report*, The Societies : Centre for Advanced Engineering, [Christchurch, N.Z.].

Department of Building and Housing. (2005). "Practise Advisory 5, Allow for movement, Precast hollow-core floor assemblies." Building Controls, ed.

Department of Building and Housing. (2007). "Hollowcore Floor Overview Report." Department of Building and Housing, Wellington, New Zealand.

Fenwick, R. (2007). "Letter to the Editor Re: "Hollow Core Floors - A Regulator's Perspective", a paper presented at the NZSEE Conference, Palmerston North, March 2007." *Bulletin of the New Zealand Society for Earthquake Engineering*, 40(2), 78.

Fenwick, R., Deam, B., and Bull, D. (2004). "Failure modes for hollowcore flooring units." *Journal of the Structural Engineering Society New Zealand Inc.*, 17(1), 52 - 70.

Herlihy, M. D. (1999). *Precast concrete floor support and diaphragm action : a thesis submitted in partial fulfilment of the requirements for the degree of Doctor of Philosophy, [University of Canterbury]*.

Iverson, J. K., and Hawkins, N. M. (2004). "Performance of Precast/Prestressed Concrete Building Structures During Northridge Earthquake." *PCI Journal*, 39(2), 38 - 55.

Jensen, J. (2006). *The seismic behaviour of existing hollowcore seating connections pre and post retrofit : a thesis submitted in partial fulfilment of the requirements for the degree of Master of Engineering at the University of Canterbury*, Christchurch, New Zealand.

Liew, H. Y. (2004). *Performance of hollowcore floor seating connection details : a thesis submitted in partial fulfilment of the requirements for the degree of Master of Engineering at the University of Canterbury*.

Lindsay, R. (2004). *Experiments on the seismic performance of hollow-core floor systems in precast concrete buildings : a thesis submitted in partial fulfilment of the requirements for the degree of Master of Engineering at the University of Canterbury*, Christchurch, New Zealand.

MacPherson, C. (2005). *Seismic performance and forensic analysis of a precast concrete hollow-core floor super-assemblage : a thesis submitted in partial fulfilment of the requirements for the degree of Master of Engineering at the University of Canterbury*, Christchurch, New Zealand.

Matthews, J. (2004). *Hollow-core floor slab performance following a severe earthquake : a thesis submitted in partial fulfilment of the requirements for the degree of Doctor of Philosophy at the University of Canterbury*, Christchurch, New Zealand.

McSaveney, L. (2007). "Hollow-core Precast Flooring in New Zealand - Historical Perspective." Guidelines for the assessment of hollow-core flooring in New Zealand - DRAFT - expected to be published in 2008, Department of Building and Housing, Wellington, New Zealand.

Mejia-McMaster, J. C. (1994). *Precast concrete hollow-core floor unit support and continuity : a thesis submitted in partial fulfilment of the requirements for the degree of Master of Civil Engineering at the University of Canterbury*, Christchurch, New Zealand.

New Zealand Concrete Society., New Zealand Society for Earthquake Engineering., and Centre for Advanced Engineering. (1999). *Guidelines for the use of structural precast concrete in buildings : report*, Centre for Advanced Engineering University of Canterbury, Christchurch, N.Z.

New Zealand Concrete Society. Study Group., New Zealand Society for Earthquake Engineering., and Centre for Advanced Engineering. (1999). *Guidelines for the use of structural precast concrete in buildings : report*, Centre for Advanced Engineering University of Canterbury, Christchurch, N.Z.

Oliver, S. J. (1998). *The performance of concrete topped precast hollowcore flooring systems reinforced with and without Dramix steel fibres under simulated seismic loading : a report submitted in partial fulfilment of the requirements for the degree of Master of Civil Engineering at the University of Canterbury*, Christchurch, New Zealand.

Priestley, M. J. N., Sritharan. S., Conley, J. R., and Pampanin, S., (1999). "Preliminary Results and Conclusions from the PRESSS Five-story Precast Concrete Test Building." *PCI Journal*, 44(6), 42 - 67.

Standards New Zealand. (1995). *Concrete structures standard*, Standards New Zealand, Wellington [N.Z.].

Standards New Zealand. (2004). *Amendment No. 3 to 1995 Standard (NZS3101)*, Standards New Zealand, Wellington, New Zealand.

Standards New Zealand. (2006). *Concrete structures standard, NZS3101, Parts 1 & 2*, Standards New Zealand, Wellington, New Zealand.

Stannard, M., Bialostocki, R., Hopkins, D. C., Jury, R., and Saunders, D. (2007). "Hollow Core Floors - A Regulator's Perspective." NZSEE Conference, Palmerston North.

Technical Advisory Group of Precast Flooring Systems. (2002). "The Seismic Performance of Flooring Systems Executive Summary : Special Research Report." *SESOC Journal*, 15(2), 36 - 43.

Yap, K. K. (1985). *Shear tests on proprietary prestressed voided slabs using various end support conditions*, Structures Section Central Laboratories Ministry of Works and Development, Lower Hutt, N.Z.

Blank

3 Background Information required for the Assessment of Hollow-core Floors

To assess hollow-core floors, it is necessary to apply a number of general structural concepts and theories. This section gives a brief overview of these and how they relate to hollow-core floors. Understanding of these concepts allows interpretation of discussion in the rest of this thesis. The reasoning behind several of the assumptions made during the assessment of hollow-core flooring is also explained. This section is separate from the descriptions of the failure mechanisms because several aspects described here apply to more than one failure mechanism.

This chapter describes;

- Capacity design, the use of a hierarchy of strength
- Initial stress conditions in hollow-core floors
- The effect of creep and shrinkage
- The behaviour of hollow-core floors under gravity loading
- Beam elongation and the potential effect this has on hollow-core floors
- The tensile strength of concrete
- Unequal stiffness of hollow-core floors under vertical loading.

3.1 Capacity Design

The concept of capacity design is to select a failure mechanism that will result in a ductile failure. This mechanism is then designed to sustain design actions specified in the appropriate loadings standard. The potential overstrength of this mechanism is also calculated; this takes into account the possibility that the variations in material properties and geometries which could lead to higher than average strength. The rest of the structure is designed for the most adverse combination of these overstrength actions that could be transmitted to it, once the permissible failure mechanism has formed. Therefore, all brittle failure modes are avoided. This methodology is explained in more detail in section 2.6.5 of the New Zealand Concrete Structures Standard (Standards New Zealand. 2006). To successfully perform a capacity design, all potential failure modes must be identified.

For design, or retrofit, of hollow-core flooring the permissible failure mechanism is typically chosen to be at the support of the unit. The connection between the supporting beam and the floor units can be detailed as a ductile fuse, limiting actions that are transmitted into the hollow-core units.

3.2 Initial Stress Conditions in Hollow-core Units

The development and transfer of force, and eccentricity of prestressing strands in hollow-core units cause stresses to be induced in the concrete. Fenwick et al. (2004) presented three initial stress conditions in the end of a hollow-core unit that should be considered. These are transverse stresses due to the transfer of prestressing forces, shear stresses over the development length of the prestressing and tensile stresses at the top of the unit due to prestressing eccentricity. Although these stresses are not likely to cause damage to the hollow-core unit alone, they may reduce the capacity of a hollow-core floor when combined with other potential load cases.

Prestressing strands in hollow-core units are eccentric and force is developed in them over a length, which can be assumed to be approximately 45 times the diameter of the strand. The transfer of force into the concrete induces stresses perpendicular to the strand in the anchorage zone. There are tensile stresses near the ends of the member (spalling stresses) and compressive stresses further in. Figure 3-1 shows the transverse stresses. As hollow-core units contain no passive reinforcement, any tensile forces must be carried by the concrete. Therefore, tensile forces should be treated with caution, particularly in the thin hollow-core webs. A guide to good practise, published by the International Federation for Structural Concrete (FIB Commission 6 Prefabrication. and Fédération internationale du béton. 2000), recommends spalling stresses should be less than the characteristic value of concrete tensile strength at the time of prestress release. The spalling stress (σ_{sp}) can be calculated by Equation 3-1 (FIB Commission 6 Prefabrication. and Fédération internationale du béton. 2000, Eq. 1.1). Once the floors are installed the spalling stresses are partially suppressed by the vertical compression stresses from the support.

$$\sigma_{sp} = \frac{P_0}{b_w e_0} \frac{15\alpha_e^{2.3} + 0.07}{1 + (\frac{l_{bp}}{e_0})^{1.5}(1.3\alpha_e + 0.1)}$$ **Equation 3-1**

$$\alpha_e = \frac{e_0 - k}{h}$$

$$k = \frac{I_c}{0.5hA_c}$$

Where:

P_0 initial prestressing force just after release in the considered web, in N

b_w web width, in mm

e_0 eccentricity of the prestressing steel, in mm

k core radius, in mm

h depth of the section, in mm

I_c moment of inertia (second moment of area), in mm^4

A_c area of cross-section, in mm^2

l_{bp} the transmission length, in mm

Shear stresses are induced in the development length of the hollow-core unit due to the change in prestress as it develops. These shear stresses, shown in Figure 3-1, induce diagonal tensile stresses in the webs. Shear stresses may be increased by gravity loads, decreasing the shear strength of the section near the support where shear is often the highest. In low positive moment zones, the eccentricity of the prestressing strands can result in longitudinal tensile stresses at the top of the hollow-core unit. The tension from the initial prestress on the top surface of the unit can be seen in Figure 3-1 labelled “Initial Prestress”.

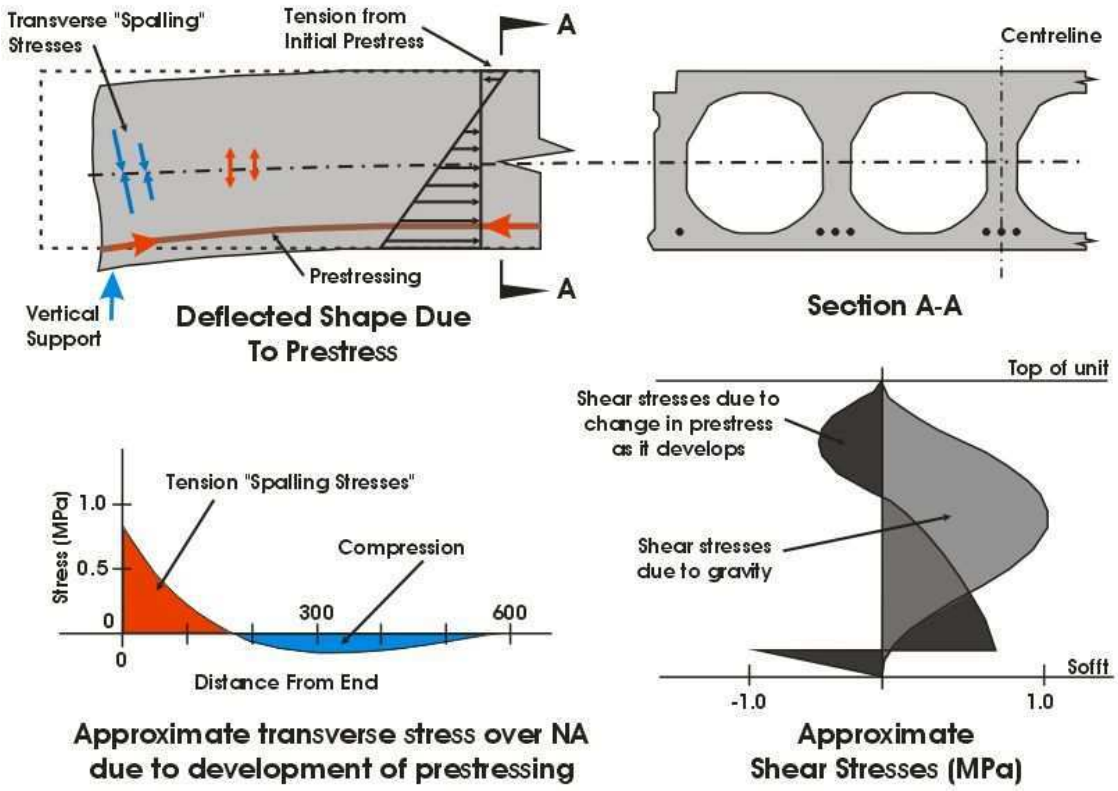

Figure 3-1 Stresses induced in hollow-core units by prestressing tendons (Adapted from Fenwick et al. 2004)

3.3 Effect of Creep and Shrinkage on Hollow-core Floors

The effects of creep and shrinkage start immediately once a hollow-core unit has been cast. In this discussion, shrinkage is defined as the change in strain over time in a specimen due to the hydration and drying of the concrete. Creep is defined as the change in strain over time as a result of an external stress. For a hollow-core floor, there are two different scenarios that need to be considered; before the floor has been installed and after, when insitu concrete has been added creating a composite section. The differential creep and shrinkage between the hollow-core unit and the insitu topping can influence the stress distribution. Shrinkage of New Zealand concrete has been observed to be greater than that in other countries; therefore, care needs to be taken when predicting the amount of shrinkage and what effect this will have on a hollow-core floor.

When a hollow-core unit is cast, creep and shrinkage cause some loss of prestress and some stress redistribution. The rate shrinkage occurs is a related to the volume to surface ratio. The

lower the volume to surface ratio the faster shrinkage occurs, as the path for water to migrate out of the concrete is shorter. Hollow-core units have a low volume-to-surface ratio; therefore, the shrinkage and creep strains develop relatively rapidly (Fenwick et al. 2004). The amount of creep depends on the age of concrete when the load is applied; the younger the concrete, the larger the amount of creep that occurs for the same loading (Bryant et al. 1984).

When the insitu concrete is poured, initially the hollow-core unit supports all the dead load and the prestressing force. Further creep, when the topping has hardened, is restrained by the composite section (hollow-core unit and topping). Therefore, some of the prestress and dead load is redistributed to the composite section. Additional stresses are formed by shrinkage of the insitu topping concrete. The rate at which shrinkage occurs in the insitu concrete is slower than in the hollow-core unit due to the higher volume-to-surface ratio. The insitu topping is cast against the unit; therefore, water can only migrate out from one surface.

Fenwick et al. (2004) performed an analysis using the modified effective modulus method to illustrate how creep and shrinkage movements influence concrete stresses in a hollow-core floor. The effective modulus method uses the elastic modulus multiplied by a coefficient to account for the effects of creep when calculating the strain under a given stress (Bryant et al. 1984). The analysis by Fenwick et al. looked at a typical 300 mm deep hollow-core unit with 65 mm of insitu concrete topping. Figure 3-2 shows the development of stresses in the hollow-core floor section over time. Two loading conditions are shown; one with and one without appreciable dead load. The section with minimal dead load acting represents a section close to the support, but beyond the length influenced by the development of the prestressing. The other represents a section at the floor mid-span. It can be seen that significant tensile stresses can be induced in the insitu topping concrete over time, when minimal dead load is applied. The analysis assumed a simply supported member, should a hollow-core floor have fixed supports, the resulting tensile stresses in the topping concrete in the negative moment region could be significantly higher.

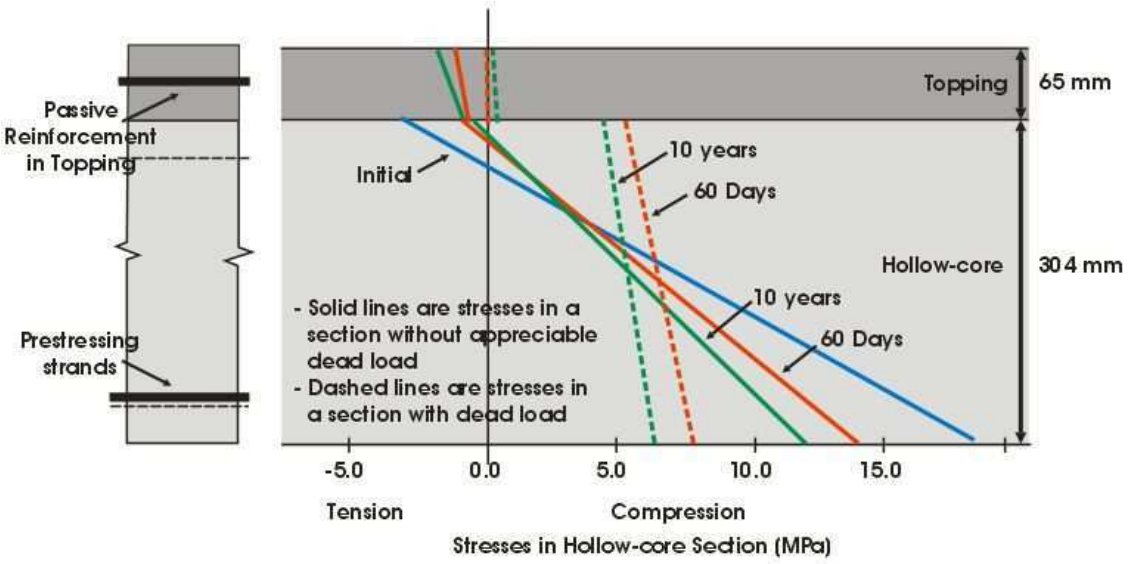

Figure 3-2 Stresses in hollow-core floor section due to prestress, creep and shrinkage (with and without dead load acting) (Adapted from Fenwick et al. 2004)

The magnitude of creep and shrinkage, which develop in New Zealand concretes, is greater than indicated by guidelines published by international bodies such as the American Concrete Institute (ACI) and the International Federation for Structural Concrete (FIB). The New Zealand Concrete Structures Standard (Standards New Zealand. 2006) recommends that as far as is practical, design values for creep and shrinkage should be based on standard test results. These need to be modified to account for the duration of damp curing, the volume-to-surface ratio and the environmental conditions. Bryant et al. (1984) compared the data from a significant number of creep and shrinkage experiments to creep and shrinkage prediction methods detailed in various overseas codes. It was concluded that realistic predictions for the magnitudes and trends for the shrinkage of New Zealand concrete are given by the CEB-FIP Model Code (Comité euro-international du béton. and Fédération internationale de la précontrainte. 1978) when these values are multiplied by a factor of two. The shrinkage predictions in the CEB-FIP 1978 Model Code are consistent with the current guidelines from the International Federation of Structural Concrete (FIB), FIB Bulletin 1 (Fédération internationale du béton. 2000). It is therefore suggested that when standard tests for creep and shrinkage cannot be performed, the shrinkage predictions from FIB guidelines be used and multiplied by a factor of two.

3.4 Hollow-core Floor Behaviour under Gravity Loads

Hollow-core floors generally have adequate strength and ductility to resist gravity loads when installed correctly. Hollow-core units have a high positive moment capacity and a low negative moment capacity because the pretensioned strands are located close to the soffit. The units are made this way because they are designed to resist gravity loads as simply-supported members. Under the self-weight of the floor and insitu topping only, this is a reasonable approximation, as when the topping concrete is placed the hollow-core unit does support this weight in a simply supported manner. However, once the topping has hardened, additional gravity loads, creep and shrinkage can induce negative moments near the supports due to continuity created by starter bars and insitu concrete topping at the floor connections. Under just self-weight loads, these negative moments are not likely to be critical. Figure 3-3 shows forces in a hollow-core unit under self-weight loading. In this case the unit is behaving as a simply-supported member. The bending moments away from the supports are resisted by a force couple comprised of the prestressing force and the centroid of the compression, separated by a lever-arm, l_a. It can be seen that the centroid of the compression force rises as the bending moment increases. This creates an inclined compression force, the vertical component of which resists some of the shear in the section.

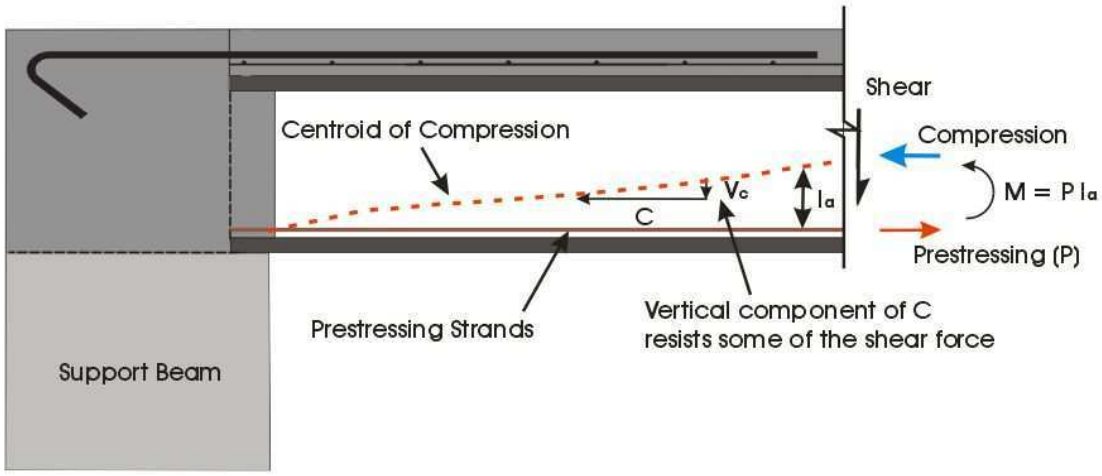

Figure 3-3 Behaviour of hollow-core flooring under gravity loads

The shear capacity can be assessed using equations from Section 19.3.11 of the New Zealand Concrete Structures Standard (Standards New Zealand 2006). There are two types of shear

cracking which should be checked, web-shear cracking and flexure-shear cracking. However, neither of these are considered critical for buildings under only gravity loads. Section 6.1.1 gives more detail on the mechanisms of web-shear and flexure-shear cracking. The development length and transfer of prestressing forces must be considered when calculating shear and moment capacities of hollow-core floors. Note that the lack of prestressing force near the ends of the floor results in a lower stiffness in this region.

There has been a significant amount of research and testing in New Zealand and internationally showing that generally hollow-core floors perform satisfactorily under gravity loads (Blades et al. 1990; Broo et al. 2005; Girhammar and Pajari 2007; Hawkins and Ghosh 2006; Pajari 1998; Pajari 2005; Pajari and Koukkari 1998; Yang 1994; Yap 1985).

3.5 Beam Elongation

When flexural cracks form in reinforced concrete members, elongation occurs unless the member sustains appreciable axial compression. The extension of frame beams parallel to a hollow-core floor, under seismic loading, can induce axial tension in the floor and potentially "pull" it away from its support. This can reduce the seating length in the connection, jeopardising vertical support. Axial tension in the floor reduces the flexural capacity and may induce negative bending moments due to the eccentricity of starter bars connecting the floor to its supporting beams. Elongation in support beams can also affect hollow-core flooring as this may induce stresses transverse to the span of the floor. The interactions between precast prestressed floor units and seismic frame systems have been observed by several researchers (Lau et al. 2007; Lindsay 2004; MacPherson 2005; Matthews 2004). It is therefore important that in the assessment of a hollow-core floor, the potential effects of beam elongation be considered. This section briefly explains the mechanisms that cause beam elongation.

When a beam cracks in flexure, the neutral axis is closer to the compression face of the beam than the tension face. Therefore, the mid-depth of the section is in tension and the tensile strains in the flexural reinforcement are larger than the compressive strains in the concrete; Figure 3-4 illustrates this. The result is axial elongation unless the member is restrained axially.

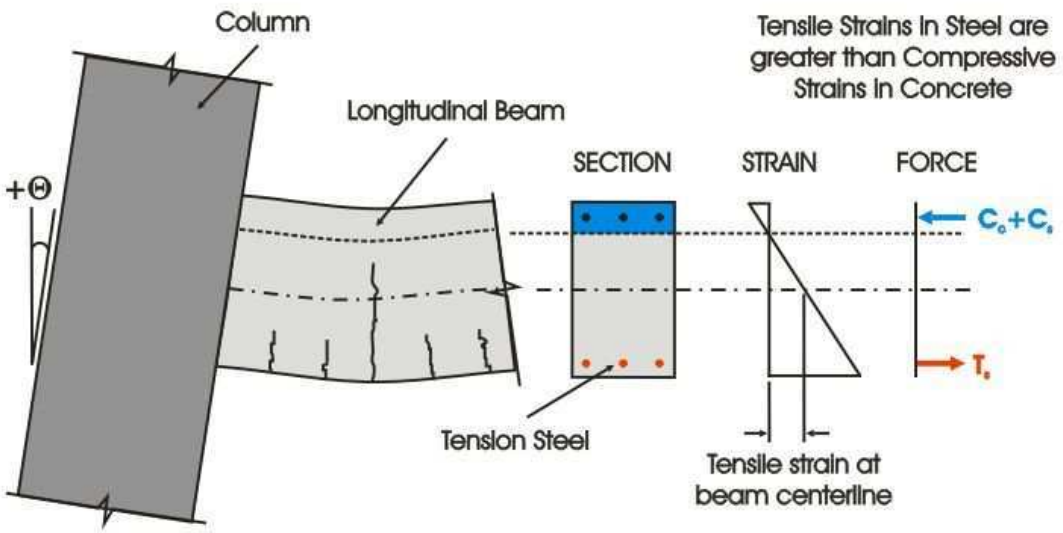

(a) Idealised beam elongation under positive rotation

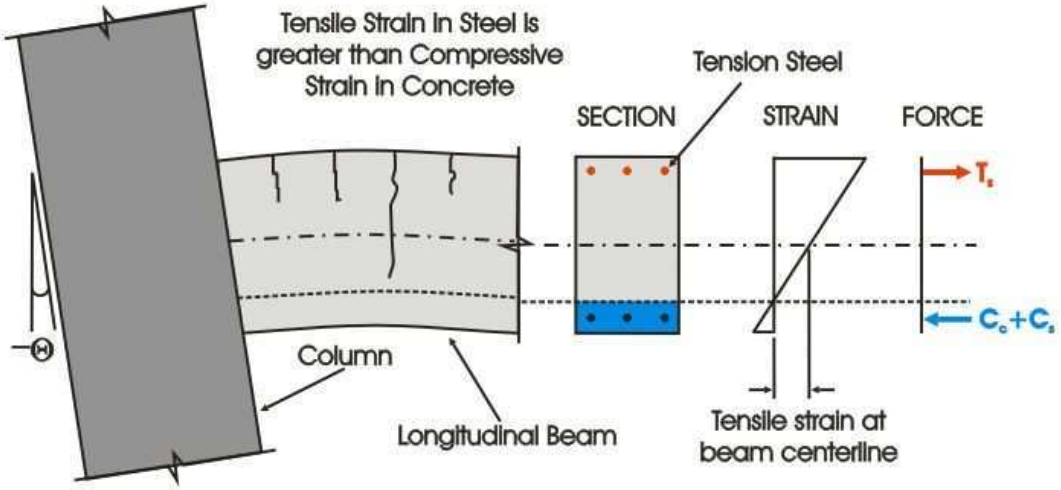

(b) Idealised beam elongation under negative rotation

Figure 3-4 Beam elongation resulting from flexure as a function of neutral axis depth (Adapted from Jensen 2006)

Plastic hinges can form when ductile beams are subjected to inelastic cyclic displacements, such as from high seismic loading. Elongation is pronounced in plastic hinge zones due to the extensive tensile yielding of the steel reinforcement and increases with each inelastic loading cycle. Figure 3-5 illustrates how the strains in a plastic hinge region are not recovered under reversed loading. Therefore, under a series of cycles the strains increase.

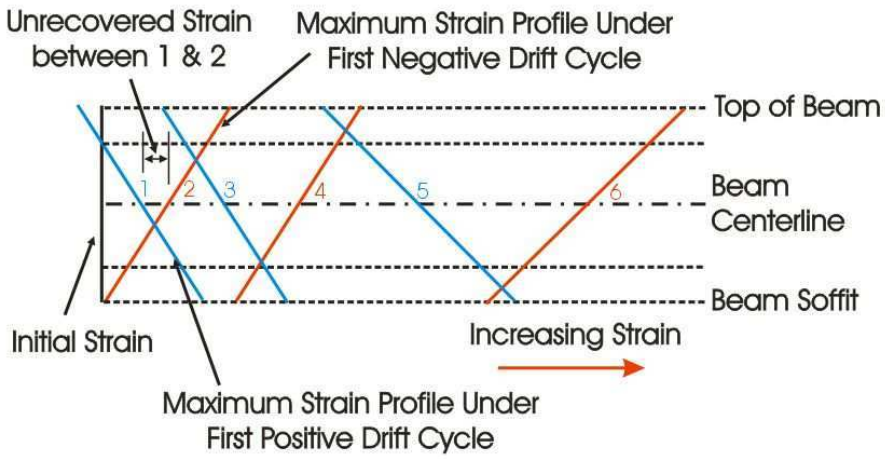

Figure 3-5 Increasing strains in a plastic hinge under inelastic cyclic displacements

Research into beam elongation has shown that plastic hinge zones, not restrained axially, can elongate from 2 to 5 % of the member depth, before strength degradation occurs (Fenwick and Megget 1993). The amount of elongation depends on the loading history and it is difficult to predict. Two types of plastic hinge can form depending on the ratio of gravity and seismic loads. These are:

- Uni-directional (gravity dominated)
- Reversing (seismic dominated)

Uni-directional hinges form in a beam when the maximum positive moment is not at the column face. As a frame sways to the right, the negative moment plastic hinge forms at the face of the right-hand column and a positive moment plastic hinge forms some distance away from the left-hand column. The opposite occurs when the loading is reversed and the frame sways to the left. Figure 3-6 (a) shows a beam containing uni-directional plastic hinges. A beam containing reversing plastic hinges is shown in Figure 3-6 (b). In this situation, seismic actions dominate, which means that both the maximum positive and negative bending moments occur at the column faces of the beam. It is likely that beams parallel to hollow-core flooring will exhibit reversing plastic hinges, as the gravity loading they carry is relatively small.

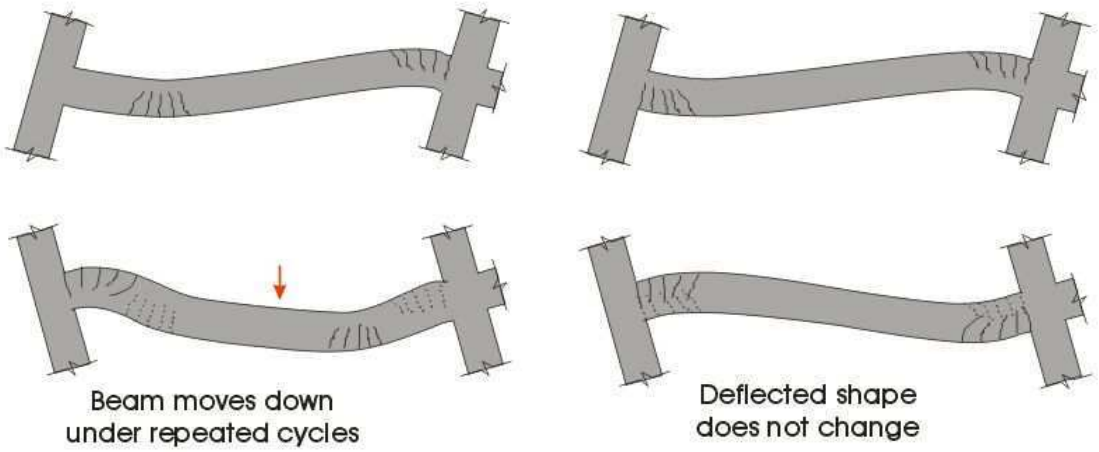

(a) Uni-directional plastic hinges **(b) Reversing plastic hinges**

Figure 3-6 Types of plastic hinge in a ductile reinforced concrete beam (Adapted from Fenwick and Megget 1993)

The magnitude of elongation experienced by both reversing and uni-directional plastic hinges is similar. In a uni-directional hinge, greater curvatures are induced as these accumulate with each inelastic displacement in an earthquake causing the vertical displacement of the floor to increase. In a reversing plastic hinge the deflected shape does not change significantly under repeated loading. During the reversal of loading direction in a reversing plastic hinge, the reinforcement in the compression zone, which had previously been yielding in tension, does not fully yield back in compression. This results in the cracks in the compression zone remaining open. There are two reasons for this, one is from aggregate particles, which have dislodged and restrict the cracks closing, the other is a function of how shear is resisted within the plastic hinge, which results in the flexural compression force always being smaller than the flexural tension force (Fenwick and Megget 1993).

It is possible in a frame system containing hollow-core floors that some axial restraint will be provided to the plastic hinges in beams parallel to the floor span. This reduces the amount of elongation as it causes the neutral axis to get closer to the centreline of the member. Axial restraint is highest in plastic hinges adjacent to intermediate columns if the prestressed floor spans past the column. Lau et al. (2007) performed several experimental tests looking at elongation of beams in ductile moment resisting frames. It was noted that including a prestressed floor slab reduced the amount of elongation. However, it does not reduce the elongation sufficiently to ignore the effect it could have on the seating width of floor slabs.

A number of numerical approaches have been proposed to predict beam elongation. Some of these predict only the maximum beam elongation (Fenwick and Megget 1993), whereas others are more complex and predict an elongation profile from a given loading history (Jensen 2006; Lee and Watanabe 2003; Matthews 2004). There is also an analytical model currently being created which should be able to be used in a computer analysis package (Peng et al. 2007).

3.6 Tensile Capacity of Concrete

Several of the potential hollow-core failure modes depend directly on the tensile strength of concrete. The modulus of rupture (the tensile strength of concrete in flexure) is generally only 10 to 15 % of the concrete compressive strength and is more variable. Generally, in strength design the tensile capacity of concrete is assumed insignificant and alternative methods of carrying tensile forces, such as steel reinforcement, are used. The New Zealand Structural Concrete Standard (Standards New Zealand. 2006) recommends that if the tensile strength of concrete is important for the integrity of the structure it should be determined by testing and used with caution. Hollow-core flooring in New Zealand contains only prestressing reinforcement running lengthwise close to the soffit and often only minimal passive steel reinforcement in the insitu topping. Therefore, any tensile stresses induced transverse to the prestressing or in the units webs, must be resisted by the concrete.

There are several ways to test for the tensile strength of concrete and several different terms used to describe it, which can be confused. These are:

- the direct tensile strength (f_t). This is not dependent on the size of the specimen, but is hard to test for, as it is difficult to apply a uniform axial tension to a concrete specimen
- the modulus of rupture (or tensile strength of concrete in flexure) (f_r). This changes depending on the size and shape of the section
- the splitting test strength ($f_{ct,sp}$). This is the strength to split a standard cube or cylinder of concrete. The strength measured from this type of test is approximately 90 % of the direct tensile strength.

As the tensile strength of concrete is variable, a number of tests need to be performed to gain an average. When gaining the concrete tensile strength from testing, account must be made

for the size effect and method of testing; the New Zealand Concrete Structures Standard gives guidelines on these. The modulus of rupture is normally found from standard flexural tests of specimens with 100 mm square cross-sections; however, it can be approximately calculated from the direct tensile strength. To do this, the direct tensile strength it must be multiplied by a factor, K_t, to account for the size effect (Standards New Zealand 2006). The modulus of rupture is generally larger than the direct tensile strength but approaches it as members get deeper. For a member depth larger than 2400 mm the modulus of rupture is approximately equal to the direct tensile strength. For a hollow-core unit, it is suggested that when finding the modulus of rupture when the extreme tension fibre is at the top of the section (in the insitu topping) the K_t factor is calculated from the member depth. However, when the extreme tension fibre is at the bottom of the section, the presence of the voids in the hollow-core unit result in very little stress redistribution and it is recommended that a K_t value of only 1.05 times the direct tensile strength is used (Department of Building and Housing 2008).

The modulus of rupture found is an average value. The New Zealand Structural Concrete Standard (Standards New Zealand. 2006) and loading standard (Standards New Zealand. 2004), state that in design, the lower characteristic tensile strength should be used along with a strength reduction factor of 0.6. To obtain the lower characteristic strength the average is multiplied by a factor of 0.68. Reliance on the concrete's tensile capacity should be exercised with caution.

3.7 Unequal Stiffness

Hollow-core units manufactured in New Zealand contain prestressing strands near the soffit. Under upward loading flexural cracking can be expected in the insitu concrete and the top of the hollow-core unit, this reduces the floor's stiffness. During downward loading, the prestressing near the soffit restricts flexural cracks from forming on the lower surface and the floor behaves as an un-cracked section with an un-cracked section stiffness. Hence, the member has different stiffness's depending on the direction of loading. Floors can experience upward and downward loading under vertical seismic forces. The equal energy and equal displacement concepts for seismic response were developed from analysis of single degree of freedom structures, which had equal stiffness in each direction. Therefore, these concepts no longer apply. These concepts are often used in seismic design rules to relate ductility to the force reduction factor. Figure 3-7 shows the hysteresis loop shape of a hollow-core floor

compared to hysteresis loop shapes with equal stiffness's in each direction for members where the equal energy and equal displacement concepts can be used.

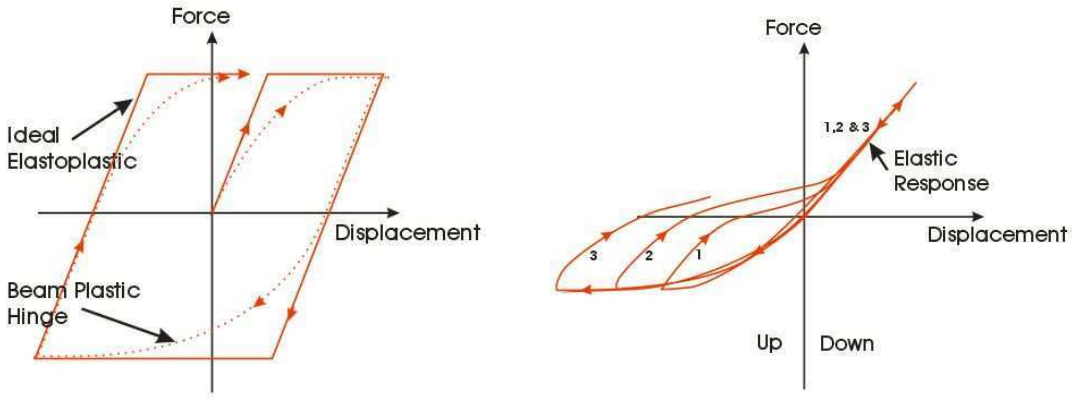

(a) Situations when equal force and equal displacement concepts can be used

(b) Hollow-core floor, stiffness changes depending on direction of loading

Figure 3-7 Difference in hysteresis loops between members that equal force and displacement concepts that can be used for and that of a hollow-core floor under vertical loading

If the equal energy and equal displacement concepts are used in the assessment of hollow-core flooring, they may lead to an under-estimate of the upwards vertical displacement (Fenwick, R., Personal Communication, 2007). This effect may be accentuated by the velocity of the floor as it returns from its maximum downward deflection, increasing the deflection under the upwards displacement under each cycle. This is illustrated in Figure 3-7 by the loop migrating to the left.

3.8 References

Blades, P. S., Jacks, D. H., Beattie, G. J., and Central Laboratories (N.Z.). (1990). *Investigation of the influence of the end support condition on the shear strength of prestressed voided slabs*, Central Laboratories, Lower Hutt, N.Z.

Broo, H., Lundgren, K., and Engström, B. (2005). "Shear and torsion interaction in prestressed hollow core units." *Magazine of Concrete Research*, 57(9), 521 - 533.

Bryant, A. H., Wood, J. A., and Fenwick, R. C. (1984). "Creep and Shrinkage in Concrete Bridges." *No. 70*, National Roads Board, New Zealand.

Comité euro-international du béton., and Fédération internationale de la précontrainte. (1978). *International system of unified standard codes of practice for structures : Volume I,*

Common unified rules for different types of construction and material : Volume II, CEB-FIP model code for concrete structures, Comite Euro-International du Beton, [s.l.].

Department of Building and Housing. (2008). *Guidelines for the assessment of hollow-core flooring in New Zealand - DRAFT*, Department of Building and Housing, Wellington, New Zealand.

Fédération internationale du béton. (2000). *Structural concrete : textbook on behaviour, design and performance : updated knowledge of the CEB/FIP Model code 1990*, International Federation for Structural Concrete, Lausanne, Switzerland.

Fenwick, R., Deam, B., and Bull, D. (2004). "Failure modes for hollowcore flooring units." *Journal of the Structural Engineering Society New Zealand Inc.*, 17(1), 52 - 70.

Fenwick, R. C., and Megget, L. M. (1993). "Elongation and load deflection characteristics of reinforced concrete members containing plastic hinges." *Bulletin of the New Zealand National Society for Earthquake Engineering*, 26 (1), 28 - 41.

FIB Commission 6 Prefabrication., and Fédération internationale du béton. (2000). *Special design considerations for precast prestressed hollow core floors : guide to good practice*, International Federation for Structural Concrete, Lausanne, Switzerland.

Girhammar, U. A., and Pajari, M. (2007). "Tests and analysis on shear strength of composite slabs of hollow core units and concrete topping." *Construction and Building Materials*, In Press, Corrected Proof.

Hawkins, N. M., and Ghosh, S. K. (2006). "Shear strength of hollow-core slabs." *PCI Journal*, 51(1), 110-114.

Jensen, J. (2006). *The seismic behaviour of existing hollowcore seating connections pre and post retrofit : a thesis submitted in partial fulfilment of the requirements for the degree of Master of Engineering at the University of Canterbury*, Christchurch, New Zealand.

Lau, D. B. N., Fenwick, R. C., Davidson, B. J., University of Auckland. School of Engineering., and University of Auckland. Dept. of Civil and Environmental Engineering. (2007). *Influence of precast prestressed flooring on the seismic performance of reinforced concrete perimeter frame buildings*, Dept. of Civil and Environmental Engineering University of Auckland, Auckland, N.Z.

Lee, J. Y., and Watanabe, F. (2003). "Predicting the longitudinal axial strain in the plastic hinge regions of reinforced concrete beams subjected to reversed cyclic loading." *Engineering Structures*, 25 (7).

Lindsay, R. (2004). *Experiments on the seismic performance of hollow-core floor systems in precast concrete buildings : a thesis submitted in partial fulfilment of the requirements for the degree of Master of Engineering at the University of Canterbury*, Christchurch, New Zealand.

MacPherson, C. (2005). *Seismic performance and forensic analysis of a precast concrete hollow-core floor super-assemblage : a thesis submitted in partial fulfilment of the requirements for the degree of Master of Engineering at the University of Canterbury*, Christchurch, New Zealand.

Matthews, J. (2004). *Hollow-core floor slab performance following a severe earthquake : a thesis submitted in partial fulfilment of the requirements for the degree of Doctor of Philosophy at the University of Canterbury*, Christchurch, New Zealand.

Pajari, M. (1998). "Shear Resistance of PHC Slabs Supported on Beams. II: Analysis." *Journal of Structural Engineering*, 124(9), 1062-1073.

Pajari, M. (2005). "Resistance of prestressed hollow core slabs against web shear failure." *Research Notes 2292*, Espoo 2005. VTT Tiedotteita.

Pajari, M., and Koukkari, H. (1998). "Shear Resistance of PHC Slabs Supported on Beams. I: Tests." *Journal of Structural Engineering*, 124(9), 1050-1061.

Peng, B., Dhakal, R., Fenwick, R., Carr, A., and Bull, D. (2007). "Analytical model on beam elongation within the reinforced concrete plastic hinges." NZSEE Conference, Palmerson North, New Zealand, paper no. 43.

Standards New Zealand. (2006). *Concrete structures standard, NZS3101, Parts 1 & 2*, Standards New Zealand, Wellington, New Zealand.

Standards New Zealand. (2004). *Structural design actions*, Standards New Zealand, Wellington [N.Z.].

Standards New Zealand. (2006). *Concrete structures standard, NZS3101, Parts 1 & 2*, Standards New Zealand, Wellington, New Zealand.

Yang, L. (1994). "Design of Prestressed Hollow Core Slabs with Reference to Web Shear Failure." *Journal of Structural Engineering*, 120(9), 2675-2696.

Yap, K. K. (1985). *Shear tests on proprietary prestressed voided slabs using various end support conditions*, Structures Section Central Laboratories Ministry of Works and Development, Lower Hutt, N.Z.

4 Potential Failure Mechanisms in Hollow-core Floors

A substantial amount of research and experimental testing has been completed on the seismic performance of hollow-core flooring, particularly at the University of Canterbury, New Zealand. Several different failure mechanisms have been observed and a number more predicted. However, several of these failure mechanisms are not fully understood and require further research. If designers are to use a capacity design approach, they are required to choose a ductile failure mechanism and then design to avoid all other failure mechanisms. To achieve this, it is essential that designers are aware of all the potential failure modes, and understand what causes them.

This chapter outlines the failure mechanisms that are currently believed to be critical for the type of hollow-core usage in New Zealand. Each failure mode is subsequently described in further detail. Where a mechanism has been observed in experimental testing, examples are given. The construction practises used and seismicity in New Zealand make some of the failure modes unique, or more pronounced, for New Zealand hollow-core buildings. Consequently, some of the modes presented have not yet been recognised by international hollow-core research. The theory behind each failure mode is outlined. Much of this information is similar to that used in a report being prepared concurrently with this thesis to be published by the New Zealand Department of Building and Housing as a guide on hollow-core assessment (Department of Building and Housing 2008).

The failure mechanisms of concern are:

- Loss of support
- Positive moment failure
- Flexural and shear actions transverse to the span of the units causing failure
- Loss of support to a web
- Failure due to incompatible displacements
- Torsional failure
- Flexural failure in negative bending moment regions
- Flexure-shear failure in negative bending moment regions.

The last two of the potential failure mechanisms mentioned are the focus of this research and are therefore are not discussed fully in this chapter, but are described in-depth in Chapters 5 and 6 respectively.

4.1 Overview of Failure modes

Performance of hollow-core flooring is complex and cannot be assessed from the projected inter-storey drift alone. Consideration needs to be given to local displacements and structural actions induced into the individual floor units, as it is these which are likely to cause a brittle failure. A short description of each failure mode, and actions or displacements that may lead to them, is given below. Combinations of the individual failure modes are also possible.

Loss of support – In this type of failure, the vertical support to a hollow-core unit is lost as a result of relative rotation between the support and the floor unit and/or elongation of parallel frame beams. Relative rotation can cause spalling from the support ledge and/or fracture of the hollow-core unit soffit at the back face, reducing the width of the ledge supporting the unit. Parallel beam elongation can cause the unit to be pulled off its vertical support.

Positive moment failure – If the connection between a hollow-core unit and its supporting beam is fixed, a flexural-shear failure may be induced near the support when a positive moment is induced. Support beam rotation from building drift may induce such positive moments at the support.

Flexural and shear actions transverse to the span of the units – Transverse to the span of the floor, hollow-core units contain no reinforcement. Hence, any flexural or shear actions induced in this direction may cause a brittle failure. Bending of the support beams is one-way flexure and shear may be induced transverse to the span.

Failure due to an unsupported web – Cutting a hollow-core unit to fit around a structural element, such as a column, may leave some of the units webs unsupported. The redistribution of forces from an unsupported web may lead to longitudinal web splitting.

Incompatible displacements – High localised forces can be induced in units due to differences in displacement between adjacent elements, such as parallel frame beams or other

hollow-core units. The localised forces can cause cracking in the unit webs, leading to the potential collapse of all or part of the unit.

Torsional failure – Hollow-core units contain no torsional reinforcement, therefore any twist induced into a floor unit could cause a brittle failure. Torsion may be induced in hollow-core units under seismic actions in some structural situations due differential displacements of floor supports or bending of supports.

Flexural failure in negative bending moment regions – Restrained supports and seismic loading can induce negative moments and axial tension in hollow-core floors. If the steel reinforcement in the insitu topping is not sufficient to resist the negative bending moments induced in the section, failure may result. This may be brittle if non-ductile mesh is used as reinforcement (see Section 5).

Flexure-shear failure in negative bending moment regions – If a series of flexural cracks are induced in a negative moment zone, shear is induced in the concrete between these cracks due to the change in tension in steel reinforcement in the topping. Under high seismic loading this shear may cause flexure-shear cracking resulting in failure (see Section 6).

4.2 Loss of Support

Loss of vertical support to a hollow-core floor can be caused under seismic loading. Two distinct mechanisms for loss of support have been identified, with and without delamination of the topping. The original provided seating length and the structural configuration of the building both affect the likelihood of a failure due to loss of support. Other factors, which may influence this failure mechanism, are spalling of cover concrete from supporting beams due to the formation of plastic hinges and the type of surface on which the units sit (for example; a mortar bed or a low friction bearing strip). Loss of support failures have been observed in several experimental tests and were the focus of research undertaken by Jensen (2006).

Vertical support to a hollow-core unit can be lost as a result of relative rotation between the support and the floor unit, reducing the size of the support ledge, and/or elongation of parallel frame beams, pulling the unit off the support ledge. There are two ways that relative rotation

can cause a reduction in the size of the support ledge. The first is due to spalling of the support ledge, which, if unreinforced, permits large chunks of concrete to break off. The other is due to a portion of the hollow-core soffit becoming trapped at the back of the support. One, or both, of these can occur and result in either a shortening of the support ledge or create a near vertical interface between the beam and the floor unit. Figure 4-1 shows the reduction of support length caused by relative rotation. With the addition of axial tension to the floor, from elongation of parallel frame beams, the floor unit is pulled away from the support beam. Ultimately all vertical support, from the ledge, aggregate interlock, friction and starter bars, is lost. Loss of support can lead to building collapse, as potentially a number of floors could fall in a progressive collapse or "pancake" type failure (Jensen 2006).

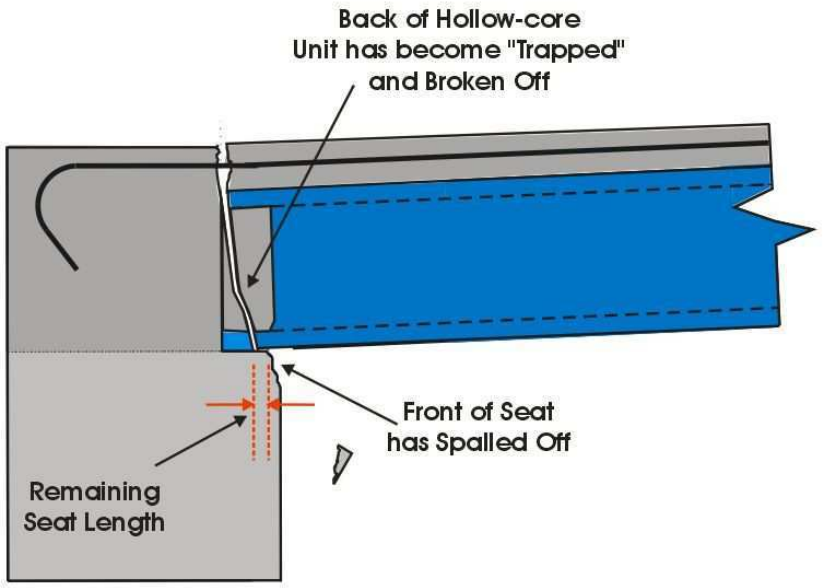

Figure 4-1 Reduction of support length due to relative rotation between support beam and floor unit

Two distinctive mechanisms of loss of support were observed in experimental tests by Jensen (2006). These are loss of support with and without delamination of the insitu topping concrete. Figure 4-2 shows four variations of loss of support failure modes. When the topping concrete does not delaminate, the starter bars rupture at the beam-floor interface. If the topping delaminates from the hollow-core unit, the strain penetration in the starter bars is increased, distributing the strain demand over a longer length, therefore reducing the chance of rupture (Jensen 2006).

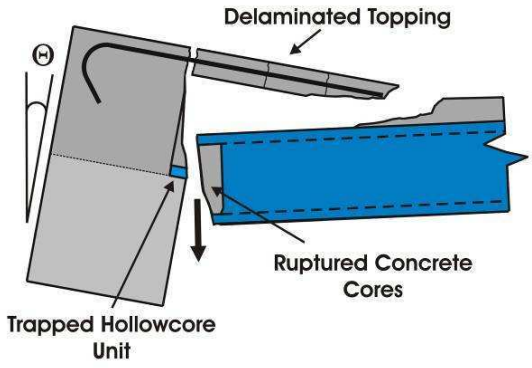

(a) Delaminated topping and trapped hollow-core unit soffit

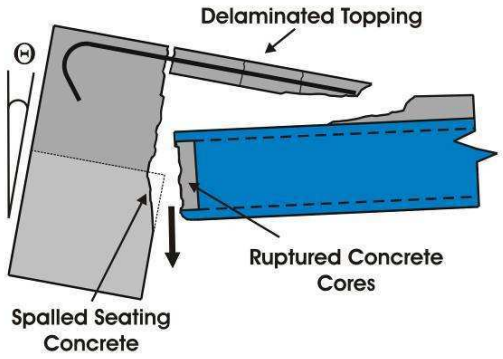

(b) Delaminated topping and spalled seating ledge concrete

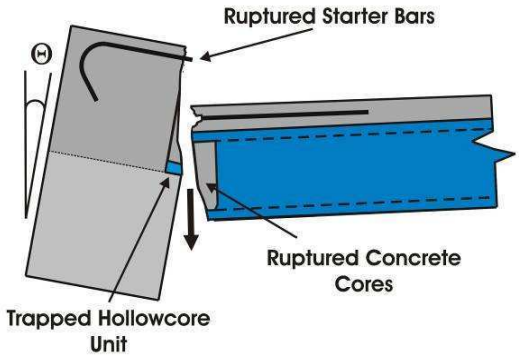

(c) Ruptured starter bars and trapped hollow-core unit soffit

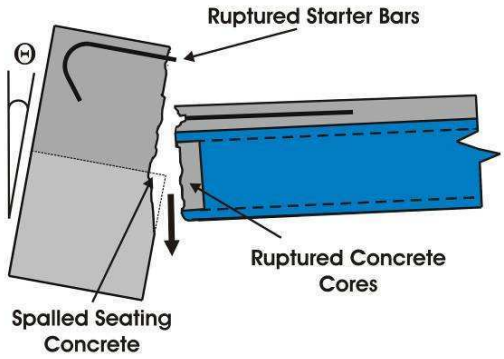

(d) Ruptured starter bars and spalled seating ledge concrete

Figure 4-2 Loss of support failure modes (Reproduced from Jensen 2006)

The loss of support failure modes are a function of the length of seating and the structural configuration of the specific building. These determine the magnitude of relative displacement that can be sustained between the support beam and the floor units. Starter bars, acting in tension across the gap between a hollow-core floor and its support cannot carry the vertical load if loss of seating occurs. This is because the starter bars could either pull out of the topping concrete or cause the topping concrete to delaminate form the hollow-core unit. This concept was emphasised in 1991 (Charleson et al. 1991).

Another issue that can add to the likelihood of loss of support to a hollow-core floor is the spalling of cover concrete from the supporting beam in plastic hinge zones. Seismic loading can induce plastic hinges in beams supporting hollow-core units. It is possible for the cover concrete of the beam in the plastic hinge zone to spall. Often, the ledge supporting the

hollow-core units is entirely cover concrete, therefore if hollow-core units are supported within potential plastic hinge zones, it should be assumed that support will be lost in this region (Lindsay 2004). Since the 2004 amendment to the New Zealand Concrete Structures Standard (Standards New Zealand. 2004) support of hollow-core units on potential plastic hinge zones has been restricted. This amendment also introduced the requirement that low friction bearing strips be used between hollow-core units and the supporting ledge. Both Lindsay (2004) and MacPherson (2005) noted that spalling of the supporting beam ledge was reduced with the inclusion of a low friction bearing strip, as opposed to seating the hollow-core unit on bare concrete or on a mortar bed.

Loss of support failure modes have been identified and investigated by several researchers. The work by Jensen (2006) is the most recent of these. Jensen performed four sub-assembly tests where support-beam to hollow-core unit connections were subjected to displacements representing those induced during seismic loading. Increasing levels of relative rotation between the support-beam and the floor unit, simulating equivalent building drift, were applied simultaneously with axial tension pulling the unit away from the support beam. Figure 4-3 shows the sub-assembly test setup used by Jensen. The first three specimens were designed to represent typical connections used in New Zealand construction prior to the work completed by Matthews (2004). Each of these three specimens had a different width of ledge supporting the hollow-core unit. The fourth specimen was used to investigate potential retrofit options for flooring believed to have insufficient seating.

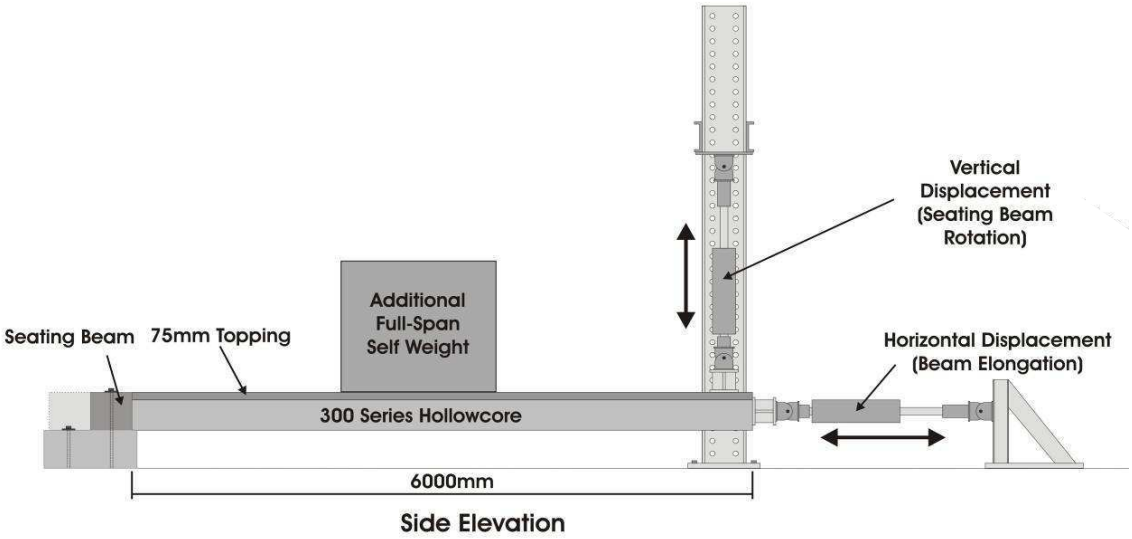

Figure 4-3 Sub-assembly test setup used by Jensen (2006)

Figure 4-4 shows the connection details tested by Jensen and photos of the failure modes. Jensen's first test specimen (HCJ1) had dropped vertically 13 mm by the completion of the 2 % drift cycle. At a drift of + 3.1 % loss of seating occurred and unit fell. The second specimen (HCJ2), which had a longer initial seating length, did not fall. Even after an extended loading protocol vertical support was maintained. However, at 40 mm of elongation, the unit had dropped 40 mm. The third specimen (HCJ3) had 50 mm seating, which has traditionally been the length of seating required. At + 2.5 % drift one side of the floor unit had dropped 15 mm, nearing - 2.0 % drift the floor unit dropped 25 mm, the starter bars ruptured and the floor collapsed. Jensen's fourth specimen (HCJ4) was the same as HCJ3 with a trial retrofit detail. The retrofit involved attaching a rectangular hollow steel section below the hollow-core unit to extend the seating length. The plane between the hollow-core unit and the support beam was also weakened by drilling vertical holes into the concrete. The retrofit was successful, as the specimen did not fail under the loading protocol, which took the specimen to 3.5 % drift. Under an extended loading protocol, the specimen was pulled 95 mm away from the support beam before vertical support was lost. However, the starter bars ruptured between and elongation of 55 and 65 mm. A summary of Jensen's results are given in Table 4-1, where LOSD stands for loss of support with delamination of the topping concrete and LOS stands for loss of support without delamination.

Table 4-1 Summary of results from sub-assembly tests performed by Jensen (2006)

	Original Seating Width (mm)	Failure Mechanism	Equivalent Building Drift at Failure (%)	Peak Elongation (mm)	Peak Positive Moment Strength (kNm)
HCJ1	35	LOSD	3.1	25	70
HCJ2	75	-	-	55	85
HCJ3	50	LOS	-2.0	20	120
HCJ4	50 + 50	-	-	85	80

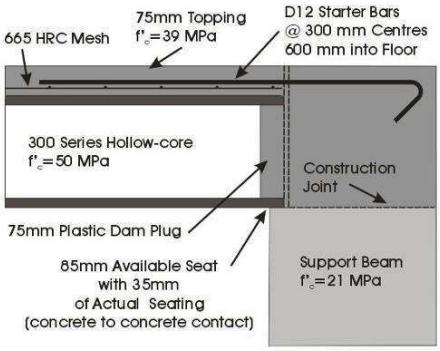

(a) HCJ1 – 35 mm seat

(b) HCJ1- Loss of support with delamination

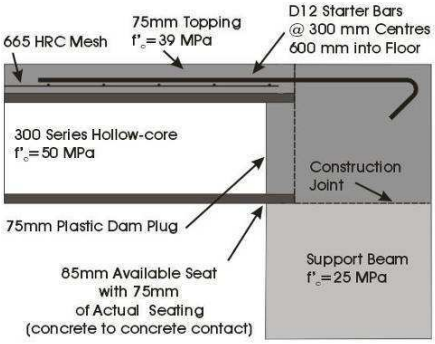

(c) HCJ2 – 75 mm seat

(d) HCJ2 – Did not fail

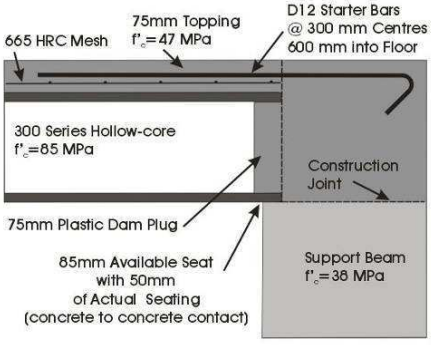

(e) HCJ3 – 50 mm seat

(f) HCJ3 – Loss of support without delamination

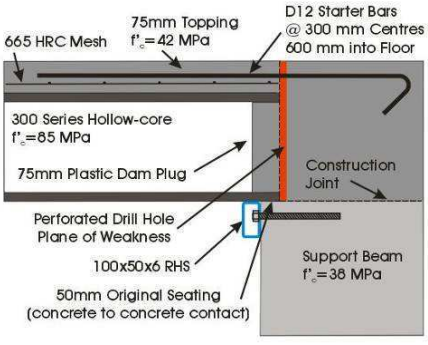

(g) HCJ4 – Retrofit detail

(h) HCJ4 – Did not fail

Figure 4-4 Connection details tested by Jensen (2006) and observed failures

Jensen concluded that in general, the existing seating connections did not perform well, but that the retrofit strategy was successful and prevented floor collapse. It was noted that the elongation required to induce loss of seating was substantially less than the length of the provided seating ledge.

4.3 Positive Moment Failure

Building drift, due to wind or seismic forces, can induce positive moments in hollow-core floors near the supports. Figure 4-5 (a) shows a support-beam to hollow-core floor connection under a positive moment. This situation can only occur if the connection has sufficient fixity. It has been observed in several laboratory tests previously mentioned in Section 2.4.4 (Bull and Matthews 2003; Matthews 2004) that positive moments at the end of hollow-core units can lead to flexural cracking close to the support. When these cracks widen and shear forces are redistributed, a brittle failure may occur (Figure 4-5 (b)). This type of failure has sometimes simply been called a flexure-shear failure (Jensen 2006).

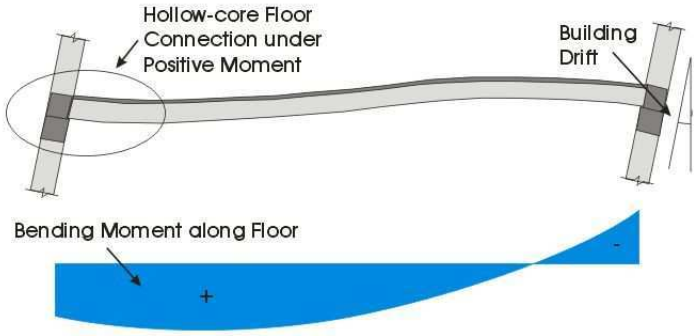

(a) Bending moments along hollow-core floor

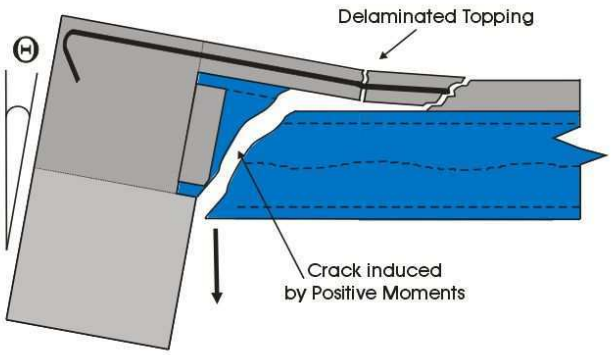

(b) Positive moment failure

Figure 4-5 Positive bending moment induced near support due to fixed connection leading to failure

Near the end of the hollow-core unit, the positive bending moment capacity of the section is reduced because the prestressing has not fully developed. At the critical section, which is at the edge of the support, the pretensioned strands are only capable of resisting a few percent of their design force. The compression force from the strands is concentrated in the webs and very little compression is induced below the voids. Figure 4-6 shows the distribution of compression force. As a result, the positive moment flexural strength depends predominantly on the tensile strength of the concrete. Once a positive moment crack has formed, it creates a weak section which widens when axial tension is applied to the floor from elongation of beams parallel to the hollow-core units.

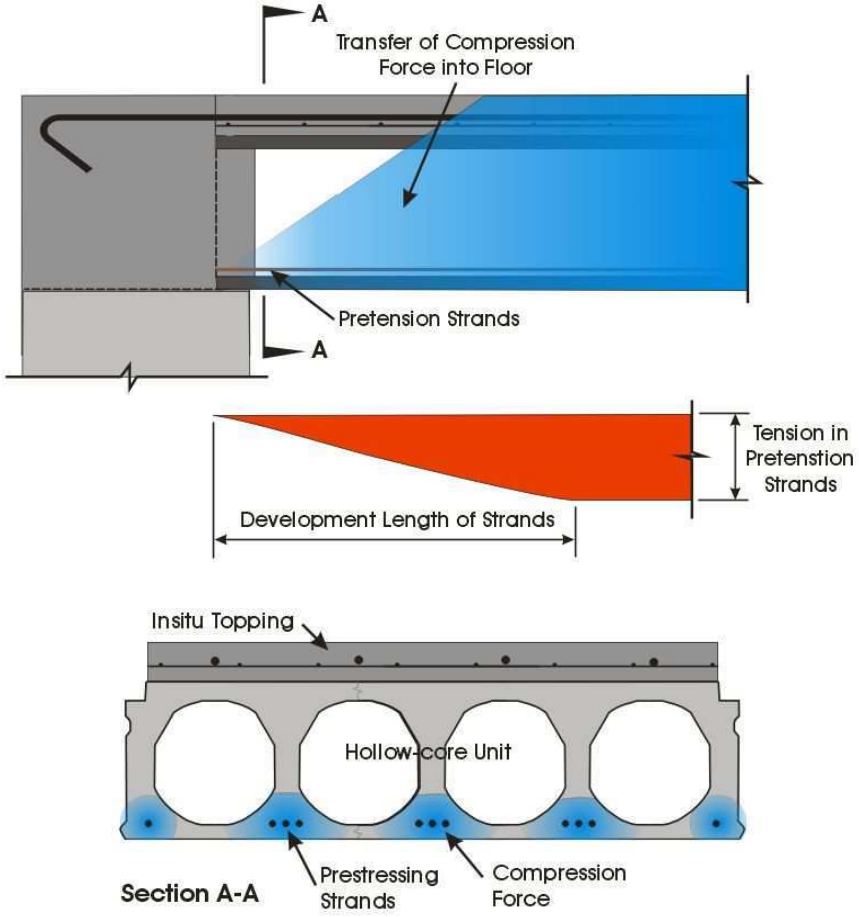

Figure 4-6 Development of compression in hollowcore due to prestressing

Once the crack is 1 to 2 mm wide, shear transfer by aggregate interlock is lost. Figure 4-7 shows the redistribution of forces at the end of the section as the cracks develop. When aggregate interlock is lost the vertical component of the tensile stresses redistributes to the

concrete in the webs and dowel action of the strands. Initially it is likely the component resisted by dowel action is small. The vertical tensile stresses in the concrete cause the flexural crack to extend almost horizontally along the unit, which results in increased displacements of the strands causing dowel action to increase. Further elongation and rotation increases the crack width until failure. A horizontal crack may also be formed by the 75 mm plug of concrete cast into the ends of the hollow-core unit acting as a dowel. If the strength of the insitu concrete is high and the bond between the plug and the hollow-core concrete poor, the magnitude of prying actions could be enough to split the hollow-core webs (Fenwick et al. 2004).

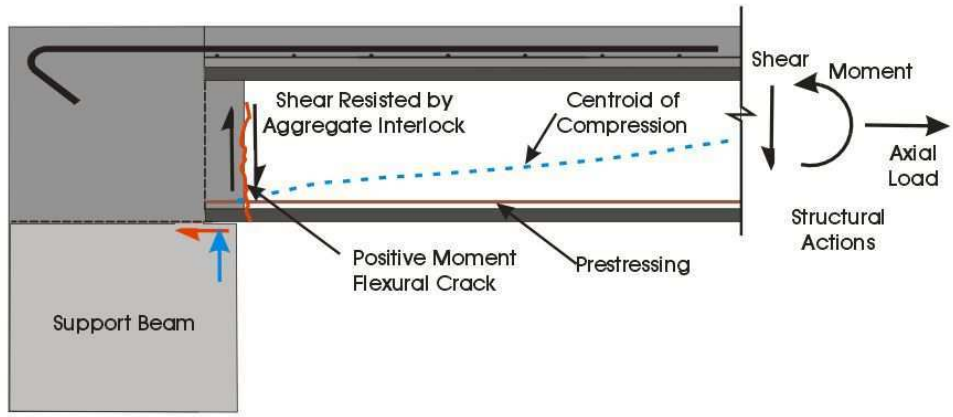

(a) Once a positive flexural crack has formed

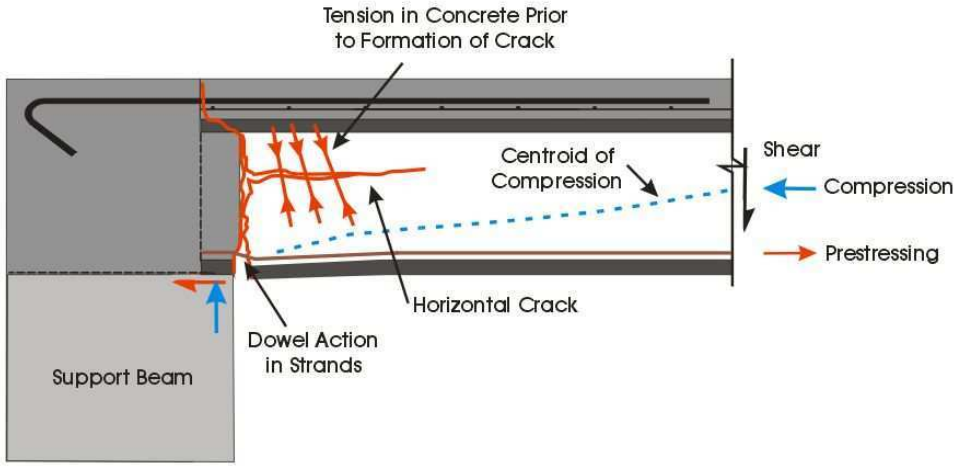

(b) When positive flexural crack is opened due to axial load a horizontal crack could form

Figure 4-7 Redistribution of forces as cracks develop

A positive moment failure is only possible if the fixity of the beam-floor interface is sufficient to transfer positive bending moments higher than the capacity of the critical section into the floor unit. This might occur if the units are supported on mortar and there is no evidence of the hollow-core unit slipping over the mortar. In tests performed by Jensen (2006), with a connection that sat on a bare ledge, positive moments up to 1.75 times those in the Bull and Matthews (2003) tests (where units sat on a mortar bed) were observed. This suggests that a bare concrete seating ledge could also induce a degree of fixity sufficient to induce a positive moment failure. However, Jensen did not observe positive moment failures in his tests. It is believed that the high concrete strength of the hollow-core units used in the Jensen tests (all had a concrete compressive strength of higher than 50 MPa) restricted this failure mode from occurring (Jensen 2006). If a positive moment flexural does occur, it is likely failure will occur when the crack width is equal to about 80 % of the diameter of the pretension strands, as at this width the strands are likely to pull through the crack and dowel action would be lost. The crack width can be taken as equal to the elongation of parallel frame beams. A positive moment failure is not likely if there is a substantial crack between the back face of the hollow-core unit and the support beam or if the unit cells have been broken out and filled with concrete and additional steel reinforcement.

4.4 Flexural and Shear Actions Transverse to the Span of the Units

Bending of supporting beams can induce actions in the ends of a hollow-core floor transverse to the span of the units. Hollow-core units contain no steel reinforcement in this direction; therefore, stresses induced may cause a shear failure in the webs, potentially leading to a brittle failure.

Figure 4-8 (a) shows a hollow-core floor and support beam under gravity load. It can be seen that the beam and the floor bend together. The friction at the hollow-core seat and the insitu concrete tie the floor and beam together. Therefore, the composite section comprised of the beam and floor ends resist the induced flexure and shear actions. This induces compression in the top of the hollow-core unit and possibly tension in the bottom of the unit. The webs of the unit connect the compression forces to the rest of the section, similar to in a Vierendeel truss type of action, which induces a shear flow in them. Figure 4-8 (b) shows actions induced in the hollow-core section. This phenomenon has been investigated by Pajari and Koukkari (Pajari 1998; Pajari and Koukkari 1998) and design recommendations based on this research

are outlined by the International Federation of Structural Concrete in the document “Special design considerations for precast prestressed hollow core floors” (FIB Commission 6 Prefabrication. and Fédération internationale du béton. 2000).

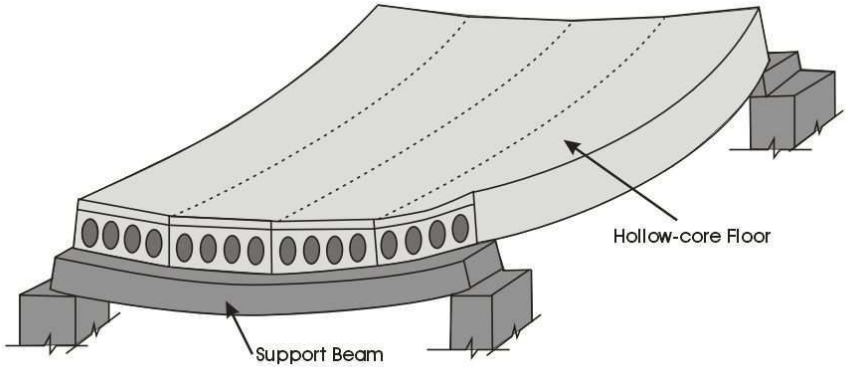

(a) Deflection under gravity load (Adapted from Pajari and Koukkari 1998)

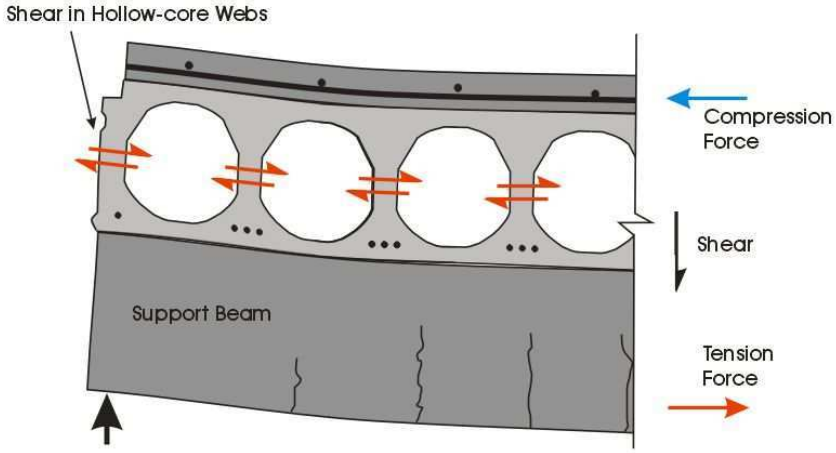

(b) Shear forces in the hollow-core unit

Figure 4-8 Hollow-core floor and support beams deforming under gravity loads

Fenwick et al. (2004) also considered the interaction between hollow-core units and supporting beams. It was suggested that the Vierendeel truss action could be reduced by supporting the hollow-core units on frictionless bearing pads and filling the voids in the hollow-core unit near the support with insitu concrete.

4.5 Loss of Support to a Web

Typically, the full width of a hollow-core unit is seated on a beam or wall. However, occasionally sections at the ends of hollow-core units are removed (cut out), resulting in part

of the width becoming unsupported. The intentional removal of support may be for several reasons; such as to allow penetrations through the floor for service ducts, or so the floor can be notched around columns and other structural elements. As other precast floor types, such as “rib and infill” floors, are structurally sound with only 16 % of their width supported, designers have been content to allow up to 50 % of the width of a hollow-core floor unit to remain unsupported (Fulford R, Personal Communication, 2007). Figure 4-9 shows two situations where support is intentionally removed from the end of a hollow-core floor.

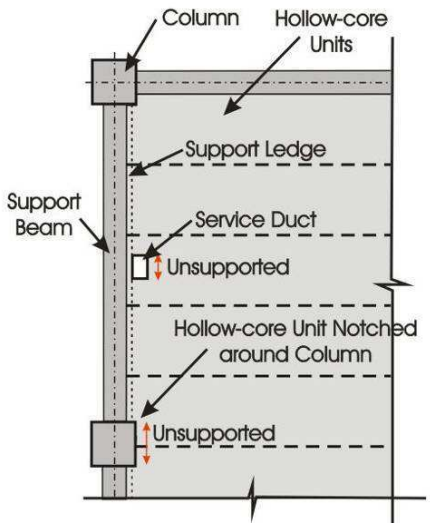

Figure 4-9 Situations where part of the hollow-core floor unit width is unsupported

Under severe earthquake loading, it is also possible for webs to become unsupported due to the curvature induced in the supporting beam. Figure 4-10 shows how this could occur.

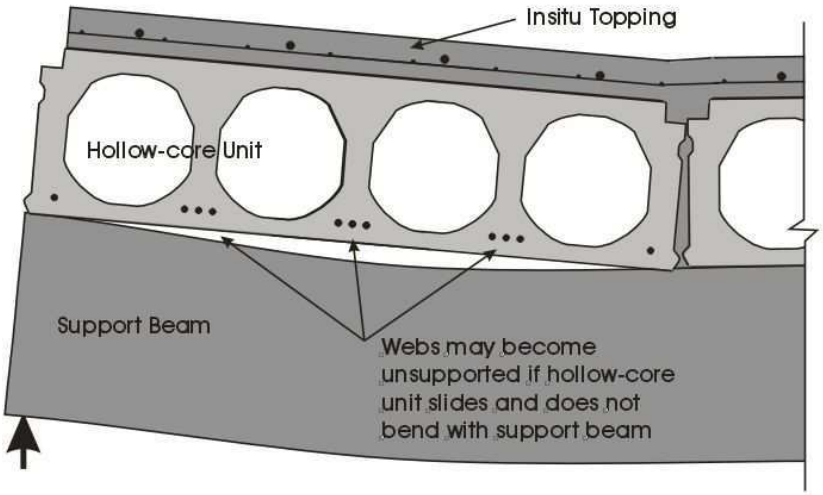

Figure 4-10 Curvature of support beam resulting in an unsupported webs

Figure 4-11 (a) shows how the forces in the end of a hollow-core unit, supported along its entire width, are distributed under a gravity load. The beam ledge provides a vertical reaction resisting the shear force from the inclined compression strut, C. The prestress force, in the development length of the strands, resists the longitudinal component of C (H_c). When the support is removed, as shown by Figure 4-11 (b), the shear force must be carried by the vertical component of tension stresses in the web. The tension is carried by shear in the top hollow-core flange and the topping concrete to adjacent webs, where it induces compression forces.

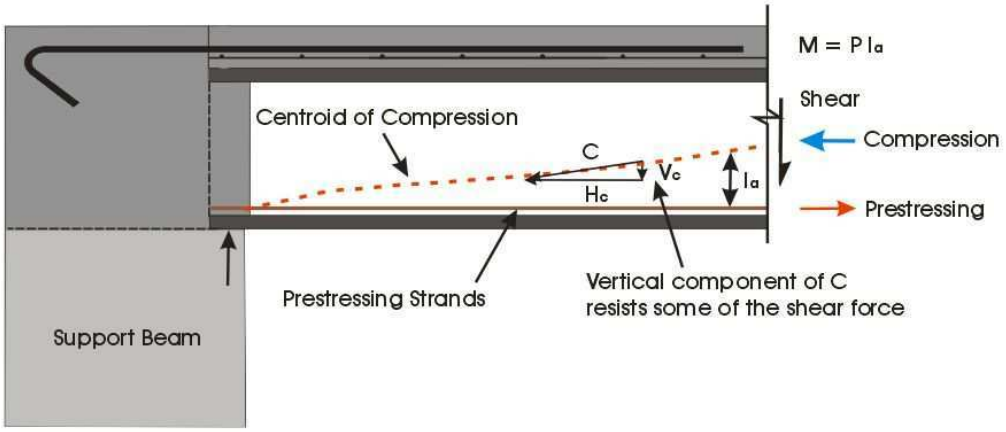

(a) Forces in a hollow-core unit supported on a beam ledge

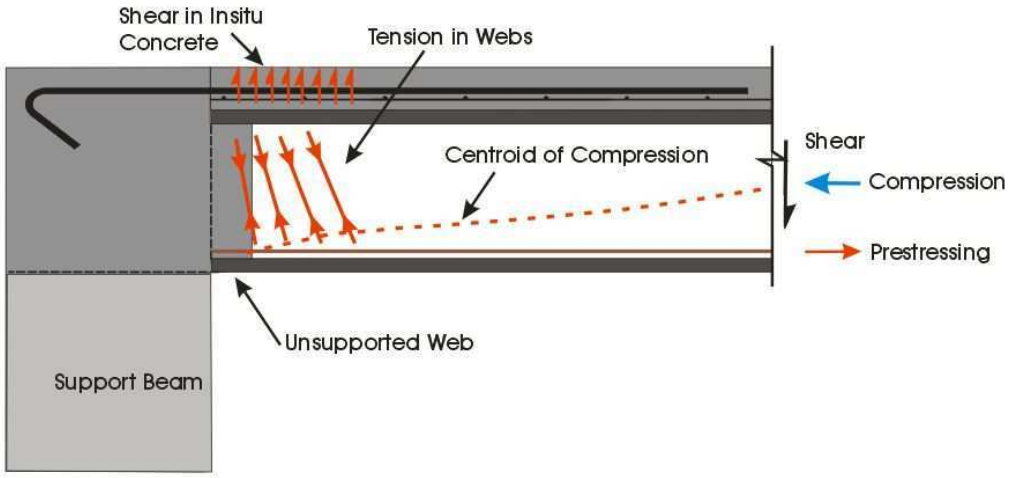

(b) Forces in a hollow-core unit when the vertical support below a web is removed

Figure 4-11 Forces in the end of a hollow-core floor unit

As the hollow-core webs do not contain any transverse steel reinforcement, tensile stresses the them may cause these to split longitudinally. Figure 4-12 shows a hollow-core unit containing longitudinal web splitting. It is unlikely that an unsupported web will induce tensile stresses in the web of a magnitude sufficient to cause web splitting under gravity loads. However, when combined with tensile stresses induced by anchorage of the pretensioned strands, the tendency for splitting to occur due to other actions is increased. As a result, the other failure modes described in this section, may occur earlier than otherwise predicted if unsupported webs are present.

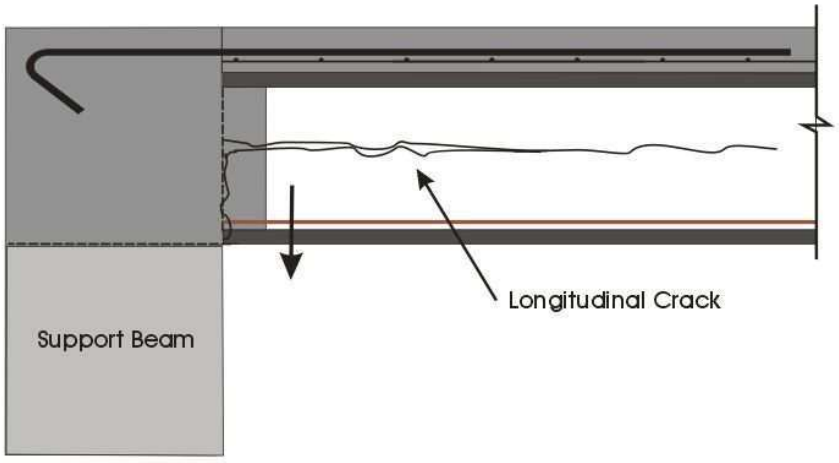

Figure 4-12 Longitudinal web splitting of a hollow-core unit caused by tensile stresses in the web

4.6 Failure due to Incompatible Displacements

There are several situations where vertical displacements induced in hollow-core units by seismic actions are different to the displacements induced in adjacent members. These incompatible displacements can cause high localised forces in the units, possibly leading to web cracking and collapse of all or part of the unit. Incompatible displacements between precast floor units and other units or parallel structural elements have been observed in experimental tests (Lau et al. 2007; Lindsay 2004; MacPherson 2005; Matthews 2004; Restrepo-Posada et al. 2000). In the Matthews test, incompatible displacements contributed to the test specimen collapse.

The two situations where incompatible displacements have been observed and induce high stresses in hollow-core units are when a hollow-core unit is placed directly adjacent a longitudinal beam and when adjacent walls support adjoining hollow-core units. The current

New Zealand Concrete Structures Standard (Standards New Zealand. 2006) recognises incompatible displacements can cause damage and requires that parallel elements, which may have differential deformation, are not directly linked. Instead, a 600 mm wide thin slab, known as a linking slab, is required to span between them. Figure 4-13 shows how the use of linking slabs can allow differential displacement without inducing high localised forces in the hollow-core units. The linking slab requirement was only introduced into New Zealand in 2004, therefore the majority of the current hollow-core building stock will not utilize a linking slab and incompatible displacements need to be assessed.

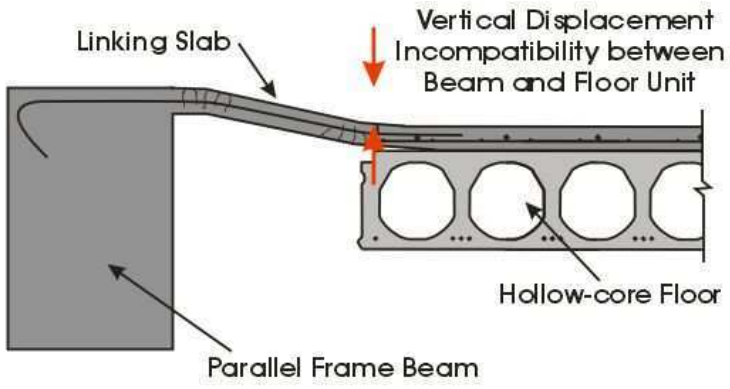

(a) Incompatible displacements between a beam and hollow-core floor unit

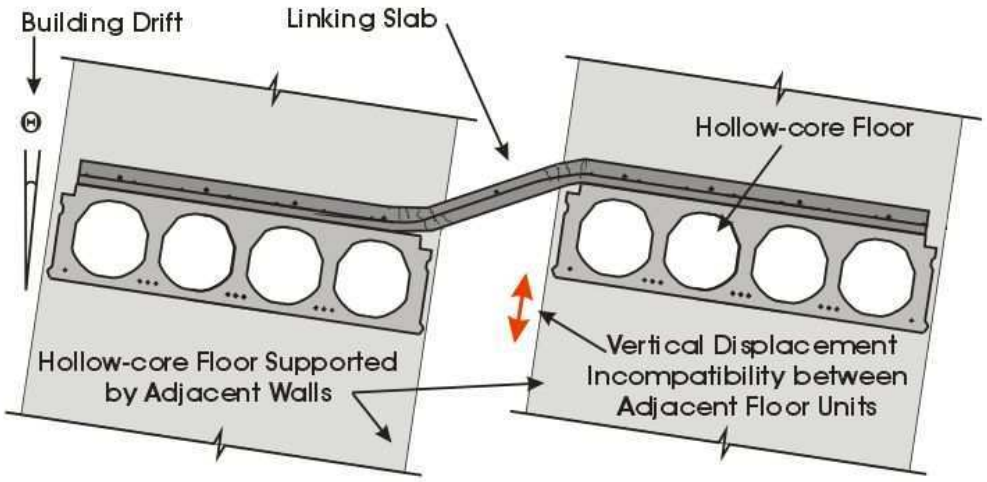

(b) Incompatible displacements between hollow-core floor units due to being supported on adjacent walls

Figure 4-13 Linking slabs used to accommodate incompatible displacements between adjacent elements

Incompatible displacements can be induced between a hollow-core floor and an adjacent beam due to differing deformation modes under seismic loading. Figure 4-14 shows an example of this. When seismic forces induce drift in the structure, the beams deform in

double curvature. The floor units, spanning parallel with these beams, often deform in a single curvature due to the difference in the support connections. The result is incompatible displacements and, if the connection between the two systems is continuous and monolithic, high forces, that the hollow-core units are not designed to sustain are induced (Matthews 2004). Figure 4-13 (b) shows how the rocking or bending of adjacent walls can cause differential displacements between the hollow-core units supported on them.

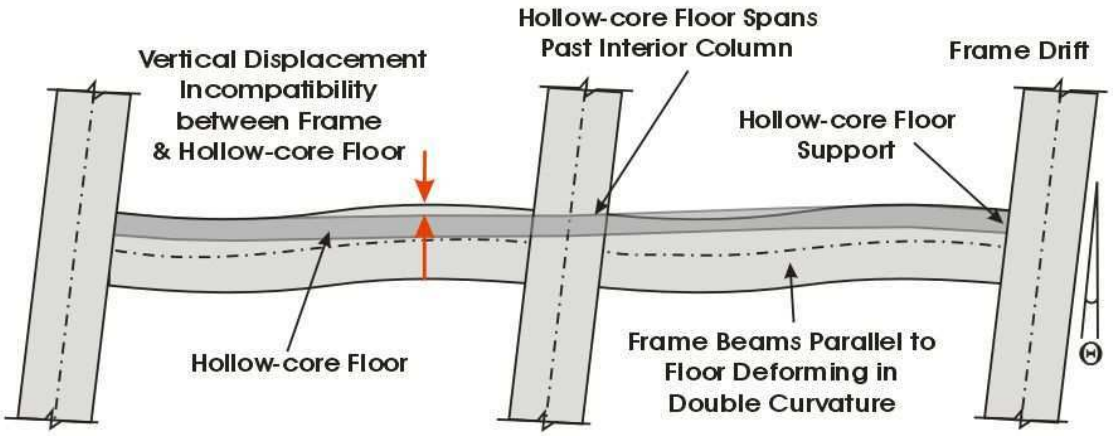

Figure 4-14 Vertical displacement incompatibility between a hollow-core floor unit and an adjacent frame beam

Figure 4-15 shows the forces and actions induced in a hollow-core floor from incompatible displacement of the adjacent member. These forces can lead to web cracking and the potential of a progressive collapse. When a beam is cast against the side of a hollow-core unit, any webs located within a distance of 450 mm from the side of the beam can be expected to split, due to the vertical movement of the beam in its elastic range. A simple model has been proposed as a tentative method for assessing the likely range of actions that may lead to failure due to incompatible displacements. This model is to be included in a set of guidelines for the use of hollow-core flooring, which is currently being prepared for the Department of Building and Housing (2008). However, due to the small amount of research in this area the model is provisional and more research in this area is required.

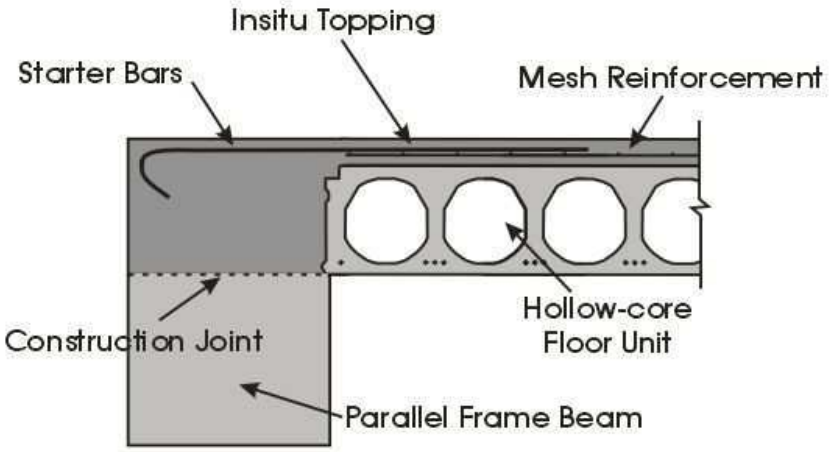

(a) Structural arrangement with concrete in the beam cast against the hollow-core unit

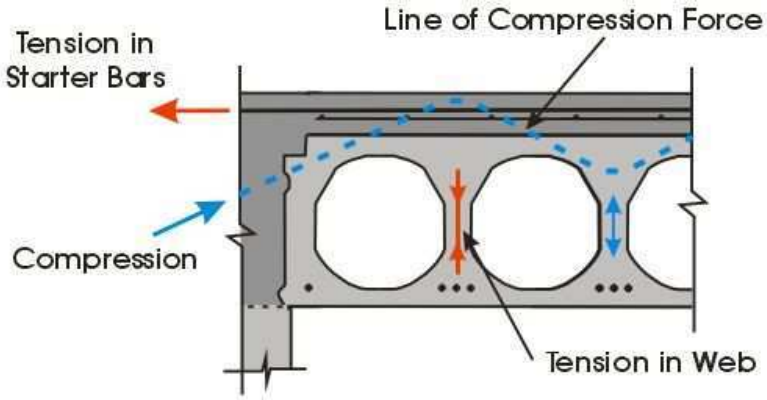

(b) Forces induced into hollow-core floor due to beam deflection relative to floor

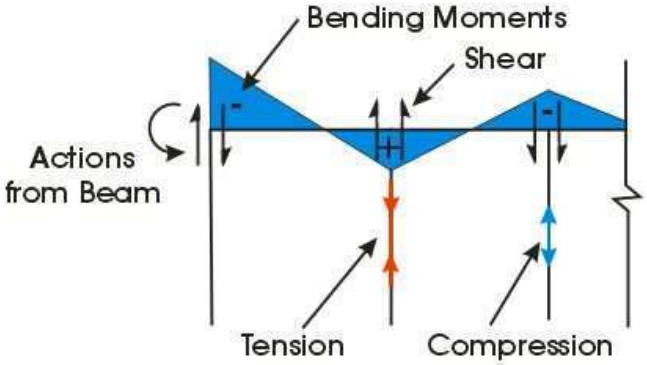

(c) Structural actions induced in the top of the composite hollow-core floor

Figure 4-15 Localised forces induced by incompatible displacement

Matthews (2004) performed a full-scale three-dimensional test, on a seismic resisting frame system, designed and constructed according to the then current New Zealand guidelines. In

the test specimen, the first hollow-core unit was directly adjacent to the parallel frame beam. Under quasi-static cyclic loading, representing earthquake excitation, the floor failed. The main cause of failure was loss of support to both ends of the hollow-core units. However, the webs of the first unit split due to incompatible displacements between it and the adjacent beam, leading to the collapse of the bottom half of the unit prior to total collapse of the floor. Figure 4-16 shows the remaining part of the hollow-core floor in the Matthews test after the lower half had collapsed due to the webs splitting.

Figure 4-16 Web splitting leading to collapse of lower half of hollow-core unit (Matthews 2004)

4.7 Torsional Failure

Torsional actions can be induced in a hollow-core floor when the supports at either end of a unit have differential rotation. This might occur if different structural systems are used, for example, a wall supporting the hollow-core floor at one end and a beam at the other. Figure 4-17 illustrates a hollowcore floor could be "twisted" by differential rotations of its supports. In the mid section of a length the "twisting" causes a torsional shear flow to develop in the hollow-core floor (see Figure 4-18). As the section is noncircular, warping accompanies twisting of the section. Theoretically, if the warping is unrestrained the section experiences only St Venant ("pure" or circulatory) torsion. However, near the ends of the member the stress state changes considerably, as the end of the member is constrained; therefore, normal

and shear stresses are developed due to warping torsion (Comité Euro-International du Béton. and Fédération Internationale de la Précontrainte. 1993).

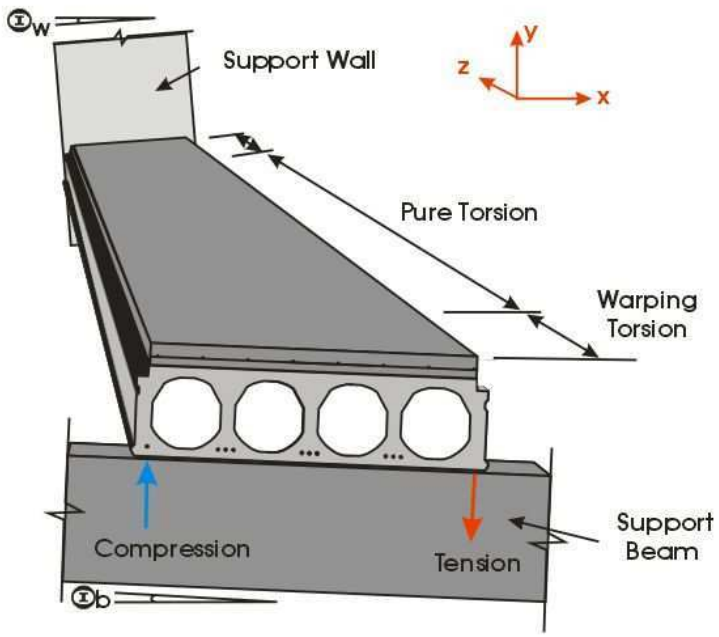

Figure 4-17 Differential displacements between supports causing torsional actions in a hollow-core floor

Thin tube theory can be used to determine the torsional strength and stiffness of the floor away from the support prior to cracking. Thin tube theory is out lined in the commentary to the New Zealand Concrete Structures Standard (Standards New Zealand 2006). Torsional resistance varies depending on the amount of longitudinal compression stress and applied bending moment, both of which fluctuate during seismic loading. Therefore, the actions leading to torsional cracking are difficult to determine. When torsional cracking occurs, the torsional resistance should decrease as the hollow-core units do not contain torsional reinforcement. Broo et al. (2005) investigated the torsion capacity in hollow-core units both analytically and experimentally. It was observed that cracks were visible in the units before the maximum loading was reached, which indicates a redistribution of actions when cracking occurs. Broo's limited tests indicated failure occurred at about 2 to 3 times the twist causing torsional cracks to form. Figure 4-18 shows how hollow-core floors have an inherent redundancy so limited cracking results in a stress redistribution, rather than failure. It must be noted however that once cracking initiates, it is likely more that one flange will crack. If the flanges below every void in the unit crack, the floor will behave as a series of individual I-beams, which have limited torsional capacity. As there has been limited research into

torsion resistance of hollow-core floors, the amount of torsional rotation that can reliably sustained without reducing the shear and flexural strength is uncertain.

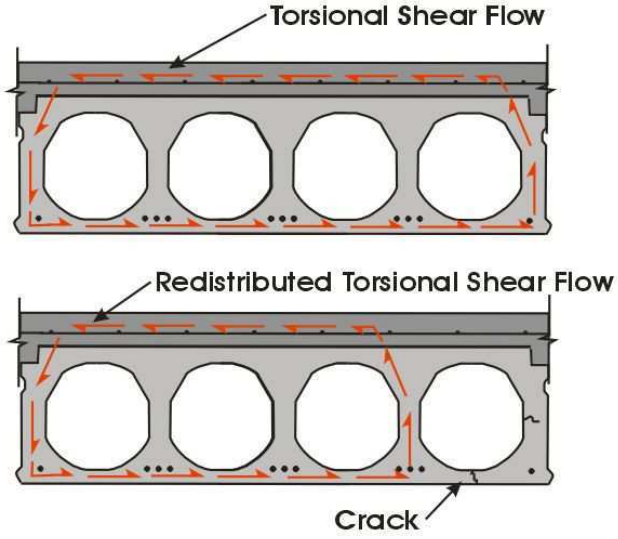

Figure 4-18 Torsional shear flow in a hollow-core unit

4.8 Preferred Hierarchy of Failure

If a hollow-core floor is going to be designed, or retrofitted, using a capacity design method, a preferred ductile failure mechanism must be selected. Hollow-core units are inherently brittle; therefore, it is preferable to limit actions entering the units by designing the connections between the units and the rest of the structure as ductile fuses. The connections must have sufficient strength and ductility to withstand actions and displacements expected under earthquake excitation. The rest of the floor unit must then be designed to withstand actions induced by overstrength forces at the “fuse”, associated displacements and any vertical seismic forces induced in them.

4.9 References

Broo, H., Lundgren, K., and Engström, B. (2005). "Shear and torsion interaction in prestressed hollow core units." *Magazine of Concrete Research*, 57(9), 521 - 533.

Bull, D., and Matthews, J. (2003). "Proof of Concept Tests for Hollowcore Floor Unit Connections." *Research Report 2003-1*, Department of Civil Engineering, University of Canterbury, Christchurch, New Zealand.

Charleson, A., New Zealand Concrete Society. Study Group., New Zealand National Society for Earthquake Engineering., and Centre for Advanced Engineering. (1991). *Guidelines for the use of structural precast concrete in buildings : report*, The Societies : Centre for Advanced Engineering, [Christchurch, N.Z.].

Comité Euro-International du Béton., and Fédération Internationale de la Précontrainte. (1993). *CEB-FIP model code 1990 : design code*, T. Telford, London.

Department of Building and Housing. (2008). *Guidelines for the assessment of hollow-core flooring in New Zealand - DRAFT*, Department of Building and Housing, Wellington, New Zealand.

Fenwick, R., Deam, B., and Bull, D. (2004). "Failure modes for hollowcore flooring units." *Journal of the Structural Engineering Society New Zealand Inc.*, 17(1), 52 - 70.

FIB Commission 6 Prefabrication., and Fédération internationale du béton. (2000). *Special design considerations for precast prestressed hollow core floors : guide to good practice*, International Federation for Structural Concrete, Lausanne, Switzerland.

Jensen, J. (2006). *The seismic behaviour of existing hollowcore seating connections pre and post retrofit : a thesis submitted in partial fulfilment of the requirements for the degree of Master of Engineering at the University of Canterbury*, Christchurch, New Zealand.

Lau, D. B. N., Fenwick, R. C., Davidson, B. J., University of Auckland. School of Engineering., and University of Auckland. Dept. of Civil and Environmental Engineering. (2007). *Influence of precast prestressed flooring on the seismic performance of reinforced concrete perimeter frame buildings*, Dept. of Civil and Environmental Engineering University of Auckland, Auckland, N.Z.

Lindsay, R. (2004). *Experiments on the seismic performance of hollow-core floor systems in precast concrete buildings : a thesis submitted in partial fulfilment of the requirements for the degree of Master of Engineering at the University of Canterbury*, Christchurch, New Zealand.

MacPherson, C. (2005). *Seismic performance and forensic analysis of a precast concrete hollow-core floor super-assemblage : a thesis submitted in partial fulfilment of the requirements for the degree of Master of Engineering at the University of Canterbury*, Christchurch, New Zealand.

Matthews, J. (2004). *Hollow-core floor slab performance following a severe earthquake : a thesis submitted in partial fulfilment of the requirements for the degree of Doctor of Philosophy at the University of Canterbury*, Christchurch, New Zealand.

Pajari, M. (1998). "Shear Resistance of PHC Slabs Supported on Beams. II: Analysis." *Journal of Structural Engineering*, 124(9), 1062-1073.

Pajari, M., and Koukkari, H. (1998). "Shear Resistance of PHC Slabs Supported on Beams. I: Tests." *Journal of Structural Engineering*, 124(9), 1050-1061.

Restrepo-Posada, J. I., Rodriguez, M., Saunders, D. B., and University of Canterbury. Dept. of Civil Engineering. (2000). *Earthquake resistant precast concrete buildings : wall-slab coupling effects in low-rise buildings*, Dept. of Civil Engineering University of Canterbury, Christchurch, N.Z.

Standards New Zealand. (2006). *Concrete structures standard, NZS3101, Parts 1 & 2*, Standards New Zealand, Wellington, New Zealand.

Standards New Zealand. (2004). *Amendment No. 3 to 1995 Standard (NZS3101)*, Standards New Zealand, Wellington, New Zealand.

Standards New Zealand. (2006). *Concrete structures standard, NZS3101, Parts 1 & 2*, Standards New Zealand, Wellington, New Zealand.

5 Negative Flexural Failure

Hollow-core flooring units are designed as simply supported members. However, frequently in construction, continuity is established between the units and supporting structure by the addition of insitu topping concrete and steel reinforcement. This change in structural form can result in negative moments and axial forces being induced in the floor by seismic and other structural actions. Negative moments induce tension on the top side of the floor which is resisted by the insitu concrete topping. There are two cases where negative moments and axial loads may result in flexural cracking leading to a brittle flexural failure. These are when topping contains either non-ductile steel reinforcement or the proportion of reinforcement is too small. Figure 5-1 shows what a flexural failure in a negative moment zone (referred to as a negative flexural failure) might look like.

This chapter describes:

- Past research and design guidelines for negative flexural failures
- Load cases which can induce negative bending moments and axial tension in floors and how to calculate the magnitude of these actions
- What situations result in hollow-core floors being vulnerable to a negative flexure failure and examples of where negative flexural failures have been observed in experimental tests
- How capacity predictions were made for the experiment undertaken as part of this research.

It should be noted that the method used to predict the capacity of a hollow-core floor section used in this chapter was shown to be unconservative by the experimental results for situations when insitu topping contains only cold-drawn wire mesh reinforcement. Hence, a revised method for predicting the capacity of a hollow-core section is presented and discussed in Chapter 10.

(a) Hollow-core floor in building subjected to earthquake drift

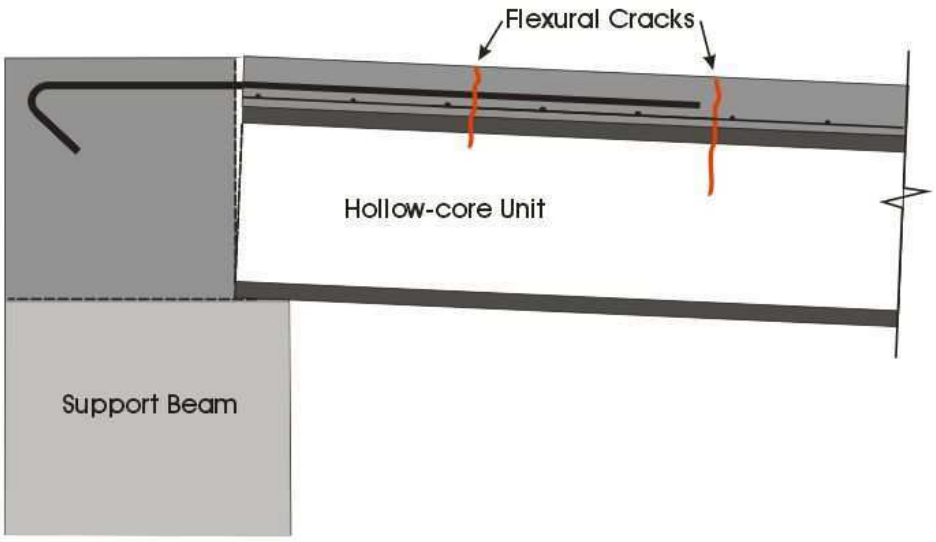

(b) Flexural crack induced near support beam

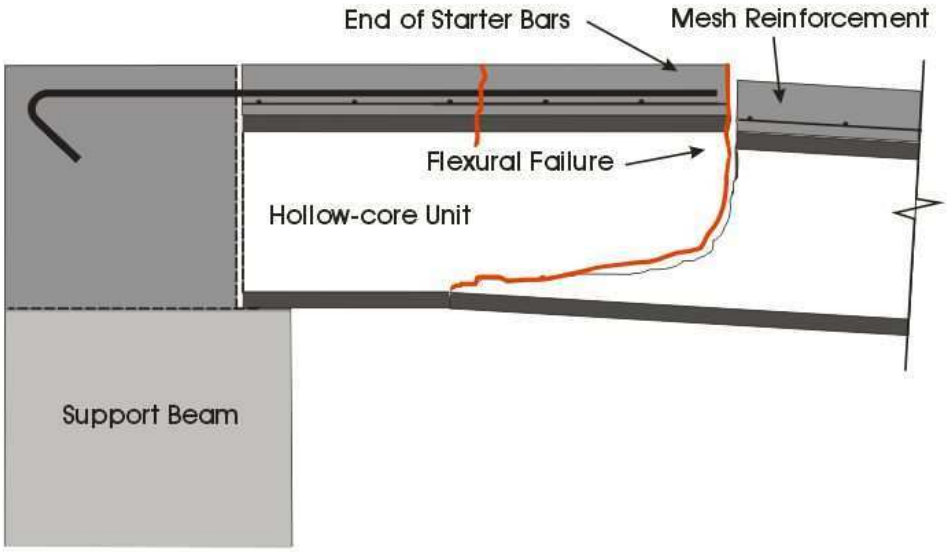

(c) Flexural failure when mesh reinforcement ruptures at the end of starter bars

Figure 5-1 Negative flexural failure in a hollow-core floor system

5.1 Past Awareness

Awareness of the potential for a negative flexural failure is not new. A guide to good practice published by the International Federation for Structural Concrete (***fib***) in 2000 specifically states that when hollow-core floors have restrained supports (whether intended or as an unintended "consequence" of design), analysis should be carried out for all critical sections near the supports. This includes checking the negative flexural capacity at a the edge of the support and at the end of any reinforcement anchored into the support (***fib*** Commission 6 Prefabrication. and Fédération internationale du béton. 2000). Most hollow-core floors in New Zealand contain restrained supports as a result of the addition of insitu topping concrete and reinforcement. This would suggest New Zealand designers should be checking for negative flexural capacity. However, the guidelines given by *fib* are predominantly for un-topped hollow-core floor slabs and gravity loads; therefore, they are not immediately applicable to New Zealand situations.

Ho (2001) investigated whether vertical earthquake accelerations could cause structural damage to a hollow-core floor system. Vertical earthquake records from three earthquakes were applied to a simple analytical model representing a hollow-core floor. It was concluded that negative moments induced in the floor could cause yielding of steel reinforcement in the topping concrete.

In 2004 the issue of flexural and axial tension failure of New Zealand hollow-core floors was raised in the Journal of the Structural Engineering Society of New Zealand Inc. (Fenwick et al. 2004). The article described several different failure modes, some previously recognised and some predicted by the authors using simple analytical models. Flexural failure of hollow-core floors due to seismically induced negative moments was one of the failure mechanisms described. The paper gives details of two critical load combinations that lead to negative bending moments. Standard flexural theory was used to calculate the flexural cracking moment and ultimate negative flexural strength of two typical New Zealand hollow-core floor construction details. It was shown that in high seismic regions, such as Wellington, the same quantity of steel that passes over the support beam to floor interface is required for the full length of the floor span. The paper concluded that negative moments may only lead to yielding of the top passive reinforcement, but if the tensile capacity of the concrete was more than that of the steel reinforcement, yielding could be limited to one section and a brittle

failure might occur. Further research in this area was recommended; the research presented in this thesis attempts to achieve this.

Negative flexural failures were observed in three sub-assembly tests performed at the University of Canterbury by Liew (2004). The tests looked at three connection details between hollow-core floors and their supporting beams (see Figure 5-3). The loading protocol induced a cyclic relative rotation between the hollow-core floor and seating beam, emulating the relative rotation induced during building drift in a seismic event. Figure 5-2 shows the test rig used. All three details exhibited a negative flexural failure. The connection details were not representative of typical construction at the time; however, the test highlighted the potential danger of a brittle failure under negative moments.

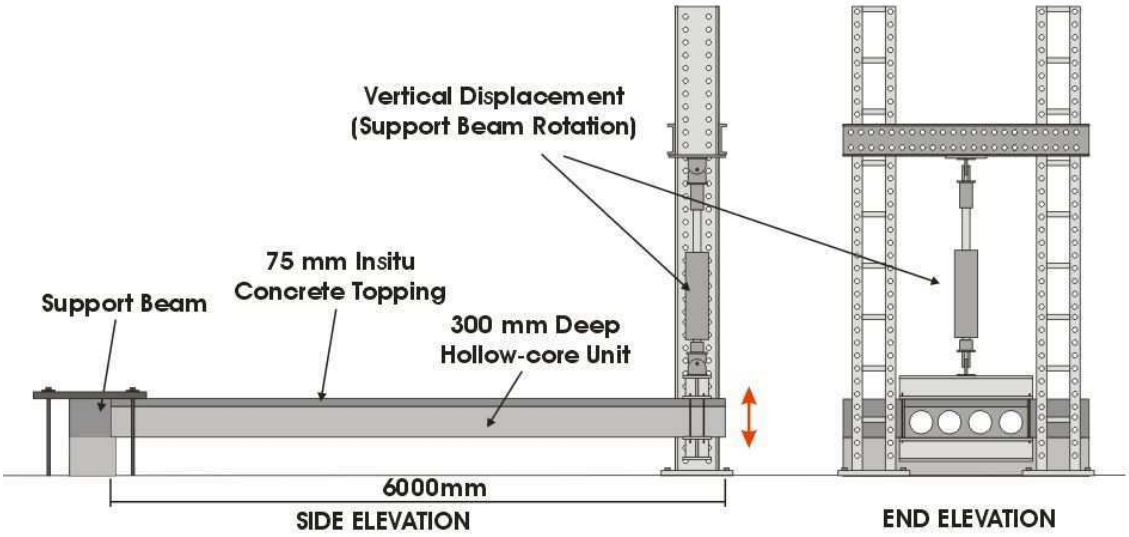

Figure 5-2 Sub-assembly test rig for applying relative rotation between the hollow-core floor and supporting beam (Adapted from Jensen 2006)

The first two specimens tested by Liew had their cores broken back and filled with concrete to around 700 mm (see Figure 5-3 (a) and (b)). An R16 paperclip of steel reinforcement was cast into each core to provide redundancy should vertical support from seating be lost (or in the case of Specimen 1, where it did not exist). The steel and concrete crossing the beam to floor interface increased the moment capacity of this section. The weakest section under negative moments is therefore moved from the beam-floor interface, to the end of the starter bars. At rotations equivalent to – 1.0 % interstorey drift, the first two of Liew's specimens formed flexural cracks at the end of the starter bars. Under further loading, the flexural cracks in both

Specimen One and Two extended near horizontally through the webs, leading to failure at 2.0 % and 4.0 % equivalent relative rotation respectively. The presence of seating was attributed to the superior performance of Specimen Two.

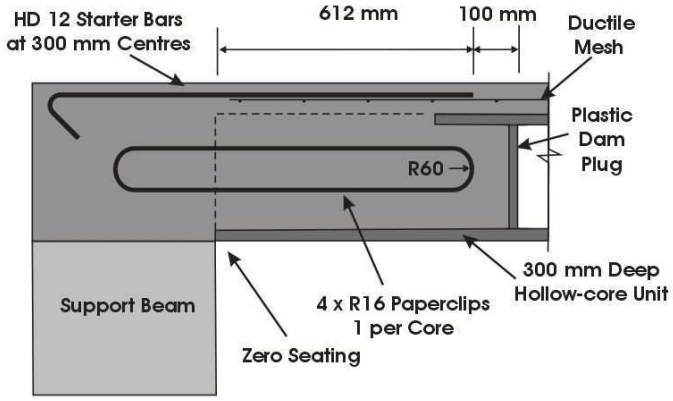

(a) Paperclip detail with zero seating

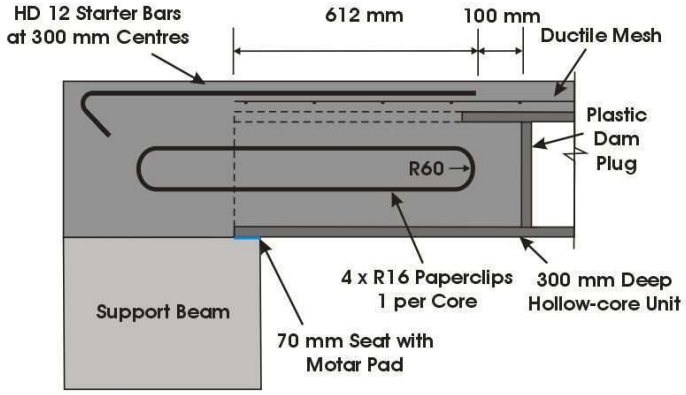

(b) Paperclip detail with 70 mm seating

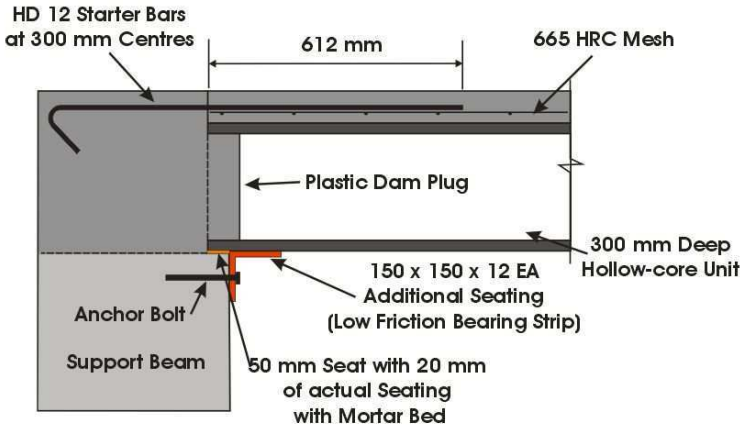

(c) Retrofit detail utilising a 150 mm steel equal angle

Figure 5-3 Seating connections tested by Liew (2004) (Adapted from Jensen 2006)

A similar test, performed by Bull and Matthews (2003), did not exhibit the same failure mechanism. The connection in this test contained only two cores broken back and filled with concrete and steel reinforcement, rather than four (see Figure 2.7(c)). The quantity of steel reinforcement in each filled core was also less, instead of a 16 mm diameter round bar paper clip, a high strength 12 mm diameter deformed bar paperclip was used. The result of less steel reinforcement crossing the beam-floor interface was that instead of a flexural crack occurring in the hollow-core unit at the end of the filled cores, a crack at the beam to floor interface opened. This specimen was taken to ± 4 % equivalent interstorey drift without failing. Comparing the tests performed by Liew with that by Bull and Matthews showed that the amount of reinforcing placed in filled cores could alter the failure mode. Liew concluded that over-reinforcement of the cores was detrimental to performance and should be avoided.

The third specimen tested by Liew (2004) did not contain cores filled with concrete (see Figure 5-3 (c)). The specimen was representative of a connection with insufficient seating; therefore, a steel angle was attached to the support beam under the soffit of the unit to act as additional seating in a potential retrofit. The angle restrained the rotation at the end of the hollow-core unit and at – 2.0 % relative rotation a negative flexural crack formed at the end of the starter bars and the mesh spanning the crack ruptured. The floor failed at 3.0 % relative rotation. Liew concluded that longer starter bars might mitigate this type of failure.

5.2 Load Cases which Induce Negative Bending Moments

Brittle failure may be expected in hollow-core floors if subjected to critical levels of negative bending moment and axial tension. These loads can be induced in a number of situations. The most critical of these are combinations of gravity loads, vertical seismic forces (up and down), together with actions transmitted through the support details. Forces transmitted through the supports can be from elongation of beams parallel to the hollow-core units and/or rotation of the support beams during building drift. Figure 5-4 shows these potential loads on a hollow-core floor.

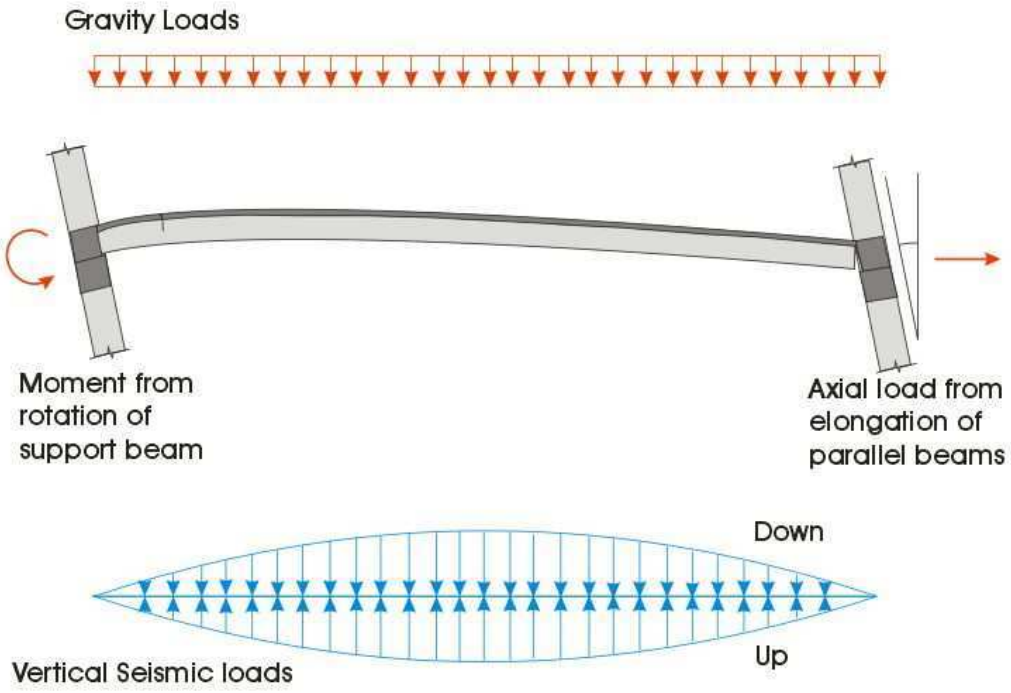

Figure 5-4 Loads that contribute to negative bending moments

To find the critical negative bending moments and axial loads in a hollow-core floor system, the bending moment components from the individual loads are summed together. Figure 5-5 shows the individual bending moments (in light blue) and their critical combinations (in dark blue). Two combinations are shown, one with axial tension (induced by parallel beam elongation), labelled A&B&D, and one without, labelled A&B&C. The method of calculating the critical bending moments for each load component are given below:

- **Gravity load** - The bending moment due to a uniformly distributed gravity load is easily determined. As the load combination includes seismic loading, the gravity load is the dead load and the live load multiplied by a short-term reduction factor. The bending moment diagram from the gravity load is shown as "A" in Figure 5-5.

- **Vertical seismic load** - The seismic actions due to vertical ground motion can be found using the New Zealand Structural Design Actions Standard (Standards New Zealand. 2004b). Generally, the vertical seismic actions are calculated from the response spectra. This is taken as 0.7 times the corresponding elastic site spectra for horizontal loading, C(T), multiplied by the seismic weight of the floor, W_t. The values to use for the structural ductility, μ, and the structural performance, S_p, factors vary

depending on the steel reinforcement used in the insitu topping, Appendix A1 explains the reasons for this and gives recommendations for appropriate values. The fundamental period, T, of a hollow-core floor span is short, generally in the range of 0.1 to 0.35 seconds; therefore, the peak values of the spectral shape factor, $C_h(T)$, should be used. When representing dynamic actions as an equivalent static force, a common assumption is to distribute the actions proportionally to the mass and displacement of the mass relative to the ground. Therefore, for a hollow-core floor, where the mass is approximately uniformly distributed, the deflected shape will be roughly a parabola. Hence, the vertical seismic actions should be distributed in the shape of a parabola along the length of the floor (Fenwick et al. 2004). The bending moments resulting from upward vertical seismic actions are shown as "B" in Figure 5-5.

- **Action transmitted through the supports** - The actions transmitted through the floor supports are likely to cause the reinforcement in the insitu topping, at the interface between the hollow-core unit and the supporting beam, to be close to its ultimate strength in a major earthquake. The way actions are transmitted over the support, and their magnitude, will vary during an earthquake and depend on the connection detail used. However, two critical situations should be considered, these are:
  - **Maximum bending moment with no axial load**: This scenario could be induced by rotation of the supporting beams due to building drift. In this case it can be assumed that one end of the floor is at its over-strength moment and the other is pinned (zero moment), with a linear variation in between. This is shown as "C" in Figure 5-5. The overstrength bending moment capacity at the floor end can be assessed assuming that the interface section acts as a singly reinforced concrete beam section.
  - **Maximum axial tension due to parallel beam elongation**: In this scenario end moments in the floor are induced by the eccentricity of the applied axial tension through the starter bars. The shape of the bending moment caused by the axial load and eccentricity is shown as "D" in Figure 5-5.

  Note that these two critical situations cannot occur simultaneously.

It is conservative to assume an over-strength end moment, due to elongation or rotation of the support beams, occurs simultaneously with the maximum vertical earthquake excitation. This

is because the fundamental period of the floor, excited by the vertical motion, is short compared to the fundamental period of the structure. It is therefore possible for both maximum moments occur at the same time.

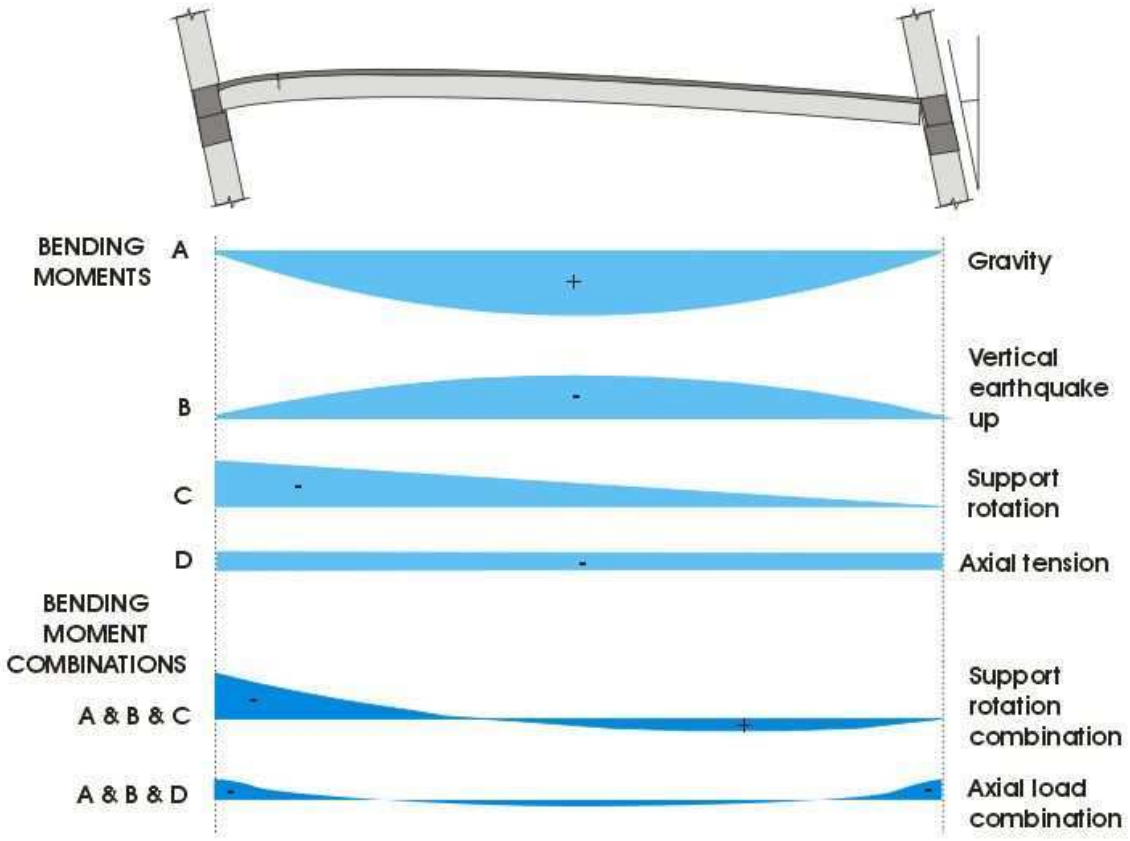

Figure 5-5 Bending moments from loads acting on a hollow-core floor span during an earthquake and their combinations

Figure 5-5 shows that the maximum negative bending moments are near the floor supports. It is therefore in these regions that the negative bending moment capacity of the floor needs to be checked. Although the case without axial tension appears to induce smaller negative flexural moments than the case with axial tension, it may still be critical as the axial tension reduces the flexural capacity of the section.

5.3 Situations Vulnerable to a Negative Flexural Failure

High seismic demand, use of non-ductile reinforcement, low reinforcement ratios and lack of shear reinforcement, all increase the potential for a negative flexural failures in hollow-core

floors. However, the characteristic of a hollow-core floor that has most effect on the likelihood of a negative flexural failure is if the beam-floor interface has a higher negative flexural capacity than sections further out in the floor. Most buildings in New Zealand will not have been designed specifically for the load combinations outlined in the previous section and may have insufficient negative flexural capacity. As the vertical seismic accelerations are included in the critical load cases, high seismic regions, such as Wellington, are most at risk.

Prior to the amendments to the New Zealand Concrete Structures Standard in 2004 (Standards New Zealand. 2004a), which state that ductile mild steel reinforcement must be used in the insitu topping concrete of buildings in seismic zones; it was typical for mesh reinforcement to be used. Mesh reinforcement has minimal ductility; it reaches its maximum stress at a strain of typically 1.5 %. The magnitude of negative moment demand along the floor is related to the capacity of the beam-floor interface (as described in the previous section). Often the negative moment capacity at the beam-floor interface is larger than the capacity of sections further into the floor due to the presence of starter bars. These typically extend 400 to 1200 mm into the floor, increasing the negative flexural capacity in this region. At the end of the starter bars the negative moment capacity of the floor decreases as only the mesh reinforcement can be relied on to sustain tension stresses at the top of the floor unit. Figure 5-6 (a) shows a typical hollow-core floor detail that contains mesh reinforcement and starter bars that extend a limited distance into the floor. The tensile capacity of the concrete cannot be relied upon, as it often contains cracks due to creep and shrinkage effects. Negative moment flexural failures at the termination point of the starter bars have been observed in several sub-assembly tests at the University of Canterbury by Liew (2004) and in this research. Hollow-core floors, where the support beam connections contain cores that have been broken out and filled with concrete and steel reinforcement, may also be prone to a negative flexural failure. The additional steel reinforcement crossing the beam-floor interface may increase the negative moment capacity at this location; the section capacity at the end of the filled cores may be insufficient to sustain the additional negative bending moment. Such a detail is shown in Figure 5-6 (b).

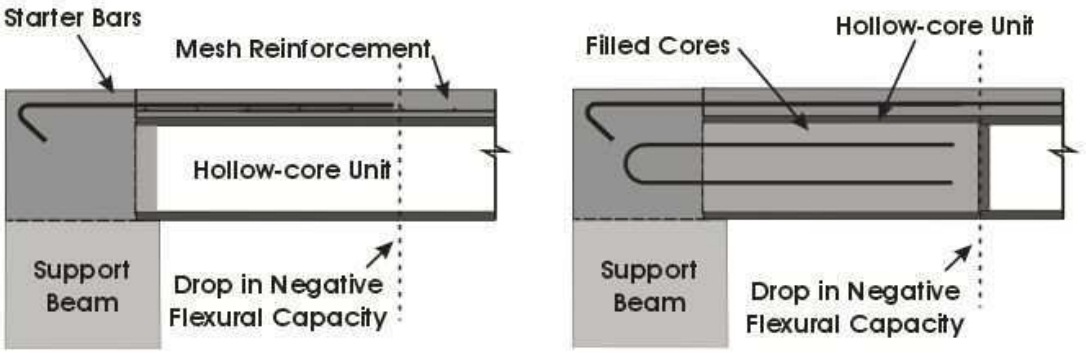

(a) Starter bars terminating a short distance into the floor leaving only mesh reinforcement

(b) Cores of the hollow-core filled with concrete and steel reinforcement for a limited distance

Figure 5-6 Connection details where the negative flexural capacity at the support is substantially higher than other sections along the floor

When the insitu topping contains only a small amount of reinforcement the tension capacity of the concrete itself may exceed that of the reinforcement. This could limit the reinforcement yielding to one section and result in a brittle failure. When assessing the capacity of a hollow-core floor, the development lengths of steel reinforcement and prestressing must be considered.

5.4 Capacity Predictions used for Experiment

The test specimen was designed to be representative of construction practice used in New Zealand during the 1980s and 1990s. The insitu topping concrete contained 665 mesh reinforcement and high-strength ribbed starter bars extending 1000 mm into the floor. More specific details of the test specimen and test set-up are described in Chapter 7. Standard flexural theory was used to calculate the negative flexural capacity of sections along the length of the floor unit. Creation of a spreadsheet allowed the neutral axis, strains, stresses and forces to be found iteratively using equilibrium and compatibility relationships, for any given loading condition. For the predictions of experimental results, the geometries and average material properties, measured from the test specimen, were used. The negative flexural capacity changed along the length of the floor unit depending on the quantity of steel reinforcement and development lengths of prestressing and passive reinforcement. The theoretical capacities were compared with the critical potential seismic load cases inducing negative bending moments. These were calculated using the method outlined in section 5.2, for an equivalent 12 m span floor located in either Christchurch or Wellington.

This following paragraphs describe:

- The basic setup of the spreadsheet used to calculate section flexural capacity
- The stress-strain relationships used for the concrete and steel in the spreadsheet
- The development lengths used for the prestressing and the passive steel reinforcement in the spreadsheet
- The difference between the predicted section capacities and the load demand for an equivalent 12 m span of hollow-core floor.

The spreadsheet created required the areas of all components in a given section and their distance from the centre line of the composite hollow-core floor section. The hollow-core section was divided into 2 mm strips. The assumption that plane sections remain plane was made and an iterative process used until the linear strain profile was found that resulted in equilibrium. Equilibrium was satisfied by ensuring the forces in the section balanced the bending moment and axial load.

The stress-strain relationship used for both the hollow-core concrete and the insitu concrete was that developed by Mander and co-workers (Mander 1982). The concrete was assumed to be unconfined and have a strain at peak stress of $0.00145 + 0.00001875 * f'_c$, this is an average value derived empirically from experimental data (Fenwick R., personal communication, 2007). The stress-strain curve used is shown in Appendix C5.3. The tension capacity of concrete was assumed to be zero. There were several reasons for this assumption. Firstly, the insitu topping concrete in an existing hollow-core floor unit is likely to contain cracks due to creep and shrinkage. Secondly, the tensile strength of concrete is variable and cannot be relied upon. Also, once a flexural crack is initiated in concrete, it generally propagates to around the level of the neutral axis. This means, exceeding the tensile capacity of concrete at the extreme tension fibre, essentially negates the tensile capacity of the concrete.

Standard monotonic tensile tests were performed on the mesh reinforcement and starter bars used in the test specimen. Piecewise functions for the stress at a given strain were approximated from the measured stress-strain relationships, see Appendices C5.4 and C5.5. The prestressing steel was assumed to remain in its elastic range. Stress levels in the

prestressing when the unit was cast, and the assumed losses, were provided by the hollow-core manufacturer.

The negative flexural capacity of the hollow-core floor unit changes along its length due to changes in the amount of prestressing and passive steel reinforcement that are active. The New Zealand Concrete Structures Standard (Standards New Zealand. 2006), gives the development length of deformed bars in tension as $L_{db} = \frac{(0.5\alpha_a f_y)}{\sqrt{f_c'}} d_b$ (Eq 8.2. p. 8-4). Where f_y is the lower characteristic yield strength of the reinforcement, f'_c is the specified compressive strength of concrete, d_b is the nominal diameter of the bar and α_a is a factor to take into account the presence of bleed water reducing the bond capacity below the bar. The factor α_a is taken as one, as in this case there is less than 300mm concrete cast below the reinforcement. The development length from the standard is a design value and therefore is conservative. To account for this in predictions, 2/3 of this value was used for development length of the starter bars. The capacity of the bars was assumed to increase linearly from zero to full capacity over this length. The mesh reinforcing was assumed to have a development length of 150 mm as this is the spacing of the transverse wires.

The development length of prestressing strands in hollow-core units is defined by the International Federation for Prestressing (FIP) (1988) as a transmission length together with an anchorage length. In a negative flexure situation, the characteristic stress in the prestressing strands is less than the effective prestress after losses. The anchorage length is a function of the characteristic stress minus the effective prestress after losses; this gives a negative value and therefore is ignored. The development length used is therefore simply the transmission length. This is defined as: $l_d = \frac{f_{se} d_b}{21}$ in millimetres. f_{se} is the effective stress in the prestressing steel after losses (in mega-Pascals) and d_b is the nominal strand diameter (in millimetres). The development length this gives is possibly conservative for the internal prestressing strands, but unconservative for the two, smaller diameter, exterior strands if compared with the transfer length assumed by the New Zealand Concrete Structures Standard, which is 50 times the strand diameter (Standards New Zealand. 2006). The stress in the prestressing strands is assumed to develop linearly over these development lengths. Figure 5-7 shows the changes in steel content along the section and the assumed development lengths.

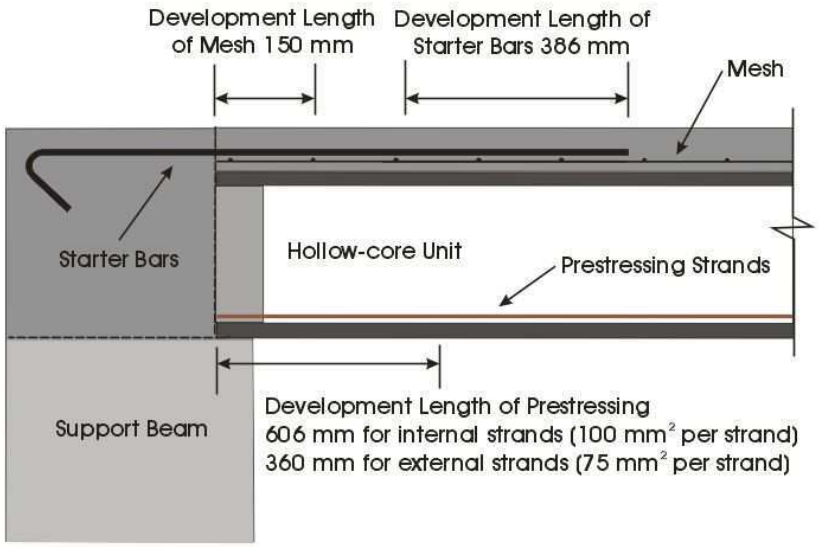

Figure 5-7 Detail near the beam support of the test specimen showing the development lengths of prestressed and passive reinforcement

When predicting test specimen capacities average material properties were used, these are given in Appendix A2. In contrast, for design, the fifth percentile material properties should be used. Appendix A3 goes through the calculation of the first yield moment for the cross-section at the end of the starter bars when no axial load is applied. Similar analyses were performed at cross-sections along the test specimen, repeated with varying amounts of axial load. Figure 5-8 shows the capacity predictions along the section compared to seismic loads calculated as described in Section 5.2. The two critical load cases are shown; one where there is a maximum negative moment at the support and no axial load (Figure 5-8 (a)) and one where axial tension is applied to the specimen, which induces a negative moment due to the eccentricity of the starter bars (Figure 5-8 (b)). Both load cases are shown for the loads scaled for Christchurch (a medium seismicity zone) and Wellington (a high seismicity zone) design values.

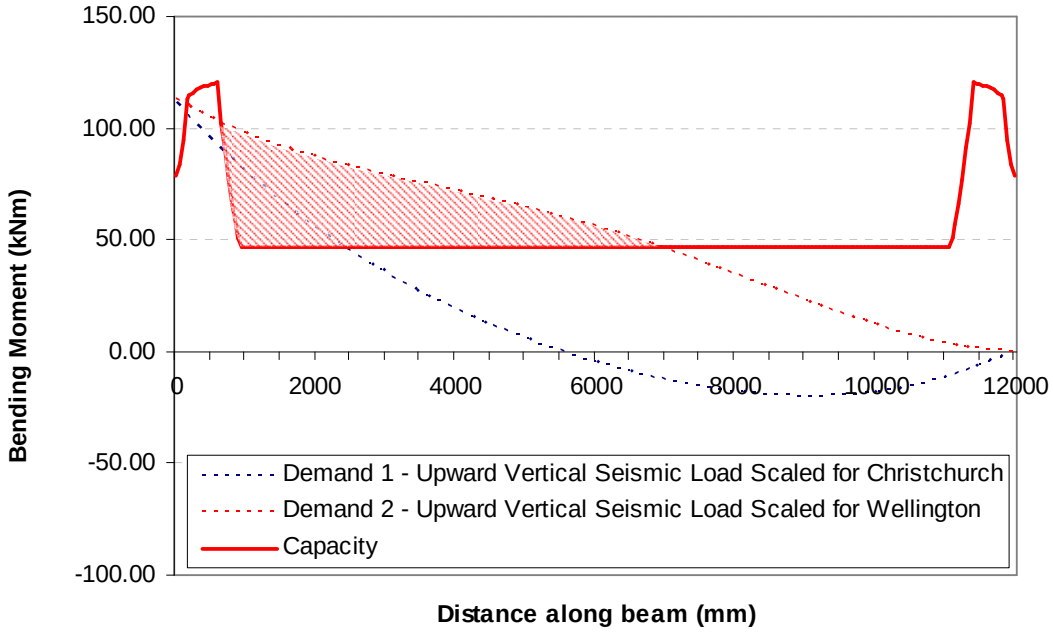

(a) No axial load, bending moment demand from rotation of supports, gravity loads and upward vertical seismic actions

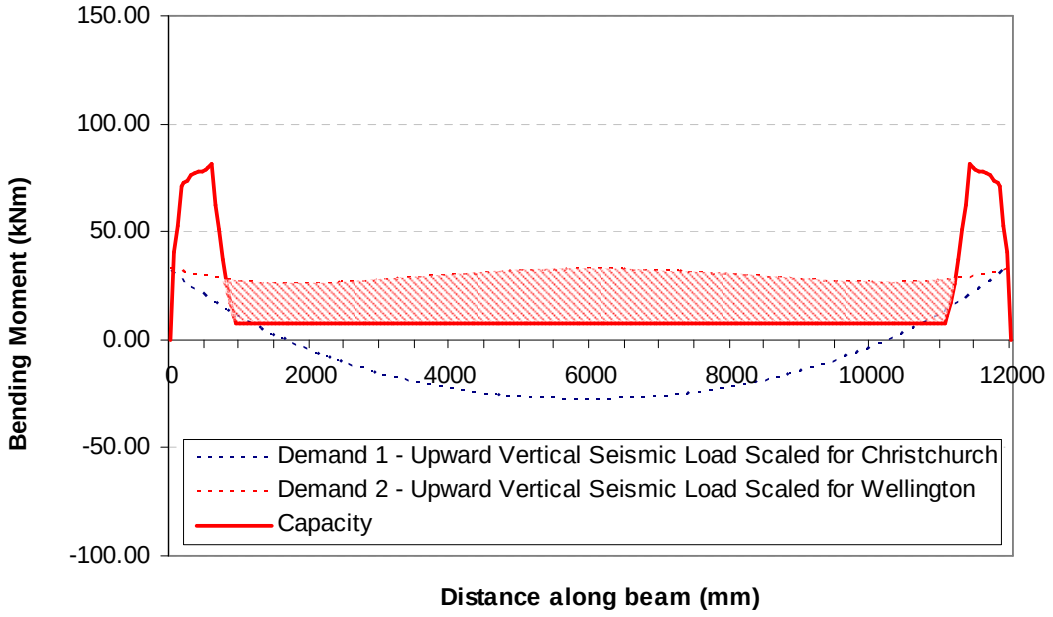

(b) With axial tension caused by elongation of parallel frame beams, bending moment demand from axial load, gravity loads and upward vertical seismic actions

Figure 5-8 Demand versus predicted capacity of a 12 m span hollow-core floor under seismic load combinations scaled for Christchurch and Wellington

The shaded area in Figure 5-8 shows that there is a deficit between the capacity of the section and demand. This raises concerns as the capacities shown were calculated from average material properties, not lower design values, and are not multiplied by a strength reduction factor. It was hence predicted that a flexural failure could be observed in experimental tests that reproduced these structural actions. In such a test, described in Chapters 7, 8 and 10, a flexural failure was observed and the experimental results showed the predictions were unconservative, the specimen failed at a flexural strength below that predicted using average material properties. It is believed this was mainly because the standard engineering assumption that plane sections remain plane needs to be revised for this situation. Discussion of this, and revised predictions compared with experimental results, are given in Chapters 8 and 10.

5.5 References

Bull, D., and Matthews, J. (2003). "Proof of Concept Tests for Hollowcore Floor Unit Connections." *Research Report 2003-1*, Department of Civil Engineering, University of Canterbury, Christchurch, New Zealand.

Fenwick, R., Deam, B., and Bull, D. (2004). "Failure modes for hollowcore flooring units." *Journal of the Structural Engineering Society New Zealand Inc.*, 17(1), 52 - 70.

FIB Commission 6 Prefabrication., and Fédération internationale du béton. (2000). *Special design considerations for precast prestressed hollow core floors : guide to good practice*, International Federation for Structural Concrete, Lausanne, Switzerland.

FIP Commission on Prefabrication. Working Group Hollow Core Units., and FIP Commission on Prefabrication. Working Group Structural Connections. (1988). *Precast prestressed hollow core floors*, Telford, London.

Ho, D. T. (2001). *Performance of hollowcore floor systems under earthquake induced vertical acceleration : a report submitted in partial fulfilment of the requirements for the degree of Master of Civil Engineering at the University of Canterbury, Christchurch, New Zealand.*

Jensen, J. (2006). *The seismic behaviour of existing hollowcore seating connections pre and post retrofit : a thesis submitted in partial fulfilment of the requirements for the degree of Master of Engineering at the University of Canterbury*, Christchurch, New Zealand.

Liew, H. Y. (2004). *Performance of hollowcore floor seating connection details : a thesis submitted in partial fulfilment of the requirements for the degree of Master of Engineering at the University of Canterbury*.

Mander, J. B. (1982). "Seismic Design of Bridge Piers." *Research Report 84-2*, University of Canterbury, Christchurch, New Zealand.

Standards New Zealand. (2004a). *Amendment No. 3 to 1995 Standard (NZS3101)*, Standards New Zealand, Wellington, New Zealand.

Standards New Zealand. (2004b). *Structural design actions*, Standards New Zealand, Wellington [N.Z.].

Standards New Zealand. (2006). *Concrete structures standard, NZS3101, Parts 1 & 2*, Standards New Zealand, Wellington, New Zealand.

Blank

6 Flexure-Shear Failure in a Negative Moment Zone

For a simply supported hollow-core floor, shear strength is controlled by web-shear cracking. However, if flexural cracks form, under negative moments induced due to continuity, the shear strength is controlled by flexure-shear cracking. Flexure-shear cracking can occur at lower shear stresses than web-shear cracking and is not considered by the manufacturers of hollow-core units as the units are designed as simply supported members. Figure 6-1 shows what a flexure-shear failure, in a negative moment zone, might look like.

(a) Hollow-core floor in a building under earthquake induced drift

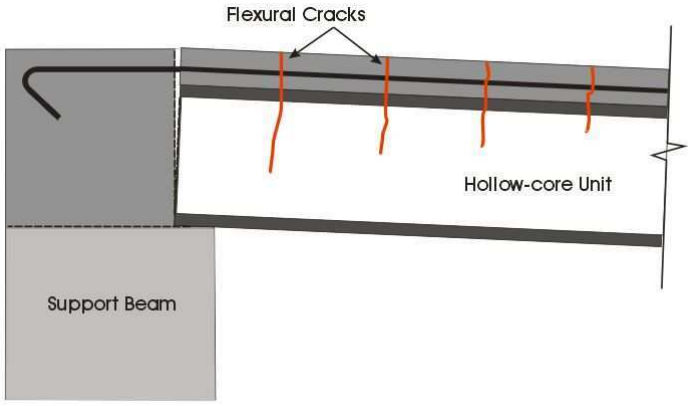

(b) Flexural cracks induced near support beam due to negative bending moment

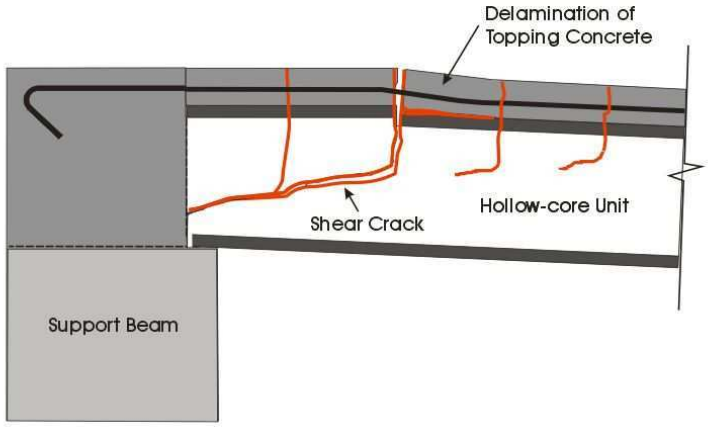

(c) Shear crack between flexural cracks induced by the change in tension force in the steel reinforcement

Figure 6-1 Shear failure in the negative moment zone of a hollow-core floor system

This chapter presents:

- Some background on shear including; the types of shear cracking possible in reinforced concrete members, flexural crack spacing and how this influences shear strength, and how shear stresses are induced in a hollow-core section
- Past research and design guidelines for negative flexural failure
- The load cases which induce negative bending moments and axial tension in a floor and how to calculate the shear stresses induced into a hollow-core unit from these
- How capacity predictions were made for the flexure-shear experiment undertaken as part of this research.

6.1 Shear

The basic variables governing the shear strength of reinforced concrete members are known; however, shear strength is complex and shear behaviour of reinforced concrete members has not been fully clarified. A number of factors influence shear strength. This section aims to describe a few of the main aspects so that a flexure-shear failure, in a negative moment region of a hollow-core floor, may be assessed.

6.1.1 Types of Shear Failure in Concrete Members without Shear Reinforcement

Subjecting a concrete element to pure shear stresses induces internal diagonal tension and compression stresses. If the tension stresses are larger than the direct tensile capacity of the concrete, a diagonal crack may form, commonly referred to as a shear crack. Figure 6-1 (a) illustrates how this occurs and shows the Mohr's circle of principal stresses associated with it. The addition of axial compression to an element (such as from prestressing) decreases the principal tensile stress induced in the element; therefore increasing its shear capacity, as illustrated in Figure 6-2 (b).

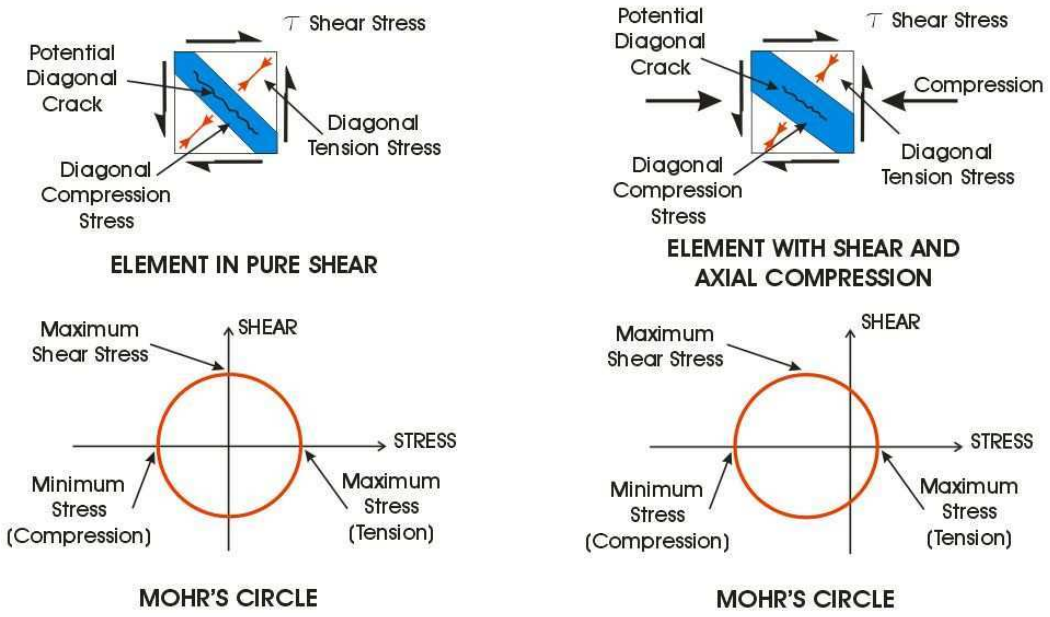

a) Under pure shear **(b) Shear with axial compression**

Figure 6-2 Principal stresses induced in an element subjected to shear

There are two types of inclined cracking that can occur in concrete beams, web-shear cracking and flexure-shear cracking. Figure 6-3 illustrates these. Web-shear cracking occurs when the principal tensile stress in the member exceeds the direct tensile capacity of the concrete. In a prestressed member this generally occurs near the mid-height of the section (Standards New Zealand 2006). Flexure-shear cracking develops after the onset of flexural cracking. When flexural cracking occurs in a prestressed member, shear stresses are induced in the flexural tension zone; diagonal cracks can form when these stresses reach a magnitude similar to the capacity of an equivalent reinforced concrete beam. Therefore, the flexural-shear capacity is often assumed to be the sum of the shear resisted by an equivalent reinforced concrete beam and the shear resisted at the decompression point of the extreme tension fibre (Standards New Zealand 2006). The flexure-shear capacity depends on the flexural crack widths, the wider the flexural cracks, the lower the flexure-shear capacity.

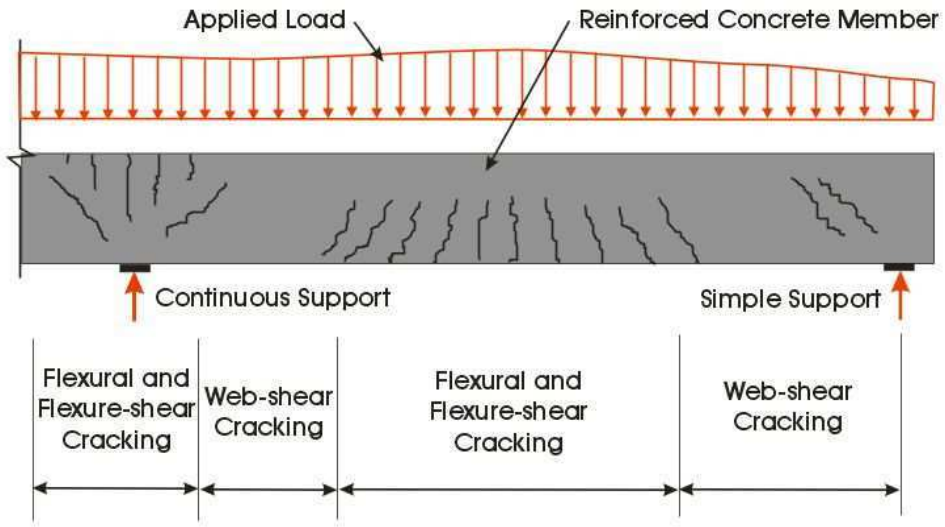

Figure 6-3 Types of cracking in concrete beams (Adapted from Standards New Zealand. 2006)

Hollow-core units are designed as simply supported members and generally, in a simply supported member the shear strength is controlled by web-shear cracking. This is because the locations of high moment, where flexural cracking occurs, commonly have low shear (for example near the middle of a simply supported span). The locations of high shear are in the uncracked, low moment zones (close to the supports). However, as illustrated in Section 5.2, negative moments can be induced in a hollow-core floor near the supports. Under negative moments, if cracks form, the shear strength is controlled by flexure-shear cracking, which is not generally considered by the manufactures of hollow-core units. Flexure-shear cracking capacity is generally less than the web-shear capacity.

6.1.2 Flexural Crack Spacing

Flexural cracking influences the flexure-shear capacity; therefore, it is important to understand what controls the spacing and width of flexural cracks. Variables that influence flexural cracking include the location of shrinkage cracks and the tensile strength of the reinforcement. However, generally for a member in flexure, crack spacing is controlled by two mechanisms. The spacing of vertical cracks, which extend close to the neutral axis is controlled by St Venant's principle. Spacing of vertical cracks near the tension face of the member is controlled by the bond characteristics of the reinforcement. These types of cracks are referred to as primary (or principal) and secondary flexural cracks respectively.

The spacing of principal cracks (S_p) is influenced by the distance required for the tensile stresses in the concrete to spread out. The angle these stresses disperse at is normally between 30 and 45 degrees Therefore, the tensile stresses in the concrete between the cracks are generally unaffected by the crack at a distance 1.0 to 1.7 times the neutral axis depth (h_0) away. Consequently, if it is assumed that the angle of dispersion is 45 degrees, subsequent cracks form at distances between h_0 and $2h_0$ away from existing cracks (Beeby 1970; as cited by Park and Paulay 1975). Figure 6-4 illustrates this, showing the zones where the presence of principal cracks reduces the tensile stresses in the concrete in yellow. This spacing is derived assuming that longitudinal reinforcement is lumped near the face of the member in tension, not dispersed over its depth.

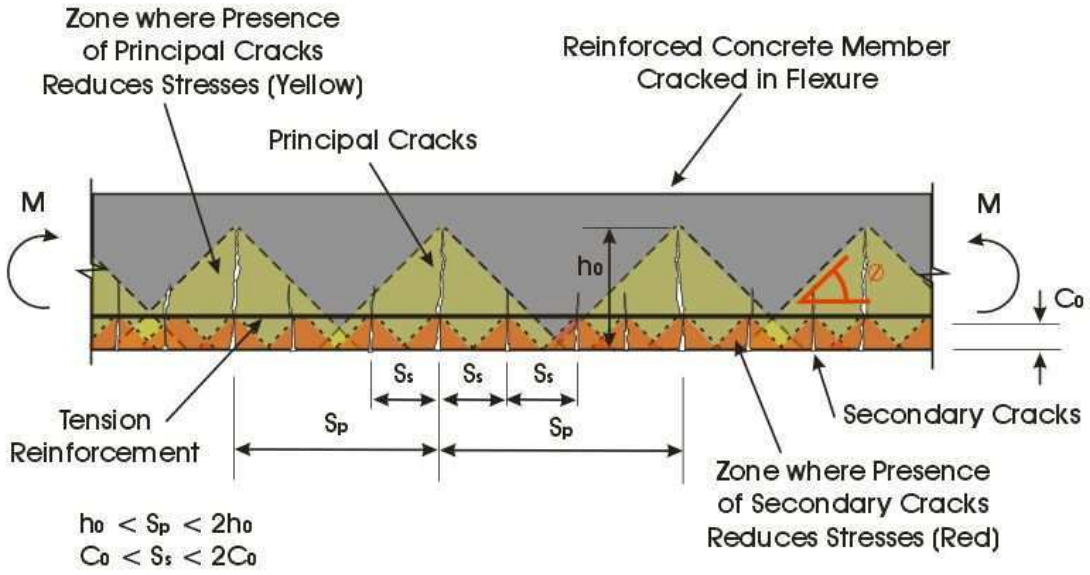

Figure 6-4 Spacing of flexural cracks in a reinforced concrete beam (Adapted from Dickson 1986)

Secondary flexural cracks are a function of bond between the concrete and the steel reinforcement. Secondary cracks form at the tension face of the member and generally only extend a distance of twice the cover depth (C_0) into the concrete. Spacing of secondary cracks (S_s) is controlled by the length of bar required to transfer sufficient tension into the concrete, through bond, to cause cracking. Several secondary cracks can form between primary cracks.

The above discussion gives a likely range for crack spacing; an exact distance can not be calculated as the spacing is often irregular because concrete does not have a uniform tensile

strength. It is often observed that cracks form at the location of transverse bars of steel reinforcement. The presence of these bars creates a weak plane in the concrete resulting in cracks more likely to form at these locations, prior to other locations. Therefore, if the assumed depth of the neutral axis, $h_{0,}$ is close to a multiple of the transverse reinforcement spacing, a valid assumption would be to assume the crack spacing will be this multiple of the transverse reinforcement spacing.

For a member in flexure a linear strain profile is normally assumed. When cracks form, the strain and the crack spacing determines the width of these. Figure 6-5 illustrates how the presence of secondary cracks results in the maximum crack width being between the level of the steel reinforcement and the neutral axis, not at the tension face of the member. Even though the maximum strain occurs at the tension face of the member, this is distributed over more cracks than the strain at the mid-depth. As the beam depth increases, the crack width in this mid-depth region also increases unless there is longitudinal reinforcement at the mid-depth. The varying crack widths affect the location that diagonal cracking might originate due to different amounts of aggregate interlock and shear transfer across the cracks.

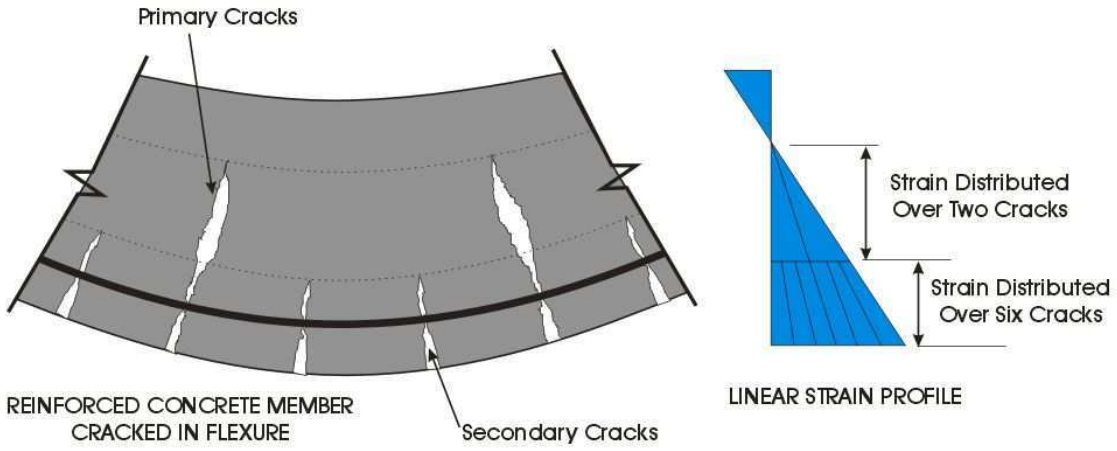

Figure 6-5 Flexural crack widths

The relative tensile strengths of the steel and concrete in a reinforced concrete member can also influence flexural cracking. If the ratio of tension reinforcement to the cross-sectional are of the member is low, it is possible that the tensile force able to be sustained by the concrete is greater than that by the steel reinforcement. Therefore, if a flexural crack formed, the steel would commence yielding and possibly rupture prior to further flexural cracks forming. In this scenario, it is likely a flexural failure would occur.

6.1.3 Development of Shear Stresses

To explain how shear stresses are developed in a hollow-core member, the development of shear stress in a simply-supported reinforced concrete beam is reviewed. Figure 6-6 (a) shows an idealised simply supported beam, with a clear span greater than 2.5 times its effective depth (d), under a point load, P, and with no shear reinforcement. The bending moment along the beam, induced by this load, is also illustrated (in blue). At the location of flexural cracks, all the tension in the section is assumed to be taken by the flexural tension reinforcement. This tension force, multiplied by the internal lever-arm, D_a, to the centroid of the compression force, equals the bending moment at this location, as shown at section "a". Away from the supports and assuming that plane sections remain plane, the lever-arm remains constant along the beam. Therefore, as the bending moment changes along the section, so must the tension force in the steel reinforcement (Collins et al. 2007).

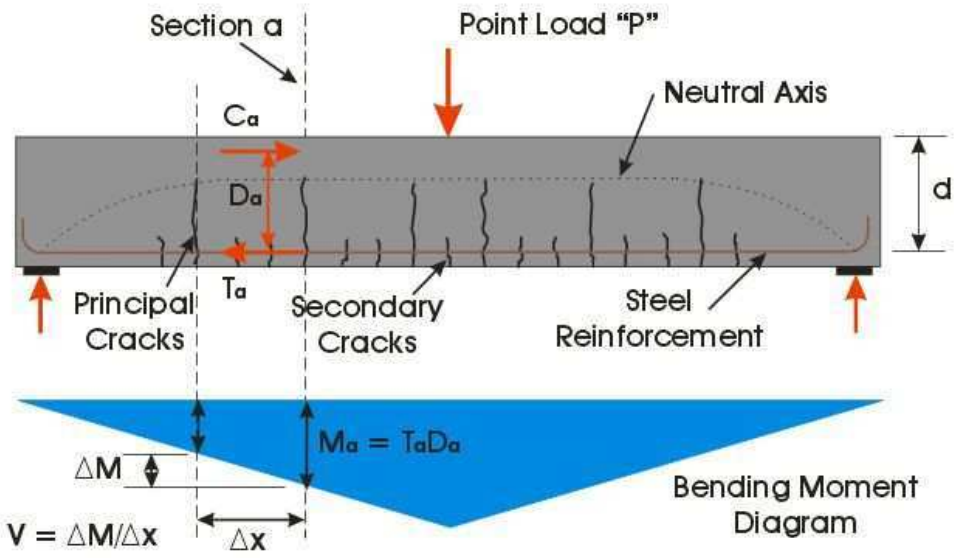

(a) Idealised simply supported reinforced concrete beam

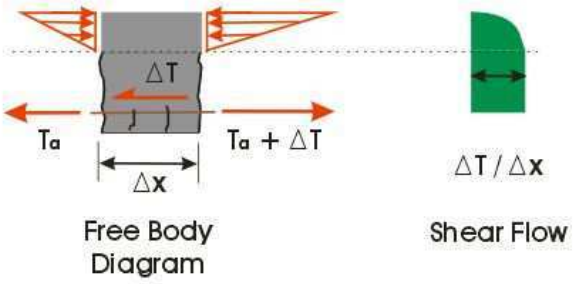

(b) Forces on a segment of beam between cracks and the shear flow induced

Figure 6-6 Idealised shear in a simply supported beam under a point load at its centre (Adapted from Collins et al. 2007)

Figure 6-6 (b) shows a free-body-diagram of a segment between two flexural cracks. The change in tension in the steel reinforcement induces a shear flow in the concrete, which is constant between the neutral axis and the tension reinforcement (the flexural tension zone). The shear flow can be found from the change in tension in the steel reinforcement similar to how the average shear force in the section is found from the change in moment. If the shear flow is divided by the width over which it acts, the shear stress in the concrete is found. In the case of this rectangular beam, the width is constant; therefore, the shear stress will also be constant in the flexural tension zone of the beam. If the magnitude of shear stress reaches a critical level, diagonal shear cracks can form. These can lead to brittle failure unless the beam contains shear reinforcement.

The critical level of shear stress decreases as the flexural cracks widen. When the cracks are narrow, shear transfers across them occurs by aggregate interlock action (also known as interface shear transfer). If the entire shear is transferred this way, the element is in pure shear as described in section 6.1.1, and the shear capacity is equal to the direct tensile capacity of the concrete. However, as this transfer of shear across the cracks breaks down, due to the cracks widening, the element is no longer in pure shear but develops bending stresses. The tension induced reduces the shear capacity. Collins et al (2007) suggest that when cracks are wide the shear capacity might be as little as one sixth of the direct tensile strength of the concrete.

The same basic theory to calculate the shear stress applies to hollow-core floor spans. Although in this case, allowance has to be made for prestressing, the irregular cross-section and the composite interaction of the precast units and insitu topping. Hollow-core units currently used in New Zealand contain prestressing near the bottom of the section, which restricts flexural cracks from forming when positive bending moments are applied. However, flexural cracks may form in a section under negative flexural actions. Figure 6-7 shows a section of hollow-core flooring near one of its support beams and a potential negative bending moment profile.

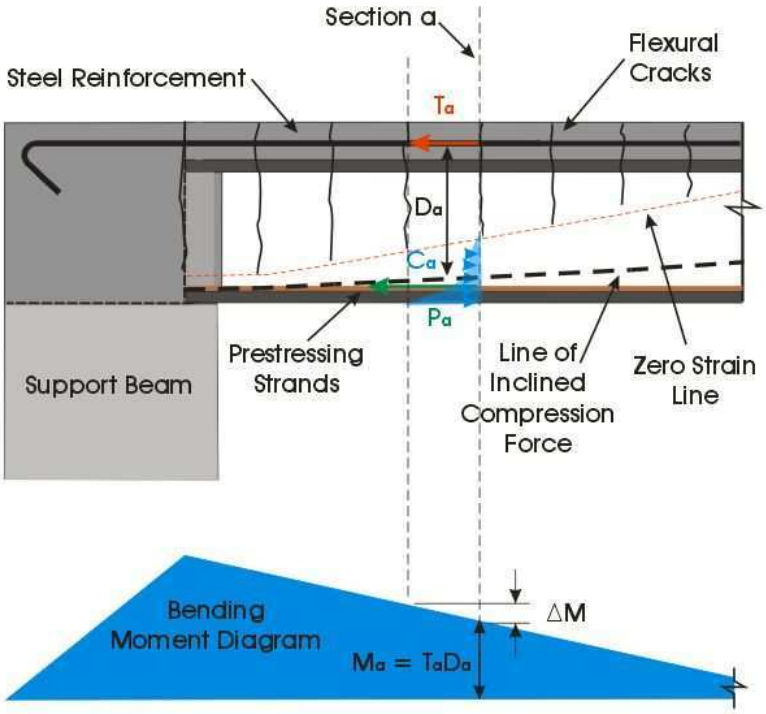

Figure 6-7 Section of hollow-core floor close to its support under negative moments exhibiting flexural cracks, forces at section "a" are shown

Like a standard reinforced concrete beam, the tension at crack locations, induced by negative flexure, is assumed to be resisted by the steel reinforcement and the change in tension (ΔT) between adjacent cracks induces a shear flow into the section, see Figure 6-8. Unlike the reinforced beam, the change in tension in the steel reinforcement is not directly related to the applied moment. This is because the lever arm from the steel to the centroid of the compression force does not remain constant. The prestressing force causes the zero strain position in the section to rise as the negative bending moment decreases, which results in the centroid of the compression forces also rising (referred to as the inclined compression force). Therefore, the shear flow induced from the change in tension force cannot be calculated from the change in bending moment alone. Figure 6-7 shows the line of the inclined compression force. For a prestressed section, the change in the bending moment is a function of both the change in lever arm and the change in tension force in the steel.

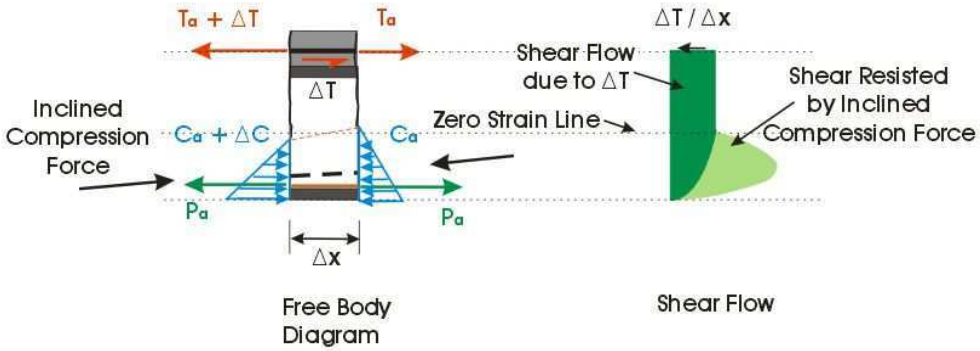

Figure 6-8 Shear flow between cracks in a section of hollow-core floor

Figure 6-8 shows a free-body-diagram of a hollow-core floor segment between two flexural cracks and the shear flow induced in that segment. The shear flow is not linear; the inclined compression force resists a large proportion of the shear. When calculating the shear stresses, by dividing the shear flows by the width over which they act, the change in width of the web, due to the voids in the hollow-core unit, must be allowed for (see Figure 6-9). In this research, the critical shear stress is defined as the maximum shear stress in the flexural tension zone; this is generally at the narrowest section of the hollow-core unit above the zero strain line. As hollow-core units do not contain any shear reinforcement, diagonal cracking can be expected to lead to failure. As mentioned previously in Section 6.1, the crack width will also influence when diagonal cracking occurs, this is not included in this assessment of "critical" shear stress; however its effect is discussed in Section 11.2. Section 6.3 details loading conditions under which a shear failure may be induced and shows the full methodology used to estimate the magnitude of shear stresses in the test completed as part of this research.

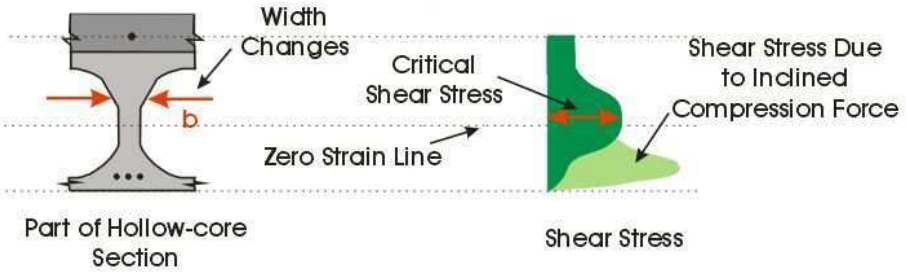

Figure 6-9 Shear stress between flexural cracks in a hollow-core floor section

6.2 Past Research and Guidelines

Shear failure, in a negative moment zone, of precast floor units is currently not explicitly mentioned in the New Zealand Concrete Structures Standard (Standards New Zealand. 2006) as a potential failure mechanism. The likelihood for this type of failure has been discussed by Fenwick et al (2004) and The International Federation for Structural Concrete (***fib***) recognise it in a bulletin titled "Special design considerations for precast prestressed hollow core floors" (***fib*** Commission 6 Prefabrication. and Fédération internationale du béton. 2000).

Fenwick et al. (2004) completed a series of simple hand analyses calculating the shear stresses where the web thickness of the hollow-core unit is a minimum. A number of loading conditions were considered. It was noted that close to the beam-floor interface, even under gravity loading, the shear strength may be exceeded. Under seismic loading, the shear strength could be exceeded out to a distance of 1.5 m from the support. The authors recommended that the issue of shear stresses in negative bending moment zones be examined in more detail.

The ***fib*** bulletin on hollow-core floors looks at situations where floors have restrained ends, resulting in negative bending moments. The guidelines recommend checking the shear strength of the floor at several locations out from the support beam interface in the negative bending moment zone. These include at a distance equal to half the equivalent depth away (d/2), at the end of the tension reinforcement and at the end of any filled cores. For the first section (d/2), no contribution from the prestress is considered and the section is assessed assuming it behaves as a standard reinforced concrete beam. The shear strength contribution from prestressing is considered for the other two locations, where both the flexure-shear cracking and web-shear cracking capacities are checked (***fib*** Commission 6 Prefabrication. and Fédération internationale du béton. 2000).

Checking for web-shear failure and flexure-shear failure in positive moment zones is part of the design criteria for precast members in the New Zealand Concrete Structures Standard (Standards New Zealand 2006). However, the concept of flexure-shear failure in a negative moment zone is not considered. The author is unaware of any experimental testing into flexure-shear failure under negative moments in hollow-core flooring.

6.3 Load Cases and Calculating the Shear Stresses Induced by these

To induce a flexure-shear failure in a hollow-core floor, it must contain negative flexural cracks. The same loading conditions that can induce a negative flexural failure (as described in Chapter 5) can induce a series of flexural cracks along a hollow-core floor. The quantity and arrangement of steel reinforcement in the topping concrete dictates which failure mode is more likely to occur.

Once negative flexural cracks are present in a hollow-core floor system, high shear stresses in a negative moment zone could produce a shear failure. These can result under load combinations including the downward vertical component of seismic motion. Section 5.2 describes two load cases, which could induce critical negative bending moments. These load combinations included; loads transferred to the floor through the supports, gravity loads and upward vertical seismic loads. If, instead of the upward vertical seismic loads, the downward vertical seismic loads are used in these combinations then, high shears are created in the negative flexure zone near the support beam. The magnitude of the downward vertical seismic load is the same as the upward vertical seismic load and can be calculated using the method described in Section 5.2. Figure 6-10 shows the bending moments induced by the individual loads (light blue) and the critical combinations. The load combinations are shown using both upward (medium blue), and downward (dark blue) vertical seismic forces. The slope of the bending moment near the support is steeper for the combinations including downward vertical loads, this results in larger shear forces. Shear force diagrams for upwards and downward seismic load combinations are shown in orange and red respectively.

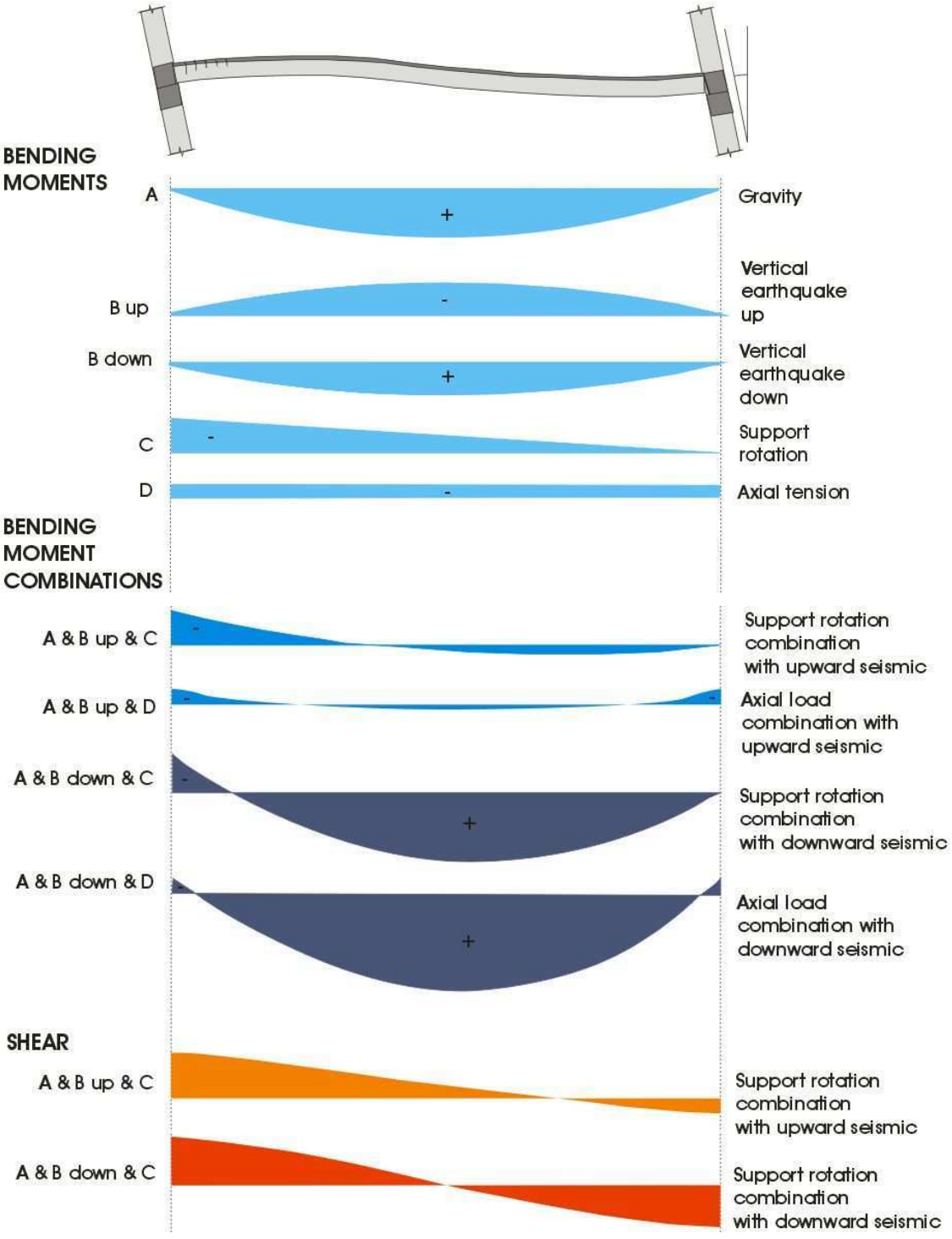

Figure 6-10 Potential bending moments and shear forces induced along a hollow-core floor

Once the critical bending moment demand has been determined, the shear stresses induced in sections along the specimen can be found. The steps to find the shear stresses induced along a section of hollow-core floor are:

- Assume a negative flexural crack spacing
- Calculate the bending moments at the crack locations
- At each crack location, find the forces in the section to resist the bending moment
- Find the shear flow induced between adjacent cracks by finding the difference between the forces induced in these sections
- Find the shear stresses in the concrete between the crack locations by dividing the shear flow by the width over which it acts.

The critical shear stress between each crack is the maximum shear stress in the concrete in the flexural tension zone, this is above the zero-strain line. Below the zero strain line, longitudinal compression reduces the magnitude of the diagonal tension force induced by shear; the shear strength is therefore higher and as a result is not critical. The following paragraphs describe each of the above steps for determining the critical shear stress.

Flexural crack spacing, along a hollow-core floor, is difficult to predict as a number of factors influence it. These include the location of transverse reinforcement, the neutral axis height of the section, the bond characteristics of longitudinal reinforcement and the relative tensile strengths of the reinforcement and concrete. Section 6.1.2 describes some of the mechanisms that affect flexural spacing and suggested that the primary crack spacing was likely to be between h_0 and $2h_0$, where h_0 is the distance between the zero strain line and the tension face of the member in flexure. In a prestressed member, the height of zero strain line, changes depending on the magnitude of moment applied to the section. Theoretically, the depth h_0 that will dictates crack spacing is when the magnitude of bending moment corresponds to the moment required to crack the concrete. This is difficult to predict however, as the tensile strength of concrete is variable.

For the hollow-core floor connection shown in Figure 6-11, the depth to the zero strain line, when a moment applied is likely to cause the section to crack, is shown as h_0. The spacing of

the transverse reinforcement is approximately $2h_0$; therefore, the flexural cracks are assumed to form at the locations of the transverse reinforcement and possibly mid-way between these.

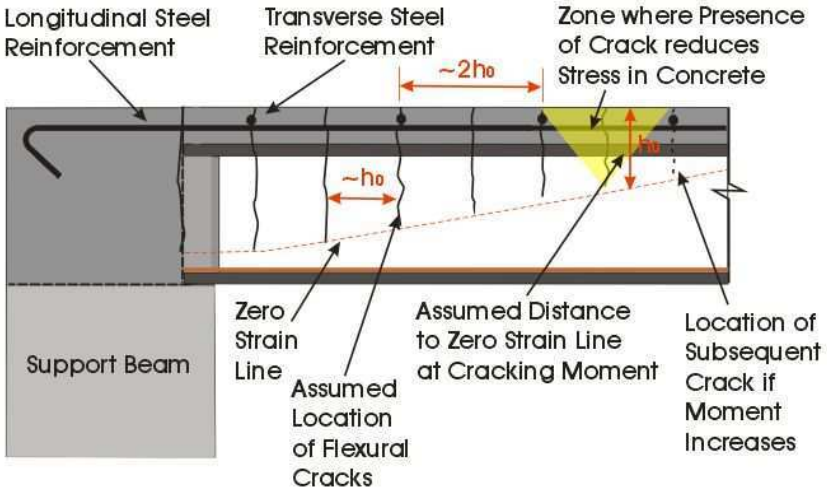

Figure 6-11 Negative flexural crack along a hollow-core floor

The next step is to find the magnitude of critical bending moment at each of the crack locations. Figure 6-12 shows a bending moment profile with the bending moments at crack locations assumed in Figure 6-11 individually specified.

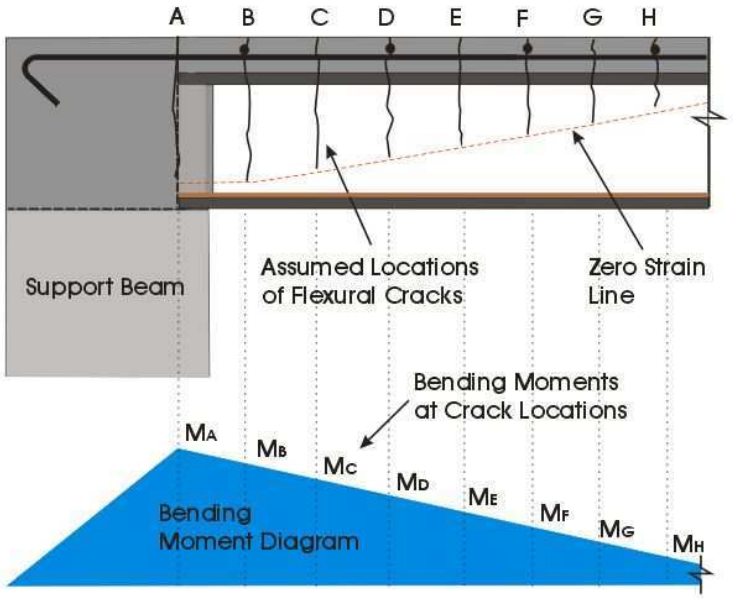

Figure 6-12 Bending moment near support beam with magnitudes of moments at the crack locations

The moment at each crack location must be resisted by the concrete and steel components of that section. The forces in each component can be calculated using standard flexural theory. In this research, a spreadsheet that allowed the neutral axis, strains, stresses and forces to be found iteratively, using equilibrium and compatibility relationships was used. Consideration was made for the development length of the prestressing reinforcement and any other change in the section, such as the quantity of steel reinforcement in the insitu topping. Figure 6-13 shows typical forces at four crack locations along a hollow-core floor (sections D, E, F and G). The tension force in the steel reinforcement (labelled "T_x") gets smaller as the negative bending moment reduces and the zero-strain line gets higher. The green forces labelled "P_x" are from the prestressing, while the forces labelled "C_x" in blue are the compression forces.

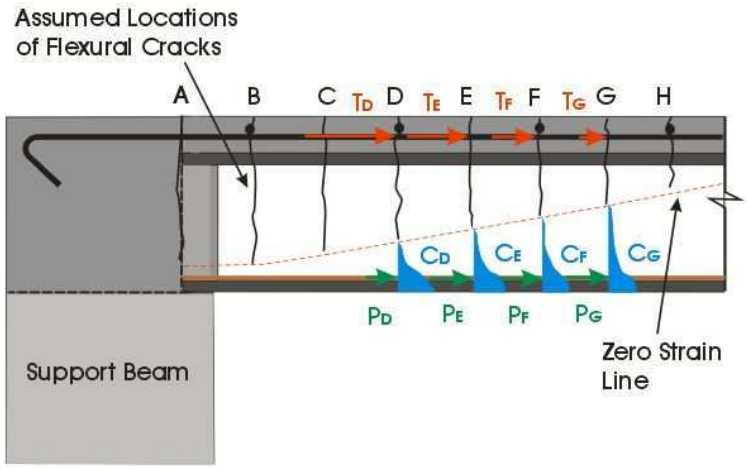

Figure 6-13 Typical forces at crack locations along a length of hollow-core floor

The shear flow (q) in the sections of concrete between cracks is the difference in forces between adjacent cracks divided by the distance between them (Δx). Figure 6-14 shows the shear flow between the cracks D and E, E and F, and F and G. The reason the shear flow labelled "q_{DE}" contains a large "jump" is because at this section the prestressing force is still developing, resulting in a difference in the prestressing force between the two crack locations.

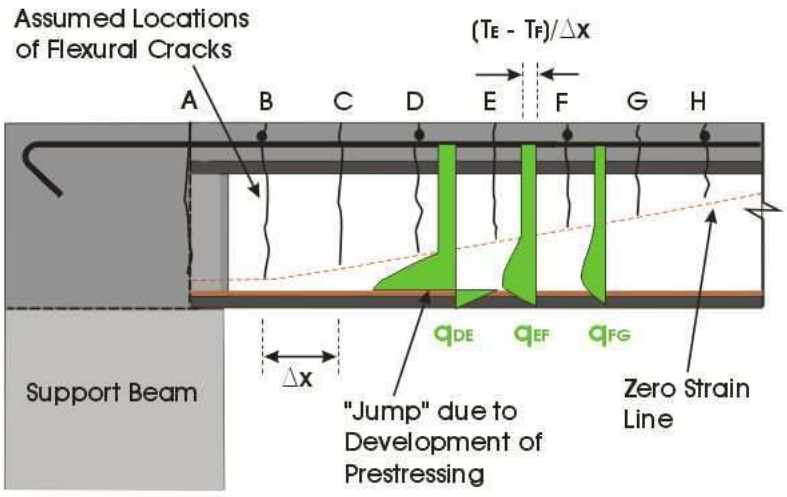

Figure 6-14 Shear flow between cracks shown in Figure 6-13

To convert the shear flow into a shear stress (v) it must be divided by the width (b) over which it acts. This width changes over the height of the section due to the changing profile of the hollow-core unit. Figure 6-15 shows the shear stresses related to the shear flows in Figure 6-14.

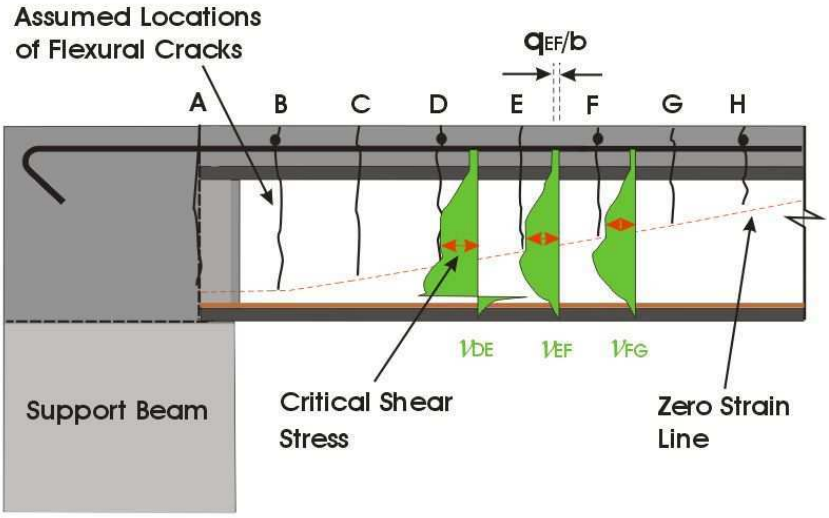

Figure 6-15 Shear stress between cracks shown in Figure 6-13

The critical shear stress was defined in Section 6.1.3 as the maximum shear stress in the flexural tension zone (above the zero-strain line); a red arrow in Figure 6-15 marks these. Below the zero-strain line, the concrete is in compression, this reduces the diagonal tensile stresses induced by shear, reducing the likelihood of shear failure. By taking this critical shear

stress from between adjacent cracks, the critical stresses along the section can be plotted. This allows a prediction to be made of where a shear failure might occur. Figure 6-16 shows the critical stresses along the hollow-core floor for the example. The critical stresses become smaller away from the support as the negative moment reduces. Where the zero strain line reaches the top of the section at around 1950 mm from the support, the critical shear stress becomes zero. The development length of the prestressing and the changing width of the hollow-core section cause the non-linearity of the critical shear stress line. As hollow-core floors in New Zealand do not contain shear reinforcement, all of the shear stress must be resisted by the shear capacity of the concrete.

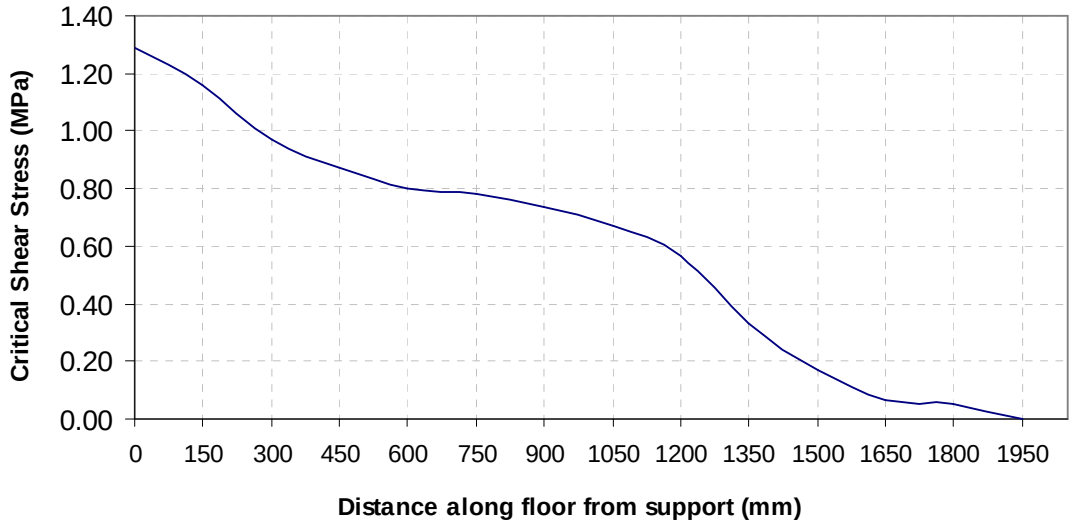

Figure 6-16 Critical shear stresses along the hollow-core floor used in the example

6.4 Capacity Predictions used for the Experiment

The insitu concrete topping of test specimen HCW2 contained high-strength, deformed bar, steel reinforcement. The bars were placed at 300 mm centres each way. A detailed description of the test setup and materials used is given in Chapter 7. It was assumed that a series of flexural cracks would form along the test specimen when a negative bending moment was applied. The crack spacing of these was assumed to be approximately 150 mm. This spacing resulted in every second crack coinciding with a bar of transverse reinforcement. In the test specimen, cracks were initiated in the topping concrete at 150 mm centres in an attempt to ensure instrumentation was positioned at crack locations.

The shear strength capacity of a hollow-core floor depends on the geometry and concrete strength of the hollow-core unit used. The New Zealand Concrete Structures Standard (Standards New Zealand. 2006) gives guidance on the allowable shear strength of concrete. Different values are provided for normal reinforced concrete members to those recommended for prestressed members. The flexure-shear capacity of a prestressed member (such as a hollow-core unit) is given by Equation 6-1 (Standards New Zealand 2006, Eq. 19-15). Where V_b is the shear resisted by an equivalent reinforced concrete beam and the second term is the shear resisted at the decompression point of the extreme tension fibre.

$$V_{ci} = V_b + \frac{V^* M_O}{M^*} \qquad \textbf{Equation 6-1}$$

As prestressing strands in New Zealand hollow-core units are near the soffit, decompression of the bottom fibre occurs at a positive moment. Therefore, as we are considering the scenario when the unit is subjected to negative moments, the inclusion of the second term decreases the shear capacity. In this case, it is appropriate to simply use the allowable shear strength for a non-prestressed member. In the New Zealand Concrete Structures Standard the shear strength provided by the concrete, $v_{c,}$ is given by Equation 6-2 (Standards New Zealand. 2006, Eq. 9-5).

$$v_c = k_d k_a v_b \qquad \textbf{Equation 6-2}$$

Where k_d is a factor between 0.85 and 1.00 to account for the effect of aggregate size. A value of 0.85 is used when the maximum aggregate size is 10 mm or less. A value of 1.00 relates to a maximum aggregate size of 20 mm or more. The aggregate in the hollow-core units used for the experimental component of this thesis had a maximum aggregate size of 13 mm. Interpolating between 0.85 and 1.00 results in a k_d factor of 0.90. k_a is a factor that takes into account the member depth. It is known that deeper members fail at lower shear stresses than shallow members, this is called the "size effect". The k_d factor equals 1.0 for members with an effective depth less than 400 mm. v_b is the basic shear stress, this is equal to the smaller of $(0.07 + 10p)\ f'_c$ or $0.2\ f'_c$, but not less than $0.08\ f'_c$. The value of f'_c, the compressive strength of the concrete, is not to be taken as more than 50 MPa. This is because in higher strength concretes, the aggregate has been observed to split and therefore does not have an increased

shear capacity. The compressive strength of hollow-core units given by the manufacture was 45 MPa; however the actual compressive strength of hollow-core units is often well above 45 MPa. A compressive strength of over 50 MPa was assumed for the hollow-core units used in the experiment; therefore, a value of 50 MPa was used in the calculation. In the equation for v_b, p is the ratio of tension reinforcement (the area for steel reinforcement in the topping divided by $b_w d$, where b_w is the minimum width of the web and d is the distance between the extreme compression fibre and the centroid of the tension steel).

Calculating the nominal shear stress capacity of the hollow-core unit used in the experiment, using Equation 6-2, gives 0.82 MPa. This is a design value and is therefore conservative. The reduction factor for shear, to find the reliable design shear stress is 0.75 (Standards New Zealand. 2006, 2.3.2.2). The nominal shear stress multiplied by 0.75 gives 0.62 MPa.

The loading protocol devised for testing specimen HCW2 is described in Section 7.3.3. The loading protocol consisted of different load combinations, each line in Figure 6-10 represents a different load combination discussed in Section 7.3.3 and is the shear stress calculated that these would theoretically induce in a hollow-core floor near one of the support beams for an equivalent 12 m span hollow-core floor. Different combinations included changing the amount of axial load and using different magnitudes of vertical seismic actions. Figure 6-17 shows the critical shear stresses, calculated using the method outlined in Section 6.3, that were predicted for several of the different load scenarios applied during the test. Abbreviated names for the load cases are given in the key for Figure 6-17 and can be matched up with the load cases described in Section 7.3.3. Measured material properties were used and the critical shear stress calculation method assumes that the specimen already contains a series of flexural cracks down to the level of the zero strain line. Many of the calculated critical shear stresses are well above the nominal code design capacity of 0.62 MPa near the support and even the unfactored nominal capacity of 0.82 MPa. It was therefore predicted that a flexure-shear failure would be observed in the test. The experimental results are given in Chapter 9, a shear failure was not observed. Possible reasons for this are discussed in Chapter 11 along with further discussion of the theoretical method for calculating the potential shear stresses such as those shown in Figure 6-17.

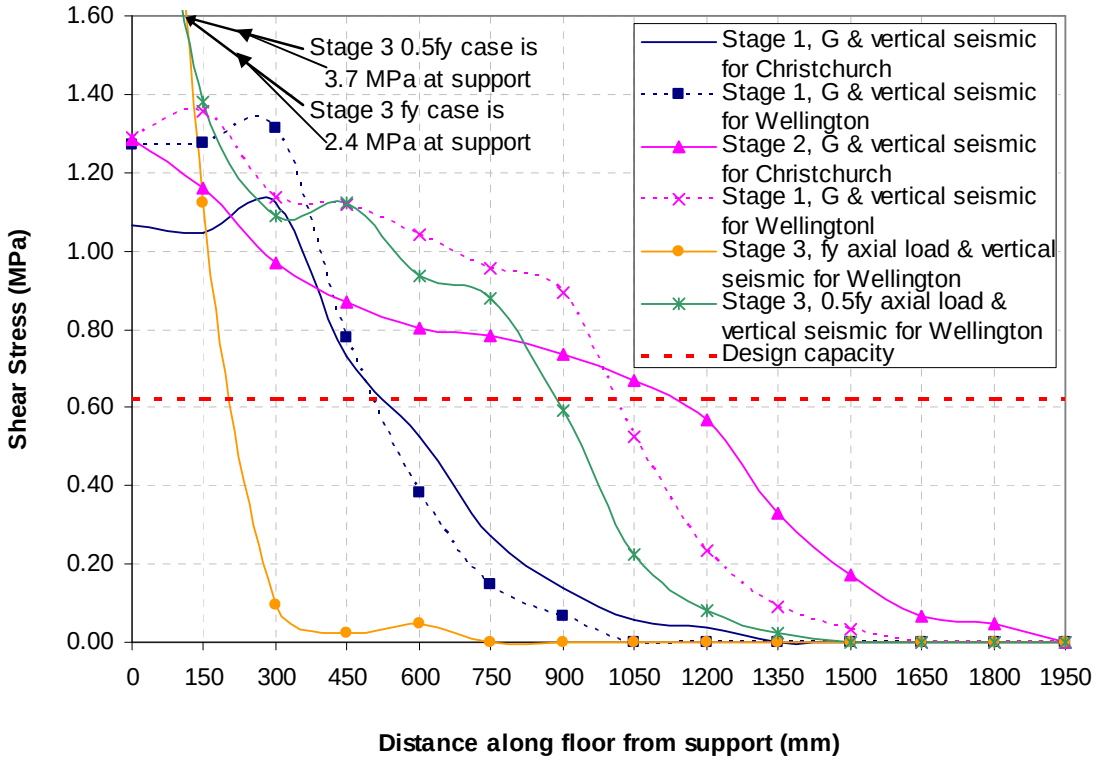

Figure 6-17 Critical shear stresses predicted along the specimen HCW2 from planned loading

6.5 References

Beeby, A. W. (1970). "An Investigation of Cracking in Slabs Spanning One Way." *Technical Report TRA 433*, Cement and Concrete Association, London.

Collins, M. P., Bentz, E. C., Sherwood, E. G., and Xie, L. (2007). "An Aduquate Theory for the Shear Strength of Reinforced Concrete Structures." Morley Symposium on Concrete Plasticity and its Application, University of Cambridge, UK.

Dickson, A. R. (1986). "The Response of Reinforced Concrete Slabs to Concentrated Loading." *Report No. 408*, Department of Civil Engineering, University of Auckland, Auckland.

Fenwick, R., Deam, B., and Bull, D. (2004). "Failure modes for hollowcore flooring units." *Journal of the Structural Engineering Society New Zealand Inc.*, 17(1), 52 - 70.

fib Commission 6 Prefabrication., and Fédération internationale du béton. (2000). *Special design considerations for precast prestressed hollow core floors : guide to good practice*, International Federation for Structural Concrete, Lausanne, Switzerland.

Park, R., and Paulay, T. (1975). *Reinforced concrete structures : R. Park and T. Paulay*, Wiley, New York.

Standards New Zealand. (2006). *Concrete structures standard, NZS3101, Parts 1 & 2*, Standards New Zealand, Wellington, New Zealand.

Standards New Zealand. (2006). *Concrete structures standard, NZS3101, Parts 1 & 2*, Standards New Zealand, Wellington, New Zealand.

7 Experimental Investigation Outline

The focus of the experimental component of this research was to demonstrate the failure mechanisms already predicted by theory, therefore validating these predictions. One sub-assembly test was performed to investigate a flexural failure in a negative moment zone (HCW1) and another to investigate a flexure-shear failure in a negative moment zone (HCW2). Different seating connections and reinforcing steel used in the topping concrete of hollow-core floors can change the type of failure expected. This chapter describes the two connection details and reinforcing steel layouts used in the two experiments. The sub-assembly test rig, loading protocol, instrumentation and limitations of the testing procedure are also described. Detailed construction drawings for the test setup, individual specimens and instrumentation layout are presented in Appendix C1 and a photographic log of construction is presented in Appendix C2.

7.1 Sub-Assembly Setup

A full-scale sub-assembly unit representing a segment of a hollow-core floor in a typical New Zealand building was used for both tests. Earlier experimental testing at the University of Canterbury into hollow-core floors used full-scale, three-dimensional super-assembly floor and frame systems (Lindsay 2004; MacPherson 2005; Matthews 2004). It was noted in these tests, that when looking at the seating connection detail of the individual hollow-core units (other than the first unit adjacent to the frame) the predominant damage causing actions were the relative rotation between the floor unit and the supporting beam, along with the longitudinal elongation of the beam parallel to the unit. It is possible to simulate these actions using a sub-assembly test rig. The first unit adjacent to the frame can not be represented in this manner; as in a real building, this unit is significantly influenced by the deformation of the adjacent beam. The performance of these perimeter hollow-core units is not investigated in this testing programme.

Sub-assembly test rigs, which incorporate both rotation and elongation actions, have been used by several researchers (Jensen 2006; MacPherson 2005; Trowsdale 2004) with results comparable to the super-assembly experiments. To create the sub-assembly, a single flooring unit, with dimensions the same as the super-assembly, is reduced to half span. This isolated hollow-core unit is then seated on a length of beam and supported at the pseudo-mid-span by

a hydraulic ram. The supporting beam is bolted to the laboratory floor enabling hydraulic rams at the pseudo-mid-span to move the hollow-core unit to simulate the relative movements between the floor and the seating beam. Casting the lower half of the two supporting beams back-to-back allowed movement between the supporting beam and the floor to be minimised as more floor bolts could be utilised. The top half of the support beams were cast at the same time as the insitu concrete topping. Figure 7-1 shows how the sub-assembly unit originates from the super-assembly.

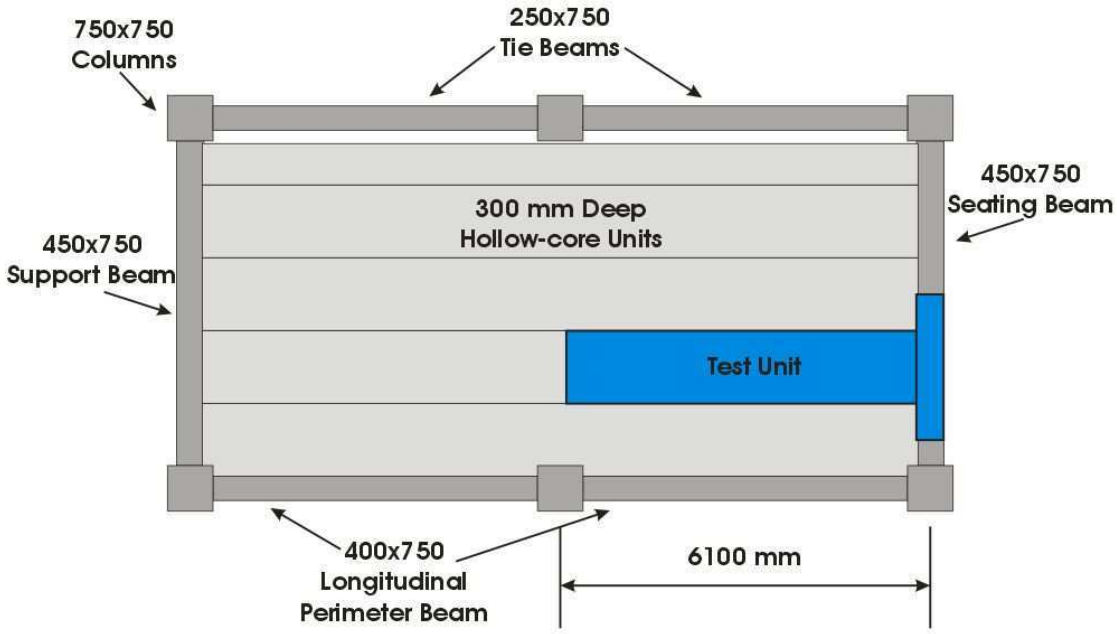

Figure 7-1 Plan of hollow-core super-assembly tests showing sub-assembly test origin (Jensen 2006)

The sub-assembly set-up used for this research was very similar to those used previously; however, an additional hydraulic ram was attached at the pseudo-quarter-span to aid simulation of vertical earthquake acceleration effects. The hollow-core sub-assembly test set-up is shown in Figure 7-2. The two vertical hydraulic rams can be used to create different bending moments and shear forces in the floor emulating those in an equivalent full-span system. These are referred to as Actuator V1 and Actuator V2. The horizontal ram (Actuator H3) imposes the effect of the floor being pulled off its support by the elongation of parallel frame beams. When discussing the test setup, the supporting beam end of the rig is the West end and the pseudo-mid-span is the East end of the test units. At the West end, where the hollow-core unit meets the support beam, is referred to as the beam-floor interface.

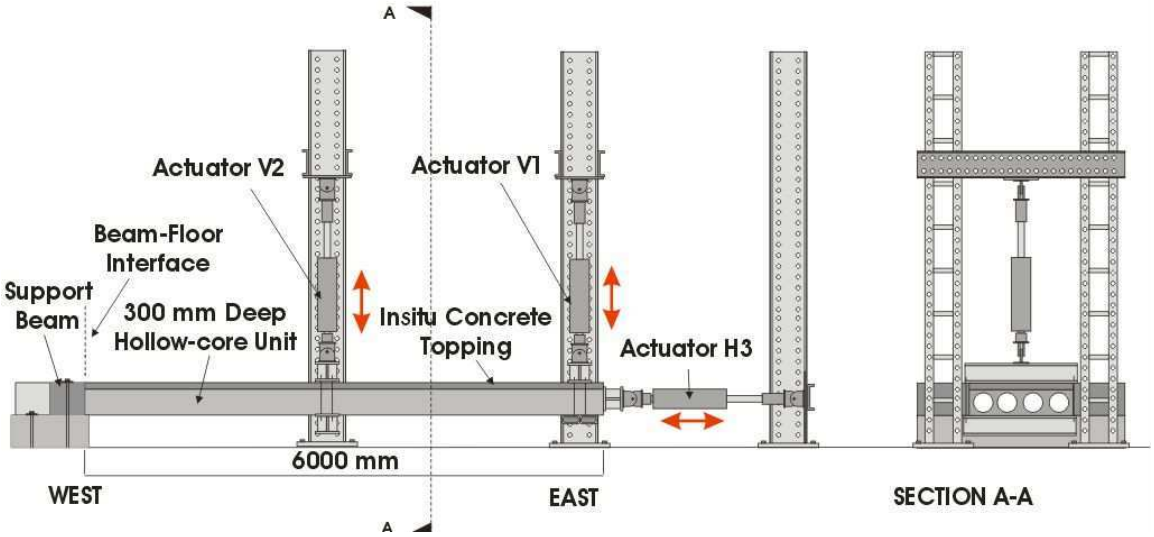

Figure 7-2 Hollow-core sub-assembly test set-up

The movements of the two vertical hydraulic rams were transferred to the specimen by steel beams placed above and below the composite floor specimen clamped together by threaded rod. The horizontal hydraulic ram was attached to a steel beam that spanned across the end of the hollow-core unit. To attach this steel beam to the hollow-core unit, the top flanges at this end of the hollow-core units were broken back to around 1000 mm. Threaded rods with steel plates attached to the ends, were then placed into the cores of the unit and bolted to the steel beam. When the insitu topping concrete was poured, the cores were filled with concrete surrounding the threaded rod, as shown in Figure 7-3.

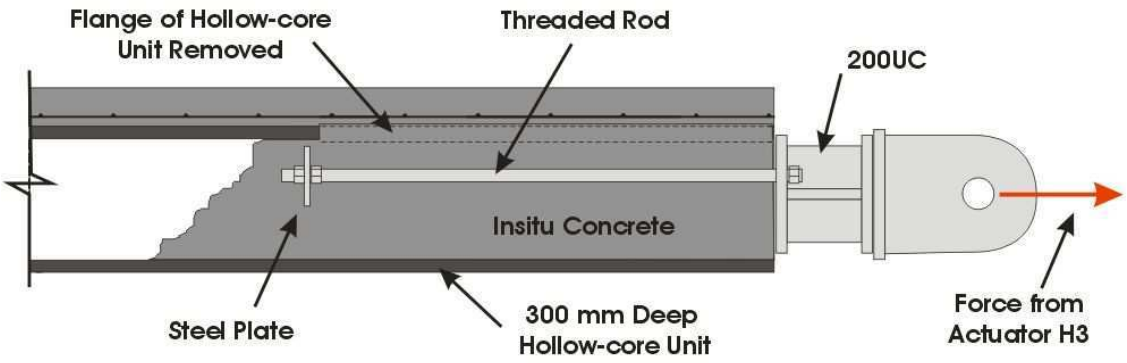

Figure 7-3 Method axial load was transferred to the test specimens

7.2 Test Specimen Details

This section describes the construction details used and the material properties of the two test specimens. The details in both test specimens were selected to represent common construction practice used in New Zealand hollow-core floor buildings. There are a wide range of construction details, and combinations of details, in hollow-core buildings; consequently, it was difficult to select a single arrangement that would represent the majority. The first test completed looked at a negative moment flexural failure; this will be referred to as test HCW1. The second test, which looked at the flexure-shear strength of hollow-core floors in negative moment regions, will be referred to as test HCW2. A photographic log of construction is given in Appendix C2.

Both hollow-core units used were 300 series *Dycore* units. These units were sourced from the Otaki Stresscrete yard in Wellington and were believed to be between one and a half and two years old when tested. The units came from an older style machine; however, the units appear to have a cross-section more consistent with the current, thicker webbed units. A comparison between the dimensions measure from the specimens and those given in product literature is given in Appendix C4. The minimum web width in the test specimens was as thick as 48 mm; it is believed that some older style units had webs as thin as 38 mm. Different webs thicknesses can change the units' performance. The thickness of the unit flanges were also greater than those specified in the product literature, resulting in the units overall depth to be around 315 mm, rather than the specified 300 mm.

Dycore units that are 300 mm deep contain eleven stress-relieved seven-wire prestressing super strands. At the base of each of the interior webs there are three 12.9 mm diameter super strands stressed to 73 % of the nominal tensile strength (73 % of 184 kN). A 11.3 mm diameter super strand stressed to 50 % of the nominal tensile strength (50 % of 138 kN) is located at the bottom of each of the exterior webs. Losses of 16 % are assumed by the manufacturer. The strand centroids were located, on average, at 37 mm up from the soffit.

7.2.1 Negative Flexure Test Specimen: HCW1

This section describes the physical arrangement and dimensions of test specimen HCW1. The connection and insitu topping details are described, and irregularities in the hollow-core unit are noted. Figure 7-4 shows the HCW1 test seating details.

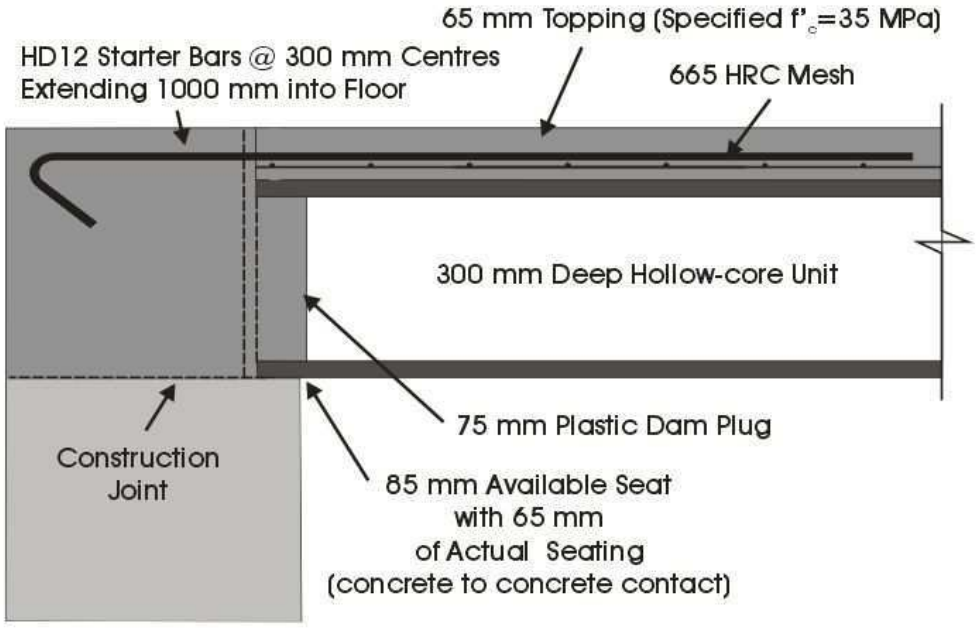

Figure 7-4 Connection detail used in test specimen HCW1

The reinforcing steel in the insitu topping concrete of test HCW1 was 665 HRC mesh. This was made from 5.3 mm diameter round bars, spot welded at 150 mm centres and was supported by 25 mm high plastic bar chairs. Deformed starter bars, with a 12 mm diameter, were used at 300 mm centres to connect the hollow-core unit to the seating beam. These starter bars were Grade 500 MPa steel. When the term "Grade" is used in reference to steel in New Zealand it is referring to the fifth percentile characteristic yield strength of the steel. Prior to 2002, the grade of steel commonly used for starter bars in this type of connection was Grade 430 MPa, but as this grade is no longer available, Grade 500 MPa was substituted. The starter bars extended 1000 mm into the floor past the beam-floor interface. The length of starter bars in existing buildings varies between 250 mm to 2000 mm. This range was observed in surveys of existing buildings in Christchurch and Wellington, which contain hollow-core flooring, made for the Department of Building and Housing (Beca Carter Hollings and Ferner Ltd 2004; Beca Carter Hollings and Ferner Ltd 2005). The starter bars were also supported on 25 mm high plastic bar chairs. The average depth of the insitu topping concrete for specimen HCW1 was approximately 60 mm. This average was calculated from spot heights taken at various locations over the specimen prior to casting. It was less than the originally planned value of 75 mm due to the unit being thicker than

expected and the camber in the unit caused by prestressing. This is a typical problem on construction sites.

In existing hollow-core floors the insitu topping concrete typically contains shrinkage cracks. Because of these cracks, and the inherent variability of its tensile strength, the tensile capacity of the topping concrete is generally assumed to be negligible. The New Zealand Concrete Structures Standard (Standards New Zealand. 2006) states that the tensile strength of concrete shall be neglected in flexural strength calculations of reinforced concrete. As the topping concrete of the HCW1 specimen was cast and then tested in a short time period, shrinkage cracks did not form. To overcome this difference between reality and the test setup, a crack was induced in the topping concrete at the end of the starter bars by placing a thin piece of Formica board at this location prior to concrete placement. The Formica was then removed once the concrete began to cure. The crack was positioned half way in between two of the transverse wires of the 665 HRC mesh. It was assumed that the strain in the mesh at the crack location would be the crack width divided by the mesh spacing (150 mm). The location of the induced crack, before and after insitu concrete placement, is shown in Figure 7-5.

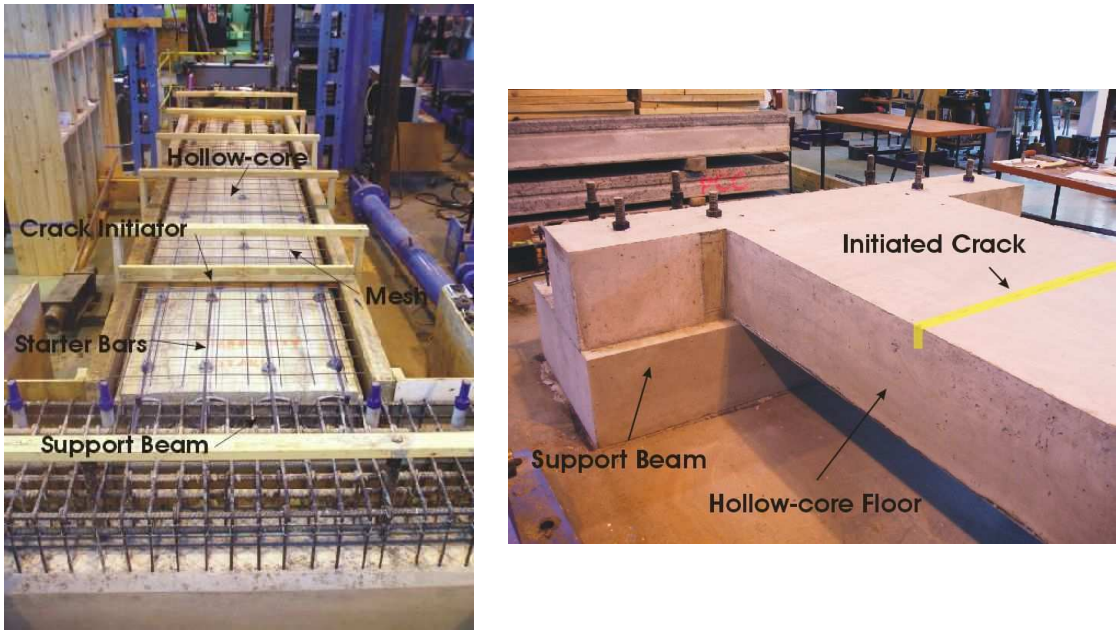

(a) HCW1 prior to concrete placement **(b) Crack induced in the topping concrete of HCW1**

Figure 7-5 Construction details of HCW1

Prior to placement of the insitu concrete topping, the hollow-core unit was inspected for defects such as web splitting. Unit HCW1 had several defects; these included, longitudinal cracks running down the top of the unit and ends that were not cut perpendicular to the unit sides. Figure 7-6 (a) shows the east end of the unit where the longitudinal cracks above the exterior cores, further down the unit they were above the first internal webs. Figure 7-6 (b) shows how when the unit was placed perpendicular to the seating beam, the north side of the unit had 70 mm seating, while the south 58 mm, this was because the end of HCW1 was not cut perpendicular to the sides of the unit. There was no visible web cracking in unit HCW1.

(a) Longitudinal cracks down top of HCW1

(b) "Skewed" end of HCW1 resulting in uneven seating

Figure 7-6 Defects in hollow-core unit HCW1

Dam plugs, 75 mm long, were used to stop concrete from entering the cores of the hollow-core unit. The unit was seated on a bare concrete ledge which followed common practice in New Zealand until the 2004 Amendment to the Concrete Structures Standard (Standards New Zealand. 2004), that requires hollow-core be seated on a low friction bearing strip.

7.2.2 Flexure-shear in a Negative Moment Zones Test Specimen: HCW2

This section describes the physical arrangement and dimensions of test specimen HCW2. The connection and insitu topping details are described, and irregularities in the hollow-core unit are noted. The HCW2 test specimen arrangement is shown in Figure 7-7.

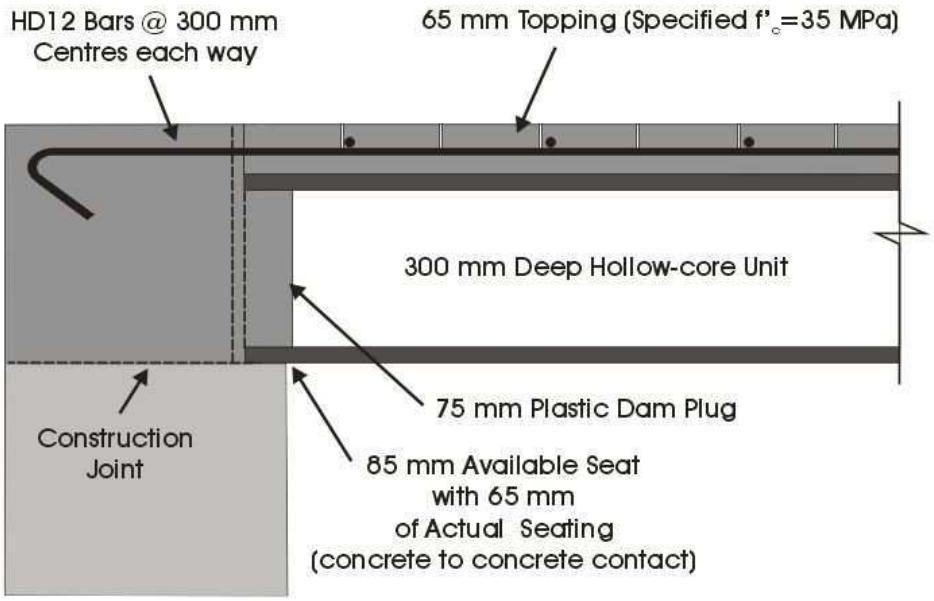

Figure 7-7 Connection detail used in test specimen HCW2

The reinforcing steel used in the insitu topping concrete of the HCW2 specimen was Grade 500 MPa, 12 mm diameter deformed bars, at 300 mm centres in both directions. The bars were continuous along the length of the floor and hooked down into the support beam. The use of continuous mild steel reinforcement in hollow-core insitu topping concrete is currently recommended in the New Zealand Concrete Structures Standard (Standards New Zealand. 2006). Grade 300 MPa reinforcement is suggested; however, Grade 500 MPa is also commonly used. The longitudinal bars were supported by 20 mm plastic bar chairs.

The loading sequence applied to this specimen was expected to open up a series of vertical flexural cracks in the topping concrete near the support beam. To assess this failure mechanism it was important to be able to measure the strain of the reinforcing steel crossing these cracks. To accurately measure the strain of steel crossing a crack, strain gauges and other measuring devices must be placed exactly over the crack. Cracks patterns in concrete are difficult to predict, so to ensure the instrumentation was correctly positioned, a series of cracks were initiated in the insitu topping concrete at predicted crack locations. The cracks were initiated by placing a steel sheet in the topping concrete down to the level of the steel reinforcement; these were removed when the concrete began to cure. As mentioned in the previous section, inducing cracks into the specimen should not have a dramatic effect on the

test. This is because older hollow-core floors would already contain similar cracks due the shrinkage of the topping concrete and the tensile capacity of concrete is often neglected in strength design.

The cracks spacing chosen to initiate cracks in the HCW2 specimen was 150 mm. This spacing was chosen considering the principal crack spacing as described in Section 6.1.2. The cracks coincided with the transverse steel reinforcement (at 300 mm centres) and mid-way between these bars. Cracks were initiated out to a distance of 1500 mm from the beam-floor interface. No crack was induced at the beam-floor interface as in tests from previous research a crack had always formed in this location with no initiator. Figure 7-8 shows test specimen HCW2 prior to the placement of the insitu topping concrete. The timber spanning across the hollow-core unit is supporting the steel plates used to initiate cracks in the topping.

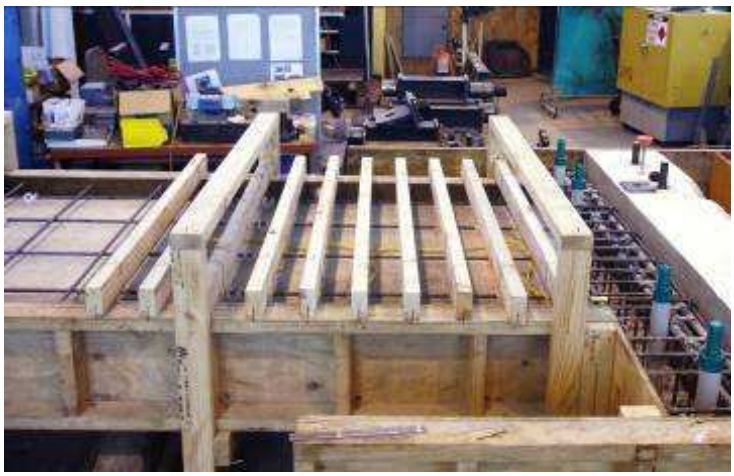

Figure 7-8 Specimen HCW2 prior to the placement of the insitu topping concrete

On inspection of the hollow-core unit used in the HCW2 test, it was noted that there was a crack in one of the central webs at one end. To avoid any weakness of the unit caused by this crack, the damaged end was placed at the East end of the test, where it would not influence the support connection. Figure 7-9 shows the extent of the crack. Similar to, but not as prominent as unit HCW1, there were some longitudinal cracks present above the exterior cores in the top of unit HCW2.

Figure 7-9 Crack in one of the webs of hollow-core unit HCW2

The HCW2 unit had 65 mm seating on a bare concrete ledge. Dam plugs of 75 mm length were used in the cores to prevent concrete from entering them at the beam-floor interface. The unit appeared to be slightly twisted along its length, once in position the south-east corner sat lower than the other corners by approximately 3 mm.

7.2.3 Concrete Properties

The properties specified for the base block beam and insitu topping concrete for both specimens were: a compressive strength (f'_c) of 35 MPa, containing 19 mm aggregate and with a 100 mm slump.

Typically in New Zealand buildings, a compressive strength of 25 to 30 MPa would be specified for the insitu topping concrete of a hollow-core floor. For the test specimens a higher strength concrete was ordered because the test specimens were representing existing hollow-core floors. When 30 MPa concrete is ordered, the supplier targets 37.5 MPa at 28 days. Aging also increases the concrete strength. Therefore, if tested today, the compressive strength of topping concrete from a ten to twenty year old building could be as high as 45 MPa. For this reason, concrete with a compressive strength of 35 MPa was ordered so that the likely strength at 28 days (the approximate time of testing) would be 45 MPa.

Standard 100 mm by 200 mm cylinders were taken from each batch of concrete delivered. These were vibrated on a shake table and cured horizontally. Table 7-1 shows the mean concrete compressive strengths (f'_c). Values were gained from standard cylinder tests performed in accordance with the New Zealand standard for testing fresh concrete (Standards

New Zealand. 1986). Cylinders tested after 28 days were cured in a fog room, those tested on test days were cured with the specimen. The test day for specimen HC1 was 34 days after casting and for specimen HC2 was 19 days after casting. All of the concrete was under strength; especially that used for the base block.

Table 7-1 Concrete compressive strength of test specimens

	f'_c (MPa)		
	28 Day	**HC1 Test Day**	**HC2 Test Day**
Base Block Beam	25.80	26.48	29.52
Topping HCW1	25.73	32.46	-
Topping HCW2	25.76	-	34.09

The manufacturer specifies that concrete used in the production of hollow-core units shall have a standard-cured 28 day cylinder strength of 45 MPa, with not more than 5 % of tests falling below this limit (Stresscrete 2007). It is believed that average compressive strengths are well above this, ranging from 60 MPa to 100 MPa. Core samples were taken from both hollow-core units once testing was complete. The compressive and tensile strengths of the cores were found using standards tests, as detailed in Appendix C5.2. Table 7-2 shows the compressive strength and direct tensile strength (calculated from the measured indirect tensile strength as shown in Appendix C5.2.). It can be seen that both specimens had compressive strengths almost twice the lower characteristic strength.

Table 7-2 Concrete compressive strength of hollow-core units used in test specimens

	f'_c (MPa)	f_{ctm} (MPa)
HCW1	87.6	6.2
HCW2	84.8	6.9

7.2.4 Steel Properties

The properties of the steel reinforcement used in the topping concrete of both specimens are shown in Table 7-3. These values were gained by carrying out standard monotonic tensile tests, the stress-strain relationships observed are shown in Appendices C5.4 and C5.5.

Table 7-3 Properties of steel reinforcement used in test specimens

	f_y (MPa)	f_u (MPa)
HD12	557	677
HRC 665 mesh	656	697

7.3 Loading Protocol

The focus of the experimental tests was to demonstrate failure mechanisms predicted by theory. It is difficult to devise a loading protocol that will adequately represent real loading scenarios. Many of the past hollow-core tests have used displacement-based quasi-static cyclic loading sequences. These were not considered appropriate for the current tests. Both the HCW1 and HCW2 tests used force-based loading protocols. This was because the critical variable in the failure mechanisms under consideration was the ultimate strength of the section, rather than the permissible deflection.

This section describes how different load scenarios were induced in the test specimens using the three hydraulic actuators. The specific loading protocols used for each specimen is then described and justified.

7.3.1 Actions Induced by the Hydraulic Actuators

As the test specimens are a half span, it is not possible to exactly emulate the forces that a full span member would experience. The failure mechanisms investigated in these tests were expected to occur near the beam-floor interface. The use of two vertical rams allowed bending moments and shear forces of a full span member to be approximated in this region. Figure 7-10 shows the bending moments induced in the member by the individual loads applied and how they can be superimposed to create a bending moment profile near the support beam consistent with one that might occur under seismic loading. At the beginning of testing it was assumed that the beam-floor interface connection performed as fixed.

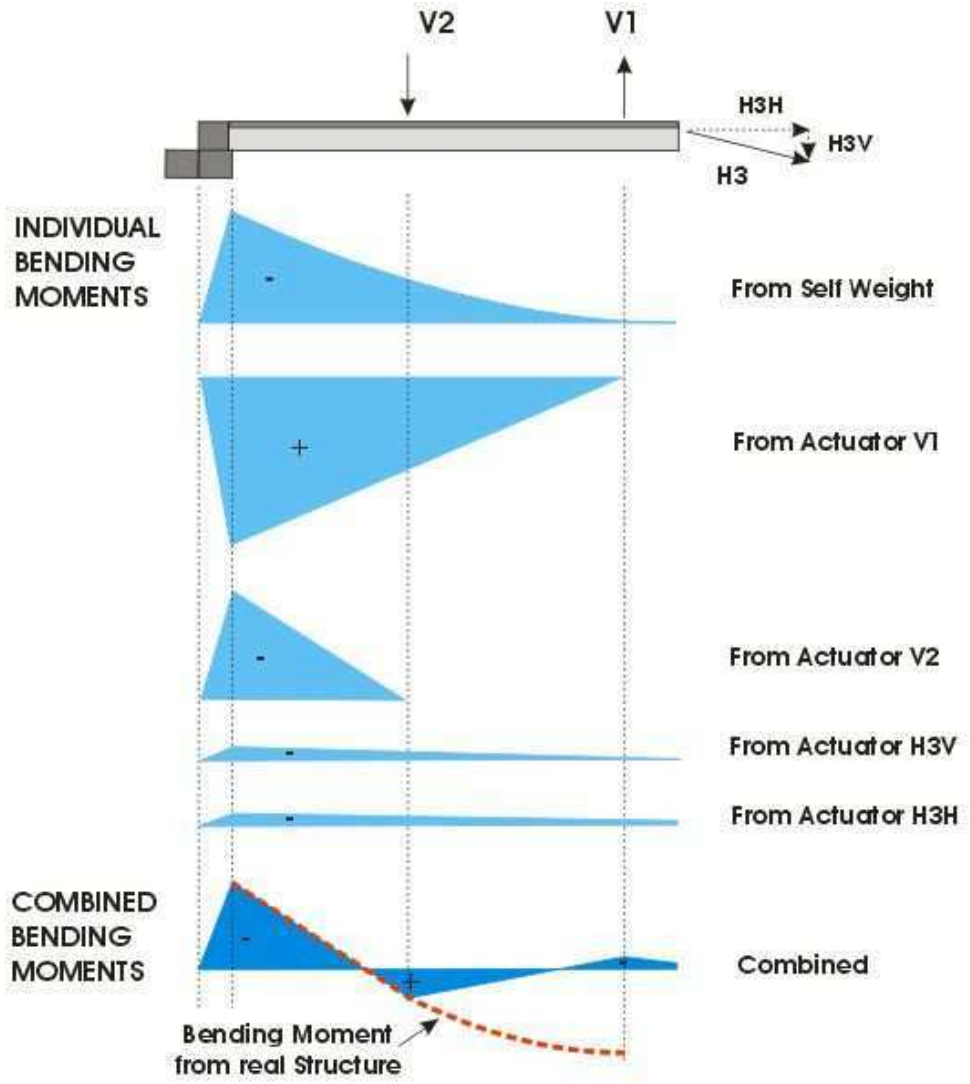

Figure 7-10 Bending moments resulting from self-weight and rams when beam-floor interface connection is fixed

The application of axial tension from actuator H3 also induced bending moments along the section as it was not connected at centre of the floor depth and its inclination changed with the deflection of the unit. An allowance had to be made for the vertical component of the load applied by actuator H3 due to its inclination. Both of the moment contributions from actuator H3 are illustrated in Figure 7-10. When axial tension is applied the fixity of the beam-floor interface connection is reduced, this is because as the floor is pulled away from the supporting beam. Figure 7-11 illustrates the forces that contribute to the moment induced at the interface; these are, the eccentricity of the tension in the starter bars (T*e) and the friction (F) of the hollow-core unit on the supporting ledge.

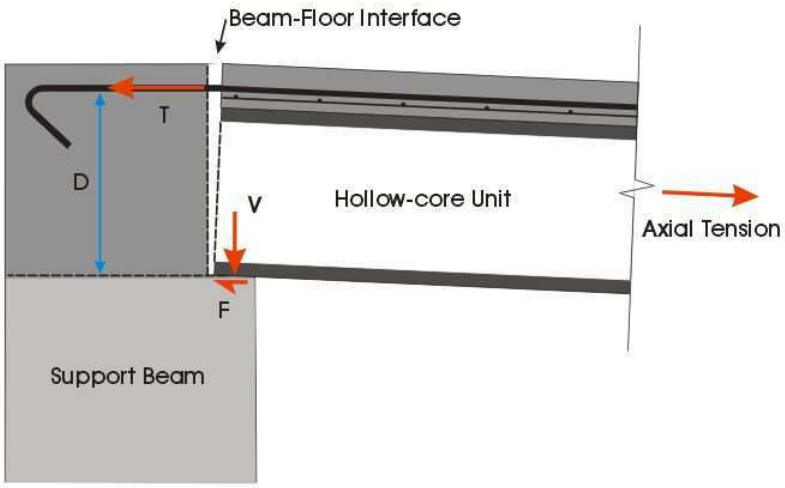

Figure 7-11 Moment at beam-floor interface in test setup when axial load applied

7.3.2 Loading Protocol for HCW1

The aim of this test was to find the negative yield moment capacity of the hollow-core section at several different axial loads. This test was not designed to emulate any specific loading conditions. Instead, the critical sections were exposed to different combinations of negative bending moment and axial load up until the steel reinforcement in the insitu concrete yielded. It was predicted by calculation that the critical section would be at the termination point of the starter bars. A three stage, monotonic force based loading sequence was proposed as outlined below. At the beginning of the test, the specimen was supported as a propped cantilever by the beam-floor interface connection at one end and the actuator V1 at the other.

- **Stage One**: The aim of Stage One was to find the negative yield moment capacity of the beam-floor interface. To achieve this it was planned to induce a negative moment in the floor by lowering actuator V1. This induces a bending moment profile in the floor that is greatest at the beam-floor interface. Once the starter bars had yielded, it was planned that the specimen would be taken back to its initial position.
- **Stage Two**: The aim of Stage Two was to find the negative yield moment capacity of the floor out from the interface with no axial load applied. It was predicted that the negative bending moment required to induce yielding in the floor section beyond the starter bars would be less than that at the beam-floor interface. Increasing the loads in the two vertical actuators at a ratio of V1/V2 = - 0.8 produces a bending moment

profile that is reasonably flat near the beam-floor interface. By increasing the loading monotonically in this manner the bending moment that would cause the mesh to yield could be found without causing excessive damage to the beam-floor interface. Once the 665 HCR mesh was observed to yield, the loads in the vertical actuators would be reduced slightly, still kept in the – 0.8 ratio.

- **Stage Three**: The aim of Stage Three was to observe the effect of axial tension on the negative yield moment capacity of the hollow-core section and therefore allow a moment and axial load interaction diagram to be plotted. Axial tension lowers the negative bending moment capacity of the section. It was proposed that from the termination point of Stage Two, where the moment at the critical section was below the yield moment of the section under no axial load, axial load would be applied until the mesh began to yield again. From this point, the moment would be reduced, and the axial load increased until another yield moment, under a different axial load, was reached. If possible, this process would be repeated several times before all loads were increased until the mesh ruptured causing failure.

7.3.3 Loading Protocol for HCW2

Flexural cracks must be induced in the negative moment region of a hollow-core floor before a flexure-shear failure can occur. Once these have formed, high shear inducing a change in the tension force in the steel reinforcement between these cracks could cause flexure-shear cracking. Therefore, to explore this failure mechanism experimentally, the loading must be somewhat cyclic; inducing high negative moments to cause flexural cracking, followed by high shear forces, in a negative moment zone, to cause flexure-shear cracking. A monotonic loading protocol like that used for specimen HCW1 can not be used. There were two seismic loading scenarios that were described in the analytical study where negative bending moments are induced in the floor;

- where a negative moment is induced at one end due to the relative rotation between the floor and supporting beam
- where a negative moment is induced at the end of the floor due to axial load and the eccentricity of starter bars.

The loading protocol developed for test HCW2 attempts to emulate both of these, as well as different intensity design levels of earthquake. Four loading Stages were planned.

- **Stage One**: The aim of Stage One was to observe the behaviour of the floor before the beam-floor interface connection had yielded. The moment at the beam-floor interface was set to that which corresponded to the tension force in the steel reinforcing bars crossing this section being half the measured force required to yield the bars (132.03 kN). Figure 7-12 shows the different bending moment profiles that were planned to be achieved during the test (dashed lines) and the bending moments in an equivalent 12 m span hollow-core floor that they aimed to represent (solid lines). First, the bending moment profile equivalent to the 12 m span gravity load was induced using actuators V1 and V2. Then, the moments caused by design level vertical earthquake actions (first for Christchurch and then for Wellington) upwards and then downwards were then applied. How to calculate the critical load combinations is detailed in Section 6.3. Only near the beam-floor interface are the bending moments and shear forces adequately represented by those produced by the actuators. However, since this is where the failure mechanism was predicted to occur, this was all that is necessary.

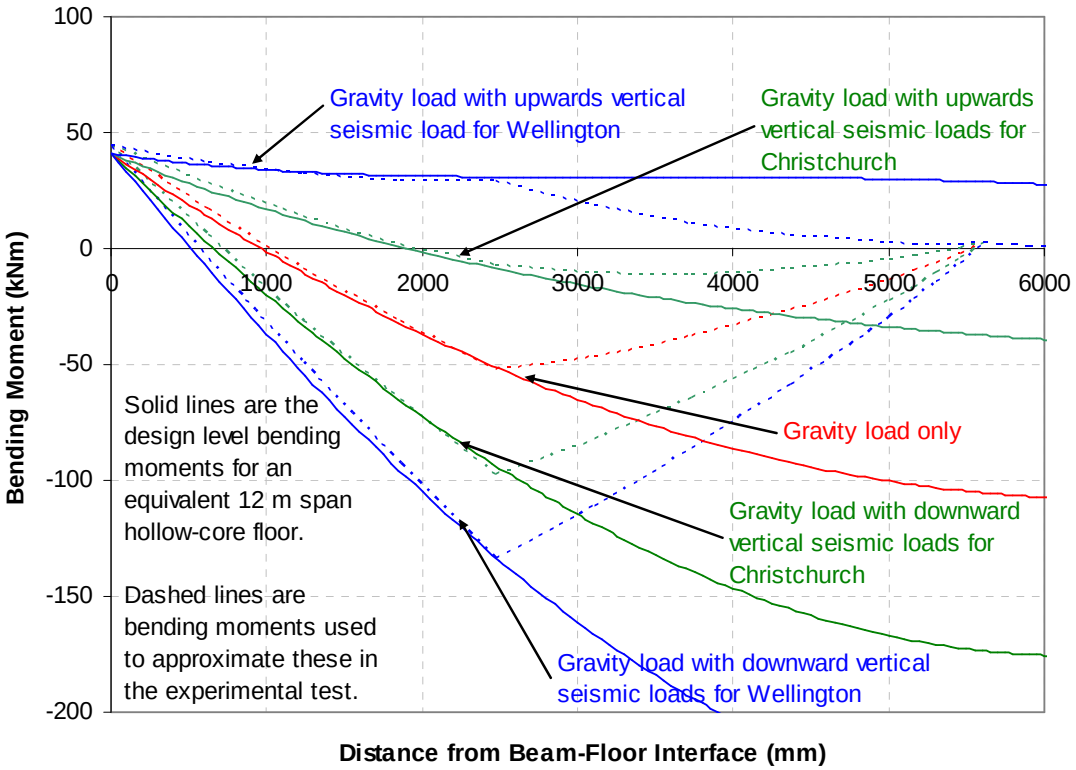

Figure 7-12 Bending moment scenarios emulated in Stage One of HCW2

- **Stage Two**: The same loading procedure as Stage One was utilised in Stage Two with the exception that the moment at the beam-floor interface was increased to the yield moment. This corresponded to the force in the steel reinforcement which crossed the section being 264.05 kN. Figure 7-13 shows the loading sequence for Stage Two.

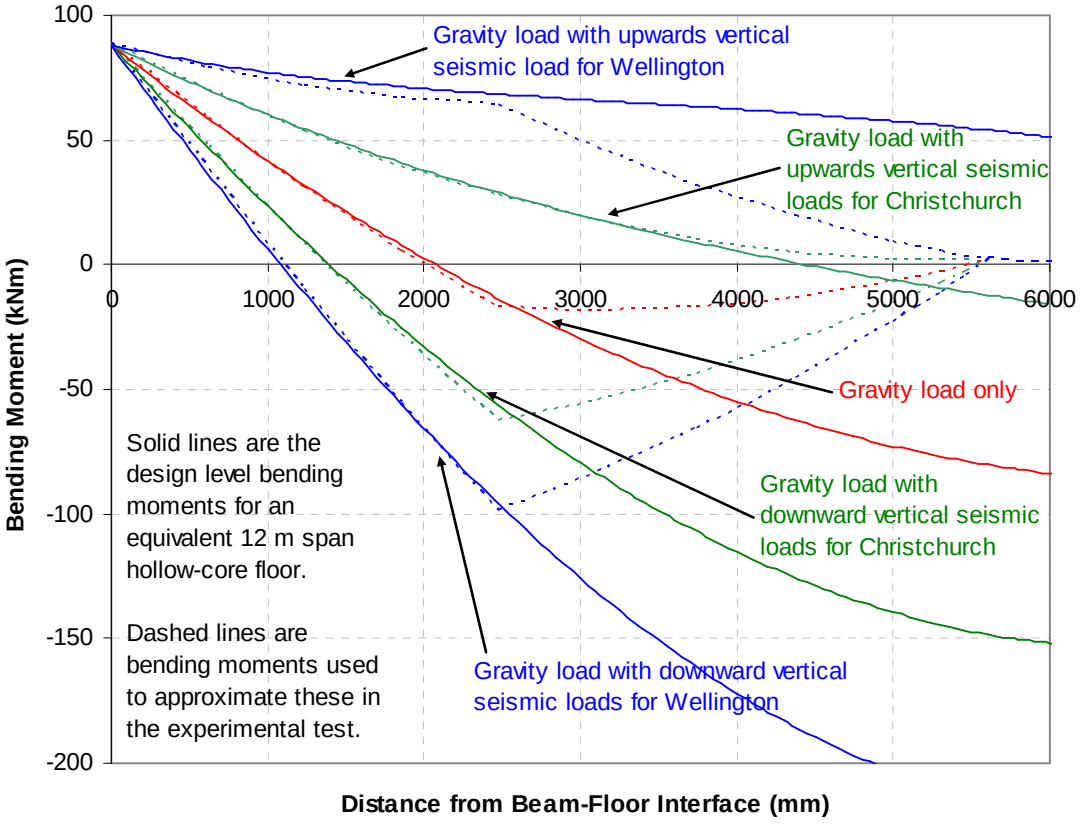

Figure 7-13 Bending moment scenarios emulated in Stage Two of HCW2

- **Stage Three**: The aim of Stage Three was to observe the behaviour of the floor when axial load was applied. An axial load of 132.03 kN (half the yield force of the steel reinforcing bars) was applied to the floor. This induced a moment at the beam-floor interface. Figure 7-14 shows the moments caused by load combinations including design level vertical earthquake actions (first for Christchurch and then for Wellington) upwards and then downwards and how actuators V1 and V2 were used to emulate them.

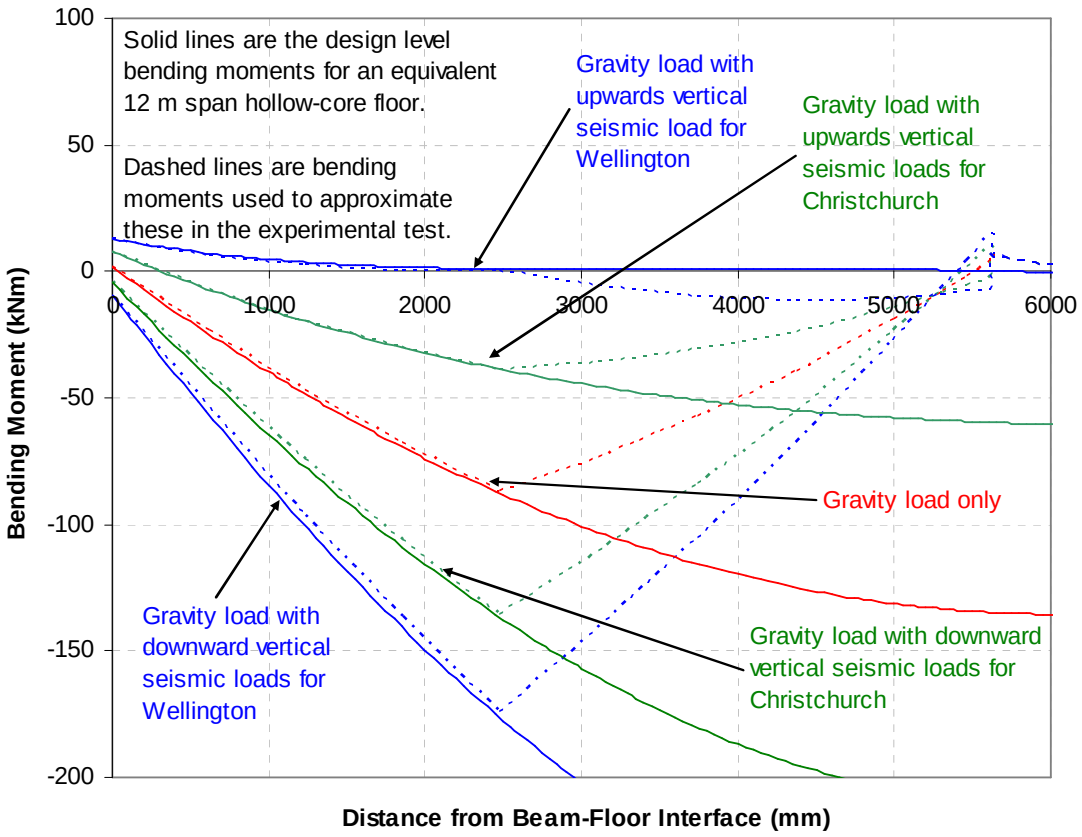

Figure 7-14 Bending moments emulated in Stage Three of the HCW2 test

- **Stage Four**: The same loading procedure as Stage Three was utilised in Stage Four with the exception that the axial load was increased to the yield force capacity of the steel reinforcing bars (264.05 kN). Figure 7-15 shows the Stage Four loading sequence.

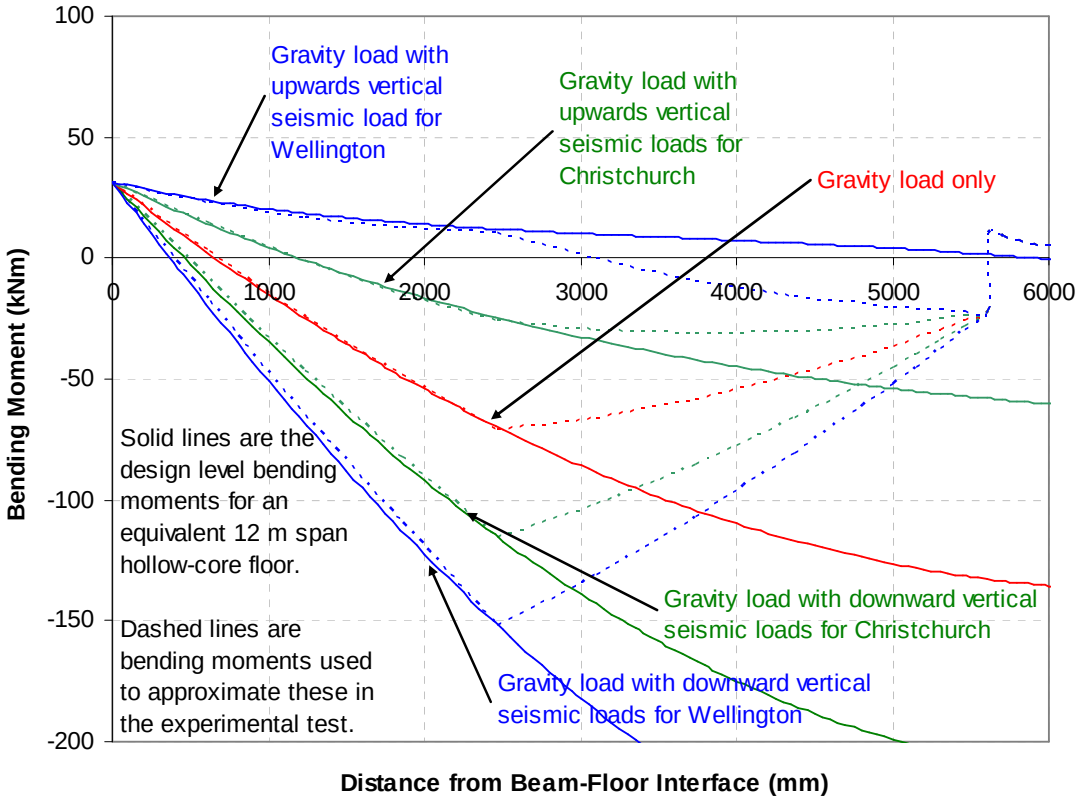

Figure 7-15 Bending moment profiles emulated in Stage 4 of test HCW2

7.4 Instrumentation

This section discusses the instrumentation used in the two tests to:

- monitor the rotation and sliding of the support beam (base block)
- monitor the relative movement between the support beam and the hollow-core unit
- determine the strain demand on steel reinforcement in the insitu topping concrete
- measure cracks induced in the hollow-core unit
- control and monitor the hydraulic actuators.

Photos of some of the instrumentation are shown in Appendix C3.

Potentiometers were used to monitor the rotation and sliding of the support beam relative to the laboratory strong floor. Figure 7-16 shows the positions of these.

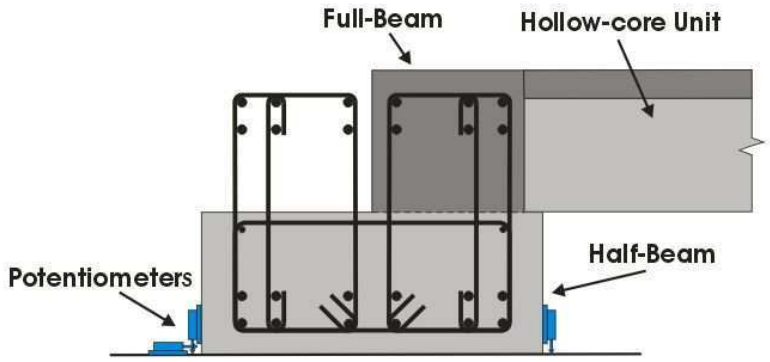

Figure 7-16 Seating beam instrumentation (Adapted from Jensen 2006)

Potentiometers were also used to measure the relative movement between the support beam and the hollow-core floor, as shown in Figure 7-17. The three potentiometers up the side of the unit were attached to the face of the seating beam and measured rotation. The potentiometers attached to the soffit of the floor and the seating beam ledge measured the "pull off" caused by axial load and vertical movements of the floor respectively.

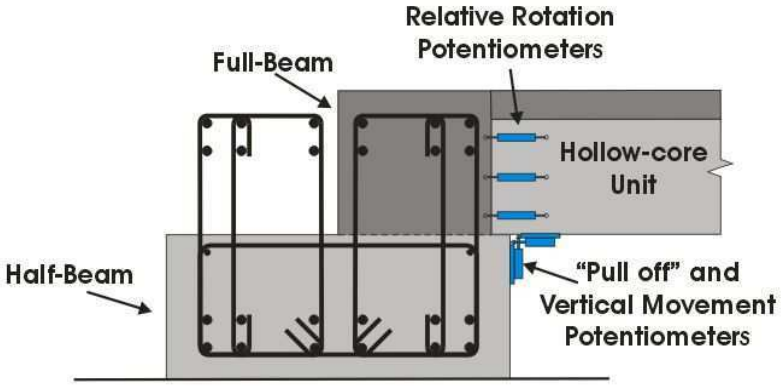

Figure 7-17 Seating beam to floor interface instrumentation (Adapted from Jensen 2006)

The majority of the instrumentation was used to monitor the strain demand on the steel reinforcement across the beam-floor interface and in the insitu topping concrete. Each test specimen had a slightly different arrangement of instrumentation and so is described separately.

In test HCW1 the sections of interest were the beam-floor interface and the location of the crack initiated at the termination point of the starter bars. For this reason, potentiometers were placed to span these sections, measuring displacement so that strain in the steel

reinforcement could be assessed. Figure 7-18 shows these potentiometers; it can be seen that those over the beam-floor interface were attached to studs welded directly to the starter bars. Small gaps were left around each coupler so that they were free to move with the steel reinforcement and not be interfered with by the surrounding concrete. The steel reinforcement which crossed the induced crack was 665 HRC mesh, couplers could not be welded to this and hence these potentiometers were attached to threaded rod drilled into the concrete topping.

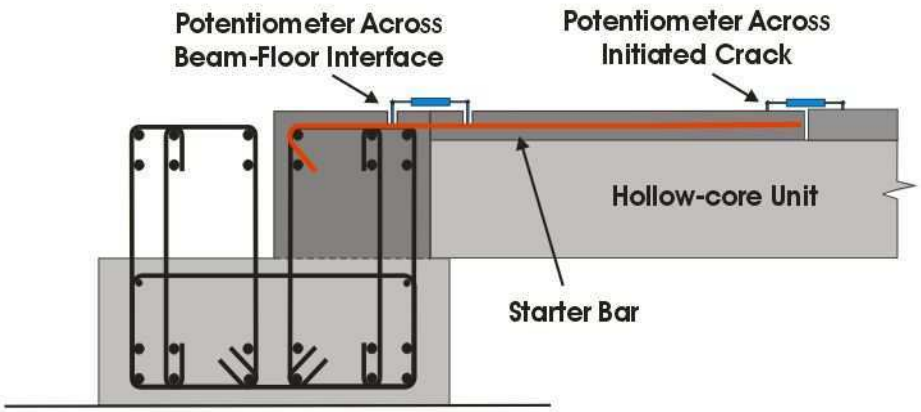

Figure 7-18 Potentiometers to determine strain in steel reinforcing in test HCW1 (Adapted from Jensen 2006)

Strain measurements were made on the top and side surfaces of unit HCW1 with Demec gauges. Demec points are small metal dots with a hole drilled into the centre. The Demec points were glued directly to the concrete surface and a measuring gauge, which uses several potentiometers and is calibrated for temperature, used to measure between the drilled centres. This method of measurement is more accurate than standard potentiometers attached to the specimen as the measurement is taken at the concrete surface. Figure 7-19 shows how in test HCW1 Demec points were glued to the insitu concrete. Demec readings allowed crack widths in the concrete to be measured and therefore strain in the steel reinforcement to be assessed.

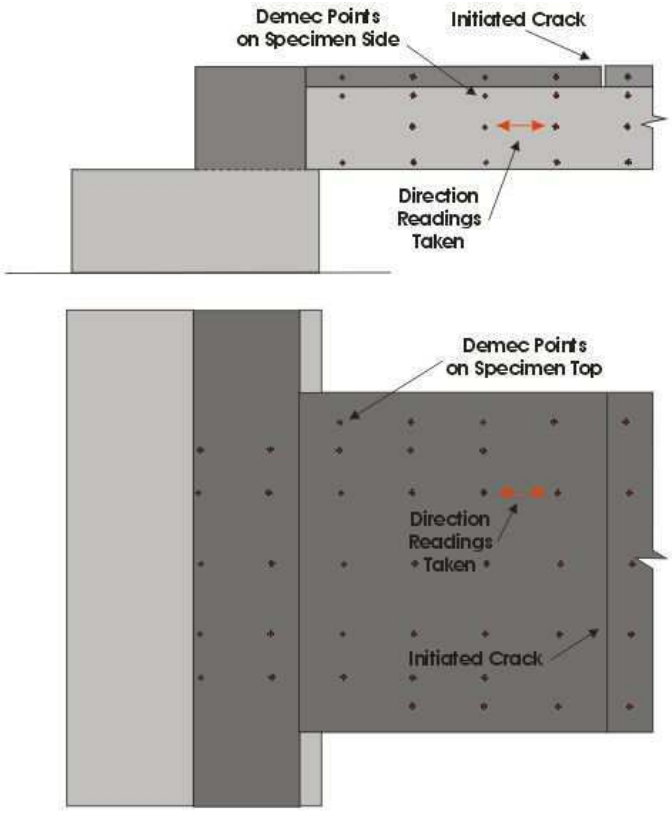

Figure 7-19 Specimen HCW1 showing Demec points

Potentiometers, Demec points and strain gauges were all used to monitor the strain demand in the steel reinforcement used in test specimen HCW2. As well as across the beam-floor interface, a line of potentiometers were positioned across the initiated cracks in the topping concrete. Figure 7-20 shows the potentiometers used to monitor the strain demand in the steel reinforcement. The potentiometers were attached to threaded rod drilled into the topping concrete and not the steel reinforcement itself.

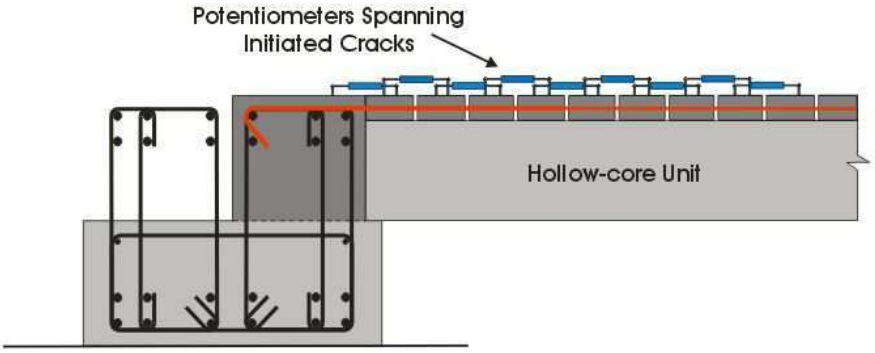

Figure 7-20 Potentiometers to measure extension of initiated cracks in test specimen HCW2 (Adapted from Jensen 2006)

Demec points were used on the top of specimen HCW2 to measure the extension of the initiated cracks. Another line of Demec points was placed down the centre of the specimen to measure overall extension and to capture cracks that formed past the initiated ones. Figure 7-21 shows the Demec point layout.

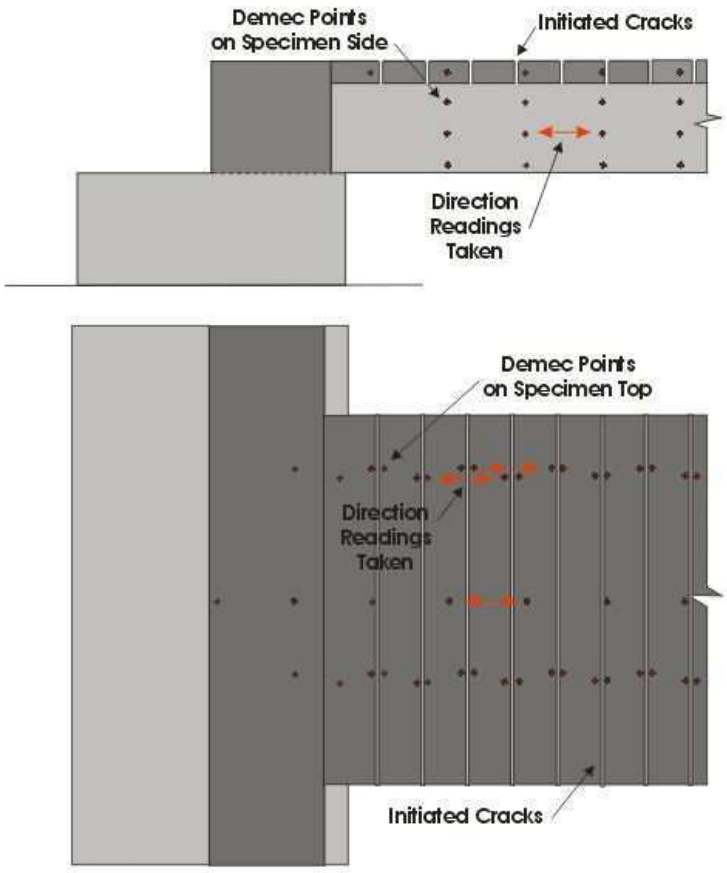

Figure 7-21 Demec point layout for specimen HCW2

Two of the longitudinal reinforcing bars were strain gauged at the locations of the crack initiators. At each location, two strain gauges were attached, one on either side of the steel bar. Placing the gauges on the sides of the bars helps reduce the effect of local bending of the bar on the strain readings. An average of the two readings at each location was taken, to give more reliable results than a single reading.

Demec points were also attached along the sides of both the test specimens to monitor any cracks that developed in the hollow-core unit. To control and monitor the hydraulic actuators,

rotary potentiometers and load cells were associated with each one. These measurements allowed the equivalent drifts and bending moment forces that were being induced in the specimens to be calculated. The rotary pots measured deflection between the hollow-core floor and the laboratory strong floor. This gave a true deflection, not effected by the possible deflections of reaction frames.

7.5 Test Setup Limitations

To create a viable test setup several simplifications had to be made. It was not practical to produce and test full-scale three-dimensional buildings under real-time earthquake loadings. By using a two-dimensional single hollow-core unit and support beam sub-assembly, several features have been neglected. This section discusses the justification behind the simplifications and the potential influence these have on the test specimens' performance.

Fenwick et al (2004) suggested the factors that influence structural seismic performance of hollow-core floors are;

- Details at support
- Stresses in unit due to; prestress, creep and shrinkage, and redistribution of stress when the insitu concrete topping is added
- Interactions arising due to elongation and deformation of beams due to the formation of plastic hinges
- Flexural deformation of supporting beams

As well as these factors, which influence the seismic performance in a real structure, the list can be extended to include factors that influence experimental tests. These include:

- Type and location of loading
- Absence of adjacent elements, such as other hollow-core units and the interactions from these.

The influence of support details on how the floor performs under negative bending moments is one of the focuses of this research. The construction details looked at in these tests are typical of construction practise used in existing buildings in New Zealand. Some of these buildings can be up to 25 years old. The test specimens did not represent the aged nature of these hollow-core floors. Over time, creep and shrinkage affect concrete. Creep and

shrinkage can cause high stresses, especially in hollow-core floors because of their prestressed and composite nature.

The effect of beam elongation was captured in the test by the application of axial loading to the specimens. However, the presence of plastic hinges in the support beam was not represented. The presence of plastic hinges could cause the seat supporting the unit to spall and the beam to have large rotations. These would be detrimental to the performance of the floor. For this reason, results from these tests should not be applied to floors seated in potential plastic hinge regions.

In a real building, the support beams are free to bend and rotate about the longitudinal axis. In the tests, the support beams were rigid and bolted to the laboratory strong floor. Relative rotations between the floor unit and support beam were applied by moving the unit. This could have had some effects on the results; however, the failure modes investigated are located out from the beam-floor interface so the effect should have been minimal.

Loading transverse to the span of the hollow-floor was neglected. However, tests using the three-dimensional super-assembly floor system by previous researchers (Lindsay 2004; MacPherson 2005; Matthews 2004) showed that the predominant damage causing mechanisms to vertical support of the hollow-core floor were relative rotation between the floor and support beam and “pull off” due to elongation of the parallel beams. Both these effects were captured in the test.

The loading applied to the specimen was in two-dimensions only and was quasi-static, hence dynamic effects are not emulated. The loads were applied as point loads, rather than the distributed loading that would be caused by earthquake accelerations. It should also be noted when interpreting the results that only two tests were performed; one looking at the negative flexure failure mechanism and one looking at a flexure-shear failure in a negative moment zone. Hence, it is not known whether the results are typical or not.

7.6 Conclusions

The experimental investigation undertaken as part of this research involved completing two sub-assembly tests on a portion of floor comprising of a segment of support beam and

hollow-core floor. The details used to connect the floor to the beam are presented, along with the material properties used. The loading procedures for the two test have been discussed along with the limitations of these. A full understanding of the test setup and loading protocol assists the interpretation of experimental results.

7.7 References

Beca Carter Hollings and Ferner Ltd. (2004). "Survey of Hollowcore usage in Christchurch." Report for the Department of Building and Housing, October.

Beca Carter Hollings and Ferner Ltd. (2005). "Survey of Hollowcore usage in Wellington." Report for the Department of Building and Housing, February.

Fenwick, R., Deam, B., and Bull, D. (2004). "Failure modes for hollowcore flooring units." *Journal of the Structural Engineering Society New Zealand Inc.*, 17(1), 52 - 70.

Jensen, J. (2006). *The seismic behaviour of existing hollowcore seating connections pre and post retrofit : a thesis submitted in partial fulfilment of the requirements for the degree of Master of Engineering at the University of Canterbury*, Christchurch, New Zealand.

Lindsay, R. (2004). *Experiments on the seismic performance of hollow-core floor systems in precast concrete buildings : a thesis submitted in partial fulfilment of the requirements for the degree of Master of Engineering at the University of Canterbury*, Christchurch, New Zealand.

MacPherson, C. (2005). *Seismic performance and forensic analysis of a precast concrete hollow-core floor super-assemblage : a thesis submitted in partial fulfilment of the requirements for the degree of Master of Engineering at the University of Canterbury*, Christchurch, New Zealand.

Matthews, J. (2004). *Hollow-core floor slab performance following a severe earthquake : a thesis submitted in partial fulfilment of the requirements for the degree of Doctor of Philosophy at the University of Canterbury*, Christchurch, New Zealand.

Standards New Zealand. (1986). *Methods of test for concrete - Tests relating to fresh concrete*, Standards New Zealand, Wellington [N.Z.].

Standards New Zealand. (2004). *Amendment No. 3 to 1995 Standard (NZS3101)*, Standards New Zealand, Wellington, New Zealand.

Standards New Zealand. (2006). *Concrete structures standard, NZS3101, Parts 1 & 2*, Standards New Zealand, Wellington, New Zealand.

stresscrete. (2007). *Precast Concrete Manual 2007, flooring specification clauses*, stresscrete, Auckland, New Zealand.

Trowsdale, J. (2004). *Seismic performance of hollowcore seating detail specified by Ammendment No 3 NZS 3101:1995 : Final Year Project, Department of Civil Engineering, University of Canterbury*, Christchurch, New Zealand.

Blank

8 Experimental Observations and Results: Negative Flexural Failure

The observed performance and behaviour of the negative moment test specimen (HCW1) is described in this section. The focus of this test was to compare the negative yield moment capacity of a hollow-core section under several different axial loads with theoretical values and to demonstrate a negative flexural failure mechanism. During the test, it was difficult to identify when the steel reinforcement commenced yielding, thus the proposed loading protocol was not strictly adhered to; of the three loading stages described in Section 7.3.2 only Stages 1 and 3 were performed. A negative flexural failure was observed during Stage 3.

This chapter presents:

- The initial stresses in, and position of, test specimen HCW1 and how these were calculated
- The behaviour of the specimen during Stage One, including when the specimen cracked and how the stiffness, bending moments, crack widths and curvature induced in the specimen changed over the stage
- The behaviour of the specimen during Stage Three. How the axial load and bending moments were varied during this stage and how these affected the crack widths, up to when the mesh ruptured and the specimen exhibited a brittle negative flexural failure.
- The key outcomes of the test

In all stages of the results section, the measured results are compared with theoretical results calculated from the measured material properties and using standard flexural theory. The main finding from this test was that the theoretical predictions of strength appear to be unconservative (the specimen failed under actions below the predicted strength). Discussion and interpretation of these test results are presented in Chapter 10, including possible reasons for the discrepancy between the observed and predicted strengths. A photographic log of testing and the raw loads and displacements at each of the actuators are presented in Appendix D.

8.1 Initial Condition of Test Specimen HCW1

The test specimen was intended to be representative of construction practice commonly used in New Zealand throughout the 1980s and 1990s. Figure 8-1 shows the connection detail used. A full description of the experimental setup is given in Section 7. At the beginning of the test the floor unit was level, held up by the support beam at the West end and actuator V1 at the East end (see Figure 8-2). Testing took place 34 days after the insitu topping concrete was placed. At an age of 34 days the concrete shrinkage experienced by the topping is approximately 50 % of what the shrinkage would be after one year. This was calculated by taking twice the shrinkage predicted by CEB-FIP recommendations, as suggested by Bryant (Bryant et al. 1984). Because of this, shrinkage cracks similar to those seen in existing concrete structures were not pronounced, but some were visible. A crack was initiated in the topping concrete, across the floor unit at the end of the starter bars when the insitu concrete was placed. The presence of the crack allowed the tensile capacity of the insitu topping concrete to be neglected, as would be the case if the specimen was older and contained shrinkage cracks. Initiating the crack also allowed instrumentation to be located so that it spanned the crack and measurements could be taken of its development.

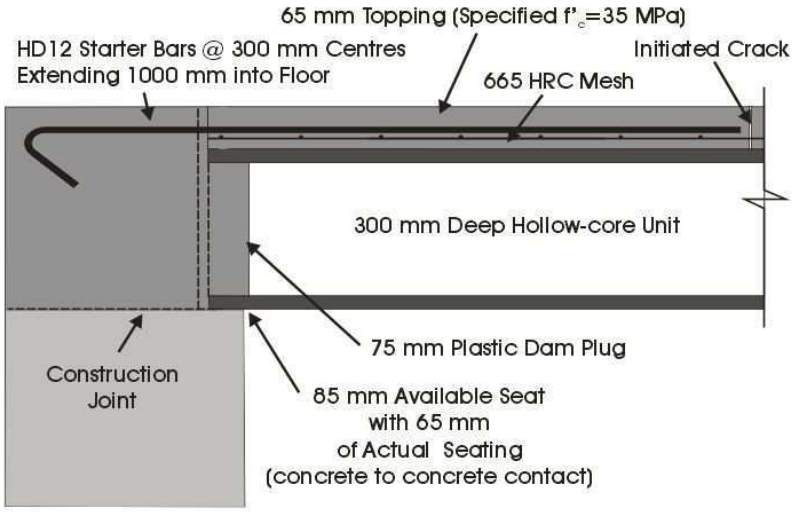

Figure 8-1 Connection detail used for test specimen HCW1

Before placement of the insitu topping concrete, the hollow-core unit acted as a simply supported member. Shrinkage of the insitu topping concrete, after placement, could have changed support condition at the West end. Theoretically, by knowing the weight of the floor and the reaction at actuator V1, the fixity moment at the West support can be determined.

Figure 8-2 illustrates this by showing the reaction at actuator V1 when the West end is fixed and when it is simply-supported. The reaction recorded in actuator V1, when the floor unit was in its initial position, was 26.7 kN. This suggests that the system acted as a simply supported span; however, there are uncertainties associated with this assumption. The self-weight of the specimen was not measured, but calculated from assumed material densities and volumes of concrete, as shown in Appendix C6. There is also uncertainty in the accuracy of readings taken from actuator V1; this reading could have an error of ± 1 kN.

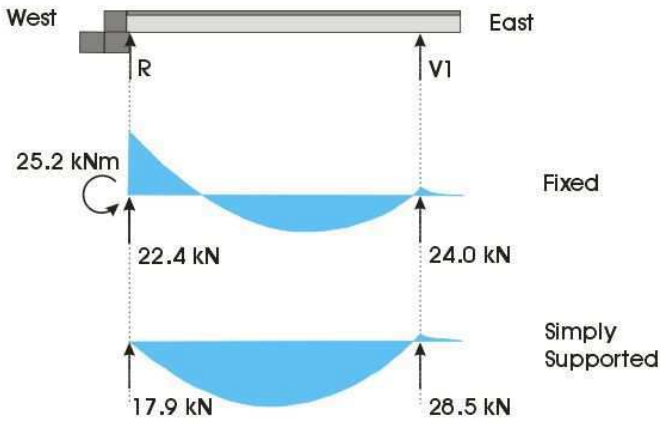

Figure 8-2 Possible bending moments and reactions induced in specimen HCW1 under self weight

8.2 Stage One HCW1: Lowering Actuator V1

Stage One of the loading protocol involved lowering actuator V1 monotonically. V1 was lowered from its initial position, to a maximum displacement of 37.5 mm from this point. Lowering actuator V1 induced a negative moment in the floor unit. It had been predicted that during Stage One the beam-floor interface would rupture. Once this had occurred, the intention was to continue loading until the starter bars at the interface yielded. The specimen did not behave as predicted; instead of only the beam-floor interface cracking, the hollow-core unit cracked at two other locations along the specimen. This is shown in Figure 8-3. The cracks, labelled “A”, “B” and “C”, developed in that order. Crack A was at the beam-floor interface, at this location the starter bars were the only steel reinforcement in the section. Crack B formed 530 mm out from the floor-beam interface; at this point the topping concrete contained both the starter bars and the mesh reinforcement. This location was also beyond the length of hollow-core floor unit assumed to be effected by the development length of the prestressing strands. Crack C occurred at the location of the initiated crack in the insitu

topping concrete. This location was the point the starter bars ended; consequently, the topping concrete contained only the mesh reinforcement.

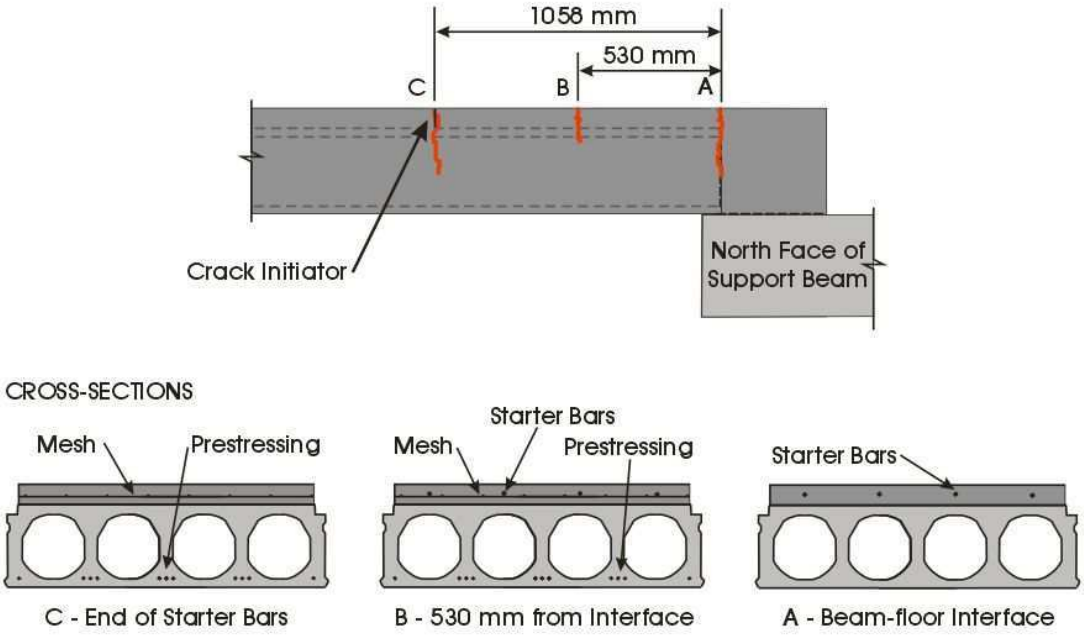

Figure 8-3 Locations cracks formed during Stage One of test HCW1 and cross-sections of the specimen at these locations

This section presents the data obtained during Stage One of the test and compares it with theoretical predictions. Items presented include:

- The stiffness of the specimen and how this changed when the specimen cracked
- The visual performance indicators
- The bending moments induced along the section and how these compare with the theoretical first yield moment
- A record of crack widths
- The curvature induced in the specimen.

The loading protocol was displacement controlled. Figure 8-4 shows the force in actuator V1 versus its displacement (the amount actuator V1 was lowered). The jumps in the graph labelled A, B and C coincide with the points during the loading protocol where the specimen cracked. The slope of force-displacement graph is the stiffness of the specimen. The initial stiffness, K_1, is 1.33 kN/mm. The theoretical stiffness, calculated from the specimen geometry and material properties, is 1.7 kN/mm. After the beam-floor interface cracked (at the point

labelled A), the stiffness reduced by more than 50 % to 0.60 kN/mm. After the second crack (B), the load dropped but the stiffness remained constant. When the specimen cracked at the end of the starter bars (C), the load in actuator V1 dropped again and the stiffness of the specimen reduced to 6 % of the value of initial stiffness. This suggests that the specimen was yielding as displacement is occurring under very little additional load. The blue data points, numbered 1 to 16 on Figure 8-4, are the increments during the test used in subsequent figures to represent a consistent "duration of test" scale. Generally, these were times when sets of Demec readings were taken.

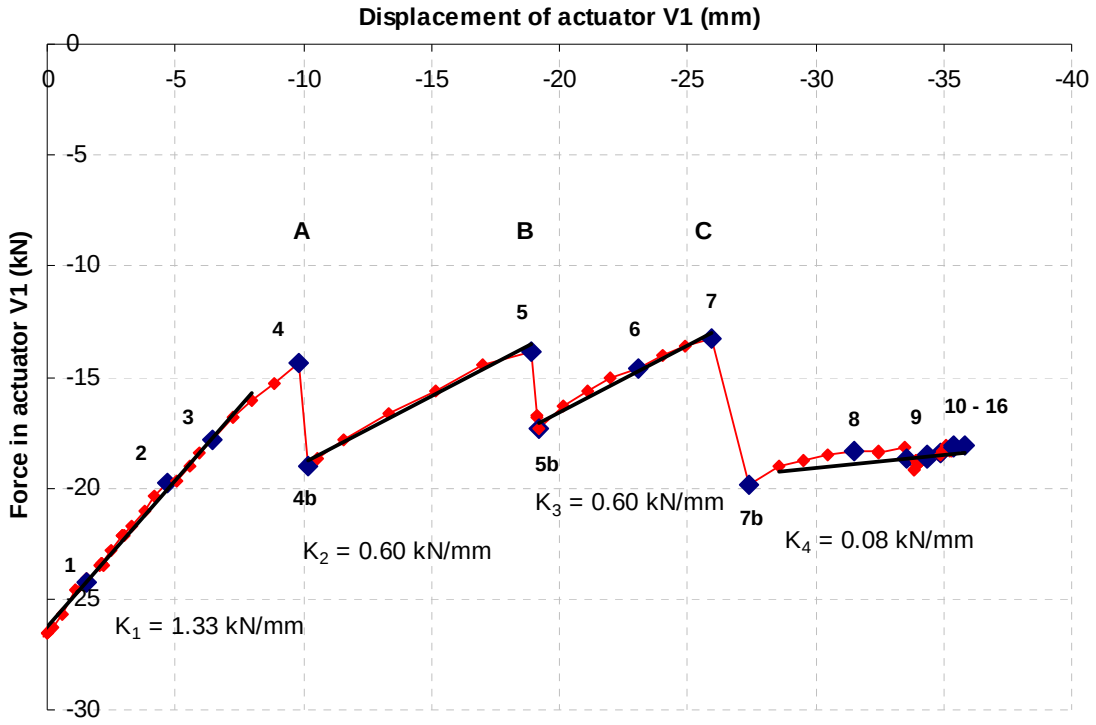

Figure 8-4 Force versus displacement of actuator V1 during Stage One

Until increment number four, only small flexural cracks were observed in the topping concrete. The first of these occurred at 100 mm from the beam-floor interface, it is likely that the topping concrete delaminated from the hollow-core unit between the beam-floor interface and this location. When the beam-floor interface cracked, shown in Figure 8-5 (a), the insitu concrete extending 75 mm into the cores of the hollow-core was broken off at the interface. Figure 8-5 (b) shows increment five, where the hollow-core unit cracked at a location 530 mm from the beam-floor interface. The hollow-core unit cracked at the end of the starter bars

(1058 mm from the beam-floor interface) at increment seven. Figure 8-5 (c) shows this crack. Although two cracks are seen in the photo that spread out diagonally from the initiated crack, this was merely how the crack propagated through the insitu concrete poured down the side of the hollow-core unit, the crack in the hollow-core unit itself was vertical. Figure 8-5 (d) shows the specimen at the end of Stage One, flexural cracks formed in the insitu concrete out to around two metres from the beam-floor interface, but only the cracks mentioned above extended down into the hollow-core unit. A more detailed photographic log of testing is shown in Appendix D 1.

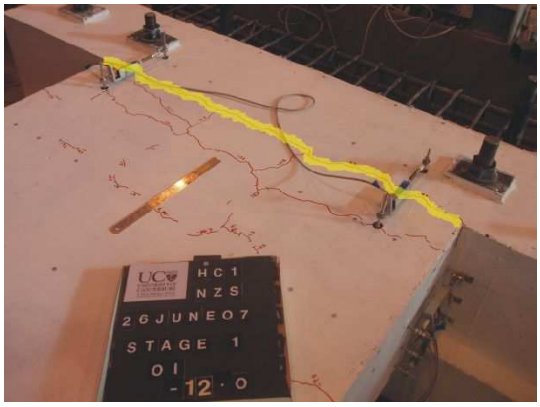

(a) Increment 4 - beam-floor interface has cracked

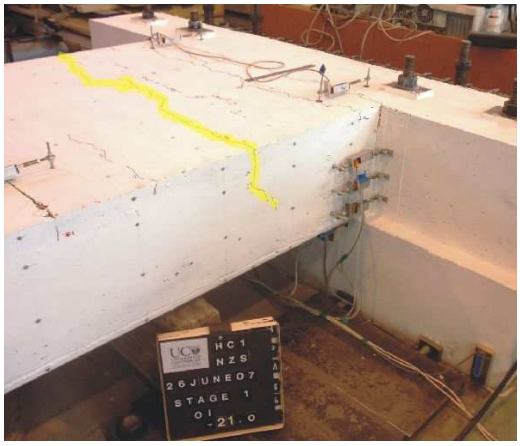

(b) Increment 5 – unit has cracked 530 mm from the beam-floor interface

(c) Increment 7 – hollow-core has cracked at the end of the starter bars

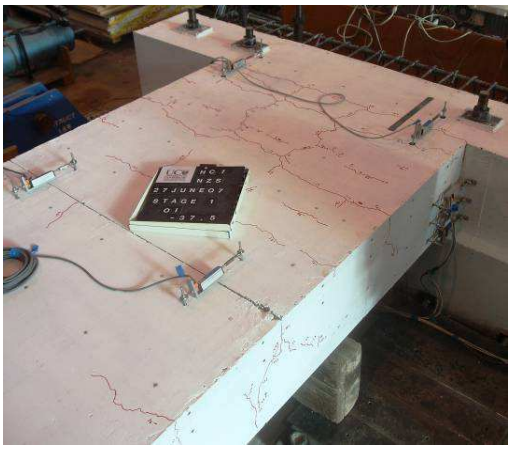

(d) End of stage one

Figure 8-5 Specimen HCW1 during stage one of testing

Each time the test unit cracked, the stiffness reduced causing the force at actuator V1 to increase. This is illustrated in Figure 8-6 where the bending moment profiles along the specimen are shown immediately before and after the beam-floor interface cracked. The displacement of actuator V1 is the same for the two profiles shown. The bending moment induced at different locations along the test unit was calculated from self-weight of the test unit and the load recorded in the actuator V1. Both of these values had uncertainties associated with them; consequently, the bending moments shown have a maximum error of ± 16.8 kNm at the beam-floor interface (derivation shown in Appendix D3), but the shape and trends are correct.

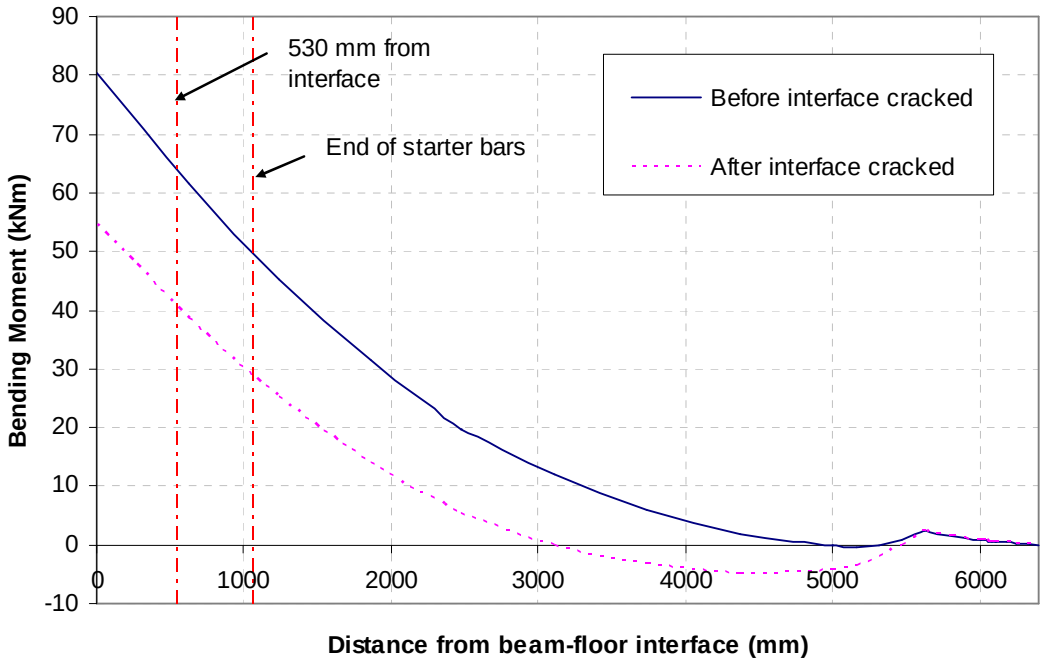

Figure 8-6 Distribution of moments along specimen before and after beam-floor interface cracked (increment 4)

Figure 8-6 is useful as it shows us the distribution of bending moments along the length of the specimen. However, this is only for two discrete times during the test, how the magnitude of the moments change over the duration of the test are not illustrated. Figure 8-7 shows how the bending moment, at the three crack locations, changed during Stage One of the loading protocol. Each line on the graph represents one of the crack locations. The vertical axis is a normalised bending moment (M_t/M_y). Where M_t is the bending moment induced during the test at a particular section along the floor, calculated as described in the previous paragraph,

and M_y is the first yield moment at the same section (this is the moment predicted to yield the reinforcement in the insitu topping at the section of interest in a cracked section). The first yield moment predictions were calculated from the measured geometry and average material properties gained from laboratory tests, not design values. The assumption that plane sections remain plane was used. The M_t and M_y values are unique for each of the crack locations. If the normalised bending moment (M_t/M_y) is equal to one at a cracked section, it would suggest that the steel reinforcement in the topping of this section is yielding. The horizontal axis represents the duration of the Stage One. The increments are not time, merely key points during the test and the numbers correspond to those shown on Figure 8-4.

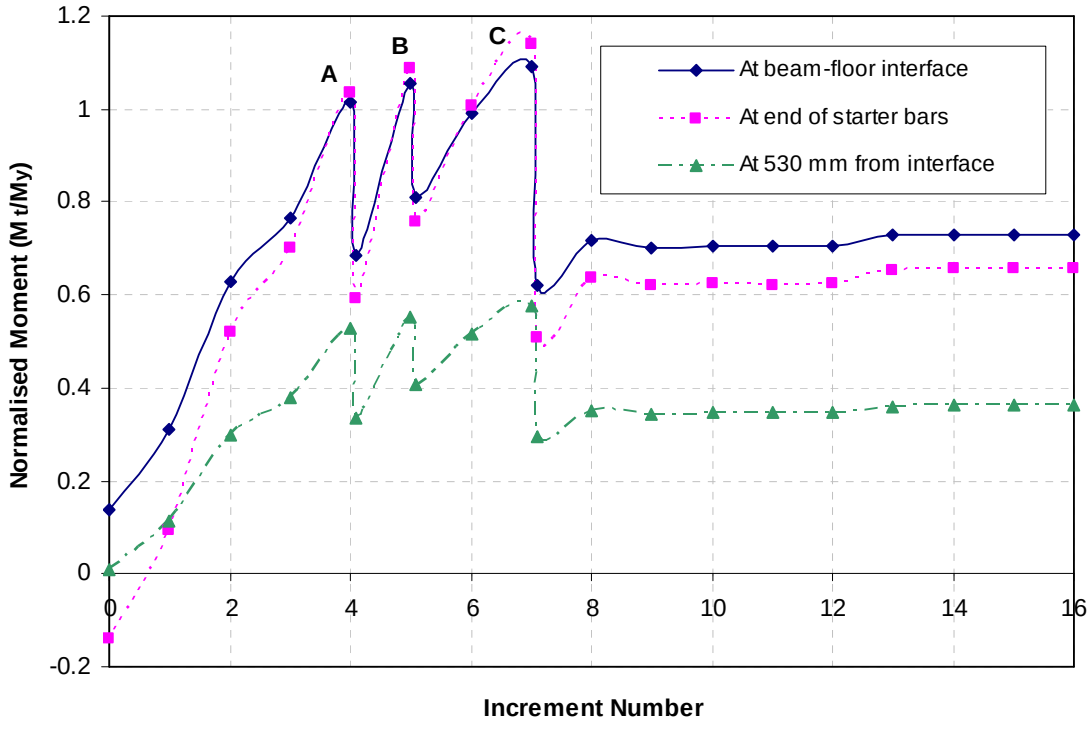

Figure 8-7 Yield moment during Stage One at the three crack locations

Figure 8-7 shows three drops in bending moment in the specimen, these correspond to the specimen cracking and the load reducing in actuator V1. It appears that the beam-floor interface is yielding at increments five and seven. However, when looking at the measured crack widths, shown later in Figure 8-8, this is probably not the case. After increment eight, further lowering of actuator V1 increased the moments only slightly before they became reasonably constant. This slight increase could be due to the change in length of the internal lever arm. It appears that a section along the specimen had yielded even though the bending

moments are below the predicted first yield moment (neither the green or pink line rise above 1 once their respective sections have cracked). By looking at the crack widths (in Figure 8-8) it can be deducted that the section that was yielding was the section at the end of the starter bars and that this section yielded immediately once the concrete had cracked at increment 5.

Figure 8-7 shows that the observed yield moment at the end of the starter bars is not equal to the predicted first yield moment (M_y), it is approximately 64 % of this (after increment 5 the pink line is approximately 0.64). There are several uncertainties related to how the values in this figure were calculated, which could account for some of the 36 % difference shown. These uncertainties can be divided into two parts; how the observed bending moment was calculated and how the first yield moment was predicted.

- Calculating the moment induced in the section during the test depended on the load measured in actuator V1 and the self-weight of the specimen, which had to be estimated. These two factors could have induced an maximum error of around ± 17 kNm (see Appendix D3).
- Predicting the first yield moment of the section at the end of the starter bars involved several assumptions. These included the level of prestress in the section. Prestressing losses of only 16 % were assumed, as this was the value provided by the manufacturer; however, higher losses of prestressing would lower the predicted yield moment. With no prestressing the predicted first yield moment capacity of the section would be around 30 % lower than the assumed value. Material properties and the section geometry used in the calculation could also have had small errors. However, it is likely the main contributor to the predicted moment, being higher than the observed, is the assumption that plane sections remain plane. It appears that when a low ratio of tension steel reinforcement is used this assumption is not valid. In the yield capacity predictions, a linear strain profile was used; however, the effects of tension stiffening make this unconservative. This concept is discussed in more detail in Chapter 10.

Demec gauge readings taken during the test allowed cracks in the topping concrete to be monitored. The amount the three main cracks opened, over the duration of Stage One, is shown in Figure 8-8. Crack widths in millimetres are shown on the vertical axis versus the increment number on the horizontal axis. Demec readings were taken at discrete times during the test, where data was not available from Demec readings it was sourced from the

potentiometers which spanned the cracks. These data points are shown as red triangles in Figure 8-8. Potentiometer readings are not used for the whole duration of the test because they were attached to threaded rods above the surface of the topping concrete and the measurements are not as accurate as those from the Demec gauge.

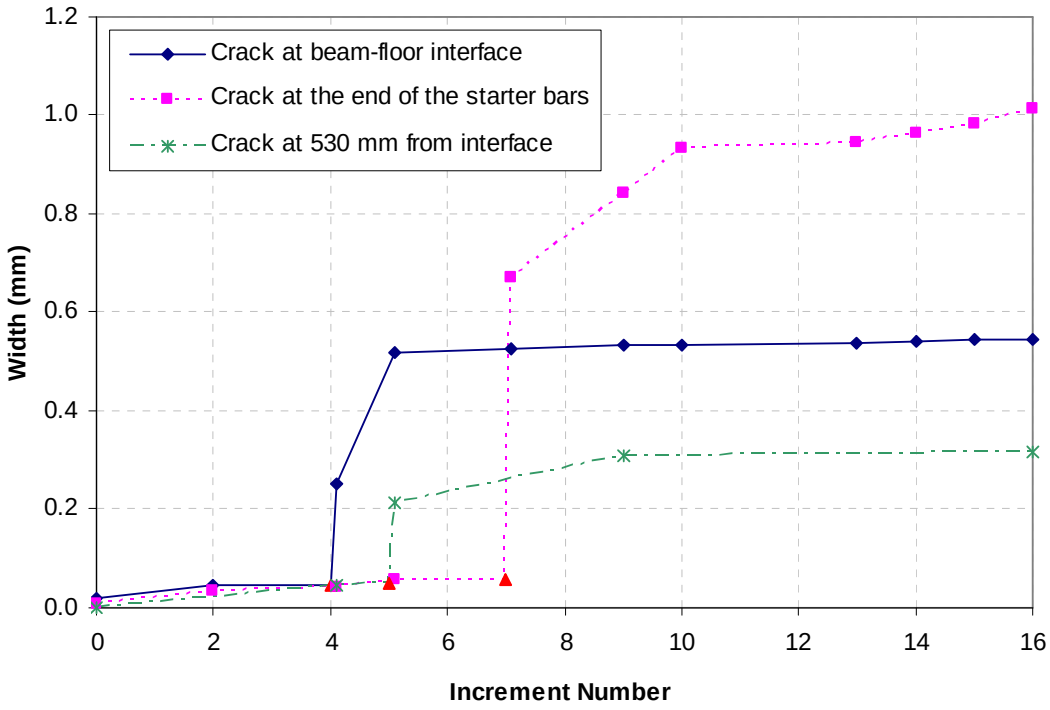

Figure 8-8 Crack widths of the three cracks formed during stage one

Figure 8-8 shows that at the increment corresponding to when a location along the specimen cracked, there is a considerable opening at that crack location. The crack at the floor-beam interface is the first to occur but only opens until the specimen cracks at 530 mm from the interface. Similarly, when the specimen cracked at the end of the starter bars (increment seven) the crack at 530 mm slows opening (as no data was available at increment seven for the crack at 530 mm it is possible that this crack actually stopped enlarging at this point).

The crack widths that correspond to the point that the steel reinforcement begins to yield can be estimated. Taking the average yield strain, found from standard tensile tests (shown in Appendix C5.4 and C5.5), and multiplying it by the length of steel effected by strain penetration, approximately gives the crack width corresponding to yield. For the mesh reinforcement, the length of strain penetration is assumed to be a maximum of 150 mm. This is reasonable as the mesh is comprised of round wires and had transverse wires welded at

150 mm centres. The amount of strain penetration in the starter bars is harder to determine, as they are deformed bars and have a stronger bond to the concrete. This could cause a high strain concentration over a short length at the crack. As a rough approximation the strain penetration was assumed to extend over a length equal to two thirds of the development length of steel given in the New Zealand Concrete Structures Standard (Standards New Zealand. 2006). This gives a length of around 280 mm. As the standard is intended for design, using the full development length would have been conservative.

The crack with corresponding to the starter bars yielding was assessed as 0.84 mm. Neither of the cracks that the starter bars crossed opened to this extent. The crack width corresponding to yield of the mesh was assessed as 0.48 mm. The width of the crack at the end of the starter bars became larger than 0.48 mm at increment seven. This is the point this section cracked. This suggests that the tensile strength of the concrete was higher than the force required to yield the mesh reinforcement. This is feasible as the force that can be sustained by the eight longitudinal mesh bars in the specimen before yield is 116 kN. Assuming the centroid of the compression force is at the level of the prestressing, this correlates to a moment of 35 kNm. The direct tensile strength of the hollow-core concrete was 6.2 MPa; this was found from the standard splitting strength of drilled cores (see Appendix C5.2). Using 68 % of this (4.22 MPa), as a lower characteristic value, results in the area of hollow-core at the top of the unit required to resist the tension resulting from a 35 kNm moment being less than 1200 mm by 30 mm. This is within the top flange of the hollow-core unit.

The displacement of the specimen at actuator V1 was due to a combination of rotation at the beam-floor interface, rotation of the support beam and curvature along the floor unit. Table 8-1 shows the deflection of the specimen at actuator V1 together with the percent of the displacement due to each of the above sources. Increment 5.1 was immediately after the beam-floor interface had cracked. At this stage, the rotation at the beam-floor interface was the most significant contributor to the displacement. By increments 9 and 16 in the test, the two other cracks had formed in the hollow-core unit. At these increments, the curvature of the unit is the predominant contributor to the displacement at actuator V1.

Table 8-1 Contributions to vertical deflection at actuator V1

	Increment		
	5.1	**9**	**16**
Measured deflection at V1 (mm)	20.6	34.8	37.5
% due to rotation at interface	51	31	28
% due to rotation of support beam	7	4	3
% due to curvature in first 3000 mm	41	60	62
% unaccounted for	1	5	5

If the test specimen represented a 12 m span floor in a building with a 3 m inter-storey height then at the end of Stage One the equivalent building drift the specimen corresponded to 0.6 %. This was calculated from deflection at actuator V1, subtracting the contribution from the rotation of the supporting beam and assuming that building drift is the same as the drift that is applied to the floor. This assumption might not be entirely correct due to twisting of the support beam. During Stage One there was no sliding of the supporting beam relative to the strong floor.

Once actuator V1 was lowered to a displacement of 37.5 mm, it was decided to stop the Stage One loading protocol. The aim of Stage One was to find the moment corresponding to the point the starter bars at the beam-floor interface yielded. These bars did not yield; however, at this point in the test it was apparent that the mesh reinforcement had started to yield at the end of the starter bars. Lowering actuator V1 further would not have induced yielding at the beam-floor interface, but would have increased the strain in the mesh at the end of the starter bars potentially causing rupture. Stage Two was not implemented as the aim of this stage was to find the yield moment of the mesh reinforcement with no axial load, which had already occurred.

8.3 Stage Three

The aim of Stage Three was to observe the effect of axial tension on the negative moment capacity of the hollow-core test unit. It was hoped that the point the mesh reinforcement commenced yielding under several different bending moment and axial load combinations would be determined. This would allow a bending moment versus axial load interaction diagram to be plotted. From the end of Stage One, negative bending moments in the specimen were reduced by raising actuator V1 from 37.5 mm to 28.6 mm. Axial tension was applied

using actuator H3, which was attached to the East end of the test unit and pulled the specimen horizontally away from the support beam. Actuator V2, which was attached at the mid-point of the specimen, was also used during Stage Three; to control the magnitude of the bending moments along the test unit. During Stage Three it was difficult to control the three actuators simultaneously. It was also difficult to determine when the mesh reinforcement was yielding. Because of these two complications, instead of finding various yield points, the axial load and negative bending moment were merely increased until failure occurred. The mesh reinforcement crossing the crack ruptured and the crack at this point then extended horizontally, as shown in Figure 8-9, resulting in a brittle failure. A photographic log of testing is shown in Appendix D1.

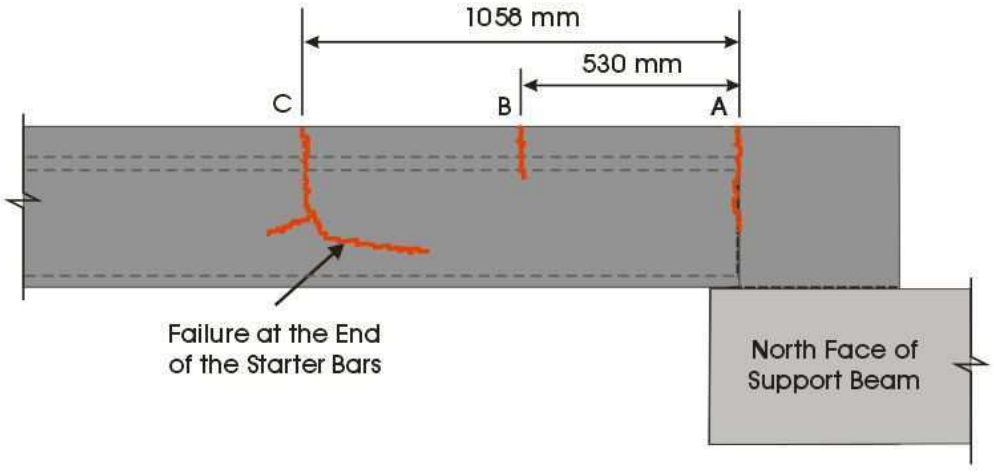

Figure 8-9 Flexural shear failure observed in test specimen HCW1

This section presents the data obtained during Stage Three of test HCW1 and compares it with theoretical predictions. Items presented include:

- The variation of moment and axial load over the duration of the stage
- Crack widths
- Visual performance indicators
- Instance and type of failure.

During Stage Three, the effects of axial tension had to be taken into account in the predictions of the first yield moments of the specimen (M_y), this adds uncertainty, as explained in Section 7.3.1.

Figure 8-10 shows a tri-axes plot of the change in moment (at the beam-floor interface and at the end of the starter bars) and the change in axial load, at increments during the test. The normalised moment (M_t/M_y) is shown on the left-hand-side vertical axis. The measured moment (M_t), is calculated from the loads in the actuators during the test and self-weight of the specimen. The negative first yield moment (M_y), is that which corresponds to the level of axial load applied at that increment in the test and is defined as being the moment when steel reinforcement in the insitu concrete topping of a cracked section first commences yielding. The axial load, shown in brown, is not normalised, its magnitude is shown on by the right-hand-side vertical axis (the negative sign indicates that the force it is a tension force). Other measurements of interest during Stage Three are the widths of the cracks at the beam-floor interface and at the two locations where the hollow-core unit cracked. Figure 8-11 shows these crack widths at increments during the test, as calculated from Demec points glued to the insitu topping concrete.

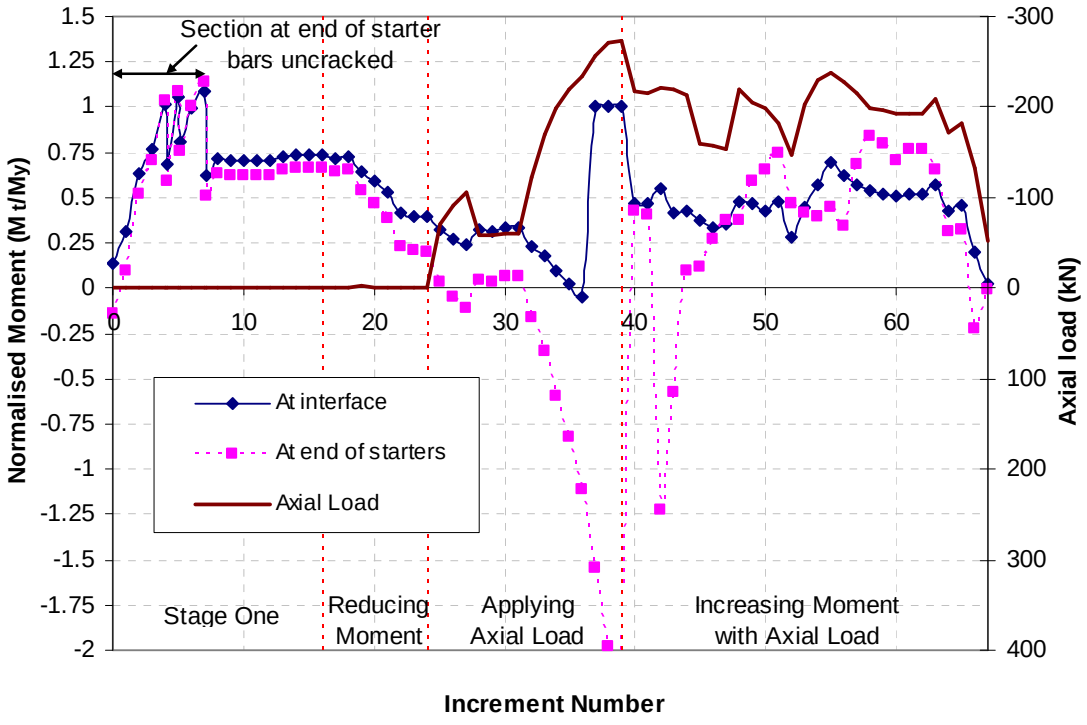

Figure 8-10 Tri-axis plot showing the change in moment, at the beam-floor interface and at the end of the starter bars, and the change in axial load during Stage three

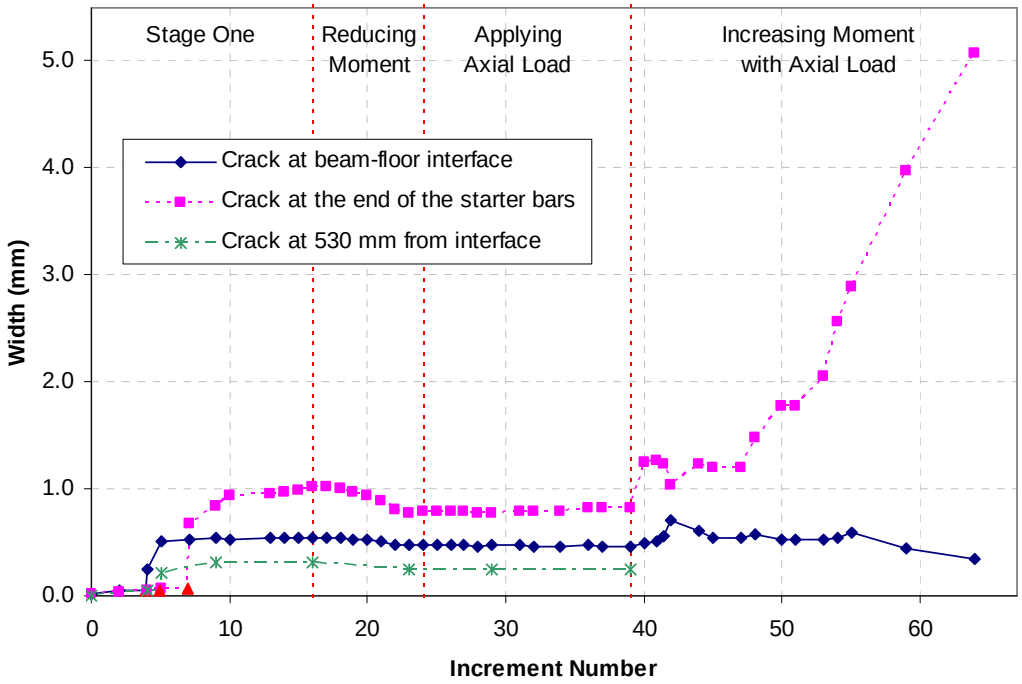

Figure 8-11 Crack widths during stage three

There are four loading segments shown in Figure 8-10 and Figure 8-11, these are:

- Up to increment 16 - Stage One
- Increments 16 to 24 –actuator V1 raised (to decrease negative bending moment)
- Increments 24 to 39 – axial load applied
- Increments 39 to 67 – combined increase of axial load and bending moment.

Apart from Stage One, which was discussed in the previous section, each of these segments is discussed in the following paragraphs.

Between increment 5 and the end of Stage One, the mesh reinforcement was yielding under negative bending moment (no axial tension applied) at the end of the starter bars. Between increments 16 and 24, actuator V1 was raised from a level of 37.5 mm below its initial position to a level of 29 mm below its initial position. This reduced the bending moment at the end of the starter bars by over 65 % and reduced the crack at the end of the starter bars from 1.01 mm to 0.78 mm.

Between increments 24 and 39 the vertical actuator V1 was held constant while the load in actuator H3 was increased to induce a maximum axial tension in the specimen of 273 kN.

Figure 8-10 shows that increasing the axial tension from this position decreased the negative bending moment in the specimen at the two sections of interest. This was because the load applied by actuator H3 contained a vertical component as well as a horizontal one due to the angle at which the load was applied. Because of the long lever arm between the beam-floor interface and the position of this vertical load it had a significant effect on the overall bending moment in the specimen. The other reason that small variations of bending moment applied to the specimen (M_t) appear to have a large effect on Figure 8-10, where the normalised moment is plotted (M_t/M_y), is that when axial tension is applied to the specimen the predicted first moment capacity (M_y) decreases. There are several increments during the test, shown in Figure 8-10, where negative normalised moment values are shown; this indicates that the section had a positive bending moment during these increments.

Between increments 37 and 39, Figure 8-10 shows that the beam-floor interface section should be yielding, as the normalised moment is equal to one. At this point the axial load, even without additional moment, is more than the yield capacity of the starter bars. However, the bars did not show signs of yielding during the test. This is likely to be because the friction between the floor unit and the supporting beam also added to the tensile capacity of the section. With the addition of axial tension, the supporting beam, which was bolted to the laboratory strong-floor, was pulled 2.5 mm horizontally across the strong-floor towards actuator H3. The rotation of the seating beam relative to the laboratory strong-floor also increased during this segment from 0.02 degrees to 0.06 degrees. Over the 6000 mm length of the specimen, this rotation creates a 6 mm vertical displacement at the location of actuator V1. Until increment 39, the relative rotation between the supporting beam and the floor remained constant and the cracks induced in Stage One did not increase in size.

At increment 39 actuator V2 was attached to the specimen. This actuator was attached mid-way between the supporting beam and actuator V1. By using a both actuators V1 and V2 the negative moment at the end of the starter bars could be increased without increasing the moment at the beam-floor interface excessively. However, it was difficult to change the load in one of the vertical actuators without significantly altering the load in the other. With axial tension still applied to the specimen the aim of this stage was to increase the negative moment at the end of the starter bars to find another yield point. In Figure 8-10 it can be seen that axial tension and the induced bending moments fluctuate. Because of these fluctuations and the difficulty experienced controlling the three rams simultaneously it was not possible to

accurately determine the yield moment at different axial loads, instead the specimen was merely loaded until failure.

Looking at the crack widths in Figure 8-11 it would appear that by increment 41 the mesh should have been yielding, as this crack extension is more than previously experienced by the mesh. Apart from increment 42, where the specimen was accidentally loaded the wrong way, the crack width at the end of the starter bars was always increasing. Figure 8-12 (a) shows the crack at the end of the starter bars down the south side of the specimen at increment 55. The crack has not propagated further than during Stage One but has widened considerably. At this point the width of the crack at top surface of the specimen was 2.6 mm. At increment 58 the ultimate capacity was nearly reached, this was the last reading taken before one of the longitudinal mesh reinforcement wires, at the end of the starter bars, snapped. Figure 8-12 (b) shows a mesh wire after fracture.

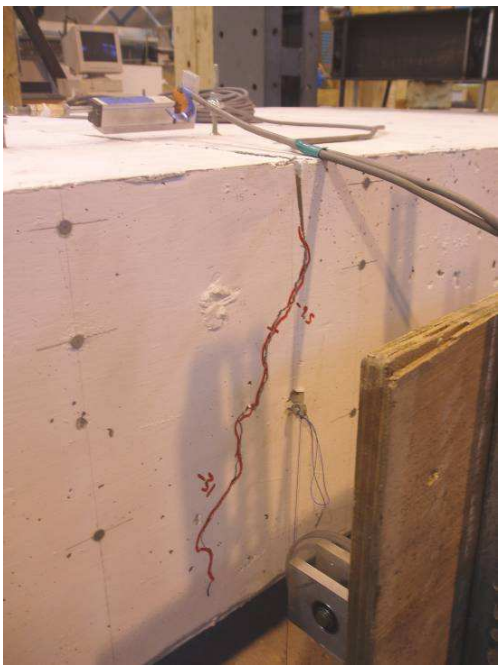

(a) Crack at end of starter bars on south side of specimen at increment 55

(b) Mesh reinforcement, after fracture, crossing crack at the end of the starter bars

Figure 8-12 Photos during Stage Three of HCW1 test

Increment 65 was the last reading taken before complete failure occurred by all the remaining longitudinal wires of the mesh reinforcement snapping. A shear crack then propagated out from the bottom of the vertical flexural crack at the end of the starter bars. The readings for

increment 66 were taken immediately after the failure occurred. Increment 67 was after the specimen had been left sitting for a couple of days, no additional loading had been applied, but the crack width increased significantly. Figure 8-13 shows the specimen, specifically the cracks down either side at the end of the starter bars, at increment 66 and then increment 67. The photos of increment 67 show the insitu concrete from down the sides of the unit removed. It can be seen that the flexural crack turns into a shear crack which runs back towards the support beam, but there is also a smaller horizontal crack extending in the opposite direction.

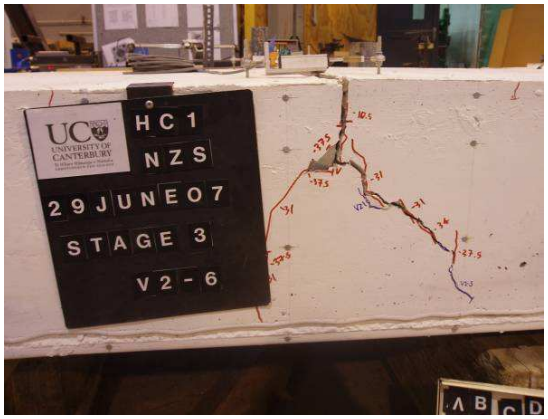

(a) North side crack at increment 66

(b) South side crack at increment 66

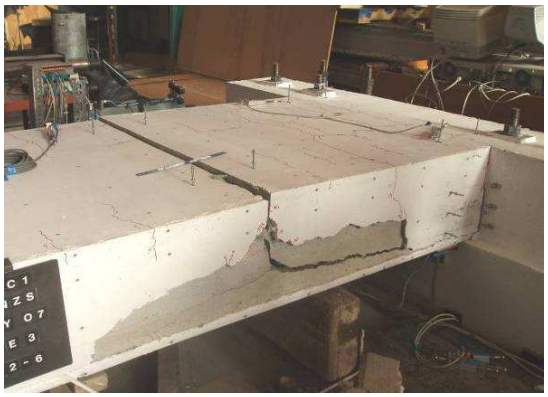

(c) North side crack at increment 67, insitu concrete removed

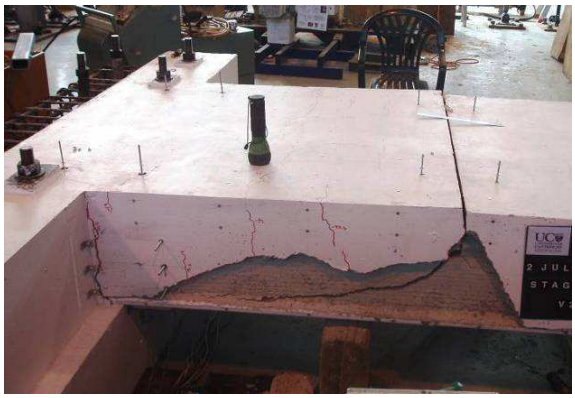

(d) South side crack at increment 67, insitu concrete removed

Figure 8-13 Specimen HCW1 after failure

The last measurements taken before the point of failure (increment 65) show -182 kN of axial tension was applied to the specimen. The negative bending moment induced at the beam-floor interface was 21.6 kNm and at the end of the starter bars 8.3 kNm. These values were well

below the predicted first yield moment (M_y); this can be seen in Figure 8-10 as the normalised moments are less than one. However, as for Stage One, the uncertainties in calculating both the applied moment and predicted first yield moment give these values are large error. The total elongation of the specimen at increment 65 was 7.7 mm, 5.6 mm of which occurred at the crack at the end of the starter bars. The rest was due to movement of the support beam relative to the laboratory strong-floor and the crack at the beam-floor interface. A crack width at the end of the starter bars of 5.6 mm before failure, could mean the mesh had a higher ductility than that expected.

During the final segment of loading, the supporting beam did not slide any further along the laboratory strong-floor, nor was there significant further rotation of the supporting beam relative to the strong-floor. There was rotation induced between the supporting beam and the test unit, this was in the opposite direction to the small 0.07 degree rotation caused during Stage One. Actuator V2 was moved vertically upwards, while actuator V1 held down, this caused the specimen to be rotated at the supporting beam interface as shown in Figure 8-14. The maximum relative rotation between the support beam and the hollow-core unit before the specimen failed was measured to be 0.7 degrees. During Stage Three there were very few additional cracks induced in the specimen. For the entire test, the seating ledge of the supporting beam remained intact and did not suffer any spalling.

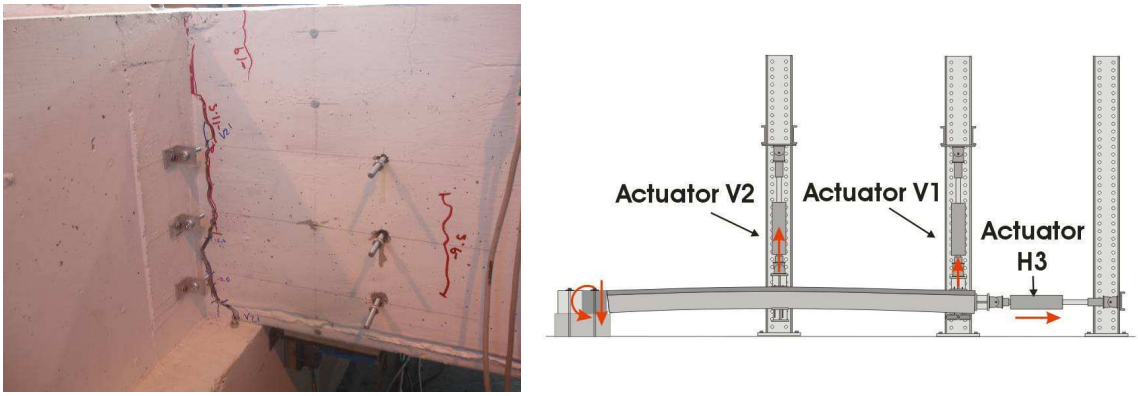

Figure 8-14 Rotation at beam-floor interface

The aim of Stage Three was to observe the effect of axial tension on the negative moment capacity of the hollow-core section. Although the yield moment under several different axial loads was not able to be observed, a flexural failure was induced. This failure occurred at the

end of the starter bars when the axial tension in the specimen was around -181 kN and the negative bending moment at the end of the starter bars was 8.3 kNm. If this was a typical hollow-core building in Wellington with the hollow-core units spanning 12 m, this load combination is below the design values when the effect of parallel beam elongation is incorporated.

8.4 Key Outcomes of Test HCW1

- The beam-floor interface cracked under a negative moment of 80 kNm
- The starter bars crossing the beam-floor interface did not yield as the moment capacity at the end of the starter bars restricted the moment that could be applied to the interface
- The section at the end of the starter bars started yielding as soon as the hollow-core cracked, suggesting that the concrete had a higher tensile capacity than the mesh
- The observed first yield moment at the end of the starter bars was around 31.6 kNm, this was 64 % of the predicted first yield moment.
- A negative flexural failure was observed at the end of the starter bars under a combination of axial load and negative bending moment that were less than Wellington based seismic design loads and a total elongation of the specimen of 7.7 mm.

8.5 References

Bryant, A. H., Wood, J. A., and Fenwick, R. C. (1984). "Creep and Shrinkage in Concrete Bridges." *No. 70*, National Roads Board, New Zealand.

Standards New Zealand. (2006). *Concrete structures standard, NZS3101, Parts 1 & 2*, Standards New Zealand, Wellington, New Zealand.

9 Experimental Observations and Results: Flexure-Shear Failure

The behaviour of test unit HCW2 is described in this section. The aim of this test was to observe a flexure-shear failure in a negative moment zone of the floor. Crack initiators were used in an attempt to induce cracks forming at locations where there were strain gauges on the steel reinforcement in the insitu topping concrete. Loads applied to the test specimen were based on the actions induced for an equivalent 12 m span hollow-core floor, when design loads from the New Zealand Structural Design Actions Standard were applied. A shear failure in the negative flexural zone was not observed, even after the loading protocol was extended. Test results are presented together with discussion of visual performance indicators.

9.1 Initial Condition of Test Specimen HCW2

The test specimen used in this test was different from test unit HCW1 in that it contained continuous deformed steel reinforcement in the topping, instead of starter bars and mesh. The topping concrete also had a series of crack initiators in the top 20 mm of the insitu concrete as it was anticipated that, had the concrete been older when tested, shrinkage cracks would likely have formed. The West end of the HCW2 test specimen is shown in Figure 9-1; the experimental setup is described fully in Chapter 7. Testing took place 20 days after the insitu topping concrete was poured. At the beginning of the test, the floor unit was level. It is believed that at the time of testing the hollow-core unit had an age of between 1.5 and 2.0 years. This indicates that any creep of the unit would have been small and shrinkage negligible.

The HCW2 test incorporated two features that allowed an improved understanding of the specimen's state at the start of the test. These were,

- that some of the steel reinforcement in the insitu topping concrete had strain gauges attached
- throughout construction of the test unit, the hollow-core unit was supported by actuator V1 at the East end and the load this carried was recorded.

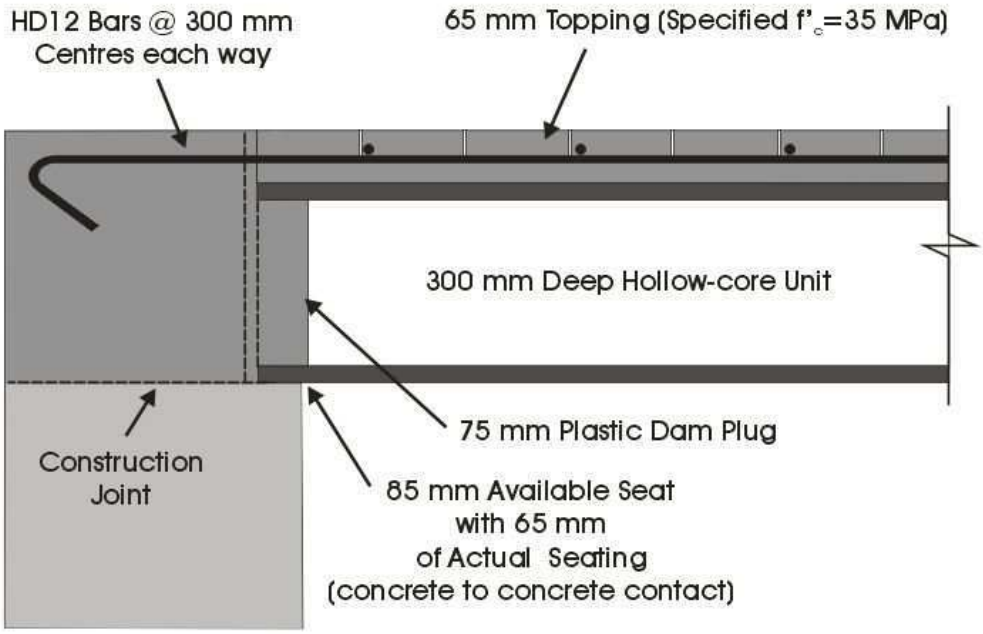

Figure 9-1 Connection detail used for test specimen HCW2

Eleven sets of strain gauges were located at 150 mm centres on two of the longitudinal steel reinforcing bars. The first set of gauges was located above the end of the hollow-core unit at the beam-floor interface. Figure 9-2 shows the average readings taken from these strain gauges at four times between placement of the topping concrete and when the specimen was tested. The first of these measurements was taken the day after the placement. The change in strain over this period shows the effect of the topping concrete shrinking. It would be expected that the concrete shrinking would cause negative strains (compression) in the steel bars. This is not the case. Apart from at the beam-floor interface, the strain gauges were positioned at the locations of the initiated cracks. The shrinkage of the concrete appears to have induced tensile strains at the cracks. Strains were not recorded in the steel between the initiated cracks but it is assumed compression strains would have been induced. The beam-floor interface, where no crack was initiated, did experience a compressive strain, which reached 150 x 10^{-6} strain (equivalent to 30 MPa) before the first load was applied.

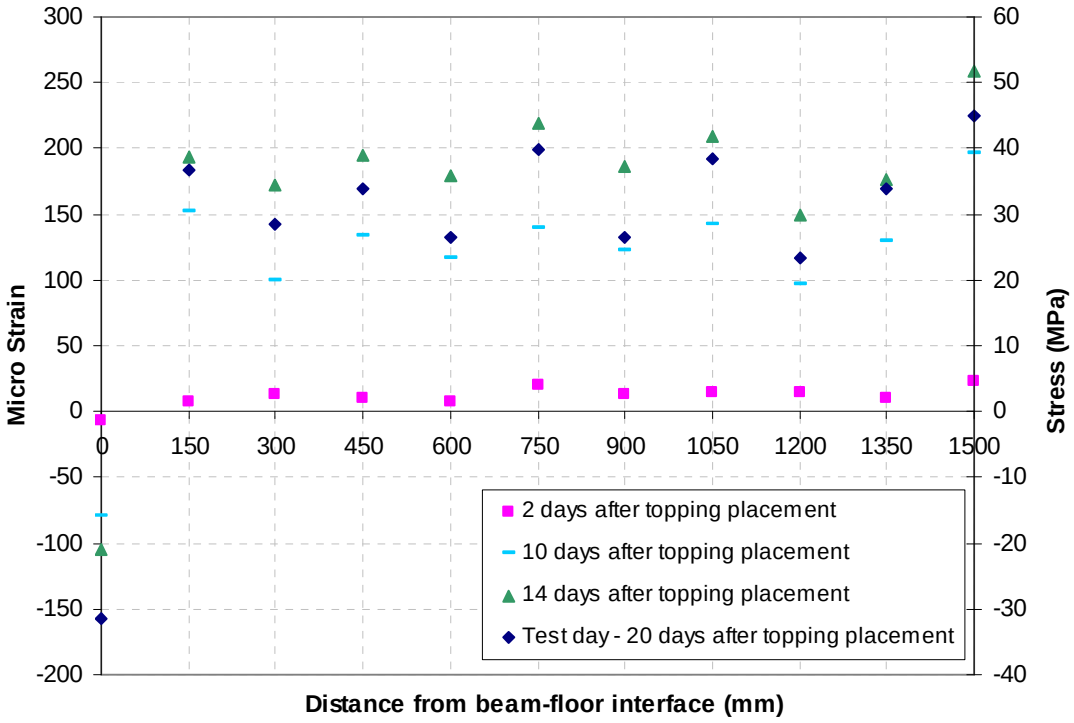

Figure 9-2 Average strain (or stress) in steel reinforcement prior to testing

Transverse reinforcement was placed in the insitu topping concrete at 300 mm centres, which coincided with every second crack initiator, the first one being 150 mm from the beam-floor interface. Figure 9-2 shows that the strain gauges at these locations had slightly higher readings than those that were mid-way between the transverse bars. It is likely that the presence of the transverse reinforcement weakened these sections, which resulted in greater shrinkage cracks forming. The steel reinforcement crossing the furthest initiated crack from the interface sustained a higher strain than the rest. This could be because there were no initiated cracks past this point and therefore a larger amount of concrete shrinkage was accommodated by this one location. The test-day measurements were taken after the specimen had been levelled, this involved raising actuator V1 slightly, which could explain the decrease in strains between the 14-day readings and the test-day readings. At the beginning of the test, the strain in the steel reinforcement at the initiated crack locations was in the order of 150 micro strain. This is around 5 % of yield strain (ε_y = 3000 micro strain). The initiated cracks were not visually observed to widen. Even if the 150 micro strain had occurred over the entire 150 mm between cracks, this would lead to a relatively small 0.02 mm extension of the steel.

Having actuator V1 supporting the hollow-core unit as the specimen was built allowed a better assessment for the self-weight of the test specimen to be obtained than for the first test. Appendix C6 Presents what the self-weight of the specimen was assumed to be and how this was derived.

9.2 Testing

The loading protocol for the HCW2 test was divided into four stages. The first two of these stages examined situations where a negative bending moment is induced at the beam-floor interface due to relative rotation between the supporting beam and the floor unit when no axial tension was applied to the floor. The second two stages examined situations where elongation of frame beams, parallel to a hollow-core unit, results in the floor being subjected to axial tension. To cause a shear failure in a negative bending moment region there first must be flexural cracks due to negative moments in the units. With the formation of these cracks the shear stresses induced in the flexural tension zone of the units may cause flexure-shear cracking, potentially leading to failure. This is explained fully in Section 6. The planned loading protocol, which is described in Chapter 7, was cyclic and aimed to induce flexural cracks during upward loading and high shear stresses in the negative moment zone during downward loading. The magnitude of forces applied to the specimen were derived from the New Zealand Loadings Code (Standards New Zealand. 2004b) for both Christchurch and Wellington.

The performance of the specimen during the four stages of planned loading is described in this section, along with the performance of the specimen under an additional loading sequence (referred to as “Phase Two”). During the four planned stages, it appears that insufficient flexural cracks formed in the negative moment region, making it very unlikely that a flexure-shear failure would occur. Once the planned loading protocol was completed and the specimen had not failed, an extended protocol was developed and implemented. This phase (Phase Two) involved inducing flexural cracks in the specimen by placing a prop under the floor specimen in the location of the desired crack and applying load to induce a negative bending moment at the prop. Several cracks were successfully formed in this manner; however, it was not possible to induce cracks at a close spacing. Applying shear to the cracked specimen still did not cause failure and therefore testing was concluded. Post test

analysis showed that the negative bending moment zone induced in the test when high shear was applied was smaller than sought. This may have been why the unit did not fail.

9.2.1 Stage One

Stage One of the planned loading protocol examined the behaviour of the floor before the steel reinforcement crossing the beam-floor interface yielded. Figure 9-3 shows the bending moment profiles that were planned (dashed lines) and those that were achieved (solid lines). The test started by applying the gravity load, which is shown in red on Figure 9-3. Actuators V1 and V2 were then adjusted to induce the additional action corresponding to vertical seismic forces for Christchurch; up and then down (shown in green). Subsequently, the additional seismic actions for Wellington were induced, up and then down (shown in blue). Near the beam-floor interface, the negative bending moments induced were larger than the intended bending moments. This is partly because the self-weight of the specimen used to calculate the planned loading was lower than the improved self-weight used to calculate the results, as illustrated in Appendix C6.

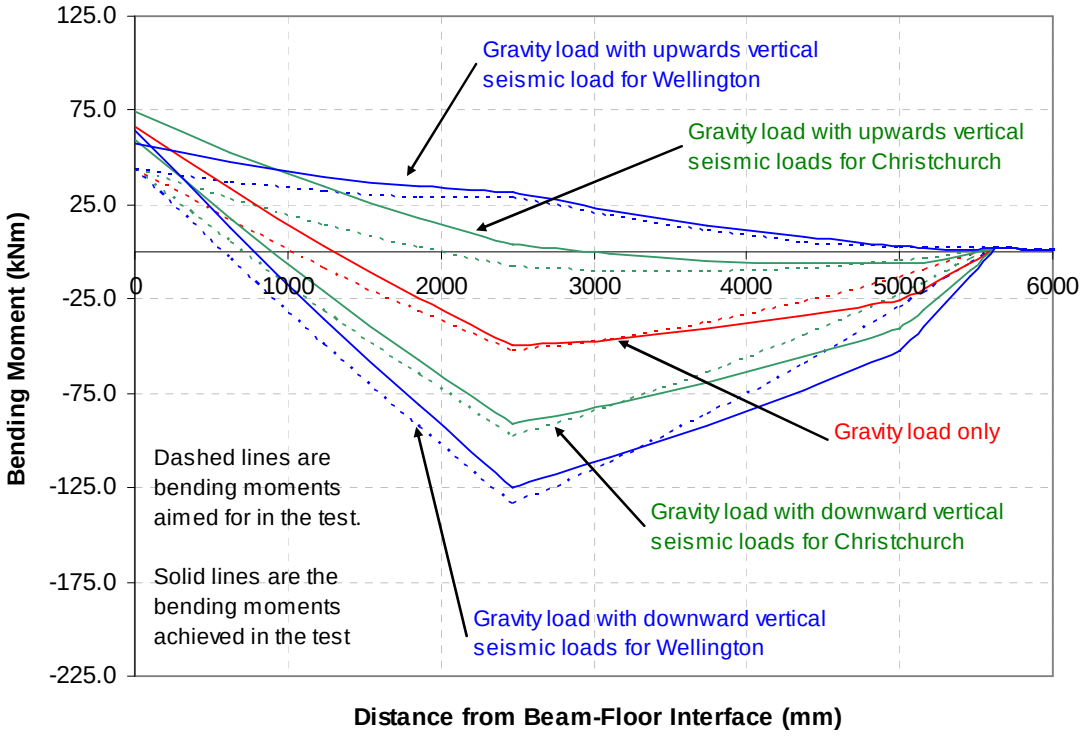

Figure 9-3 Planned and achieved bending moments along specimen HCW2 during Stage One

During Stage One, it was observed that the beam-floor interface cracked (shown in Figure 9-4); probably breaking off the 75 mm concrete plugs which extended into the cores of the hollow-core unit. This occurred when the bending moments induced were those scaled for Wellington and with downward vertical seismic forces. Some longitudinal cracking in the topping was also observed above the two interior bars of the longitudinal steel reinforcement, see Figure 9-4.

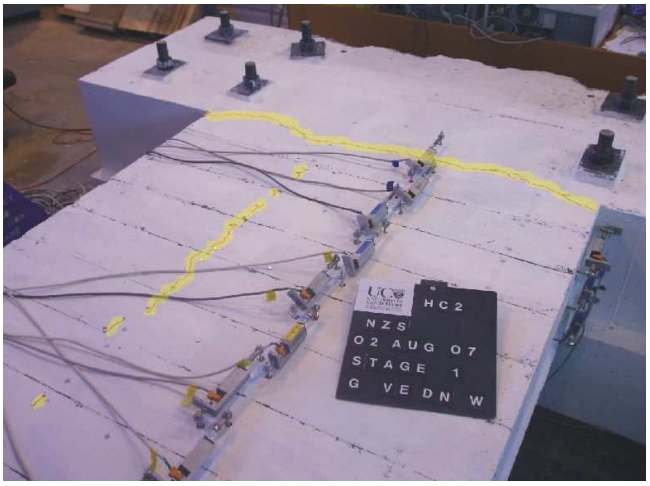

Figure 9-4 Specimen HCW1 during Stage One of testing after the beam-floor interface had cracked

Average strains recorded by the strain gauges along the longitudinal steel reinforcement are shown in Figure 9-5. These are given as a fraction of the first yield strain (ε_y = 3000 micro strain) at different load stages. As the stress-strain relationship is linear up until yield, this ratio is also the fraction of yield stress experienced by the steel. The values labelled “Start of test” are the same values recorded in Figure 9-2 for the test day. During testing strains increased, from those recorded prior to the test, in the reinforcement out to a distance of 1000 mm from the beam-floor interface. Beyond this section, some of the strains became less than those at the start of the test. When we compare the strains with the bending moments shown in Figure 9-3, it can be seen the strains decrease where the unit was subjected to positive bending moments. When the interface cracked the strains at this location went from compressive strains, due to shrinkage, to tensile strains. During Stage One, the steel reinforcement was well below yield.

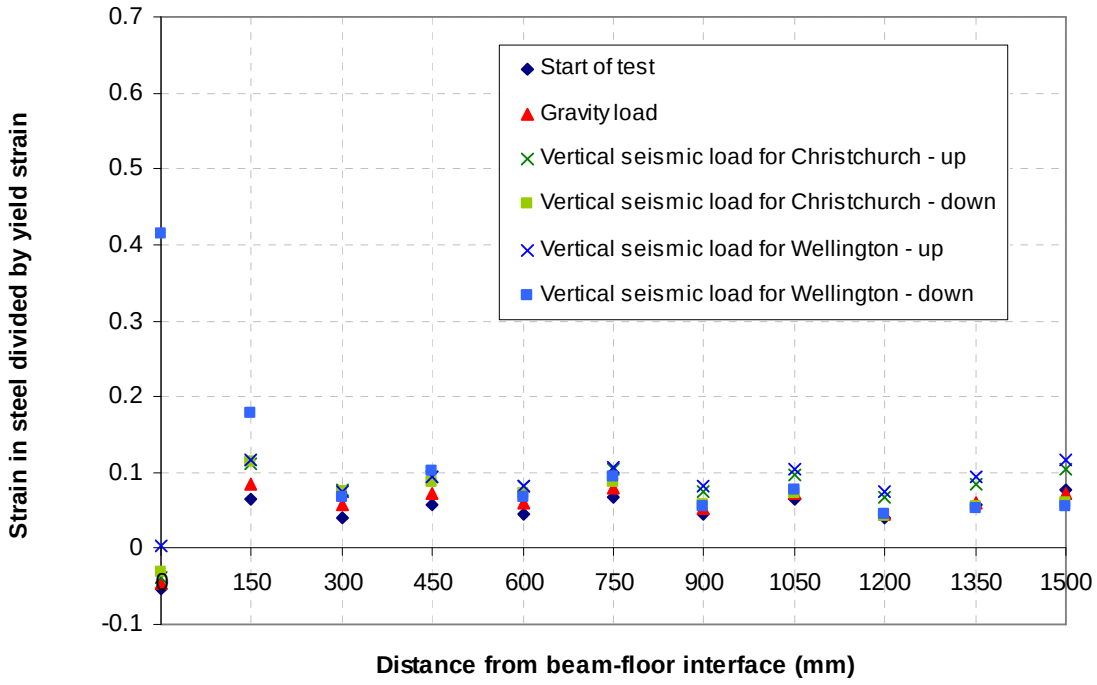

Figure 9-5 Average strains in steel reinforcement during Stage One of testing

9.2.2 Stage Two

Stage Two of the planned loading protocol followed the same pattern as Stage One, except that the negative bending moment at the beam-floor interface was increased to cause the steel reinforcement at the support to yield. The negative bending moment predicted to induce yield at this section was 88 kNm. Figure 9-6 shows that this magnitude of moment was first achieved when upward vertical seismic design loads for Christchurch were induced in the specimen. Readings from the strain gauges at this location confirmed that the steel reinforcement was yielding (shown in Figure 9-8). This load case also induced a crack in the hollow-core unit, which could be seen on the South side, 150 mm from the beam-floor interface (shown in Figure 9-7 (a)), but did not form at the same location on the North side of the unit. It appears that the crack was diagonal and terminated at the beam-floor interface near the central web. Figure 9-7 (c) shows the end of the hollow-core unit after the specimen had been dismantled, this flexural crack can be seen in the first two webs.

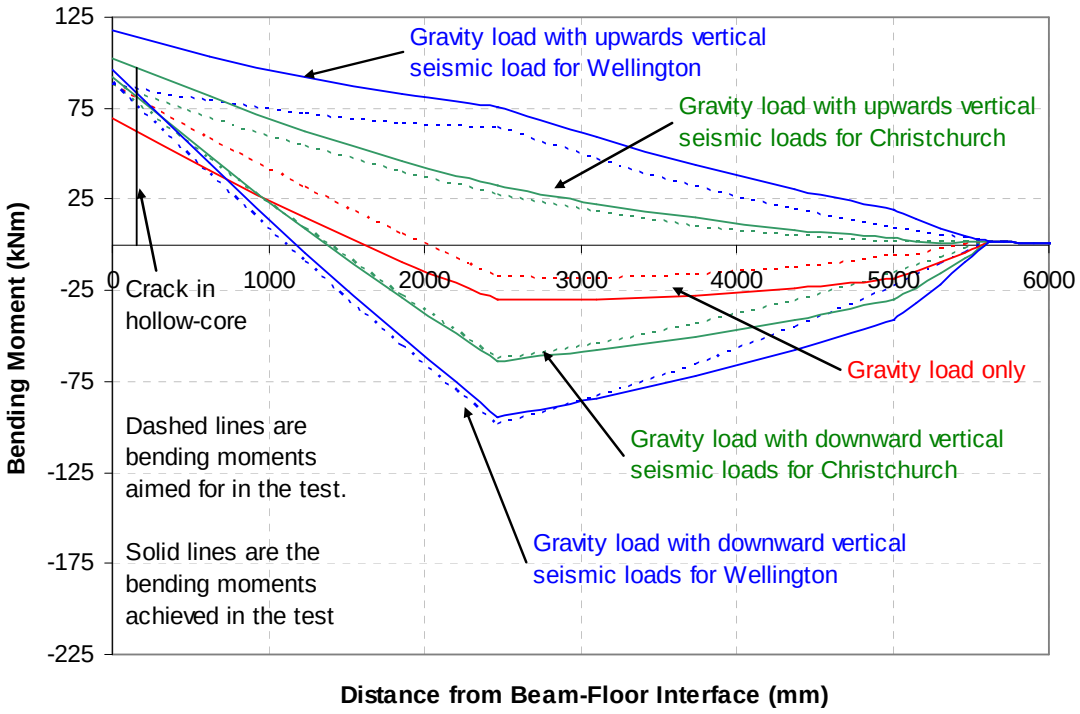

Figure 9-6 Planned and achieved bending moments along specimen HCW2 during Stage Two

The upwards Wellington seismic load case induced a horizontal crack in the South side of the hollow-core unit. This extended from the flexural crack, formed previously, to the beam-floor interface, see Figure 9-7 (b). During both upward vertical seismic load cases, flexural cracks were opened up in the insitu topping concrete, perpendicular to the span, past the extent of the initiated cracks (shown in Figure 9-7 (d)). The first of these was 150 mm past the last initiated crack; this was the location of a transverse steel reinforcement bar. Subsequent cracks were at 300 mm or 150 mm spacing. The last load applied during Stage Two was the downward vertical seismic design load for Wellington. This induced a diagonal crack in the hollow-core unit at the beam-floor interface on the North side, which is shown in Figure 9-7 (e) and in Figure 9-7 (f) when the specimen was dismantled.

(a) South side of unit , hollow-core cracked under upwards vertical loads for Christchurch

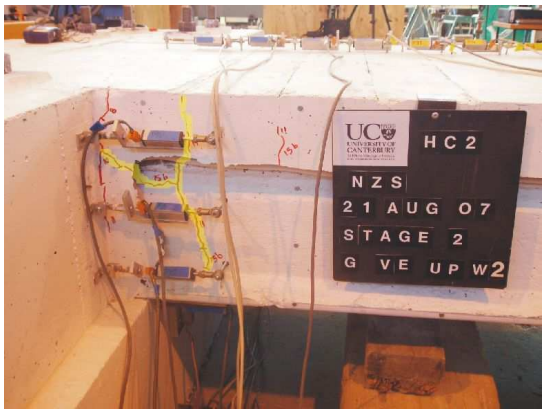

(b) South side of unit, horizontal crack in hollow-core under upwards vertical loads for Wellington

(c) Cracks observed in end of hollow-core unit when specimen dismantled

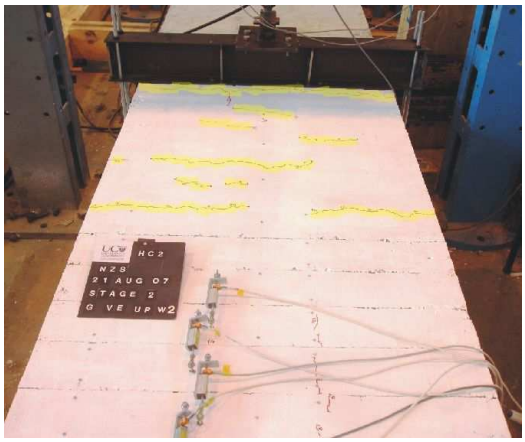

(d) Flexural cracks in topping past induced cracks formed during Stage Two

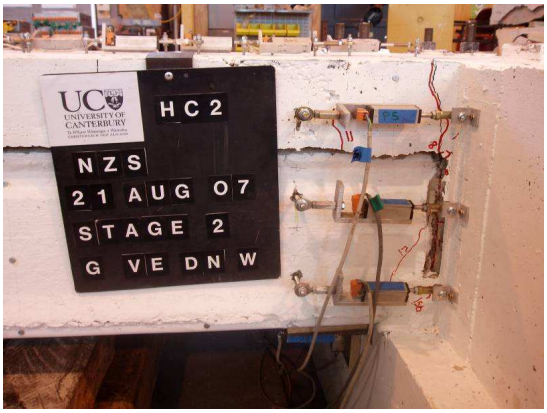

(e) Crack in hollow-core at support induced under downward vertical loads for Wellington

(f) Crack in hollow-core at ledge when specimen dismantled

Figure 9-7 Photos of specimen HCW2 showing cracking induced during Stage Two of the planned loading

Figure 9-8 shows the average strains (or stresses) in the longitudinal reinforcement at the locations of the initiated cracks as a fraction of the first yield strain. Where the data points are not shown on the plot, such as at the beam-floor interface, the bars in this location had yielded. The strain in the bars 150 mm from the beam-floor interface has increased. The induced crack on the South side of the specimen at this point opened up when the hollow-core unit cracked.

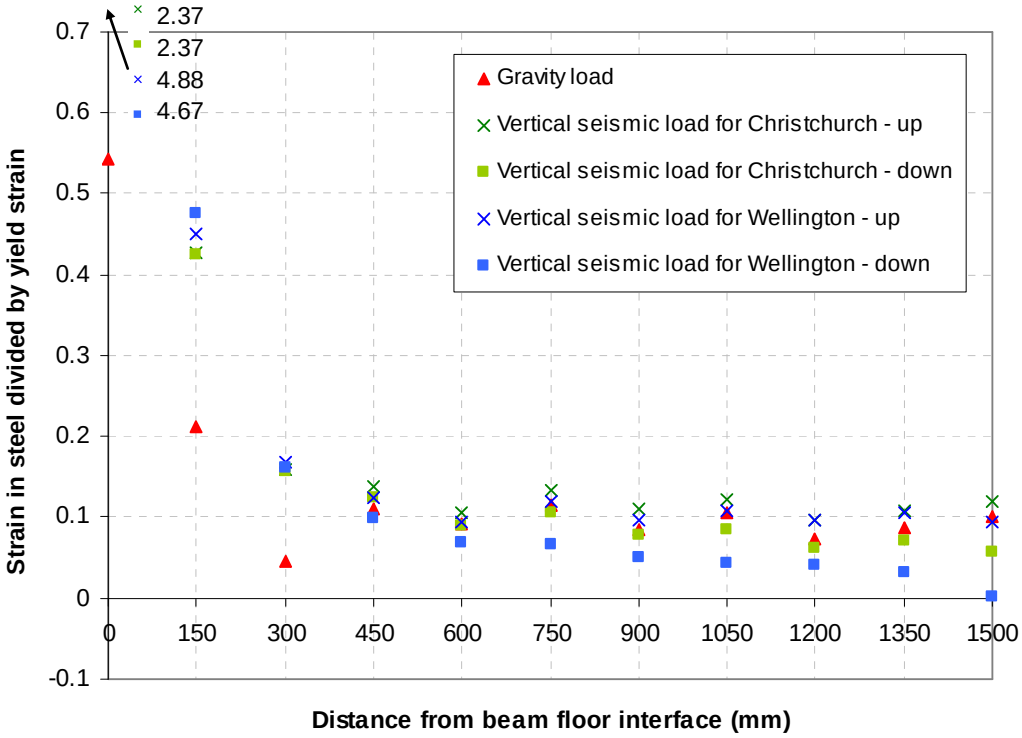

Figure 9-8 Average strains in steel reinforcement during Stage Two of testing shown as a fraction of yield strain

9.2.3 Stage Three

To commence Stage Three the specimen was taken back to its initial position where the East end, supported by actuator V1, was level with the end at the supporting beam. An axial tension of 132 kN was then applied by actuator H3, this induced axial tension and bending moments as the application of load was eccentric to the member and inclined. The same vertical seismic forces applied during Stages One and Two were applied in this stage. Figure 9-9 shows the target bending moments and those achieved during Stage Three. The negative bending moments were higher than the planned values, especially in the case with the upwards vertical seismic forces for Wellington. This was partly due to the self-weight of the

specimen being larger than predicted and partly due to the uncertainties contained in the calculations for the planned loading. The bending moment induced at the beam-floor interface depended on the friction between the hollow-core unit and its support, which varied.

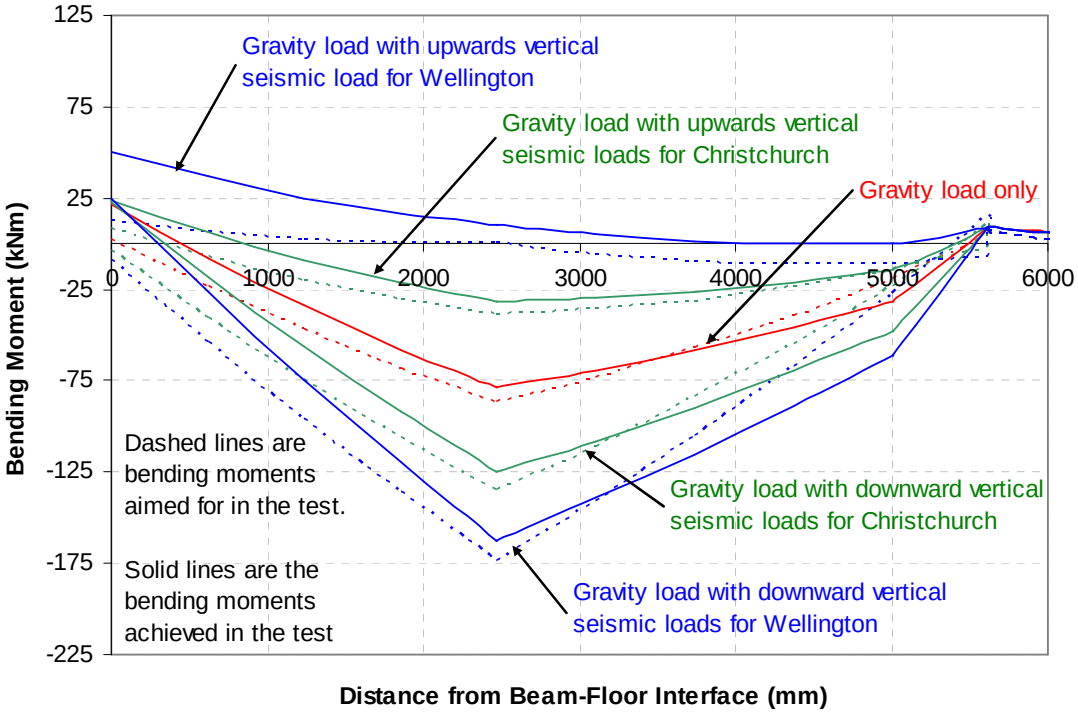

Figure 9-9 Planned and achieved bending moments along specimen HCW2 during Stage Three

When the axial tension was applied, the floor unit was pulled away from the supporting beam. This opened up a crack of about 1.5 mm between the hollow-core unit and the face of the supporting beam, as shown in Figure 9-10.

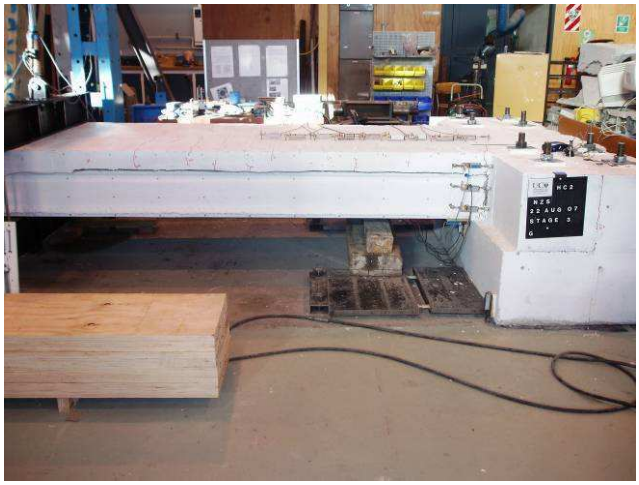

(a) North side of HCW2 during Stage Three

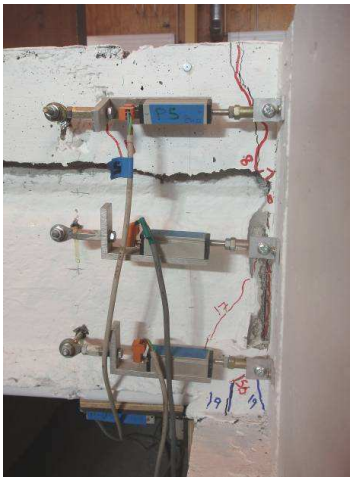

(b) Beam-floor interface on North side after axial load applied

Figure 9-10 Photos of specimen HCW2 during Stage Three

Figure 9-11 shows the average strains, as a fraction of the first yield strain, in the longitudinal reinforcement at the locations of the initiated cracks. The strains at the beam-floor interface are in excess of the yield strain. On average, the stains are smaller than those in Stage Two.

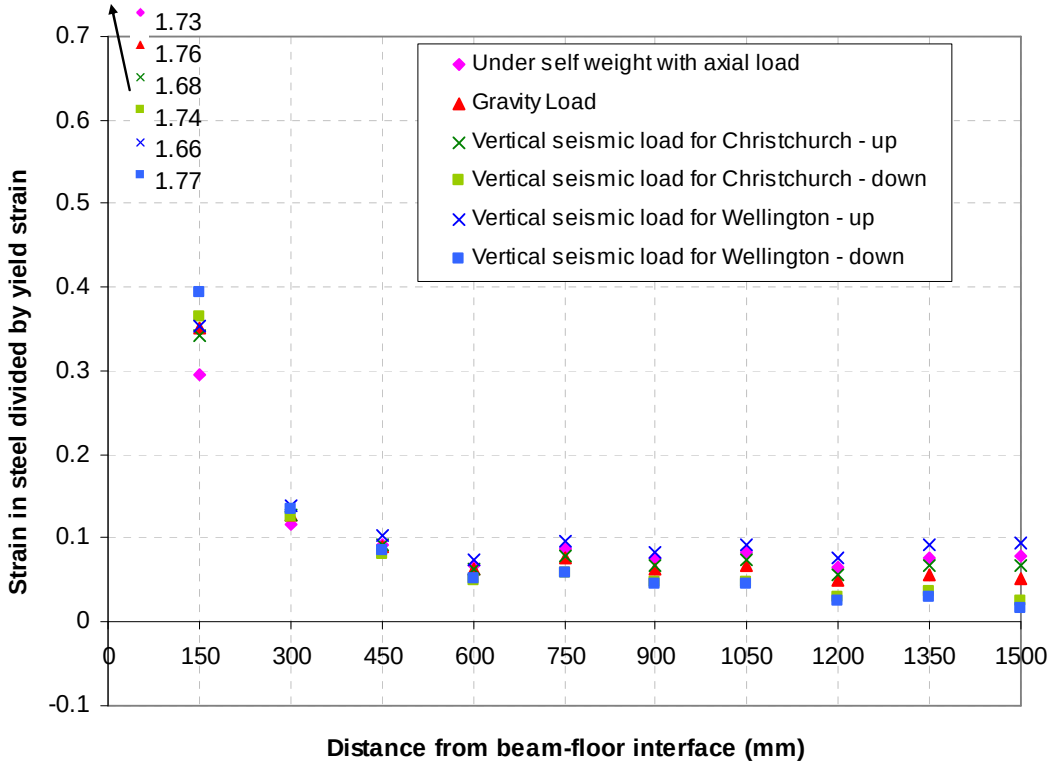

Figure 9-11 Average strains in steel reinforcement during Stage Three of testing

9.2.4 Stage Four

Stage Four involved increasing the axial tension applied to the specimen to 264 kN, this corresponds to the yield capacity of the longitudinal steel reinforcement. The same cyclic loading protocol applied during the previous three stages was implimented. Figure 9-12 shows the planned and achieved bending moments in the specimen. Apart from the crack at the beam-floor interface becoming larger no further cracking was observed in the specimen. As the specimen had not failed at the end of the planned loading protocol, an additional load cycle was added, which is shown as a solid orange line in Figure 9-12. Even under these increased loads flexural cracks were not formed and the specimen did not fail.

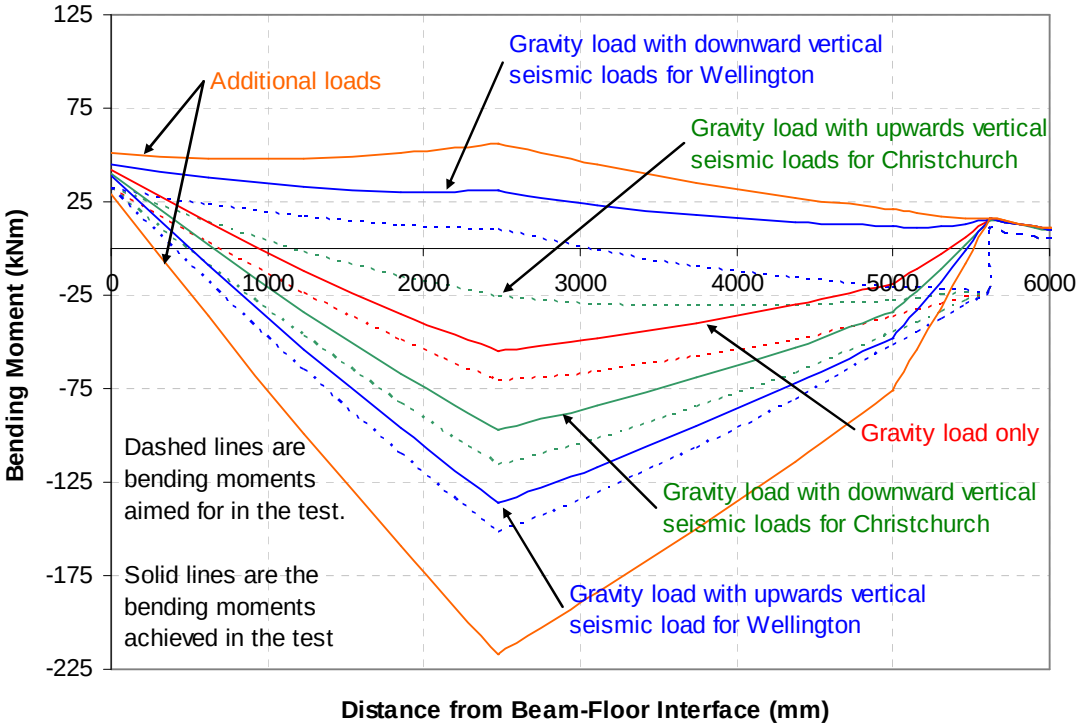

Figure 9-12 Planned and achieved bending moments along specimen HCW2 during Stage Four

Figure 9-13 shows the beam-floor interface during Stage Four. The floor unit was pulled on average 3.5 mm away from the face of the support beam. The implication of this was that when a moment was applied, only the steel reinforcement crossing the interface and the friction at the seat could resist it.

(a) Beam-floor interface on north side when axial load applied

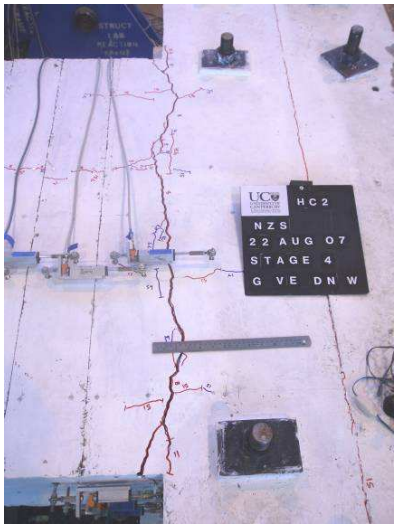

(b) Looking down at beam-floor interface when downward load case for Wellington is applied

Figure 9-13 Photos of specimen HCW2 during Stage Four

The beam-floor interface was the only crack to open significantly; however, it can be seen in Figure 9-14 that the strain is the longitudinal reinforcement 150 mm from the beam-floor interface increase to around 0.6 of the yield strain.

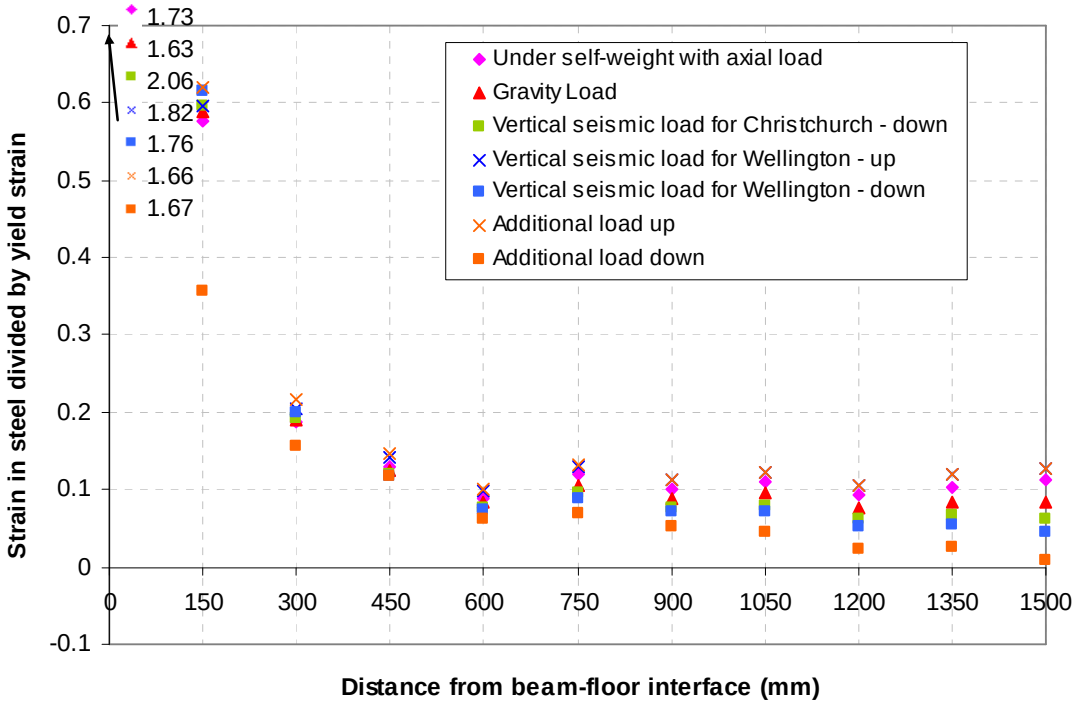

Figure 9-14 Average strains in steel reinforcement during Stage Four of testing

In the additional loading cycle, the magnitude of negative bending moments along the test unit were planned to be increased until sufficient flexural cracks had formed in the negative moment zone near the beam-floor interface. The negative bending moment achieved on the upwards part of this cycle can be seen in orange in Figure 9-12. The maximum negative moment was created at around 2500 mm from the beam-floor interface; this was the location of actuator V2. The hollow-core unit cracked at this location when the axial load was -271 kN and the negative bending moment 56 kNm. The crack at actuator V2 can be seen at the left side of Figure 9-15 (a). The bending moment capacity at the beam-floor interface was limited; so at this stage in the test it was not possible to create a bending moment of 56 kNm at this location. When the downward part of the additional cycle was applied the crack at the interface opened at the top surface to more than 6.5 mm; at this width the steel reinforcement could be seen. Figure 9-15 (b) shows the beam-floor interface crack. The initiated cracks remained small.

(a) Hollow-core unit has cracked at the location of actuator V2

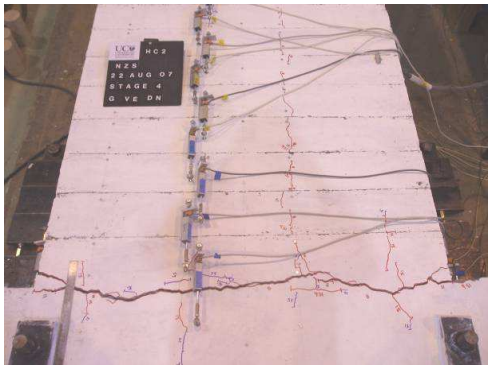

(b) Looking down at top of specimen, crack at beam-floor interface was more than 6.5 mm wide

Figure 9-15 Photos of specimen HCW2 during extended loading of Stage Four

9.2.5 Extended Testing of Specimen HCW2: Phase Two

In an attempt to induce a flexure-shear failure in a negative moment zone, flexural cracks were required at close spacing in the specimen. As sufficient flexural cracks were not induced by the original loading protocol using the hydraulic actuators V1, V2 and H3, it was decided to induce cracks by placing a wooden prop beneath the specimen and to use actuator V1 to bend the hollow-core unit over it, thus inducing high negative moments at the props location. Using this method, several flexural cracks were induced in the specimen. However, once a

crack had opened up, further loading with the prop in the same position only opened that crack further and caused cracks extending horizontally each way from the bottom of the flexural crack rather than causing additional flexural cracks to form. This resulted in the closest spacing that flexural cracks could be induced being, on average, 450 mm. Even with the presence of flexural cracks, a shear failure was not observed when a high shear was induced in the specimen. This could have been because only a small negative moment zone was induced.

Figure 9-16 shows how a negative bending moment was induced in the specimen using a wooden prop and lowering actuator V1. When the floor specimen is level, actuator V1 carries around 29 kN to support the specimen's self-weight. By reducing this load the floor is lowered at the East end inducing a moment over the prop. An upward vertical load has to be resisted at the beam-floor interface. This was achieved predominantly by friction down the crack induced at the interface. There is some uncertainty of the magnitude of the moment induced between the prop and the beam-floor interface using this method, as neither the reaction at the prop or the moment capacity at the beam-floor interface are known.

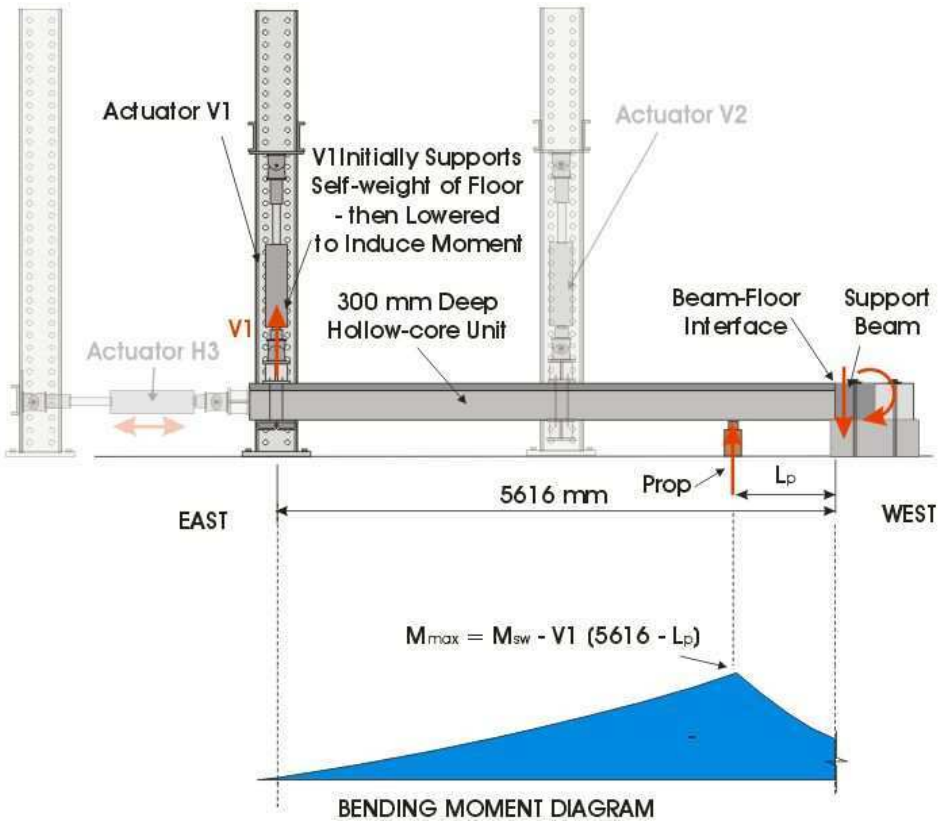

Figure 9-16 Creating negative moment in specimen using prop and actuator V1

The cracks labelled in Figure 9-17 were induced during Phase Two. Three cracks were induced on the North side of the specimen and four on the South side.

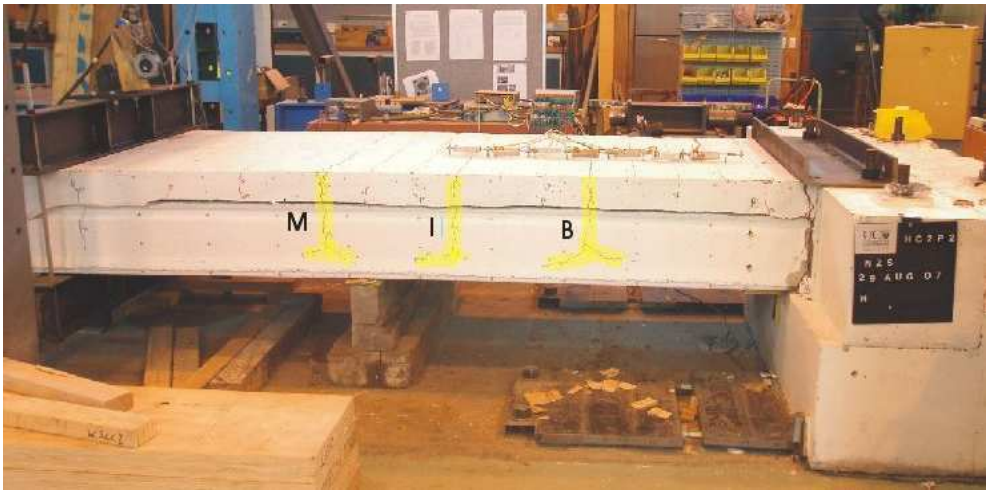

(a) North side of specimen HCW2

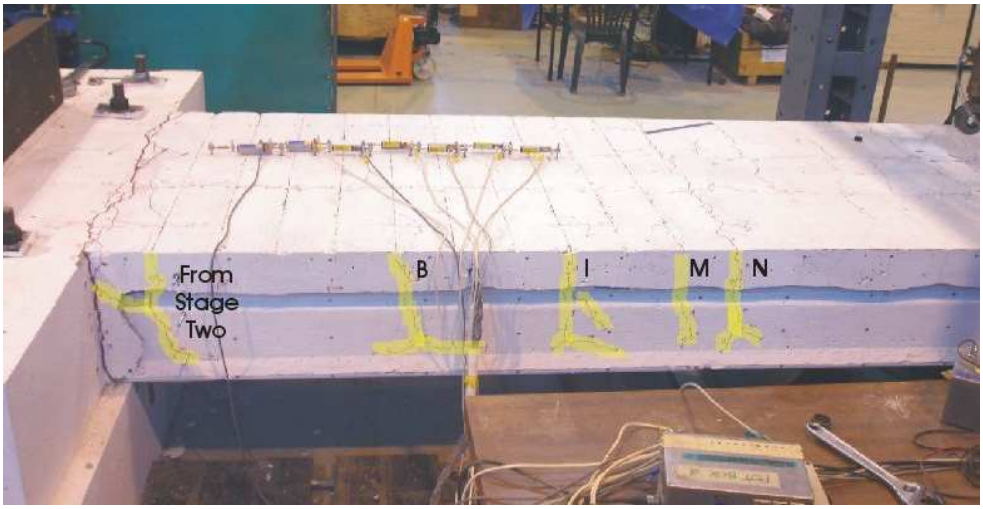

(b) South side of specimen HCW2

Figure 9-17 Flexural cracking induced during Phase Two of testing

The negative bending moments at the crack locations, which caused the cracks are given in Table 9-1. There is a considerable scatter of values. This could be partly due to the variability of the tensile capacity of concrete. It is interesting that some of the bending moments induced in the specimen during Stages One and Two were higher than these bending moments, which caused cracking, and yet did not induce flexural cracks.

Table 9-1 Negative bending moments which induced flexural cracking in the hollow-core unit

	Crack position			
	B	**I**	**M**	**N**
Negative bending moment causing cracking (kNm)	78.2	81.5	59.2	100.0

Once the flexural cracks had formed, additional negative bending moment induced horizontal cracks to form out each side from the bottom of the vertical crack. Figure 9-18 (a) shows these “tails”, the flexural crack is labelled “M” and the tails labelled “N”. It is possible that these tails formed due to stresses induced in the hollow-core unit due to incompatible displacement between the compression and tension zones. When flexural cracks are present and a negative bending moment is applied to the specimen, the concrete below the neutral axis is in compression. This causes this section of the concrete to bend. The concrete above the neutral axis is not stressed as much and remains square. The incompatibility near the base of each flexural crack induces tension and can cause the concrete to crack at this level. Figure 9-18 (b) shows this concept.

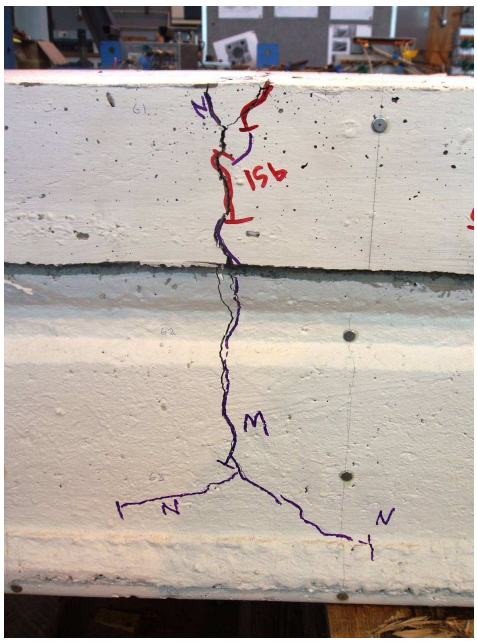

(a) Photo of flexural crack on North side of specimen showing “tails” extending horizontally

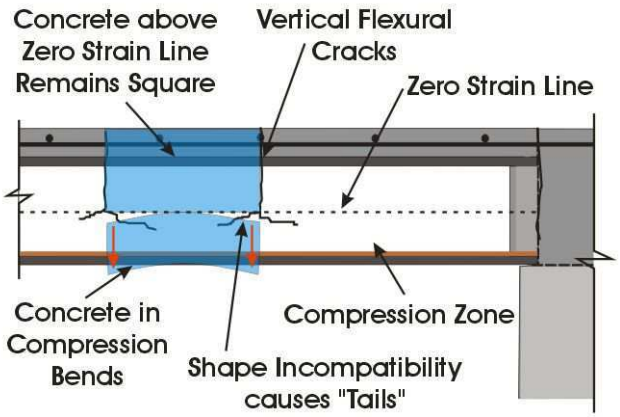

(b) Shape incompatibility causing the formation of “tails” at the bottom of flexural cracks

Figure 9-18 Incompatibility of shapes due to negative bending moment causing “tails” at the base of flexural cracks

A possible reason that cracks could not be formed at spacing closer than 450 mm was the low reinforcement ratio in the topping concrete, combined with the high tensile capacity of the hollow-core concrete. The result being that when a negative moment was induced in the specimen large enough to crack the concrete, the tensile force was larger than the force required to yield the steel. Therefore, when the crack formed, the steel yielded and larger moments could not be sustained. This prevented the formation of flexural cracks either side of the original crack.

The last flexural crack to be induced in the test specimen using the wooden prop was crack "N". Figure 9-19 shows the strains along the steel reinforcement when the prop was 1650 mm from the beam-floor interface and the load in V1 was 1.5 kN up. At the locations of cracks "B" and "I" in the hollow-core unit, the steel reinforcement is yielding. It is assumed that the steel was also yielding over crack "N"; however, this was at 1650 mm from the beam-floor interface and the steel reinforcement was not strain gauged at this location. The steel reinforcement between the flexural cracks was not yielding.

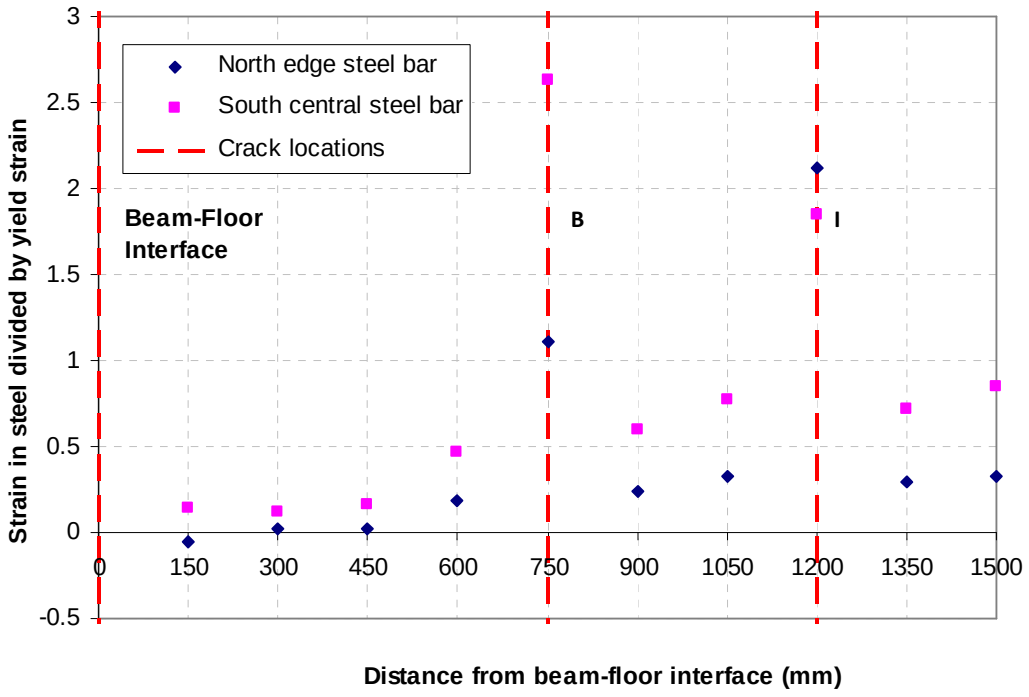

Figure 9-19 Strain in steel reinforcement along test specimen divided by yield strain

After the flexural cracks were formed, actuator V2 was used to reverse the loading and induce a high shear in the section. Unfortunately, it appears an insufficient negative flexural zone was formed to induce flexure-shear cracking when the high shear was applied. A shear failure did not occur. Figure 9-20 shows the bending moment and shear diagrams for the maximum shear that was induced in the test unit. The region of negative moment does not extend to the location of the flexural cracks. The region containing the flexural cracks was therefore in compression and a flexure-shear failure could not occur. In hindsight, actuator H3 should have been used to induce a negative moment due to the eccentricity of the starter bars.

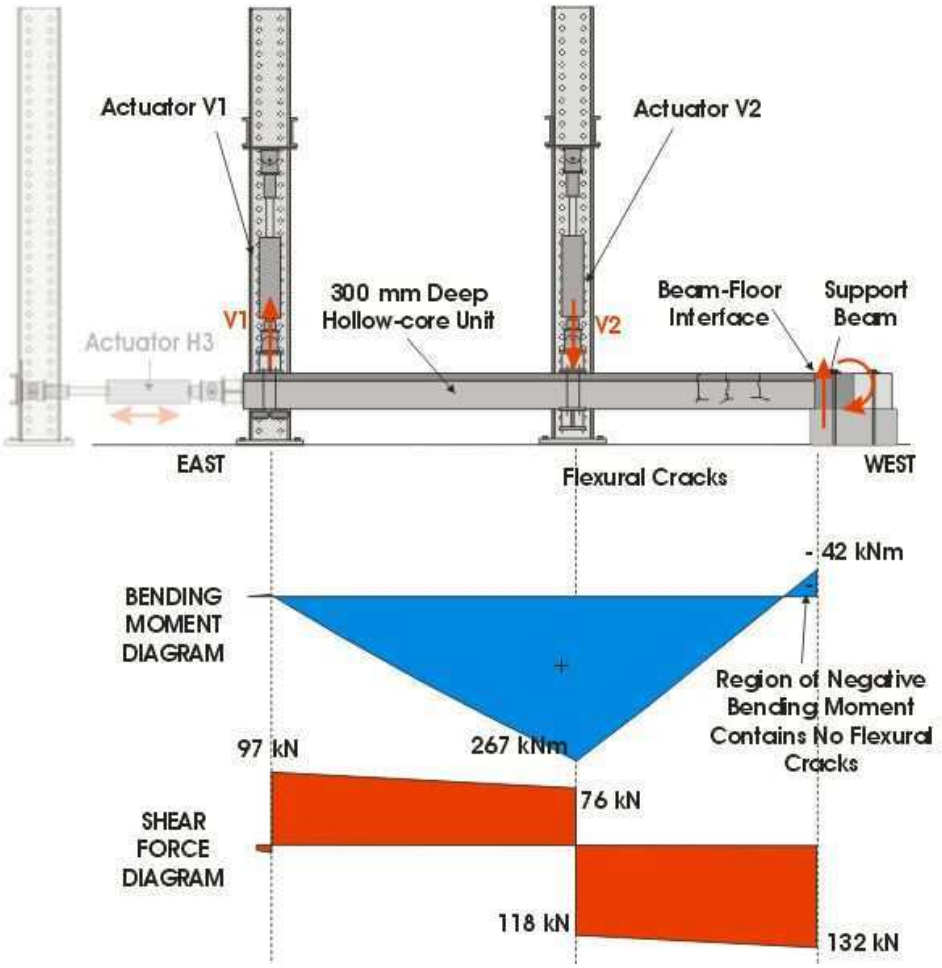

Figure 9-20 Final actions induced in test specimen HCW2

9.3 Summary and Conclusions

During Stage One, higher negative bending moment were induced in the test unit than had been planned. The beam-floor interface cracked under the load case emulating the Wellington

downward vertical earthquake design loading. Very little other cracking was observed in the specimen and the steel reinforcement was kept within its elastic range.

During Stage Two, the steel reinforcement crossing the beam-floor interface yielded. Flexural cracks were observed in the insitu topping concrete past the extent of the initiated cracks and several cracks were induced in the hollow-core unit close to the beam support.

During Stage Three, the floor unit was pulled away from the face of the supporting beam. No additional cracking was observed in the specimen due to the applied loading.

During Stage Four the test floor unit was pulled even further away from the face of the supporting beam. During the planned loading protocol no additional cracks were formed. Under a higher additional load cycle, the hollow-core unit cracked at the position of actuator V2. This occurred at an axial load of 271 kN and a bending moment of 56 kNm. It was not possible to crack the specimen closer to the beam-floor interface without causing further damage at the location of actuator V2.

During the extended loading sequence (Phase Two), flexural cracks were induced in the specimen using a prop. A shear failure in a negative moment zone was not observed, even when the planned loading protocol was extended. For this specimen this could possibly be due to the high tensile strength of the concrete and low reinforcement content in the insitu topping, which resulted in few flexural cracks forming. Once flexural cracks had been induced an insufficient zone of negative moment was induced to cause flexure-shear cracking. Therefore, the possibility of flexure-shear cracking occurring in existing hollow-core floor buildings has not been eliminated.

Blank

10 Discussion: Negative Flexural Failure

This section discusses the analytical and experimental research presented earlier in this thesis for the flexural failure mechanism possible when negative moments are induced in a hollow-core floor. Strength predictions, based on the assumption that plane sections remain plane, proved inaccurate. It appears that tension stiffening has a large influence on strains along the steel reinforcement in the insitu topping. The peak strains are much higher than the average strains predicted when assuming a linear strain profile. A consequence of this was that the test unit failed below its predicted strength. To increase the accuracy of predictions the discussion herein reviews the method for estimating flexural strength, specifically the assumption that plane sections remain plane and the influence of tension stiffening. A modified method is proposed for estimating the negative flexural strength of hollow-core flooring when the topping concrete contains cold drawn wire mesh reinforcement, which has a relatively low level of ductility. This involves finding a strain concentration factor, by which to multiply the strain in the steel reinforcement. The modified flexural strength prediction is compared to the experimental results with improved agreement. Negative flexural failures have been observed in other experimental tests at the University of Canterbury. These instances are considered and the revised method for estimating flexural capacity used to assess them. Recommendations on how to detail a hollow-core floor to avoid a negative flexural failure are given. Some hollow-core floors in existing buildings are at risk of a negative flexural failure and therefore to mitigate this risk they require retrofitting. This research has not investigated retrofit possibilities; however, a brief conceptual discussion of potential retrofit methods is included.

10.1 Prediction of Flexural Strength

In test HCW1, the steel reinforcement commenced yielding at a load below that predicted (see Section 8.2). This is of some concern as it means that the method of assessing the flexural strength used is unconservative. In assessing the flexural strength of a concrete member, several assumptions are normally made. To investigate why the flexural strength predictions for this test were unconservative these assumptions must be reconsidered. The standard assumptions in flexural assessment include;

- the steel and concrete have perfect bond
- the stress levels are uniquely related to strains

- the ultimate flexural strength is attained at specified strain levels
- the tensile strength of concrete is ignored
- an equivalent stress block can be used to describe the magnitude and position of the compression force.
- plane sections are assumed to remain plane.

When assessing the flexural strength of the test specimens in this research, the effects of first five assumptions were minimised and should have had negligible effect on the estimated capacity. The assumption of perfect bond is only true for uncracked sections, hence was ignored. Material properties were measured from standard test specimens, including the stress-strain relationship of the steel reinforcement, which was used to define when the flexural strength was reached. Two flexural strength limits were looked at, first when steel reinforcement yielded and then when it reached its ultimate capacity. Instead of using an equivalent stress block to approximate the compression force in the concrete, a stress-strain relationship for the concrete was used. The tensile strength of concrete was neglected; however, at the flexural strength limits considered the tensile contribution of the concrete at cracks is small. Section 5.4 outlines the method used to predict the flexural strength of the test specimen using all the above assumptions.

The fifth assumption, that plane sections remain plane, was also used in the strength predictions, but may not be appropriate in this situation due to the influence of tension stiffening. The following paragraphs discusses the validity of assuming that plane sections remain plane when estimating the flexural capacity of a hollow-core floor that contains non-ductile mesh reinforcement in the insitu topping concrete. By comparing test results with theoretical predictions it is proposed that, in this case, the peak strain in the steel at crack locations is four to five times the average strain predicted from a linear strain profile. In this discussion this ratio will be referred to as the "strain concentration factor".

10.1.1 Plane Sections remaining Plane and Tension Stiffening

The assumption that "plane sections remain plane" is illustrated in Figure 10-1. It can be seen that sections A-B and C-D are still straight after a moment has been applied. The upper face of the member has decreased in length and the lower face has become longer. The longitudinal line that remains the same length is the neutral axis. The assumption that plane

sections remain plane implies that the strains in a section vary linearly with distance from the neutral axis. When a member is subjected to bending and shear, it is recognised that, as the ultimate strength of a reinforced concrete member is approached, the strain profile deviates from linear. This is especially noticeable when diagonal cracks form due to high shear stresses. This non-linearity does not normally have a large effect on the flexural strength, provided adequate shear reinforcement is included, so the assumption of plane sections remaining plane is widely used (Paulay and Priestley 1992).

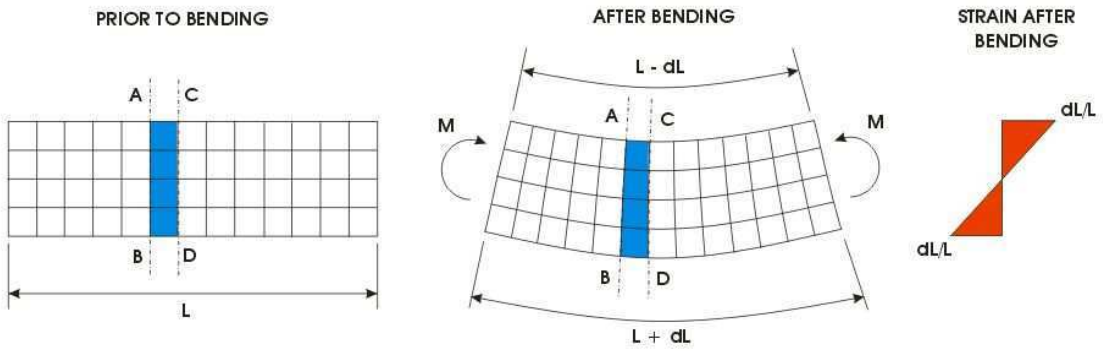

Figure 10-1 Plane sections remaining plane

The assumption is valid for uncracked reinforced concrete sections, and generally remains valid once the member cracks in flexure if the sections compared have several cracks between them and are located mid-way between cracks. The strains gained from the linear strain profile between two sections mid-way between cracks, are the average strains between these two sections. The strain profiles at any section within this region do not have to be linear. In fact, due to bond between the steel reinforcement and the concrete, the strains between the two sections will vary depending on their position relative to a crack.

Figure 10-2 illustrates the distribution of forces and strains along a segment of reinforced concrete beam in pure flexure. The bending moment (M) is constant along the section; however, the strains in the steel and the concrete vary. When assuming plane sections remain plane, it is the average strains in the concrete and steel that are found, these are less than the peak values. At crack locations, nearly all the tensile force is taken by the steel reinforcement (T_c). Away from the cracks, some of the tension in the steel is transferred to the concrete through bond. In the transfer length, the strains in the concrete and the steel differ and some slip occurs. Mid-way between the cracks, as the concrete takes some of the tensile strength,

the centroid of the tensile force moves closer to the beam centreline and reduces the length of the lever arm from l_{ac} to l_{auc}. As the same bending moment, M, is still resisted, the magnitude of forces in the section increase ($T_c = C_c$, $T_{cu} = C_{cu}$ and $T_c < T_{cu}$), the position of the zero strain line (or neutral axis) and centroid of the compression force, move towards the tension face. These changes contribute to the overall stiffness of the beam; the effect they have is termed tension stiffening. In a normal reinforced concrete beam, tension stiffening has little effect on the prediction of flexural strength, as the location of the compression force is not significantly changed and the average and peak strains are similar (see Figure 10-3 (a)).

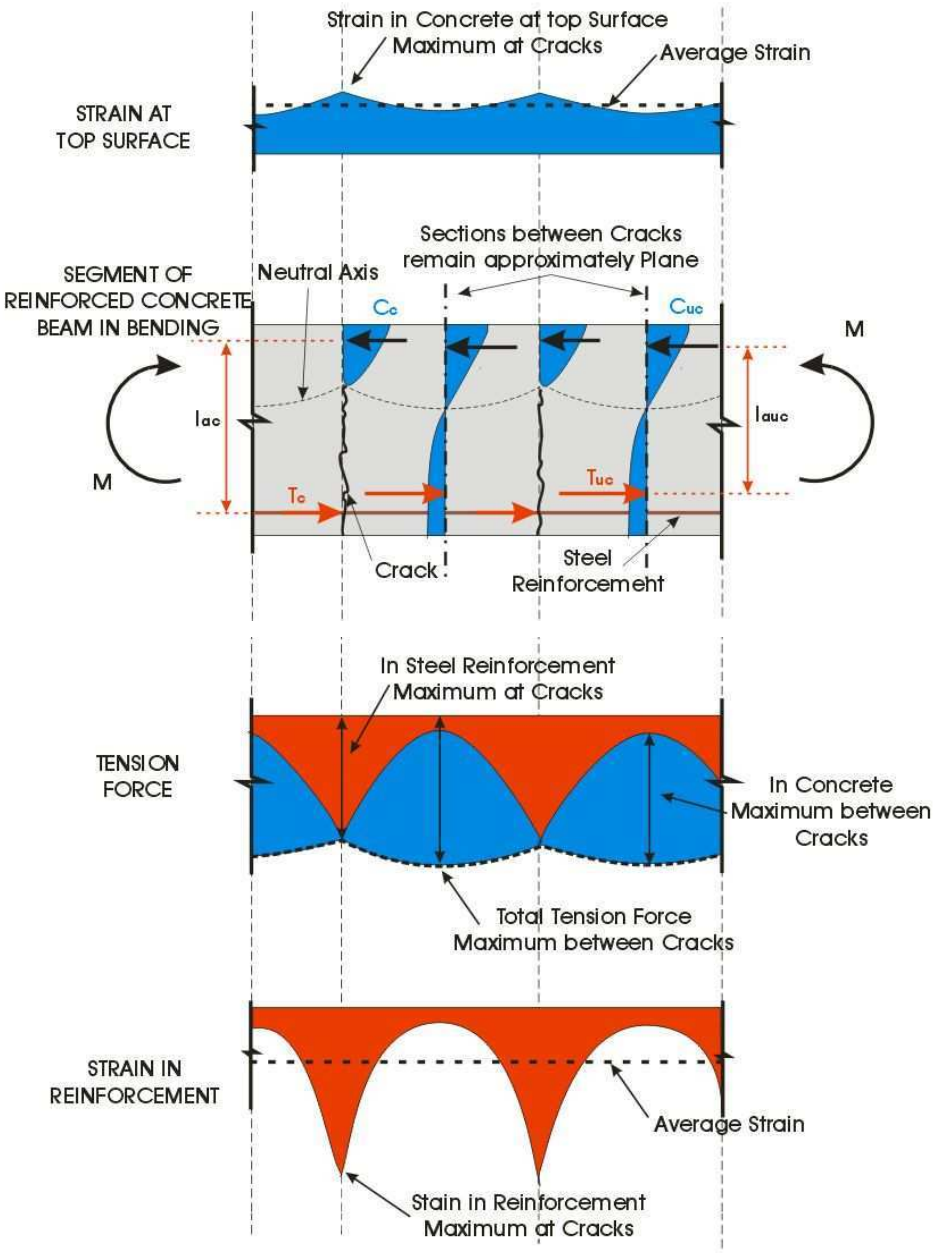

Figure 10-2 Real forces and strains in a section of reinforced concrete beam

For a section of hollow-core flooring, the effect of tension stiffening is more pronounced. Figure 10-3 compares the effects of tension stiffening between a section of standard reinforced concrete beam and a segment of hollow-core floor. For the reinforced concrete beam, the yield moment is similar whether the effect of tension stiffening is included or not. However, for the hollow-core floor the presence of the prestressing force (P) and the low quantity of steel tension reinforcement (A_s) causes the centroid of the compression force (and therefore the zero strain line) to move further towards the tension face. When the effect of tension stiffening is included the strain in the steel reinforcement in the region of the crack is over 4 times that of a linear strain profile. The example shown in Figure 10-3 (b), the reduction in ultimate bending moment when the effect of tension stiffening is included is around 20 %. The example assumed a 300 mm deep hollow-core section with 60 mm topping containing mesh reinforcement. The points shown are when the mesh reinforcement reached a strain of 2 %, which was assumed to be around its ultimate. The compressive strength of the hollow-core unit was assumed to be 88 MPa. When the mesh is at its ultimate strain the concrete is below this stress.

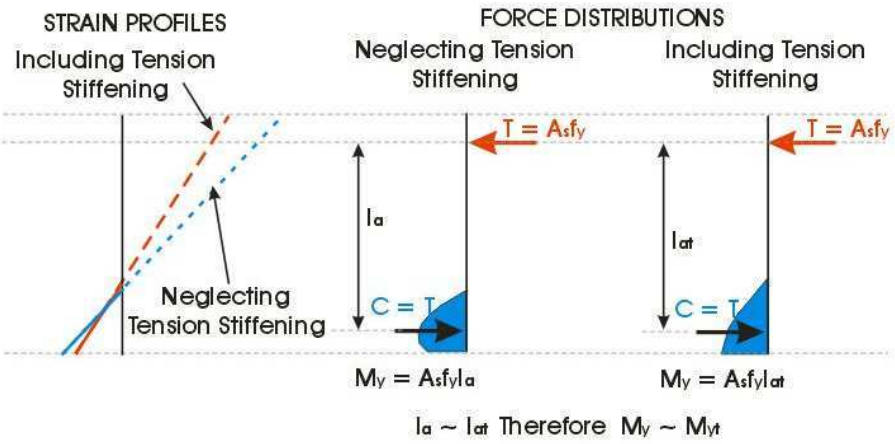

(a) Strains and forces in a normal reinforced concrete beam

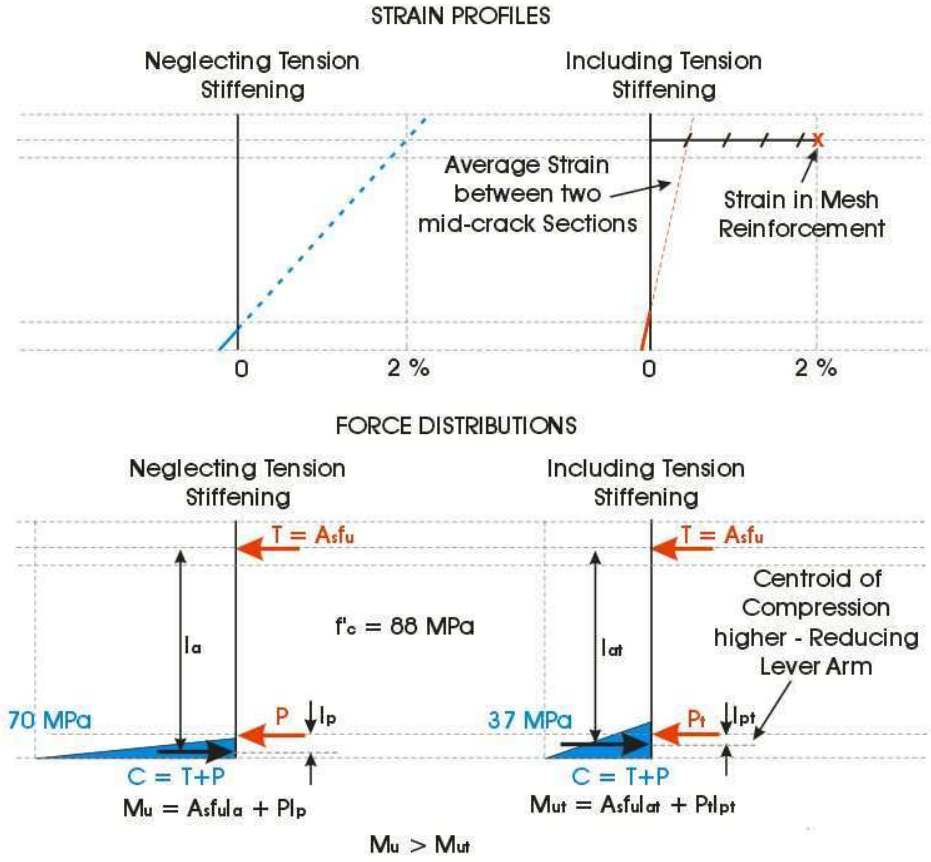

(b) Strains and forces in a prestressed hollow-core floor

Figure 10-3 Effect of tension stiffening on members in bending

To account for the effect that tension stiffening has on the negative flexural capacity of a hollow-core floor, it is proposed that the average strain gained from a linear strain profile is multiplied by a strain concentration factor. Figure 10-4 shows the difference for a hollow-core

section between the average strain and the peak strain, found between two sections mid-way between cracks. The average strain is calculated assuming plane sections remain plane, it is equal to the change in length at the level of the mesh reinforcement (dm) divided by the length between two cracks (L_c). The strain concentration factor is the number the average strain must be multiplied by to equal the peak strain. The length over which the majority of the change in length occurs in the mesh is not L_c, but the distance between transverse bars of the mesh reinforcement (D_m) or less. This is because the transverse bars fix the longitudinal bars at these locations and stop stress penetration further along them. To find the strain concentration factor it is proposed that the length between flexural cracks (L_c), is divided by the length over which the majority of the extension in the steel occurs (L_s).

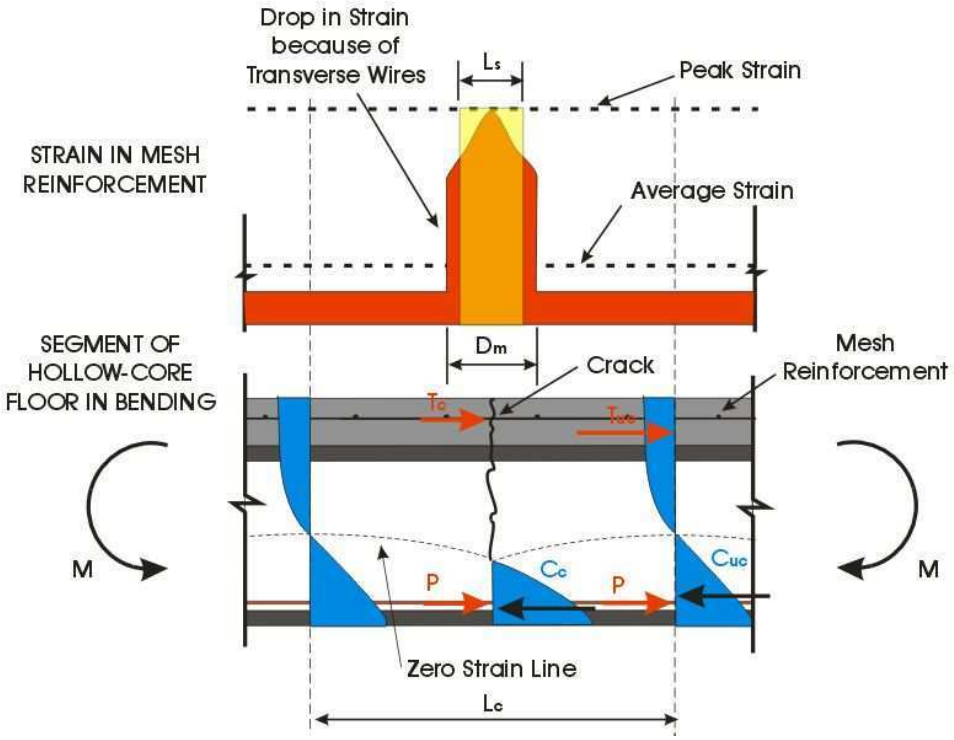

Figure 10-4 Strains in a section of hollow-core floor

In a hollow-core floor both of the spacing of the cracks and the amount of strain penetration in the steel are variable. However, the range in which the strain concentration factor is likely to be can be found. For a floor containing a 300 mm deep hollow-core unit and non-ductile mesh with transverse wires at 150 mm spacing, the crack spacing is likely to be between 200 mm and 600 mm and the strain penetration of the mesh reinforcement to be

between 50 mm and 150 mm (see Figure 10-5). These values give a strain concentration factor anywhere between 1.3 and 12.0.

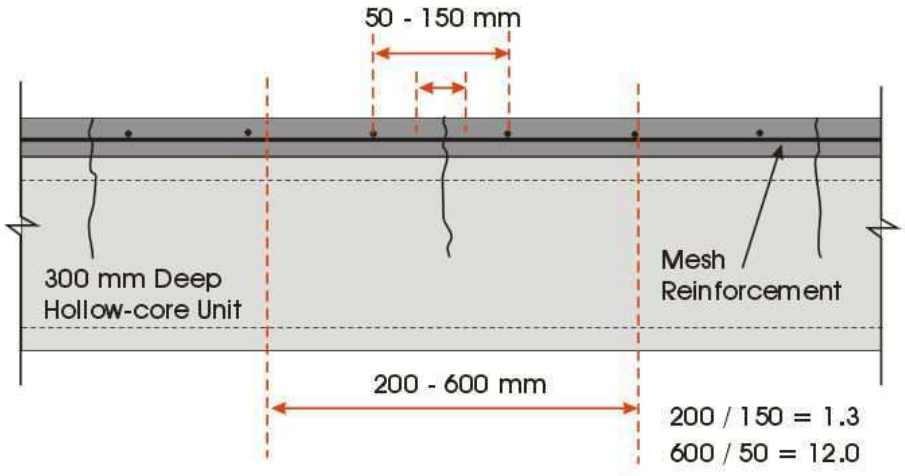

Figure 10-5 Variability of length over which strain occurs in concrete and steel

For test specimen HCW1, the crack spacing was observed and the length of strain penetration in the steel can be calculated; therefore, the strain concentration factor was assessed. The difference between the original prediction of first yield moment and the observed yield moment is known. By comparing the predicted and the observed moments, the ratio between the peak strain in the steel and the average between cracks can be assessed. This should be similar to the ratio predicted by looking at the crack spacing and strain penetration in the steel. For the test specimen HCW1, the predicted first yield moment at the end of the starter bars, using a linear strain profile, was 48.00 kNm (see Appendix A3). The moment applied to the section at the end of the starter bars during testing, which caused the mesh reinforcement to yield, was 31 kNm, that is 65 % of the estimated value. To decrease the "predicted value" to 31 kNm, the strain in the steel found from a linear strain profile must be multiplied by five.

The crack spacing in the test was observed to be 530 mm. Bond and transfer of force between the concrete and steel result in the strain in the steel varying. To find the length over which a constant strain in the mesh is equal to the yield strain, when in reality the maximum steel strain is equal to the yield strain, the bond characteristics of the mesh must be assessed. An analytical method to achieve this is presented below.

In the test specimen, the insitu topping concrete contained 665 mesh reinforcement. This is comprised of cold-drawn plain round bars with a diameter of 5.3 mm. The transverse bars were spot welded at 150 mm centres to produce the mesh. When the concrete cracks under a negative bending moment, the mesh reinforcement spanning the crack resists the tensile forces. The tensile force in the mesh reinforcement is then transferred to the concrete by: bond between the longitudinal bars and the concrete, and the anchorage effect of the transverse bars.

There are two components of bond between concrete and smooth bars in direct tension, adhesion and dry friction. The adhesive bond is due to the deformation of the cementitious layer around the bar. This breaks at relatively small displacements and is therefore not significant. Dry friction is the force due to the radial compressive stresses around the bar caused by concrete shrinkage. Factors that affect the bond are the concrete quality, surface roughness of the bar and the location of the bar in the concrete. When fresh concrete settles, water accumulates under the reinforcing bars, known as "water gain". The more fresh concrete that is below the bar, the more water accumulates, which is detrimental to the bond. Bond is also reduced when a bar begins to yield in tension; the contraction of the bar reduces the radial compressive stresses and consequently the bond due to friction (Fédération Internationale du Béton. 2000).

The CEB-FIP model code (Comité euro-International du Béton. and Fédération Internationale de la Précontrainte. 1993) defines a model for the bond stress-slip relationships of steel reinforcement in concrete. The model assumes that in the uncracked state, strains are equal in the steel and the concrete. When a crack forms in the concrete, the tension in the steel is transferred to the concrete over a transfer length, l_t, by the bond between the two. The bond stress is modelled as a function of slip (the difference between the strain in the concrete and the steel). For smooth cold-drawn bars with good bond, the relationship is given by Equation 10-1 and Equation 10-2.

$$\tau = \tau_{\max}\left(\frac{s}{0.01}\right)^{0.5} \qquad \text{For } s < 0.01 \text{ mm} \qquad \textbf{Equation 10-1}$$

$$\tau_{\max} = 0.1\sqrt{f_{ck}} \qquad \text{For } s \geq 0.01 \text{ mm} \qquad \textbf{Equation 10-2}$$

Where τ is the bond stress, s is the slip and f_{ck} is the characteristic value of the concrete's compressive strength from a standard cylinder or cube test. The relationship is a statistical

mean curve derived from experimental data. Bond strength is variable, with test results often having a coefficient of variation of up to 30 %, so the relationship is not intended for accurate design. The relationship is not appropriate for use after bars have yielded. In work completed by Soltani et al. (2004) on elements reinforced with welded wire mesh, the bond stress post yield was assumed to be zero. This work also includes a decrease of bond stress near the crack to account for bond deterioration due to splitting and crushing of the concrete.

For the cold-drawn mesh used in the insitu concrete of test HCW1, a maximum bond stress of 0.53 MPa is calculated using Equation 10-2. This is much smaller than typical values given in British literature of the 1970s. Typical ultimate allowable bond stresses for similar situations were given as in the order of 1.4 MPa (Morrell 1977).

The transverse bars of the mesh reinforcement also contribute to the transfer of tensile stress into the concrete due to the bearing of the wires against the supporting concrete. At can be assumed that the transverse bars provide sufficient anchorage to the steel that the longitudinal bars are fully restrained at this location and zero slip occurs at the weld point. If this is the case, then the width of a crack formed between two transverse bars is a function of only the slip between these two bars. If a crack forms at the location of a transverse bar then the slip may occur over a length twice this long; however, to be conservative it is assumed the crack forms mid-way between transverse wires.

Using this theory, the change in stress, and therefore strain can be found, between two transverse wires that have a crack in between them (see Figure 10-6). If we assume that the mesh yields at the crack location, then the stress at this location is around 650 MPa (see Appendix C5.5). The bond stress is 0.53 MPa (found using the CEB-FIP model code) (Comité Euro-International du Béton. and Fédération Internationale de la Précontrainte. 1993), so over 75 mm along the 5.3 mm bars the stress in the mesh is reduced to 620 MPa. Figure C30, in Appendix C5.5, shows the measured stress-strain relationship for the mesh. From this curve, the average strain between stresses of 650 MPa and 620 MPa is found to be 0.0038. Note that these strains were found from the measured stress-strain curve and not the bi-linear approximation. The change in length this corresponds to is 0.57 mm over the 150 mm between transverse wires. An equivalent length can be found if the average strain is taken as equal to the yield strain (the strain that corresponds to a stress of 650 MPa). The yield strain is approximately 0.0041, the length over which this gives a change in length of

0.57 mm is 140 mm. This length is what we compare with the crack spacing to find the ratio of steel strain to the linear strain profile. A similar can be used to estimate crack widths.

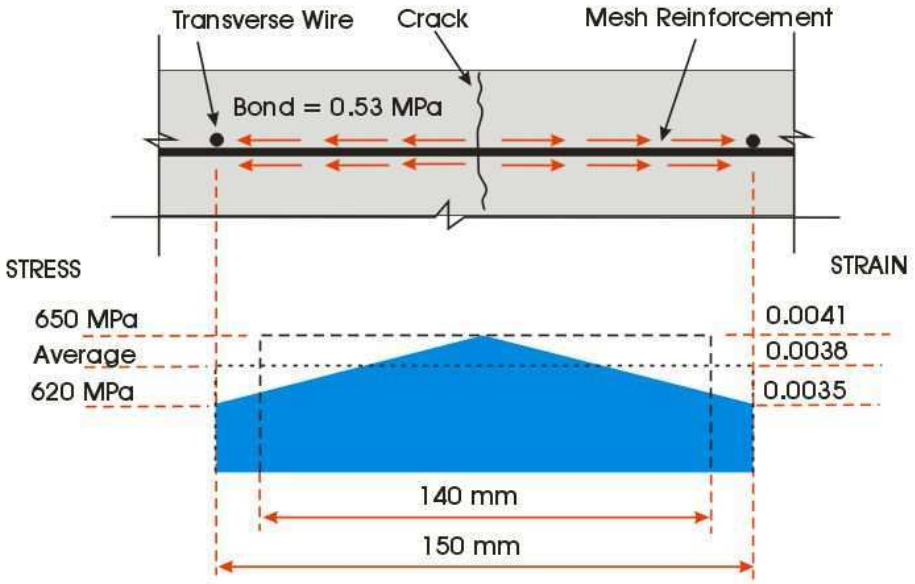

Figure 10-6 Stress and strain in mesh between transverse wires

The ratio of the peak steel stress to the stress assumed by a linear strain profile should be around 530/140 = 3.8, where 530 mm is the crack spacing and 140 mm is the equivalent length of strain penetration in the steel at yield. This is smaller than the 5.0 predicted by comparing the observed yield moment with the original prediction of yield moment. There could be several reasons for this. One is the potential error in calculating the observed yield moment, the potential magnitude of this uncertainty is presented in Appendix D3. The other reason for the error could be the assumptions used in predicting the length of strain penetration in the steel. These included the stress-strain relationship of the mesh and the amount of bond. If a higher bond stress of 1.4 MPa (as suggested by Morrell (1977)) is used the length reduced to 127 mm and the ratio increases to 4.2. It is reasonable to assume a good bond between the mesh and concrete as the concrete is thin (on average only 58 mm deep) and there would be minimal bleed water below the bars.

From the above discussion, it is reasonable to assume that the strains in the steel are around 4.2 times the strains given by assuming a linear strain profile. To investigate the strain in the steel further, the measurements from Demec readings taken during the test along the sides of

the unit are analysed. These measure a change-in-length, which can be converted to a change in strain up the section.

10.1.2 Strain profile along unit

The following discussion compares the change-in-strains calculated from Demec readings taken during the test and predicted change-in-strains for the hollow-core floor specimen using standard assumptions. To illustrate the differences, the change in strains up the sides of the hollow-core unit between the start of the test and Increment 16 are investigated.

Due to prestressing and effects such as creep and shrinkage, the real strain in the hollow-core section could not be measured, as the initial strain condition was unknown. Instead, the change in strain along the member from the beginning of the test was calculated. Several times during test HCW1, Demec gauge readings were taken along the sides of the hollow-core unit and insitu topping. The location of Demec points are shown in Figure 7.20 and Figure A1. From sets of Demec readings, the change in length during the test, between the Demec points was found. The change-in-strain, induced between Increment 16 and the beginning of the test, was calculated by dividing the change in length, by 250 mm (the original length between the Demec points). The change-in-strain found is an average between the two Demec points. Figure 10-7 shows the average measured change-in-strain profiles along the test specimen over 250 mm intervals, compared to the profiles predicted using standard theory. The change-in-strains measured and predicted at the level of the steel reinforcement are also shown. These are average values over the 250 mm intervals so the peak strains may be higher than these (as shown in yellow).

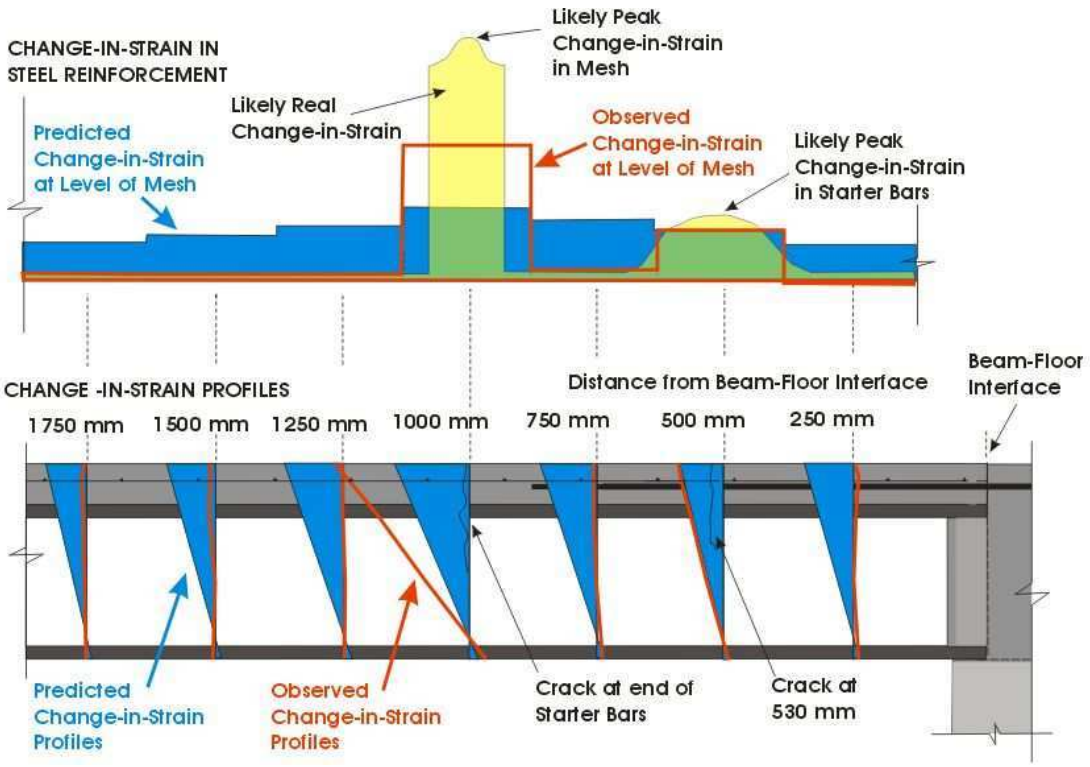

Figure 10-7 Measured versus predicted change-in-strain profiles along test specimen at Increment 16

The method used to predict the change-in-strain profiles along the floor specimen is shown in Appendix F1. The predictions were made assuming that the concrete did not have any tensile capacity, that plane sections remained plane and tension stiffening did not affect the strength of the member. At the beginning of the test, there were already strains induced in floor specimen due to the prestressing and its self-weight, therefore the change-in-strain profiles shown do not represent the real strain in the section. For example, the location the change-in-strain profile crosses the y-axis is not the location of the zero strain line. The change-in-strain profiles along the floor are used solely to illustrate that the predicted strains (or change-in-strains in this case) are not always accurate.

Increment 16 was at the end of Stage One in the loading protocol. By this time in the test, the unit had cracked at three locations; the beam-floor interface, 530 mm out from the interface and 1058 mm out from the interface, these crack locations are shown in Figure 10-8 and Figure 10-7. The measured versus predicted change-in-strain values vary in three ways in Figure 10-7. These are:

- **at the un-cracked sections**. Here the predicted values are higher than the actual change-in-strains. This could be because the prediction assumed the concrete did not have any tensile capacity, essentially assuming a cracked section.
- **at the crack 530 mm from the beam-floor interface**. Here the predicted and measured change-in-strains correlate well. The starter bars in the insitu concrete cross this crack and the moment applied at this location was below the predicted first yield moment of that section.
- **at the end of the starter bars**. Here the predicted change-in-strains are lower than the measured values. At this location, the negative bending moment predicted was below the first yield moment. However, it was shown in Section 8 that the mesh at this section was yielding. It therefore appears that the strain profile and yield moment predictions at this section are incorrect. As discussed previously, a possible explanation for this discrepancy is the effect of tension stiffening.

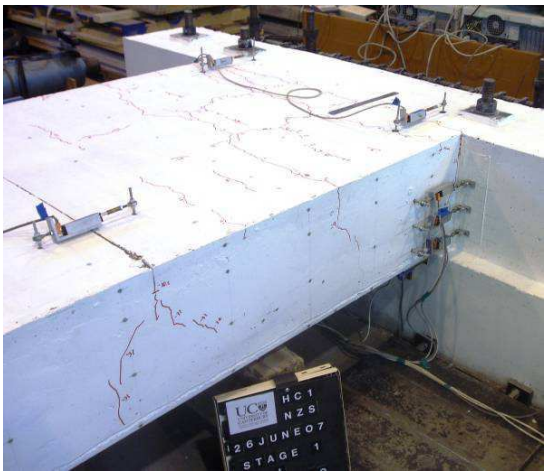

(a) Demec points down side of test unit and cracks in red, with insitu concrete down sides

(b) With insitu concrete removed real crack location is observed

Figure 10-8 Cracks down side of test unit HCW1

In Section 10.1.2 it was proposed that assuming a linear strain profile is not appropriate in this situation. Instead, the strain in the mesh is a multiple of the average strain found by a linear strain profile at that level (the average strain multiplied by the strain concentration factor). Figure 10-9 shows the change-in-strain values over the crack at the end of the starter bars between the beginning of the test and Increment 16. The measured value is shown in solid red. The other lines are predicted strain profiles when different strain concentration factors are used to calculate the strain in the mesh reinforcement. It appears a multiple between four and

five would predict a strain of around the correct magnitude at the level of the mesh. The main difference between the predicted strain profiles and the measured profile is that the measured profile is approximately linear, whereas the predicted profiles become increasingly "kinked" as the strain concentration factor was increased. If the hypothesis that the strain profile is not linear is correct then the measured values should also be "kinked". A possible reason that the measured profile was not observed to be "kinked" could be that the measurements taken from the lower Demec points did not reflect the movement of the hollow-core unit itself. The Demec points were glued to the insitu concrete; it can be seen in Figure 10-8 that the location of cracks observed in the insitu concrete was not the same as the crack in the hollow-core beneath. This suggests that there must have been some differential movement between the two. The insitu concrete was easily removed, suggesting there was little bond to the hollow-core unit. It is possible that the real strain profile was "kinked".

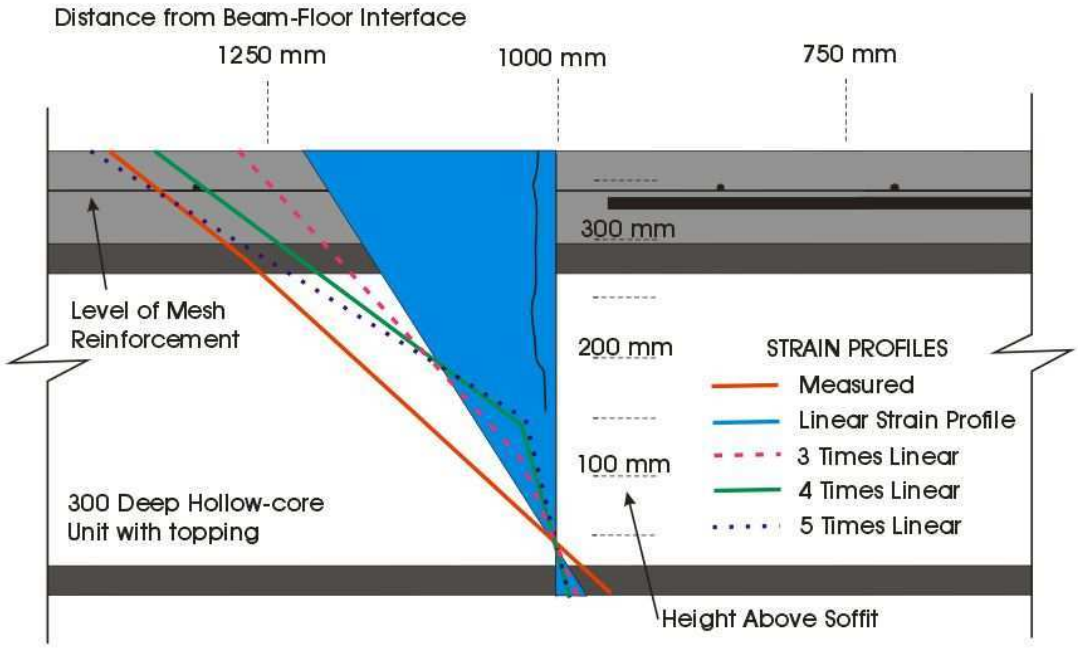

Figure 10-9 "Change-in-strain" profile spanning crack at the end of the starter bars

The above discussion aimed to derive an appropriate strain concentration factor between the peak strains in the mesh reinforcement and the average found when using a linear strain profile. To achieve this the observed versus predicted bending moments were compared, the different lengths over which strain developed were looked at and observed versus predicted strain profiles were compared. From this it appears reasonable to assume that, at the end of

the starter bars in test unit HCW1, the strain in the steel is between four and five times the strain from a linear strain profile.

10.2 Revised Predictions versus Results

The predicted bending moment capacity of the test unit at the end of the starter bars was above the observed capacity. This is shown in Figure 8.7, where the observed first yield moment (between increments 8 and 16 on the graph) of the section at the end of the starter bars is 64 % of the predicted first yield moment (M_y). The previous section suggests that this is because the assumption that 'plane sections remain plane' is not valid when crack spacing is wide and the topping concrete contains minimal reinforcement. Revised calculations are presented here, assuming a strain concentration factor of 4.2 for the strain in the mesh reinforcement. The value of 4.2 was selected because this is the ratio of the distance between flexural cracks and the equivalent length of mesh yielding when good bond between the steel and concrete is assumed. The first yield moment calculated assuming a linear strain profile (plane sections remain plane), under no axial load is 48 kNm. When a strain concentration factor of 4.2 is used, the strain in the steel is 4.2 times that given by a linear strain profile and the first yield moment reduces to 33 kNm. Figure 10-10 shows the change in bending moment at the end of the starter bars during test HCW1, along with the applied axial tension (in brown).

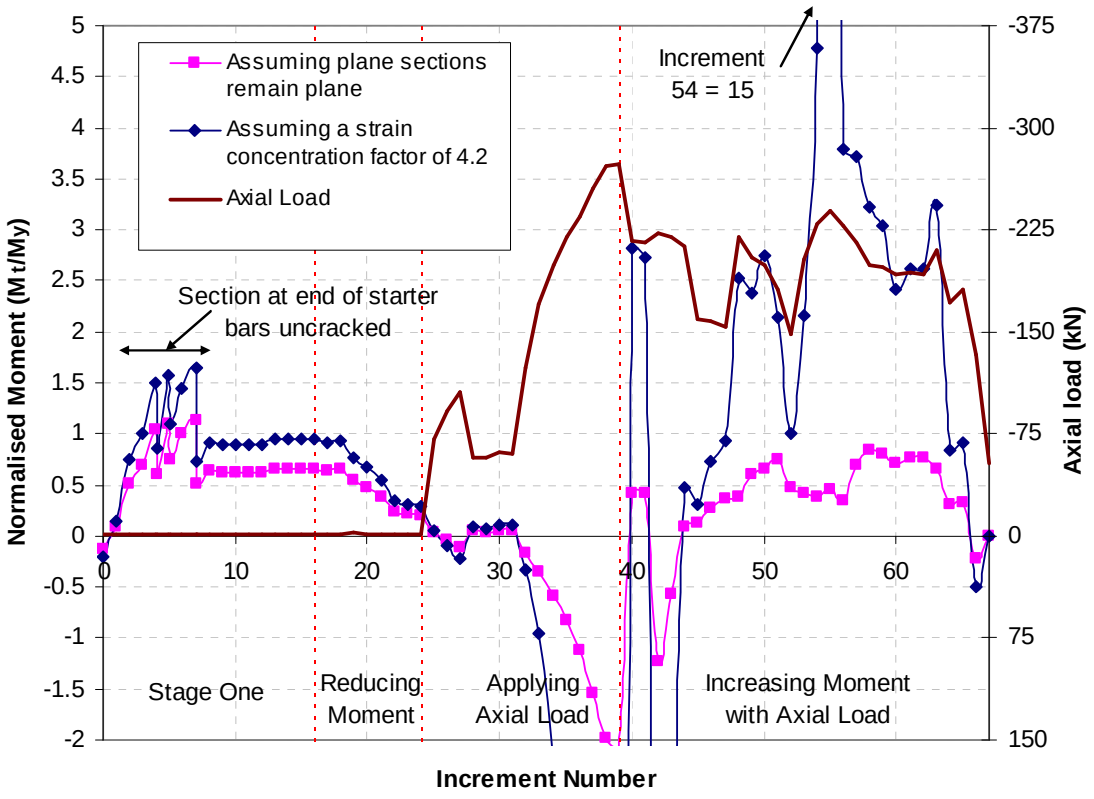

Figure 10-10 Tri-axis plot showing the change in moment at the end of the starter bars, normalised by the predicted first yield moment at the end of the starter bars, and the change in axial load during test HCW1

The measured bending moment is plotted in Figure 10-10 normalised by the predicted first yield moment (M_y). The first yield moment is defined as the moment required to cause the mesh in the topping concrete to yield. A value larger than one would suggest that the section was yielding. There are two bending moment lines on the plot; the pink line measured moment is normalised by a first yield moment calculated assuming standard flexural theory. The blue line is normalised by the revised calculation for the first yield moment where a strain concentration factor of 4.2 is used in the prediction. Where the mesh was first observed to yield during the test, between increments 8 and 16, the revised calculation gives a prediction much closer to a value of one. It appears that at increments 4, 5 and 7 the section is already yielding. However, these moments were achieved before the section at the end of the starter bars had cracked, so the tensile capacity of the concrete would have contributed to the moments and the mesh was not yielding. After increment seven, the section did crack and it is assumed that the mesh reinforcement carries all the tension force contributing to the resisted moment.

After increment 39 in the test, the specimen had both axial load and negative bending moment applied. The first yield moment used to normalise the measured moment during this stage in the test takes into account the effect of axial load. During this stage of the test, the crack width at the end of the starter bars was always increasing, suggesting that the negative moment and axial load combinations applied were above the yield moments. This is in agreement with the revised calculations as the blue line is always above a value of one. Increment 58 was the last reading taken before one of the mesh bars ruptured. Increment 65 was the last reading before the remaining mesh bars ruptured and the specimen failed. After increment 40 in the test the measured negative bending moments are up to 15 times the predicted first yield moment. This is because, due to the high axial load applied, very small negative bending moments cause the section to yield. The stress-strain relationship of the mesh reinforcement is approximately bi-linear and the there is still some strength increase after yield so higher moments can be sustained before failure. Figure 10-11 is a similar plot to Figure 10-10 except that the negative bending moments are normalised by the predicted ultimate moment rather than the predicted first yield moment.

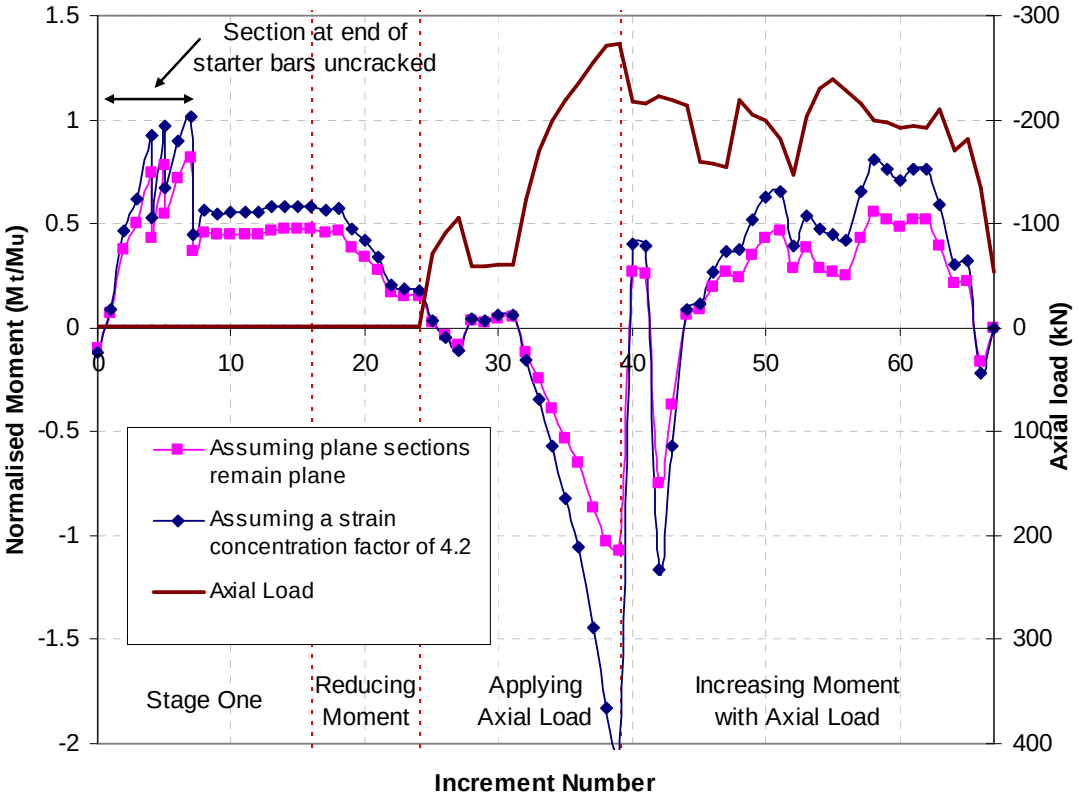

Figure 10-11 Tri-axis plot showing the change in moment at the end of the starter bars, normalised by the predicted ultimate moment at the end of the starter bars, and the change in axial load during test HCW1

Figure 10-11 shows that using a strain concentration factor of 4.2 results in the measured moments being closer to the ultimate (closer to a value of one). On this plot a value of one would suggest that the mesh had reached its ultimate capacity and should rupture. The only place that this occurs is at increment 7. As mentioned above, at this point in the test, the section at the end of the starter bars had not yet cracked and therefore the concrete resisted some of the tensile forces, hence the mesh would not have been near ultimate. After increment 7, the closest the bending moment gets to the ultimate moment is at increment 58, this is where the first of the mesh wires ruptured. After this point, it appears that the bending moment moves away form the ultimate moment; however, the reduction in the area of steel due to the first wire rupturing was not accounted for in the ultimate moment capacity calculation. Therefore, the bending moment is likely to still be near its ultimate at increment 65, when the remaining wires of mesh ruptured and the specimen failed.

The revised calculation method appears to have an improved correlation with the observed test behaviour than the original predictions. However, the calculated yield moment was still slightly less than the observed and therefore unconservative. In the discussion of Figure 8.7 in Chapter 8, other uncertainties associated with comparing the observed versus calculated bending moments are discussed, these uncertainties could easily account for the variation seen. Therefore, the revised method of calculating the negative flexural strength of a hollow-core section by increasing the strain in the mesh reinforcement is believed to be well-founded and gives a superior estimate of a sections flexural strength.

The strength reduction factor given in the New Zealand Concrete Structures Standard (Standards New Zealand 2006) for members in flexure with or without axial load is 0.85. The revised method for calculating the negative flexural strength of a hollow-core floor that contain only mesh reinforcement in the topping concrete described above, involves multiplying the strain in the mesh by a factor equal to the ratio between the crack spacing and the equivalent unbonded length of mesh. There are uncertainties involved with estimating both the crack spacing and the unbonded length of mesh; these lead to errors in the calculation of negative flexural strength. It is therefore recommended that a smaller reduction factor be used.

10.3 Negative Flexural Failure Observed in Experimental testing

Several researchers have used sub-assembly test setups to investigate the performance of connection details between hollow-core floors and their supporting beams. Section 2.4 gives a brief overview of this research and major findings. Of the researchers, Bull and Matthews (2003), Liew (2004), MacPherson (2005) and Jensen (2006) all imposed negative moments to the floor systems in their test setups. This section briefly looks at possible reasons why some of the details tested experienced negative flexural failures and others did not. Figure 10-12 shows eight connection details tested in sub-assembly tests at the University of Canterbury where negative moments have been induced as part of the loading protocol.

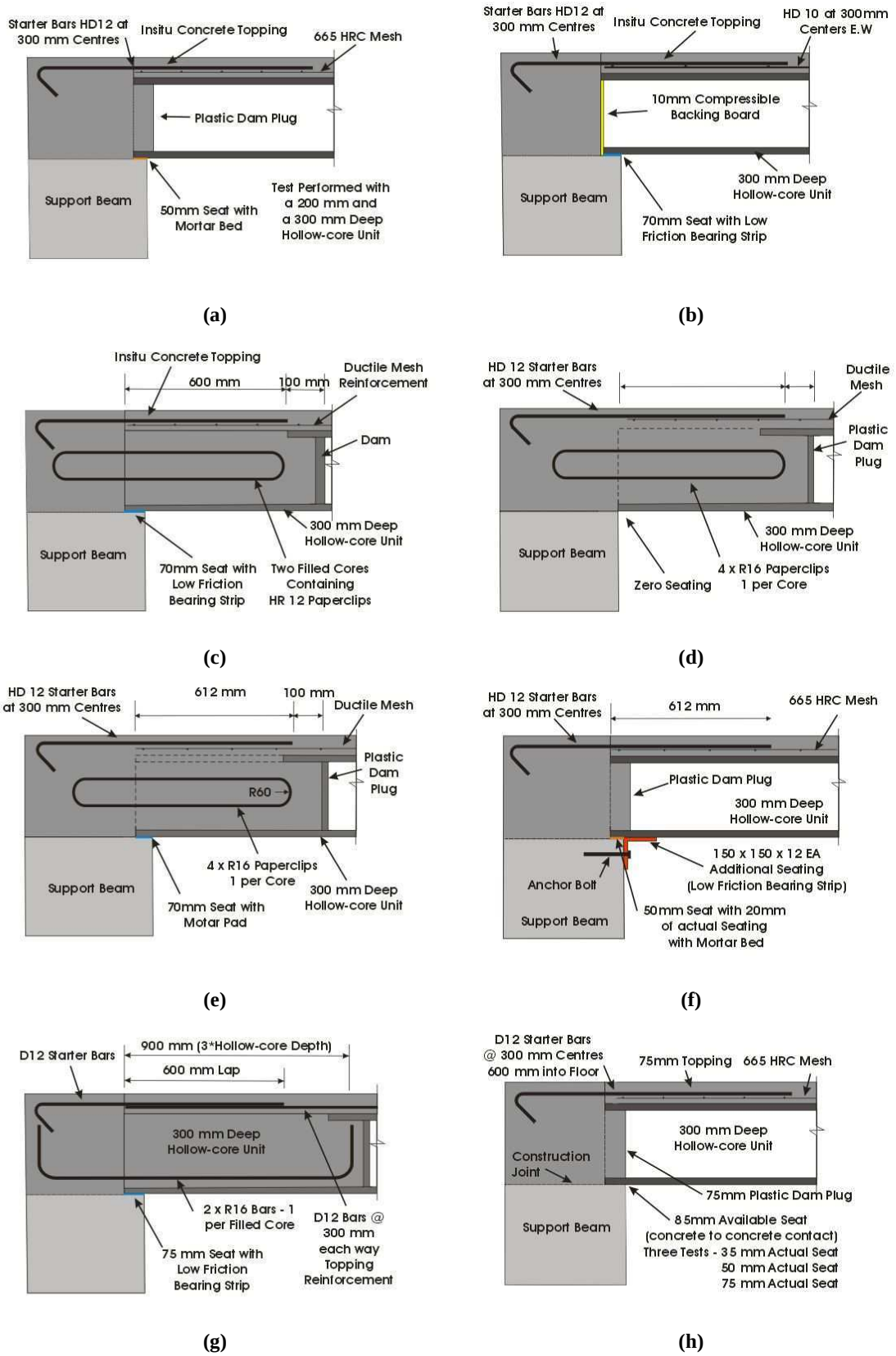

Figure 10-12 Connection details tested in sub-assembly tests where negative moments have been imposed

Table 10-1 contains a summary of the sub-assembly tests and their details, which are shown in Figure 10-12. The type of loading applied, the failure mode observed and the negative flexural capacities of the detail at both the beam-floor interface and the critical section are also presented. The critical section is defined as either the section at end of the starter bars or the end of filled cores as this is generally where there is a dramatic drop in flexural capacity. The negative flexural capacities in Figure 10-13 were calculated using average material properties and standard flexural theory. The revised method for calculating negative flexural capacity when topping concrete contains mesh reinforcement (as described in the previous section) was used where applicable. A value of 50 MPa was used for the compressive strength of the hollow-core units when this was not specifically determined by the researchers. Figure 10-13 shows a sub-assembly set-up similar to that used in these tests. Negative moment is applied by lowering the vertical actuator on the opposite end to the beam connection detail. This imposes a bending moment that is a maximum at the beam-floor interface. Apart from the MacPherson detail (g), the critical section of all the details is around 600 mm from the beam-floor interface. Therefore, assuming the dead load of the floors are similar, the critical sections should all experience a similar magnitude moment relative to the moment at the beam-floor interface. This allows comparison of the relative flexural capacities to be valid.

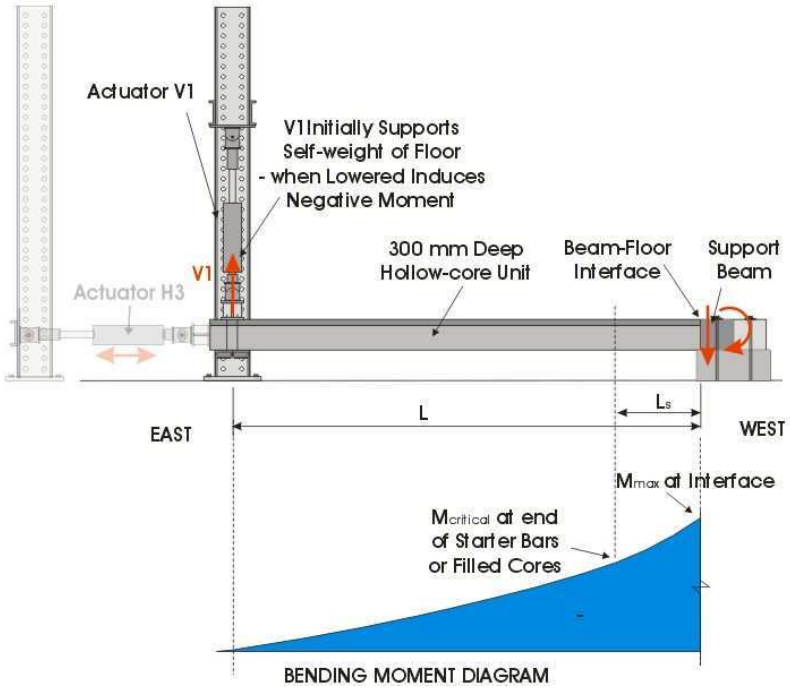

Figure 10-13 Sub-assembly test set-up used to apply negative moment and axial tension and bending moment induced

Table 10-1 Observed failure mode and negative flexural capacities of connection details

				Negative Flexural Yield Capacity (kNm)	
Detail	Researcher	Type of Loading	Failure Mode	At Interface	At Critical Section
(a) 300 series	Bull and Matthews (2003)	Relative rotation	Positive flexural	75	31
(b)	Bull and Matthews (2003)	Relative rotation	Did not fail	75	90
(c)	Bull and Matthews (2003)	Relative rotation	Did not fail	89	31
(d)	Liew (2004)	Relative rotation	Negative flexural	136	31
(e)	Liew (2004)	Relative rotation	Negative flexural	136	31
(f)	Liew (2004)	Relative rotation	Negative flexural	120*	31
(g)	MacPherson (2005)	Rotation & elongation	Did not fail	49	55
(h) 35 mm seat	Jensen (2006)	Rotation & elongation	Loss of support with delamination	49	31
(h) 75 mm seat	Jensen (2006)	Rotation & elongation	Did not fail	49	31
(h) 50 mm seat	Jensen (2006)	Rotation & elongation	Loss of support	49	31
(h) with RHS	Jensen (2006)	Rotation & elongation	Did not fail	49	31
Current research		Rotation & elongation	Negative flexural	79	33

* Interface moment calculated 200 mm from end of hollow-core as angle fixed unit up to this position. Therefore, some prestressing is activated.

Tests (d), (e) and (f) all demonstrated negative flexural failures. It can be seen that in these tests, the ratio between the negative moment capacity at the beam-floor interface and the negative moment capacity at the end of the starter bars is in the order of 4 to 1. When the moment capacity at the interface is large, large moments can be transferred into the hollow-core floor. Therefore, if the capacity of the floor is significantly lower, a flexural failure can result.

Test (a) and (c), by Bull and Matthews (2003), also had a high ratio of negative interface moment to critical section moment (almost 3 to 1). However, these details did not exhibit a negative flexural failure. For detail (a) this can be explained as prior to a negative moment being applied to the specimen, a positive flexural crack formed at a positive drift of 0.35 %. The positive flexural crack created a weak section and therefore was the location of failure. The reason the positive flexural crack formed could have been the effect of the mortar bed used "trapping" the hollow-core unit under positive moment. A crack forming in the hollow-core so early in the loading protocol also suggests the tensile strength of the hollow-core unit concrete was low. Detail (c) did not fail under the imposed cyclic loading protocol. A crack did form in the insitu topping concrete at the end of the starter bars at -0.4 % drift, but this did not appear to widen under additional loading. All rotation appeared to occur at the beam-floor interface.

It is clear in tests (b) and (g) that a negative flexural failure was not likely as the capacity of critical sections was higher than the capacity of the interface. In both cases, this was because ductile steel reinforcement was used in the insitu topping concrete rather than mesh. In specimens tested by Jensen (2006) (labelled (h) in Figure 10-13 and Table 10-1), mild steel (Grade 300) steel was used for the starter bars. This reduced the negative moment capacity of the beam-floor interface; therefore reducing the ratio between the capacity at the interface and at the end of the starter bars. These specimens were aimed to be representative of hollow-core connection details used in the 1980s and 1990s; that typically contained starter bars made of Grade 430 steel reinforcement. As Grade 430 was not available at the time of testing, Jensen substituted Grade 300 steel reinforcement. If a higher Grade of reinforcement had been used, the failure modes observed may have been different.

This brief investigation of previous testing indicates that the ratio of negative flexural capacity between the beam-floor interface and the critical section plays a crucial role in determining whether a hollow-core floor is prone to a negative flexural failure. The other major contributor is the location of the critical section. It can be seen in Figure 10-13 that the negative bending moment decreases out from the beam-floor interface. Therefore, longer starter bars can mitigate the risk. When calculating the potential negative bending moments the effects of vertical seismic accelerations must be taken into account. A method for assessing these is given in Section 5.2.

10.3.1 Conclusions – Situation that may be at Risk of a Negative Flexural Failure

A negative flexural failure may be possible in a building under seismic loading, if there is a large differential between the negative moment capacity at the beam-floor interface compared to that at a section along the hollow-core floor (for example at the end of the starter bars or filled cores). This may be a problem in existing buildings that contain short Grade 430 starter bars and non-ductile mesh reinforcement. Connection details that use steel reinforcement in filled cores increase the negative flexural capacity of the beam-floor interface and therefore may also increase the potential of a negative flexural failure. In this research, only hollow-core floors made with 300 mm deep hollow-core units have been investigated. However, it is believed that other depth floors will behave similarly.

10.4 Recommended Detailing to Avoid a Flexural Failure

If hollow-core floors are detailed according to the current New Zealand Concrete Structures Standard (Standards New Zealand 2006), negative flexural failure is unlikely. Several clauses in this standard specify practises that improve negative flexural performance. These clauses place limits on the quantity of steel that can pass over the end the of the hollow-core units and in filled cores and on how far steel, that does pass over the beam-floor interface, must extend into the floor. The Standard states that starter bars must extend a length equal to the greater of, 0.2 times the hollow-core span or 400 mm plus the development length of the bars. If the ultimate strength of the bars crossing the beam-floor interface is greater than 113 kN/m then the reinforcement in excess of this must span the entire span of the floor. The ultimate

strength of reinforcement in filled cores is also restricted to a maximum of 60 kN at not more that 600 mm centres and bars must be placed near the bottom of the hollow-core void (Standards New Zealand 2006, C18.6.7). Essentially, what this clause aims to achieve is to restrict the differential between negative moment capacity at the beam-floor interface and at the end of the starter bars. The increased length of starter bars also pushes the critical section further into the floor, which generally results in a lower magnitude of negative moment demand.

10.5 Potential Retrofits to Avoid Flexural Failures

This section briefly considers potential methods of retrofitting existing hollow-core floors that are found to be vulnerable to a negative flexural failure. The retrofit concepts discussed are only conceptual; no verification (experimental or analytical) has been competed on their validity for New Zealand situations. This is an area of potential future research. Any retrofit to a hollow-core floor must consider all potential failure mechanisms. A capacity design or hierarchy of strength approach is recommended. Hollow-core sections and grades of steel reinforcement have changed over the years, it is therefore important to ensure appropriate and conservative geometries and material properties are assumed. Consideration must also be made for differences between structural drawings and what has in reality been constructed.

The fundamental concept when retrofitting against a negative flexural failure is to ensure the negative moment transferred into the hollow-core floor is less than the floor's capacity. There are two ways of achieving this, namely by limiting the negative flexural actions entering the floor or increasing its negative flexural capacity.

Limiting the negative flexural actions entering the floor could be achieved by strategically weakening the beam-floor interface. If the beam-floor interface is over-reinforced, cutting some of the steel reinforcement crossing this section would reduce its negative moment capacity. However, this could prove to be difficult, as the exact location of steel reinforcement may not be known.

To increase the negative flexural capacity of an existing hollow-core floor, it might be possible to bond carbon fibre reinforced polymer (CFRP) strips to the top side of the floor. Hosny et al. (2006) tested six full scale hollow-core slabs strengthened using CFRP strips and

found the negative moment capacity was increased by between 183 and 574 %. Although the tests were performed on un-topped, 150 mm deep, hollow-core floors, which are not common in New Zealand, the results show that the method does have potential as a retrofit solution. The researchers found that the increase in negative moment capacity was limited by flexural crack-induced debonding of the CFRP strips. If debonding is prevented it was suggested the likely failure mode of the floors would be a shear failure (Hosny et al. 2006).

10.6 References

Bull, D., and Matthews, J. (2003). "Proof of Concept Tests for Hollowcore Floor Unit Connections." *Research Report 2003-1*, Department of Civil Engineering, University of Canterbury, Christchurch, New Zealand.

Comité euro-international du béton., and Fédération internationale de la précontrainte. (1993). *CEB-FIP model code 1990 : design code*, T. Telford, London.

Fédération Internationale du Béton. (2000). *Structural concrete : textbook on behaviour, design and performance : updated knowledge of the CEB/FIP Model code 1990*, International Federation for Structural Concrete, Lausanne, Switzerland.

Hosny, A., Sayed-Ahmed, E. Y., Abdelrahman, A. A., and Alhlaby, N. A. (2006). "Strengthening precast-prestressed hollow core slabs to resist negative moments using carbon fibre reinforced polymer strips: an experimental investigation and a cricial review of Canadian Standards Association S806-02." *Canadian Journal of Civil Engineering*, 33(8), 955 - 967.

Jensen, J. (2006). *The seismic behaviour of existing hollowcore seating connections pre and post retrofit : a thesis submitted in partial fulfilment of the requirements for the degree of Master of Engineering at the University of Canterbury*, Christchurch, New Zealand.

Liew, H. Y. (2004). *Performance of hollowcore floor seating connection details : a thesis submitted in partial fulfilment of the requirements for the degree of Master of Engineering at the University of Canterbury*.

MacPherson, C. (2005). *Seismic performance and forensic analysis of a precast concrete hollow-core floor super-assemblage : a thesis submitted in partial fulfilment of the requirements for the degree of Master of Engineering at the University of Canterbury*, Christchurch, New Zealand.

Morrell, P. J. B. (1977). *Design of reinforced concrete elements*, Crosby Lockwood Staples, London.

Paulay, T., and Priestley, M. J. N. (1992). *Seismic design of reinforced concrete and masonry buildings*, Wiley, New York, N.Y.

Soltani, M., An, X., and Maekawa, K. (2004). "Cracking response and local stress characteristics of RC membrane elements reinforced with welded wire mesh." *Cement and Concrete Composites*, 26(4), 389-404.

Standards New Zealand. (2006). *Concrete structures standard, NZS3101, Parts 1 & 2*, Standards New Zealand, Wellington, New Zealand.

11 Discussion: Flexure-Shear Failure

Test specimen HCW2 did not exhibit a flexure-shear failure. There are several possible reasons for this. The first being, that under the planned loading protocol, flexural cracks did not form. The second, was that once flexural cracks were induced in the specimen (under the extended loading protocol), a negative moment was not induced in the specimen concurrently with high shear. In this section, the shear stresses induced in the specimen during testing are shown. These are compared to the flexure shear capacity, as calculated in Section 6.4, and the web-shear capacity of the section, calculated from the New Zealand Concrete Structures Standard. Possible reasons flexural cracks did not form during the planned loading protocol are discussed. As well as why, when they were induced under the extended loading protocol, the crack spacing was larger than predicted. An analytical investigation of the shear stresses in the negative moment region of hollow-core floors is also presented in this section. The rational analysis used in Section 6.3 for determining the shear stresses is tedious. However, the alternative of using the uniform distribution of shear stress, as recommended in by the New Zealand Concrete Structures Standards, may be unconservative in some situations. The analytical investigation allows an appropriate shear stress design value to be derived from the shear force applied to the section.

11.1 Results versus Predictions

Flexural cracks did not form during the planned loading protocol; consequently, flexure-shear cracking could not occur and the shear stresses were not high enough to induce web-shear cracking. Section 6.1 describes the mechanisms behind web-shear and flexure-shear cracking. Web-shear cracking is directly related to the tensile strength of the concrete and occurs at higher shear stress values than flexure-shear cracking. Figure 11-1 shows the maximum shear stresses, above the zero strain line (referred to as the critical shear stresses), induced in the hollow-core floor during testing. The three load cases shown are all from the initial phase of testing when the specimen did not contain flexural cracks. As these stresses are above the zero strain line, the axial compression from the prestressing does not effect them, as the section is uncracked there may be some additional tensile stress in the concrete. These shear stresses were calculated from the actual loads applied to the specimen using the method outlined in Section 6.3.

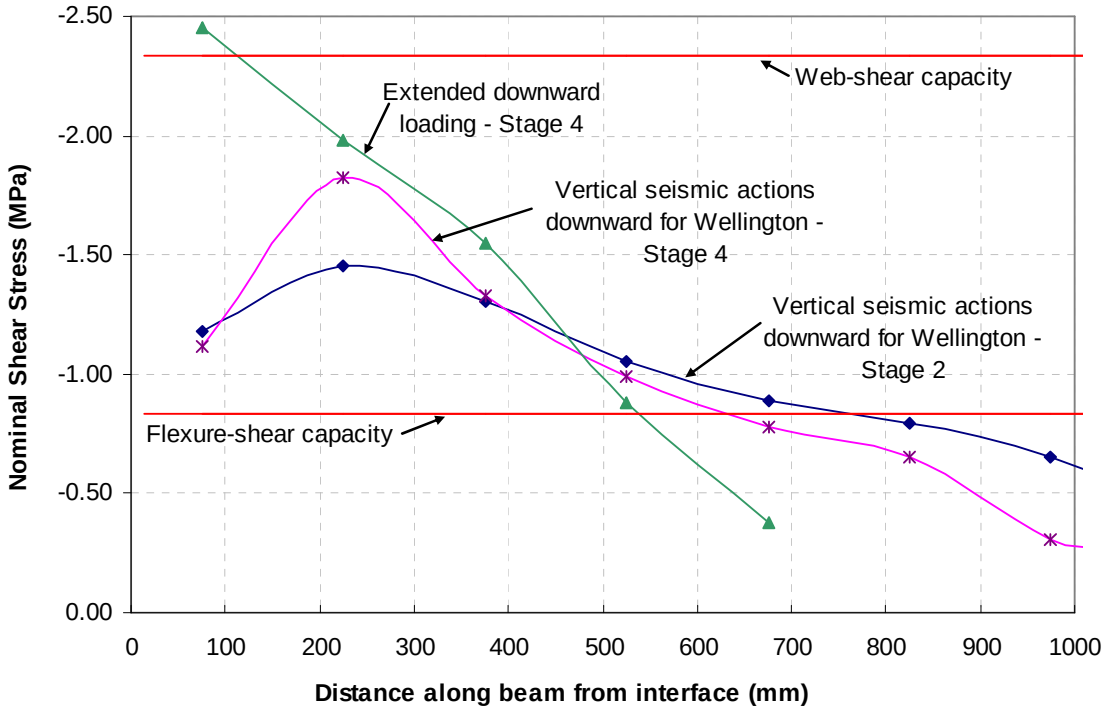

Figure 11-1 Maximum critical shear stresses induced in the hollow-core specimen during test HCW2

The two red horizontal lines in Figure 11-1 are the web-shear capacity and the flexure-shear capacity. The web-shear capacity is 2.3 MPa and was calculated from Equation 11-1 (Standards New Zealand 2006, 19.3.11.2.2 (b)), where f'$_c$, the compressive strength of the hollow-core, is taken as 50 MPa.

$$v_{cw} = 0.33\sqrt{f_c'} \qquad \textbf{Equation 11-1}$$

The nominal flexure shear capacity is 0.83 MPa, this was calculated in Section 6.4. Both are lower characteristic values and neither have been multiplied by a reduction factor. Apart the green line near the interface, the shear stresses are well below the web-shear strength of the section. Out to around 800 mm from the beam-floor interface the shear stresses are above the flexure-shear capacity. However, as the specimen did not contain flexural cracks this type of shear cracking was not possible.

11.2 Flexural Cracking and its Effect on Flexure-Shear Cracking

In test specimen HCW2, crack initiators were placed in the insitu topping concrete at 150 mm centres as it was predicted that flexural cracks would form at this spacing. However, during the planned loading protocol flexural cracks did not form, even though negative moments were applied that were above the predicted cracking moments of the sections. This could have been because the strength of the hollow-core unit was higher than predicted (f'_c = 88 MPa, as shown in Appendix C 5.2, rather than the assumed f'_c = 50 MPa).

In the extended loading protocol (referred to as Phase Two), flexural cracks were induced by placing a prop underneath the floor specimen and bending the specimen over it. Several cracks were formed this way; however, it did not appear possible to form cracks at a spacing closer than 450 mm. This could be because of the low reinforcement ratio in the topping concrete, combined with the high tensile capacity of the hollow-core concrete. The result being that when a negative moment was induced in the specimen large enough to crack the concrete, the tensile force was larger than the force required to yield the steel. Therefore, when the crack formed the steel yielded and moments large enough to crack sections, either side of the original crack, could not be formed. This is also possibly why no secondary cracks were observed.

Crack widths affect the flexure-shear capacity of a specimen. Deriving crack widths and how these affect the shear capacity is complex and its influence in hollow-core floors requires further research. For shallow floors (those that use 200 mm and 300 mm deep hollow-core units) the crack widths might be small enough that the flexure-shear strength is similar to the web-shear strength and therefore not likely to be significant. This is due to shear transfer being maintained, reducing the likelihood of high stress concentrations at points of aggregate contact and diagonal cracks forming. The effect of the change in crack width due to the formation of secondary cracks also needs to be considered. In this research the critical shear stress has been defined as the maximum shear stress in the flexural tension zone; however, due to the varying crack width, the actual location of the critical shear stress (where shear cracking is likely to originate) is unlikely to coincide with this maximum.

11.3 Amount of Shear Resisted by change in Tension along Steel Reinforcement

In the following paragraphs, shear stress distributions are derived from section analyses and these are compared with the uniform shear stress distribution assumed in the New Zealand Concrete Structures Standard (Standards New Zealand 2006). Four sets of analyses are made to assess the influence of different reinforcement contents, in the insitu topping, on the shear stress levels. From these analyses, appropriate shear stress levels for design with hollow-core floors are recommended. The analyses do not include the effects of flexural crack widths.

To calculate the shear stress demand in reinforced concrete member, the New Zealand Concrete Structures Standard (Standards New Zealand 2006) assumes that the shear stresses are distributed uniformly over an area A_{cv}. Equation 11-2 defines A_{cv} for a prestressed member in terms of the web width, b_w, and effective depth, d, which is the distance between the extreme compression fibre and the centroid of the tension steel.

$$A_{CV} = b_w d \qquad \textbf{Equation 11-2}$$

However, in Section 6.1.3 it was shown that the shear stresses in a hollow-core section are not uniformly distributed. The presence of the prestressing induces an inclined compression force, which resists a portion of the shear, in addition, the changing width of the section also has an effect on shear stresses, this is illustrated in Figure 11-2.

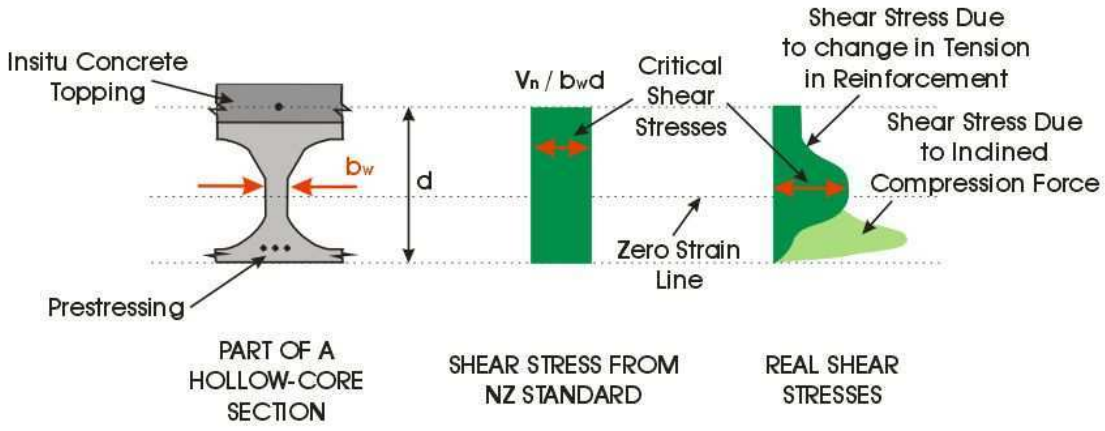

Figure 11-2 Shear stress distribution in a hollowcore unit

In the section analyses, all material properties and geometries are kept the same, with only the quantity of steel reinforcement in the insitu concrete topping being varied. The members analysed are similar to test specimen HCW2. Figure 11-3 illustrates the layout and material properties used in the analysis, further details are given in Table F6 of Appendix F2. Design material properties were used. The development and dispersion of forces of the prestressing were accounted for by allocating a development length, over which the prestressing force was assumed to increase linearly, and a dispersion length, to account for the dispersion of the compression force into the section. The development length was assumed to be that specified by the International Federation of Structural Concrete (FIP 1988), which is outlined in Section 5.4. The dispersion length was assumed to be ten times the diameter of the strands.

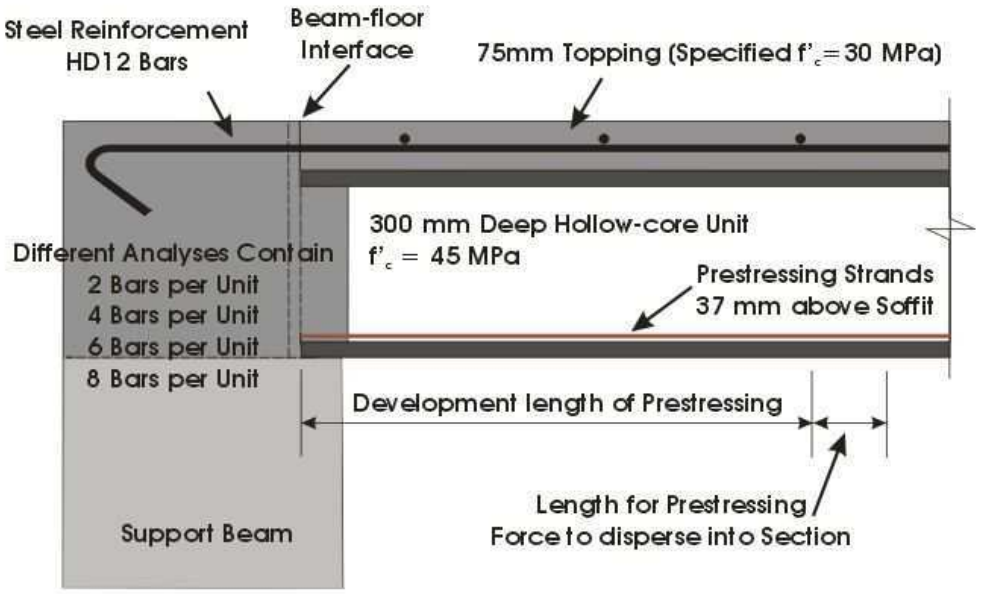

Figure 11-3 Layout and material properties used in the analysis of shear stresses

The steel reinforcement was assumed to be Grade 500, 12 mm diameter deformed bars. The number of these was varied, namely two, four, six and eight bars were used in the different analyses. The load applied to the floor was equivalent to that applied to a 12 m span hollow-core floor in Wellington. The load case applied resulted in a bending moment similar to that illustrated as "A & B down & C" in Figure 6.10. Where "A" is the moment from the gravity load, "B" is the moment from downward vertical seismic actions scaled for Wellington and "C" is the moment induced by rotation of the support beam. In this load combination, the bending moment at the beam-floor interface is assumed to be the

overstrength moment. As this bending moment is dependent on the quantity of reinforcement in the topping concrete, this changes for the four different scenarios analysed.

Figure 11-4 shows the first metre of the member out from the beam-floor interface, for the four cases analysed. On this figure are shown:

- the bending moments applied
- the region the hollow-core web where its width is the slimmest
- the location of the zero strain line

The less steel in the topping concrete over the beam-floor interface, the more rapidly the zero strain line rises.

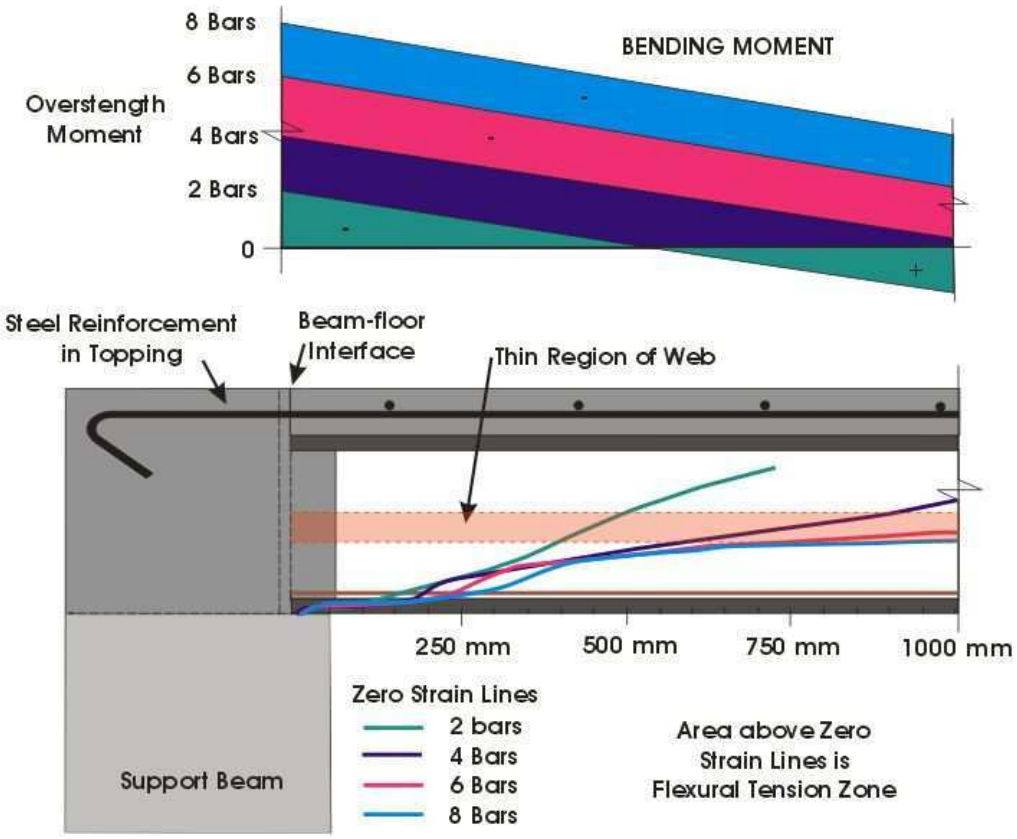

Figure 11-4 Applied bending moments and height of zero strain lines

The shear stresses in the section were calculated using the method described in Section 6.1.3 and illustrated in Section 6.3. Figure 11-5 shows the magnitude of critical shear stresses, as solid lines, in the first metre of floor from the support calculated for the four members. In the following paragraphs the term “critical shear stresses” will refer to the maximum shear stresses in the flexural tension zone. The stresses in the flexural compression zone are not

critical because the diagonal tensile stresses are suppressed by the longitudinal compression stresses in the compression zone, this is illustrated in Section 6.1.1. The dotted lines are the shear stress values calculated using the method outlined in the New Zealand Concrete Structures Standard, where the shear force is divided by the area, A_{cv}. The shear stress values from the standard may be unconservative near the support. As the shear stresses were calculated between sections 50 mm apart, not all variations in shear stress were picked up by the analyses. A common trend appears to be that the more steel crossing the beam-floor interface, the higher the average shear stress. The critical shear stress rises rapidly to its peak value at around 125 mm from the support. From this peak value, the shear stress decreases until approximately where the steel in the topping stops yielding and then it increases again.

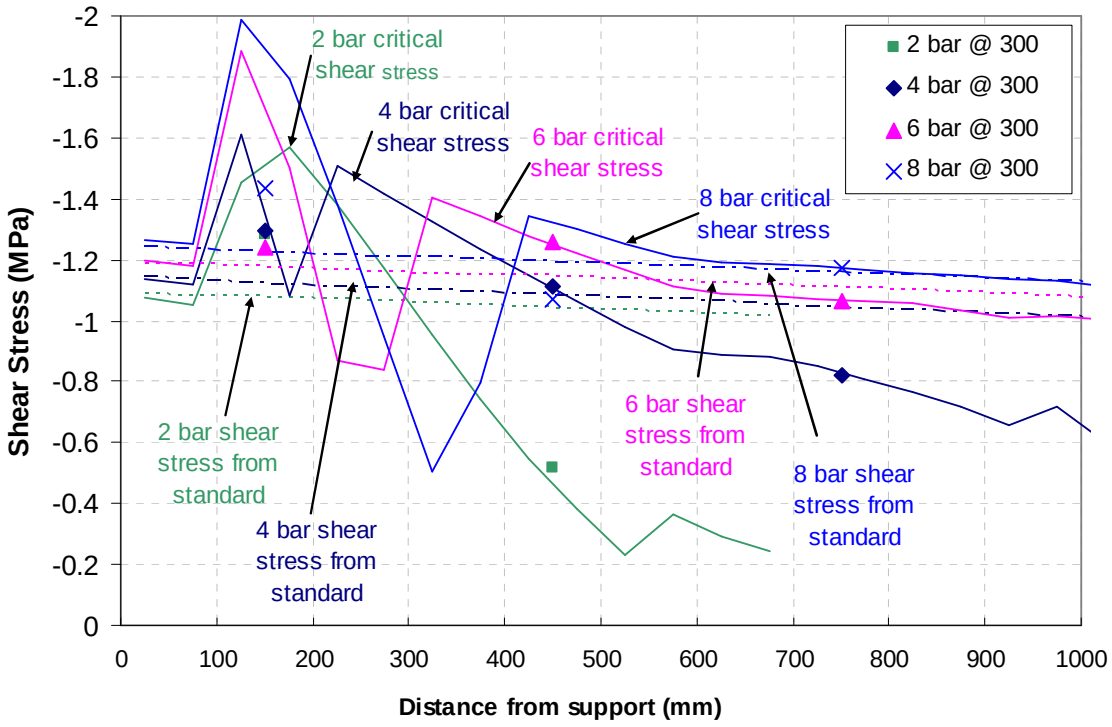

Figure 11-5 Critical shear stresses induced along hollow-core floor sections for different steel quantities crossing the beam-floor interface. The discrete data points are when shear stresses are calculated over 300 mm intervals

The critical shear stresses were found to be at the narrowest section of the web until the zero strain line moved above this level. Once this had occurred, the critical shear stress was located at the zero strain line. There are kinks in the critical shear stress lines for the two-bar and four-bar scenarios at 525 mm and 925 mm respectively (see Figure 11-5). These correspond

to the location where the zero strain line moves above the narrow web section. There is also a change of slope in all the critical shear stress lines at around 675 mm from the interface; this position corresponds to where the prestressing is fully developed.

When the critical shear stress (v_{crit}) is at the narrowest part of the web it can be found by Equation 11-3, where is ΔT is the change in tension in the steel reinforcement between two sections a distance Δx apart and b_w is the narrowest width of the cross-section.

$$v_{crit} = \frac{\Delta T}{b_w \Delta x} \qquad \textbf{Equation 11-3}$$

The critical shear stress is at the narrowest part of the section, for the majority of the first metre out from the interface and the values of b_w and Δx are constant. Therefore, the magnitude of the critical shear stress is proportional to the magnitude of the change in tension force in the steel. Hence, considering a flexure-shear failure, the property of interest is the change in tension force in the steel between two flexural cracks

To explain the fluctuations in Figure 11-5 it is helpful to look at the actual magnitudes of tension force in the steel reinforcement. Figure 11-6 shows the tension force sustained by the steel reinforcement in the four different members. The forces that cause the bars to yield are also shown (dashed lines). Forces higher than the yield force can be sustained by the bars as a stress-strain relationship including the effects of tension stiffening was used. This non-linear relationship also causes variations of the slope of the lines in Figure 11-6 when they are above the yield force. It can be seen that the location the tension force in the bars goes below the yield force is around 100 mm, 200 mm, 300 mm and 400 mm from the interface for the two-bar, four-bar, six-bar and eight-bar scenarios respectively. These locations along the member correspond to where the main fluctuations end in Figure 11-5 and the slope of the lines in Figure 11.6 become more constant.

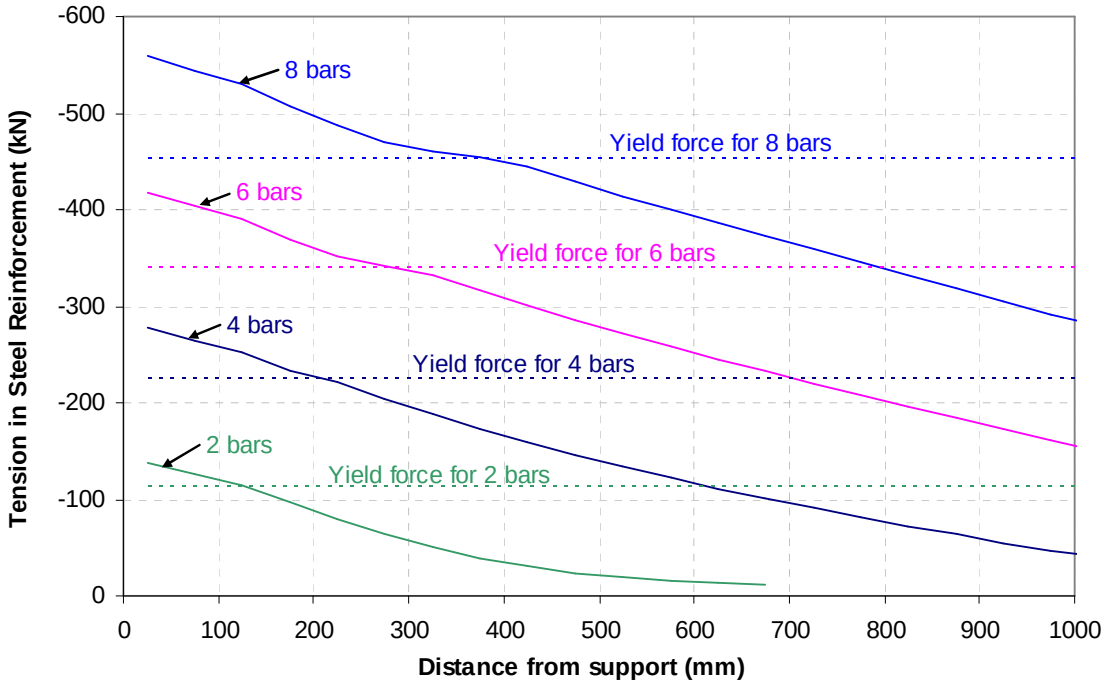

Figure 11-6 Tension in steel reinforcement along hollow-core floors in analyses

Figure 11-5 shows the change in stresses over 50 mm sections. It is unlikely that flexural cracks will form this closely. Generally, the first crack will form at the beam-floor interface. For a floor containing a 300 mm deep hollow-core units, the next crack could form anywhere between 200 mm and 600 mm out from the interface. The change in tension in the steel reinforcement over these larger distances reduces the effect of the fluctuations. The critical shear stresses calculated over 300 mm intervals are illustrated on Figure 11-5 by the data points at 150 mm, 450 mm and 750 mm out from the interface. It can be seen that the points at 150 mm out from the interface are considerably lower than the shear stresses calculated over 50 mm intervals at this location. Further out in the floor, the shear stresses over 50 mm intervals and 300 mm intervals correlate well. The eight-bar scenario is an exception to this as in this case the fluctuations extended past a distance of 300 mm from the interface. It is not likely in a real building that the quantity of steel that the eight-bar scenario represents would be used. Essentially this means, the fluctuations of critical shear stress near the support shown in Figure 11-5, which suggest the critical shear stress occurs at around 125 mm from the support, can be ignored.

For reinforced concrete beams, the New Zealand Concrete Structures Standard states that the maximum design shear force located a distance less than d from the face of the support may be taken as that at a distance d from the support (Standards New Zealand 2006, 9.3.9.3.1). Where d is the distance equivalent to the distance between the extreme compression fibre and the tension steel. This is because the closest possible inclined crack at the end of a member will terminate at a location about d away from the support and any load applied between the support and a distance d can be transferred directly to the support. Therefore, the maximum shear that must be transferred over the inclined crack is that from load applied further than a distance d from the support. Figure 11-7 illustrates this using a free-body-diagram.

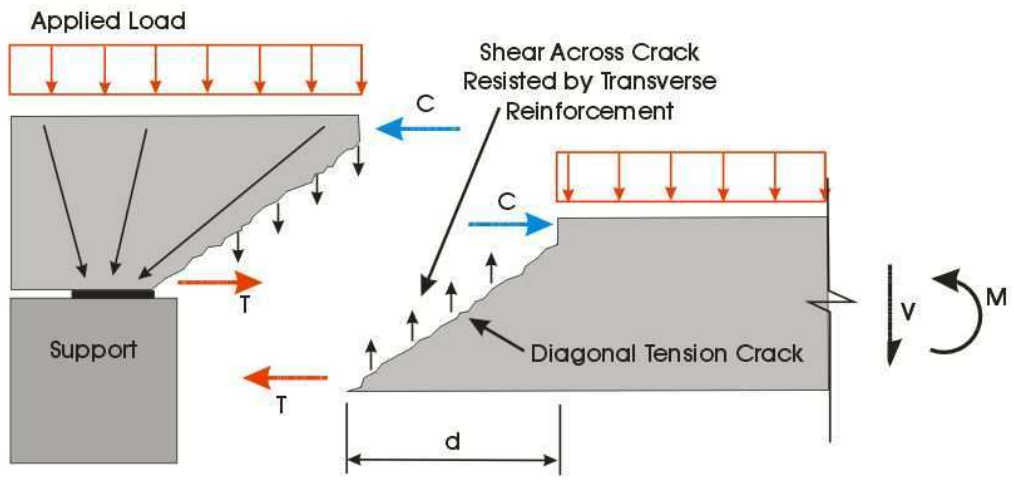

Figure 11-7 Free body diagram showing why a reinforced concrete beam can be designed for a maximum shear force equal to the shear force a distance d from the support (Adapted from Standards New Zealand 2006)

In a hollow-core floor, there is no transverse reinforcement to carry the shear force once a crack has formed. Therefore, the shear force has to be resisted by the concrete. However, it has been observed that because of the shape of a hollow-core section flexure-shear cracks tend to propagate almost horizontally. Therefore, in a negative moment zone, if the maximum shear stress is exceeded at a distance d from the support and a flexure-shear crack forms vertical support might be maintained. Figure 11-8 illustrates how the load paths might be preserved. Hence, if adequate bearing is provided, it might be assumed that within a distance d of the interface the shear stress is not critical and the maximum shear stress that needs to be checked is at a distance d from the support. The vertical compression near the support will also help to suppress the diagonal tension stresses in this region.

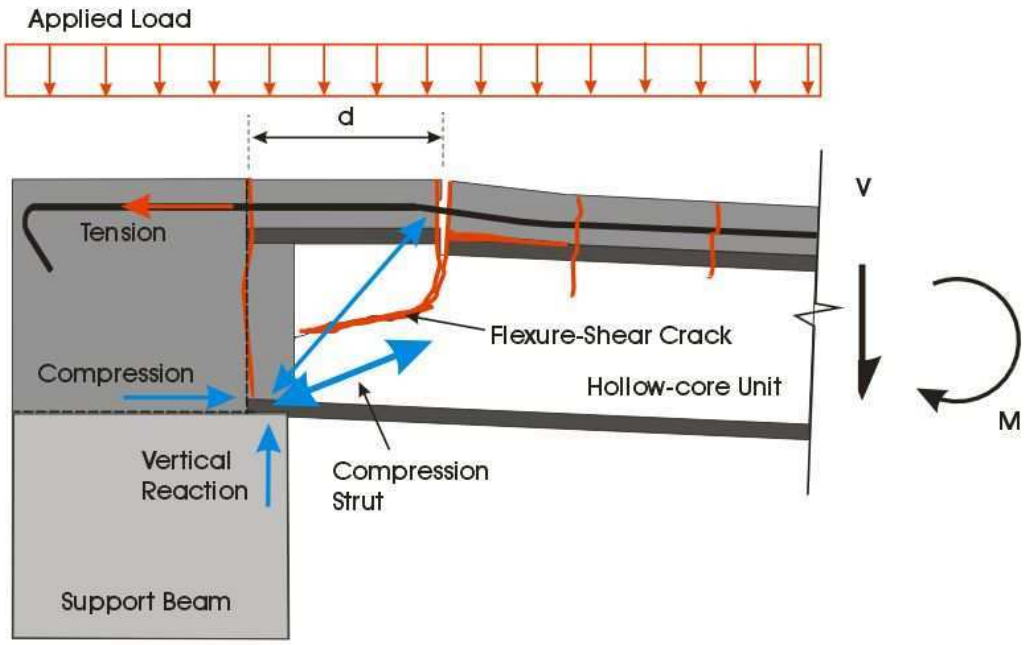

Figure 11-8 Shear crack near hollow-core floor support

In a prestressed member, some of the shear is resisted by the change in tension in the steel reinforcement, $V_{\Delta s,}$ and some by the inclined component of the compression force. It is often assumed that a large portion of the shear is resisted by the inclined component of the compression force. Figure 11-9 shows the percent of shear along the floor resisted by the $V_{\Delta s}$, where $V_{\Delta s}$, is calculated by Equation 11-4. ΔT is the change in tension, Δx is the distance over which this change occurs and d is the distance between the extreme compression fibre and the tension steel and e is the distance between the extreme compression fibre and the centroid of the compression force, which can be taken as about 0.1 times d at a distance d from the support.

$$V_s = \frac{\Delta T}{\Delta x}(d - e) \qquad \textbf{Equation 11-4}$$

The relationship between ΔT and shear stress is illustrated more fully in section 6.1.3. In Figure 11-9 it appears that near the support, $V_{\Delta s}$ resists more than the total amount of shear applied to the section. This is due to the development of the prestressing strands. In the analyses, the change in prestressing force across a section causes shear stresses in the opposite direction to those resisted by $V_{\Delta s}$. Therefore, part of the shear resisted by the inclined compression force is subtracted from $V_{\Delta s.}$ The prestressing is fully developed by a distance of

675 mm from the support and then $V_{\Delta s}$ and the shear resisted by the inclined component of the compression force are both positive and sum to the total shear applied to the section.

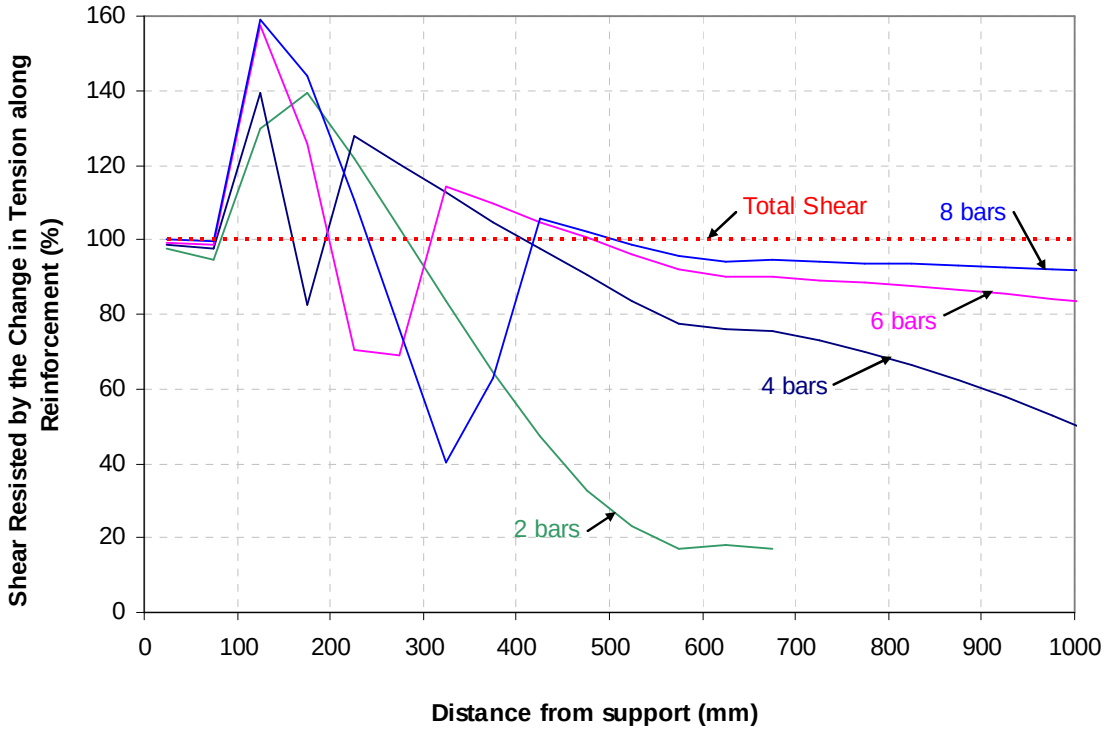

Figure 11-9 Percent of total shear along section resisted by the change in tension along the steel reinforcement

As mentioned previously, it is unlikely that flexural cracks will form at 50 mm spacing. If the change in tension was taken over larger sections, then the fluctuations near the support in Figure 11-9 would be reduced. If average values are examined between the support and 675 mm from the support it appears that for the four, six and eight bar scenarios, the shear resisted by $V_{\Delta s}$ is approximately between 80 and 100 %. This percentage is larger with more steel and drops as distance from the support increases. The quantity of steel across the beam-floor interface in a typical section is normally around four bar per unit (300 mm centres). In this case, at a distance of d (337.5 mm) out from the interface the percent of shear carried by $V_{\Delta s}$ might be taken as 100 %. It is therefore recommended that at this position the negative flexural shear capacity is checked for the full shear stress (100 %). As this shear stress occurs between flexural cracks, above the zero strain line, the prestressing has no effect and the capacity might be checked as though the member is a reinforced concrete beam.

The above investigation shows that in a hollow-core floor containing flexural cracks under a negative bending moment, the critical shear stress is likely to be at a distance d from the support. Figure 11-5 showed that the magnitude of this critical shear stress could be larger than the value predicted by the New Zealand Concrete Structures Standard (Standards New Zealand 2006). Figure 11-10 shows the magnitude of this discrepancy. The critical shear stress is shown as a percent of the shear stress calculated using the method from the standard. No reduction factor has been included. At d out from the support, the critical shear stress for all four scenarios assessed was not more than 120 % of the code value. All of this shear stress should be assumed to be taken by the change in tension in the steel reinforcement and not by the inclined component of the compression force.

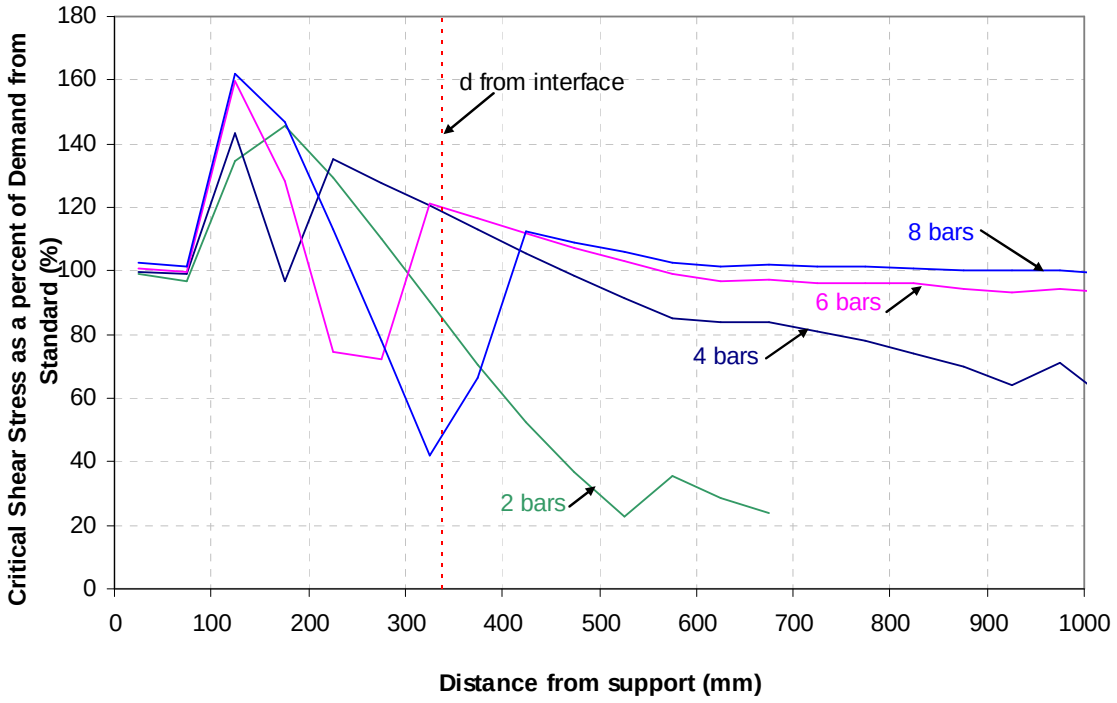

Figure 11-10 Critical shear stress along a hollow-core floor as a percent of the shear stress for design calculated from the New Zealand standard

From the analytical assessment performed above, the nominal shear stress that should be checked in a hollow-core floor containing negative flexure cracks is proposed. It is suggested that the shear stress capacity, as calculated for a reinforced concrete beam, should be checked at a distance d form the support against a value is 1.2 times the nominal shear stress currently recommended by the New Zealand Concrete Structures Standard (Standards New Zealand 2006). The factor of 1.2 is used as 100 % of the shear stress could be resisted by the change in

tension in the steel reinforcement and in some of the scenarios from the above analysis, critical shear stress values at a distance d from the support were as high as 1.2 times the value suggested by the standard.

For the four-bar scenario above, the nominal shear stress capacity, v_c, equals 0.82 MPa (calculated in Section 6.4). The shear stress demand from the New Zealand Concrete Structures Standard at d from the support, multiplied by 1.2 equals 1.75 MPa. Clearly, there is a deficit between the demand and capacity; however, this is only a problem if flexural cracks are present. It is also possible that as hollow-core floors are generally shallow members, it is possible that the width of flexural cracks will be narrow enough that shear transfer is maintained across them, reducing the likelihood of high stress concentrations at points of aggregate contact and diagonal cracks forming. Further research and experimental testing is required in this area.

11.4 Conclusions

Although a flexure-shear failure mechanism was not observed in the experimental component of this research, it is believed that the basic theory behind predicting this type of failure is valid. It would be interesting to repeat this test, ensuring that negative flexural cracks were initiated in the early stages. It was shown in Section 11.1, that had flexural cracks been formed in the specimen, the shear stresses induced could have been high enough to cause flexure-shear cracking. However, the influence of flexural crack width on the flexural shear capacity has not been fully examined and should be researched in more detail before guidelines on the flexure-shear capacity of hollow-core floors are prepared. The flexural shear capacity of a hollow-core section can not be easily increased. Therefore, perhaps the best way to prohibit a flexure-shear failure is to prevent the formation of flexural cracks. This could be achieved by the inclusion of prestressing strands at the top of the hollow-core units or by limiting the quantity of steel crossing the beam-floor interface. This would allow the magnitude of negative moments transferred to the floor to be controlled, perhaps to a value lower than the cracking moment.

11.5 References

FIP Commission on Prefabrication. Working Group Hollow Core Units., and FIP Commission on Prefabrication. Working Group Structural Connections. (1988). *Precast prestressed hollow core floors*, Telford, London.

Standards New Zealand. (2006). *Concrete structures standard, NZS3101, Parts 1 & 2*, Standards New Zealand, Wellington, New Zealand.

Blank

12 Summary, Conclusions and Recommendations

12.1 Summary

This research has investigated the seismic performance of hollow-core flooring, particularly the failure modes possible if it is exposed to negative bending moments. Prestressed hollow-core floor units are precast concrete components that have been extensively used in New Zealand for more than 30 years. However, a number of issues regarding the seismic performance of existing hollow-core floors have raised concern. It is important that their performance in earthquakes is understood, so that engineers can predict failure modes and detail to avoid these through the use of capacity design. Understanding of behaviour must be comprehensive enough to assess possible failure modes and develop a desired hierarchy of strength.

The way hollow-core floors are installed and the possibility of seismic loading, make the design and assessment criteria for hollow-core floors in New Zealand unique. Recent research has increased awareness of the potential vulnerability of existing hollow-core floors in New Zealand and has lead to revisions in the way hollow-core floors are installed; however, there are still gaps in current knowledge. The work undertaken in this research programme adds to current knowledge.

The behaviour of hollow-core flooring is complex. Eccentric prestressing, the lack of passive reinforcement and its non-uniform cross-section mean it cannot be assessed as a standard reinforced concrete member. Several factors, which influence its performance, are presented. These include aspects such as the effect of reinforced concrete frame beams elongating, its initial stress state, the effect of creep and shrinkage, and the consequence of its unequal stiffness under vertical loading.

A suite of eight possible failure modes, common to hollow-core floors, is presented.
The failure mechanisms are:

- Loss of support
- Positive moment failure
- Flexural and shear actions transverse to the span of the units
- Loss of support to a web

- Failure due to incompatible displacements
- Torsional failure
- Flexural failure in negative bending moment regions
- Flexure-shear failure in negative bending moment regions.

To complete a capacity design, all potential failure modes must be identified and a hierarchy of failure assessed. Some of the failure modes presented have been identified and observed in past experimental research, while others have been predicted from analytical work. Several are not well understood and require further research. The final two failure modes listed above are possible if a hollow-core floor is exposed to negative bending moments. It is these two failure modes that were the focus of this research.

Negative bending moment can be induced in a hollow-core floor under seismic and other actions due to continuity established by the addition of insitu topping concrete and steel reinforcement. Vertical seismic accelerations in combinations with other loading can create significant negative moments that currently are not considered in the design of hollow-core floors. Both of the negative flexure failure mechanism and flexure-shear failure modes were analytically and experimentally investigated.

A sub-assembly, comprising of a single 6 m long span of a 300 mm deep hollow-core unit with insitu topping and length of support beam at one end, was built to investigate each failure mode. The test specimens were designed to be typical of hollow-core floors used in New Zealand. Different types of reinforcement were used in the insitu topping concrete for each test as this effects which failure mode is more likely to occur. Bending moments and axial loads were applied to the sub-assembly by hydraulic actuators. The loading protocols were quasi-static and force based.

The test investigating a negative flexural failure contained mesh reinforcement, which has limited ductility, in the topping concrete. High strength starter bars extended 1000 mm into the topping concrete, connecting the support beam to the hollow-core floor. Under a negative bending moment, the test unit experienced flexural cracks in three locations. These were at the beam to floor interface, at the end of the starter bars and mid-way between these two sections. Only mesh reinforcement crossed the crack at the end of the starter bars and this was observed to yield immediately when the crack formed. This suggested that the tensile capacity

of the concrete was more than the steel crossing this section. When increasing axial load (tension) and negative bending moments were applied to the test unit, the crack at the end of the starter bars continued to widen until the mesh ruptured and the specimen experienced a brittle failure.

It was observed that the flexural capacity of the test specimen, measured in the test, was 60 % of the flexural capacity predictions. An analytical investigation was undertaken to determine what factors contributed to this discrepancy. It was proposed that due to the prestressing, the high tensile strength of the hollow-core unit concrete and low reinforcement content in the insitu topping, that under negative bending moments the effect of tension stiffening is pronounced. This results in the average strain in the steel reinforcement, predicted assuming that plane strains remain plane, being considerably less than the peak strain in the reinforcement, which determines the strength of the section. A method is described to calculate a "strain concentration factor" which is in the included in flexural strength calculations and allows for the effect of tension stiffening. This was shown to improve the flexural strength capacity predictions.

In the experimental test investigating a flexure-shear failure, continuous deformed steel bars were used in the insitu topping. The loading protocol was designed to induce high negative bending moments in the section, to create negative flexural cracks, followed by high shear and negative moments to induce flexure-shear cracking. Under the planned loading protocol, the test unit did not experience negative flexural cracking. An extended protocol was devised, which did induce negative flexural cracks. However, a flexure-shear failure was not achieved.

Possible reasons that a flexure-shear failure were not observed in the experimental investigation are presented, these included the high tensile capacity of the concrete and the low reinforcement content in the topping limiting yield to a single section when flexural cracks were formed. An analytical investigation was undertaken comparing the theoretical shear stresses induced by different quantities of steel reinforcement in the insitu topping and it was shown that shear stress values predicted by the New Zealand Concrete Structures Standard (Standards New Zealand 2006) might be unconservative (underpredicting the magnitude of shear stresses induced in the section). The understanding of this failure mechanism, and whether it might be critical, requires further research.

12.2 Conclusions

The following section presents the main outcomes from this research.

Load combinations that induce significant negative bending moments in hollow-core floors were assessed. These combinations include gravity loads, upward vertical seismic loading and actions transferred through the floor supports. Two cases are believed to be critical and should be checked during design; these depend on the type of loading transferred to the section through the supports. The first is when rotation of the support beam due to building drift induces the overstrength moment of the connection to be transferred into the floor. The second is when end moments are induced by the eccentricity of axial load applied through the starter bars.

It is possible the high tensile capacity of hollow-core concrete and the low content of steel reinforcement used in insitu topping may result in the concrete having a higher tensile capacity than the steel. Therefore, when concrete cracks yielding of the steel is limited to one section which reduces the member's ductility.

It is not appropriate to assume that plane sections remain plane when calculating the negative flexural capacity of a hollow-core section containing non-ductile mesh reinforcement in the insitu topping. This is because tension stiffening has a significant effect and the peak strain in the steel is higher than that predicted by a linear strain profile.

To gain a better estimation for the negative flexural strength of a hollow-core section that contains mesh reinforcement it is proposed that a "strain concentration factor" be included in the flexural strength calculation. This is calculated as the ratio of the distance between flexural cracks and the length over which the steel reinforcement in assumed to yield (found from bond between the concrete and steel).

Analytical investigations indicate that a flexure-shear failure might be possible in hollow-core flooring after negative moments have induced negative flexural cracking. However, this type of failure was not observed experimentally.

12.3 Recommendations for Further Research

The seismic performance of hollow-core flooring is still not fully understood. To adequately assess a hollow-core floor and use capacity design to avoid a brittle failure all failure modes must be easily identified and checked. Currently there are several failure modes that require further investigation. These include the magnitude of incompatible displacements and the forces these induce in hollow-core floors. Torsion along hollow-core floors is not well understood and the interaction between failure modes has not been investigated.

This research has increased knowledge of the potential of a negative flexural failure. However, effects of load sharing between units and deflection of support beams was not included in the experimental test or analyses.

In this research, analytical investigations suggest that a flexure-shear failure could occur in some types of hollow-core floors. However, this type of failure was not observed in an experimental test. It would be interesting to perform further investigation (including experimental tests) into the potential of a flexure-shear failure in a negative moment zone. One aspect of this which should be looked at is the crack width required for a flexure-shear failure to be induced.

12.4 Reference

Standards New Zealand. (2006). *Concrete structures standard, NZS3101, Parts 1 & 2*, Standards New Zealand, Wellington, New Zealand.

Blank

Appendix A Negative Flexural Failure

A 1 Values of S_p and μ for Calculating Vertical Seismic Actions for Hollow-core floors

It is recommended in guidelines for the assessment of hollow-core flooring in New Zealand (Department of Building and Housing 2008), that in design or retrofit of hollow-core floors the actions due to vertical seismic accelerations, calculated from the New Zealand Structural Design Actions Standard, are based on modified structural ductility factors (μ) and structural performance factors (S_p). When mesh reinforcement is used these values should be $\mu = 1.0$ and $S_p = 1.0$. When ductile reinforcement is used these values can be changed to $\mu = 2.0$ and $S_p = 0.9$. These structural performance factors are different to those given by the New Zealand Concrete Structures Standard (Standards New Zealand 2006) which would suggest $S_p = 0.81$ when $\mu = 2.0$.

There are three reasons these changes are suggested. These are:

- When mesh reinforcement is used in the topping concrete the member has very little ductility under negative moments
- As explained in Section 3.7, hollow-core floors have different stiffness's depending on the direction of loading and the commonly used equal displacement and equal energy concepts no longer apply. Using the normal structural performance factor in this situation can lead to an under estimate of the upward displacement.
- The proportion of reinforcement in the concrete topping (whether mesh or ductile bars) is generally low. This could result in yielding of the reinforcement being confined to one crack, which would limit ductility. This might occur if the tension capacity of the concrete is more than that of the steel crossing a crack (Department of Building and Housing 2008).

A 2 Properties of Test Specimen HCW1 used in Capacity Predictions

Table A-1 lists the material properties and dimensions of the hollow-core unit used for capacity predictions for test HCW1. Table A-2 lists the material properties and dimensions of the insitu topping. Note that negative values indicate tension.

Table A-1 Hollow-core unit properties used in capacity predictions

HOLLOW-CORE UNIT			
Material Properties			
Concrete Strength	f'chc	87.6	MPa
Modulus of elasticity			
Hollow-core unit	E eff	38000	MPa
Prestress Steel	Es	200000	MPa
Tension capacity of concrete	fr	0	MPa
Stress in prestress - exterior	fpse	-773	MPa
Stress in prestress - interior	fpsi	-1128	MPa
Dimensions			
No. of strands - exterior	nse	2	
No. of strands - interior	nsi	9	
Area of each strand - exterior	ape	75	mm^2
Area of each strand - interior	api	100	mm^2
Area of Prestress-exterior	Apse	150	mm^2
Area of Prestress-interior	Apsi	900	mm^2
Height of prestress from base	ht	37	mm
Hollow-core unit - dimensions in Figure C-11			
Area of hollow-core	Ahc	168471	mm^2

Table A-2 Insitu topping properties used in capacity predictions

INSITU TOPPING			
Material Properties			
CONCRETE			
Concrete Strength	f'ct	32.5	MPa
Modulus of elasticity	Ec	25800	MPa
Tension capacity of concrete	frt	0	MPa
STARTER BARS			
Reinforcing Steel	Est	200000	MPa
Grade of steel		Grade 500 test	
Yield stress topping steel	fy	-550	MPa
Ultimate stress	fus	-677	MPa
Yield Strain	eys	-0.00275	
Strain Hardening Strain	ehs	-0.016	
Ultimate strain of topping steel	eus	-0.169	
Number of starter bars	nb	4	
MESH			
Modulus of elasitcity	Em	200000	MPa
Yield stress	fym	-570	MPa
Ultimate stress	fum	-630	MPa
Yield strain	eym	-0.00285	
Ultimate strain	eum	-0.0117	
Dimensions			
CONCRETE			
Insitu conc. Width	w	1200	mm
Insitu conc. Depth (ave.)	h	58.4	mm
Area of topping concrete	At	70080	mm^2
STARTER BARS			
Assumed to be at mid height of topping			
Bar diameter	db	12	mm
Length into slab	Lb	1000	mm
Area of topping steel	As	452	mm^2
MESH			
Assumed to be at mid height of topping			
Bar diameter	dm	5.3	mm
Mesh spacing	sm	150	mm
Area of mesh	Am	176	mm^2

A 3 Prediction of Moment at First Yield

Using the assumption that plane sections remain plane and the properties specified in Table A-1 and Table A-2, the first yield moment for any section along the test unit could be calculated.

For the section at the end of the starter bars, the prestress was fully developed and the topping concrete contained only the mesh reinforcement. The yield moment when no axial load was applied was found by finding the moment when the tension force in the mesh reinforcement was equal to its yield force and the forces in the section were in equilibrium. This was calculated to be 48 kNm, where the zero strain line was 73 mm above the section soffit. Figure A-1 shows the linear strain profile used to calculate the first yield moment. Figure A-2 shows the stresses that correspond to the strains given in Figure A-1 using the stress-strain relationships shown in Appendix C5. Figure A-3 shows the forces in the section, found by multiplying the stresses in Figure A-2 by the area over which they act. The forces sum to zero and the force in the mesh reinforcement is equal to its yield force.

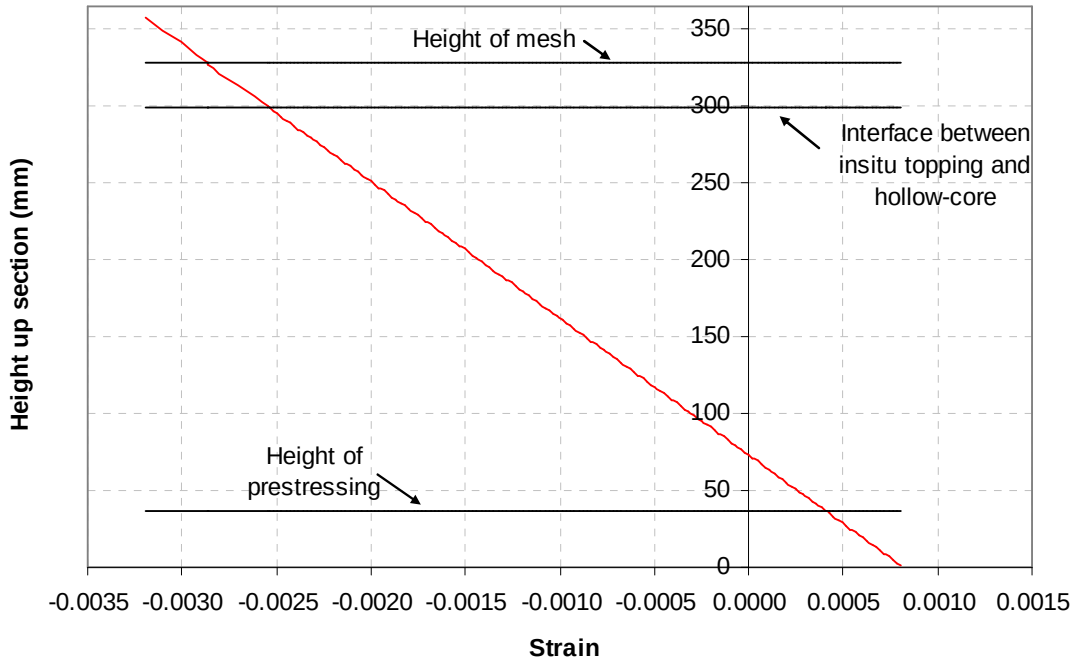

Figure A-1 Strain in section at end of starter bars at first yield moment

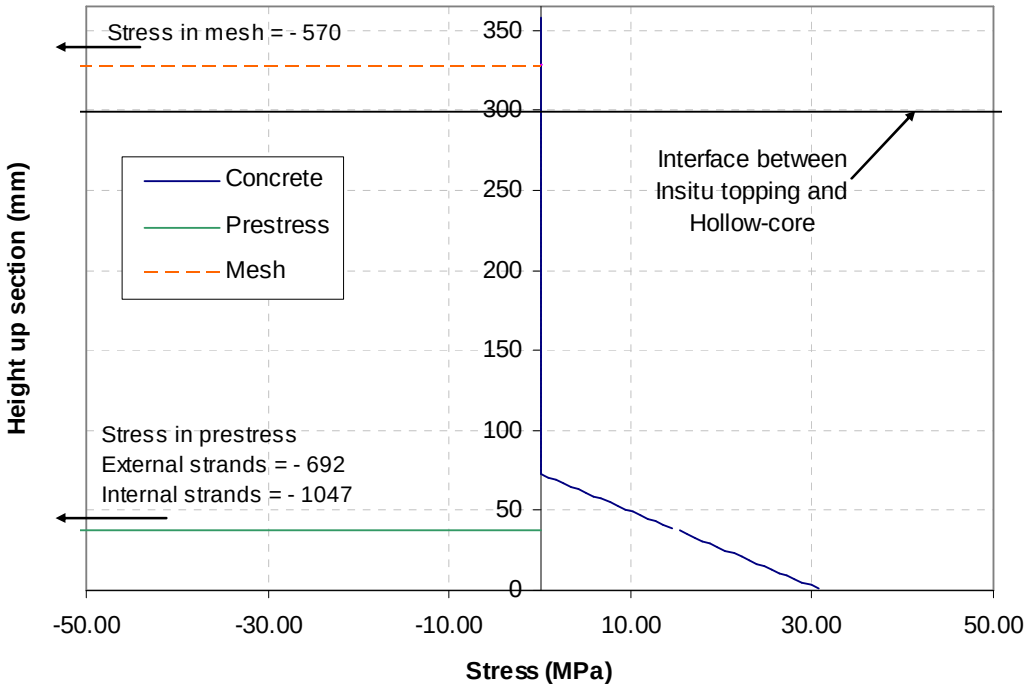

Figure A-2 Stress in section at end of starter bars at first yield moment

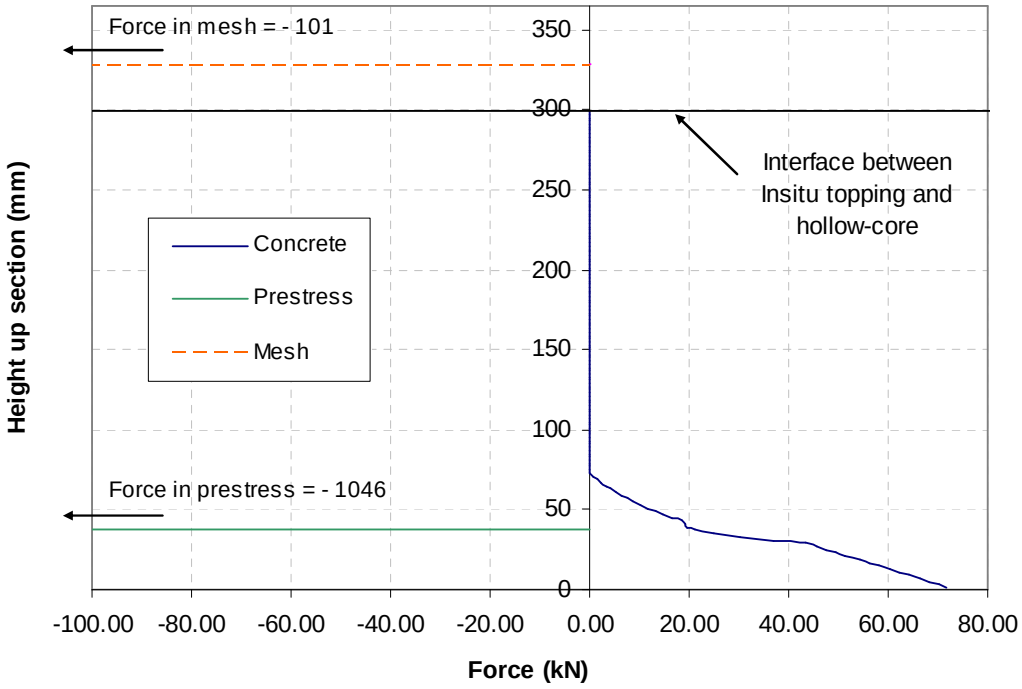

Figure A-3 Forces in section at end of starter bars at first yield moment

A 4 References

Department of Building and Housing. (2008). *Guidelines for the assessment of hollow-core flooring in New Zealand - DRAFT*, Department of Building and Housing, Wellington, New Zealand.

Standards New Zealand. (2006). *Concrete structures standard, NZS3101, Parts 1 & 2*, Standards New Zealand, Wellington, New Zealand.

Appendix B Shear Failure in a Negative Moment Zone

B 1 Properties of Test Specimen HCW2 used in Capacity Predictions

Table B-1 lists the material properties and dimensions of the hollow-core unit used for capacity predictions for test HCW2. Table B-2 lists the material properties and dimensions of the insitu topping. Note that negative values indicate tension.

Table B-1 Hollow-core unit properties used in capacity predictions

HOLLOW-CORE UNIT			
Material Properties			
Concrete Strength hc	f'chc	84.8	MPa
Modulus of elasticity			
Hollow-core unit	E eff	37500	MPa
Prestress Steel	Es	200000	MPa
Tension capacity of concrete	fr	0	MPa
Stress in prestress - exterior	fpse	-773	MPa
Stress in prestress - interior	fpsi	-1128	MPa
Dimensions			
No. of strands - exterior	nse	2	
No. of strands - interior	nsi	9	
Area of each strand - exterior	ape	75	mm^2
Area of each strand - interior	api	100	mm^2
Area of Prestress-exterior	Apse	150	mm^2
Area of Prestress-interior	Apsi	900	mm^2
Height of prestress from base	ht	37	mm
Hollow-core unit - Dycore - dimensions in Figure C-11			
Area of hc	Ahc	168471	mm^2

Table B-2 Insitu topping properties used in capacity predictions

INSITU TOPPING			
Material Properties			
CONCRETE			
Concrete Strength	f'ct	34	MPa
Modulus of elasticity	Ec	26300	MPa
Tension capacity of concrete	frt	0	MPa
STEEL REINFORCEMENT			
Reinforcing Steel	Est	200000	MPa
Grade of steel		Grade 500 test	
Yield stress topping steel	fy	-550	MPa
Ultimate stress	fus	-677	MPa
Yield Strain	eys	-0.00275	
Strain Hardening Strain	ehs	-0.016	
Ultimate strain of topping steel	eus	-0.169	
Number of bars	nb	4	
Dimensions			
CONCRETE			
Insitu conc. Width	w	1200	mm
Insitu conc. Depth (ave.)	h	67	mm
Area of topping concrete	At	80400	mm^2
STARTER BARS			
Assumed to be at mid height of topping			
Bar diameter	db	12	mm
Area of topping steel	As	452	mm^2

Appendix C Experimental Set-up

C 1 Construction Drawings

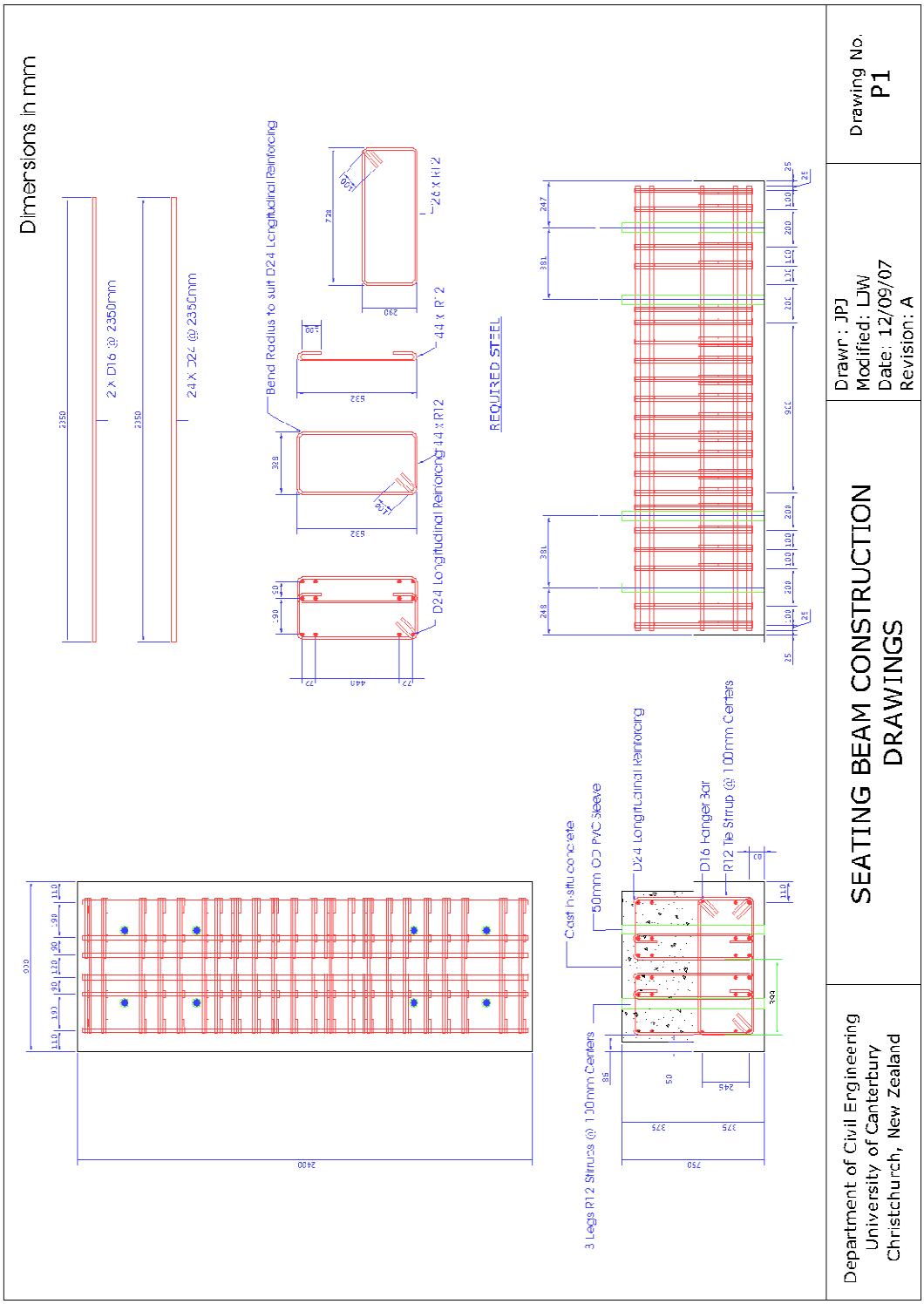

Figure C-1 Seating beam construction drawings

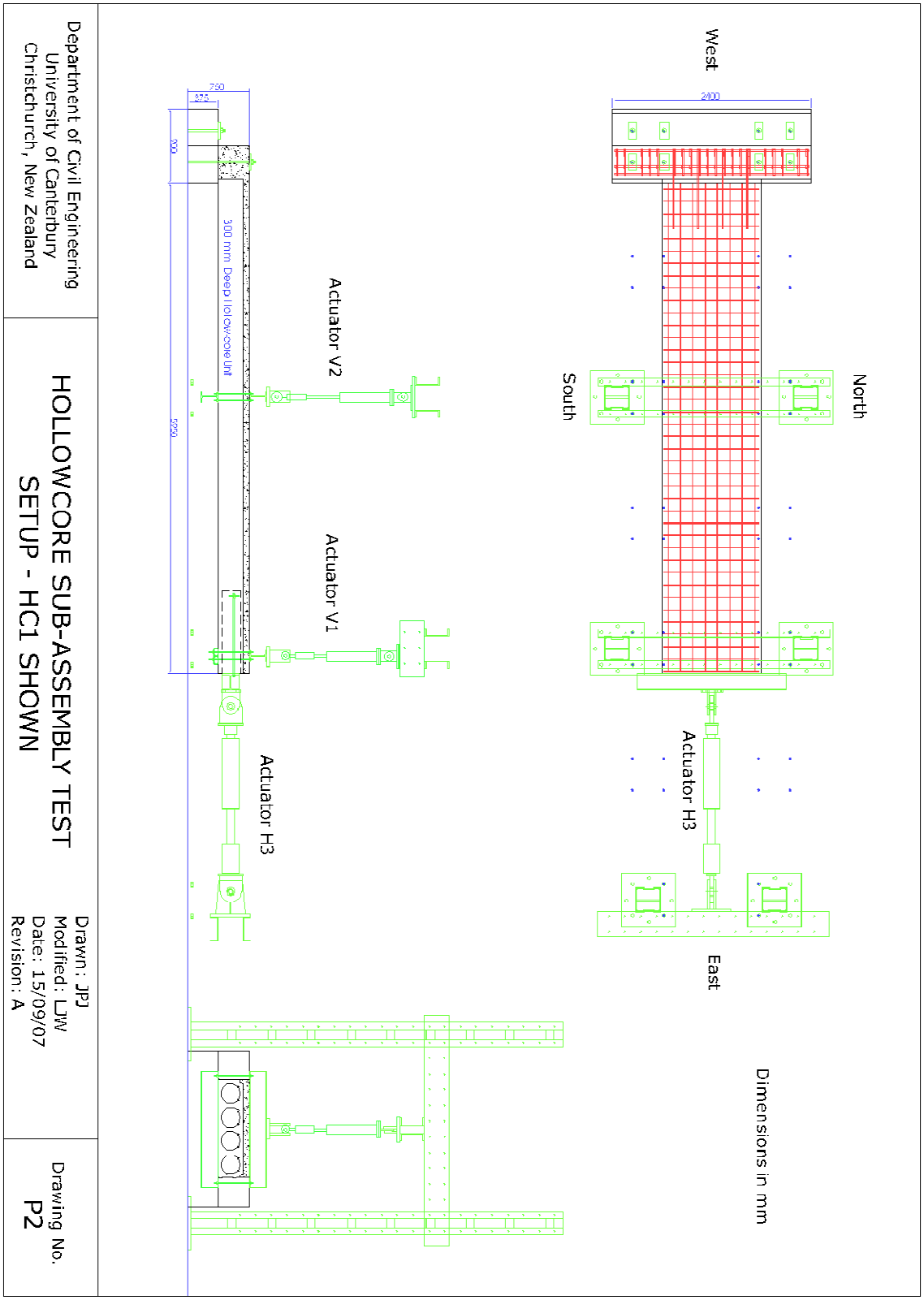

Figure C-2 Sub-assembly test setup

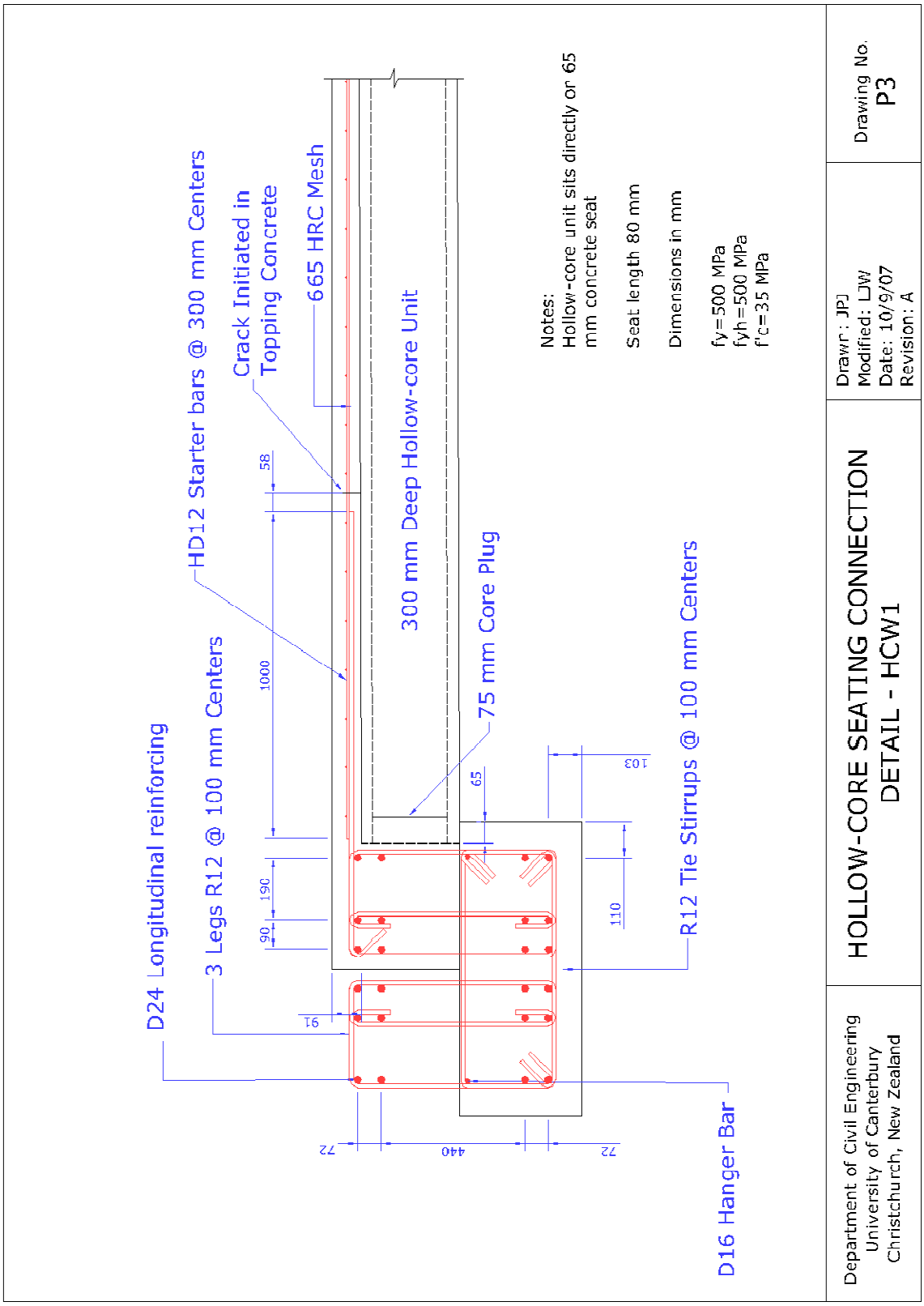

Figure C-3 Seating Connection for HCW1

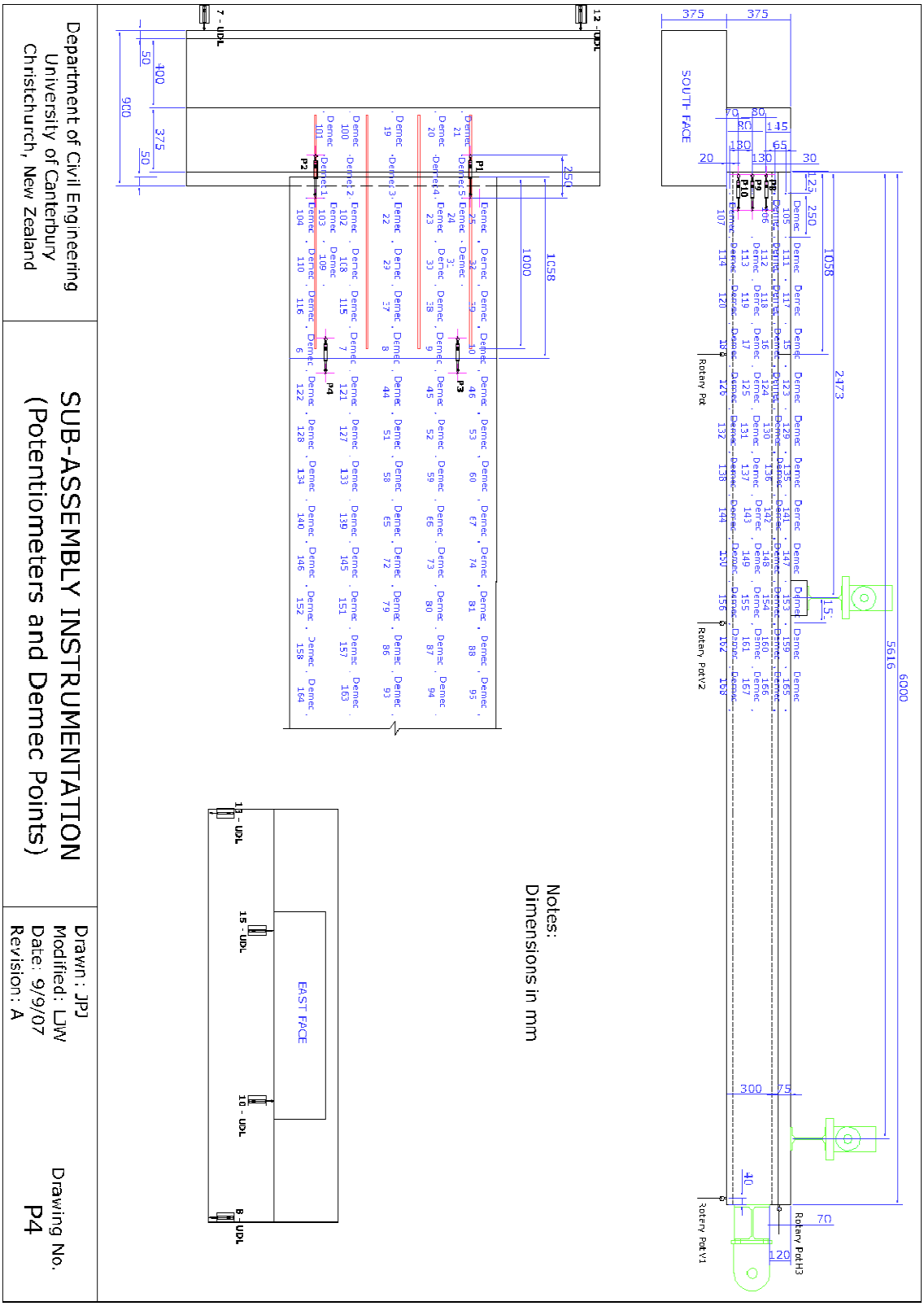

Figure C-4 Sub-assembly HCW1

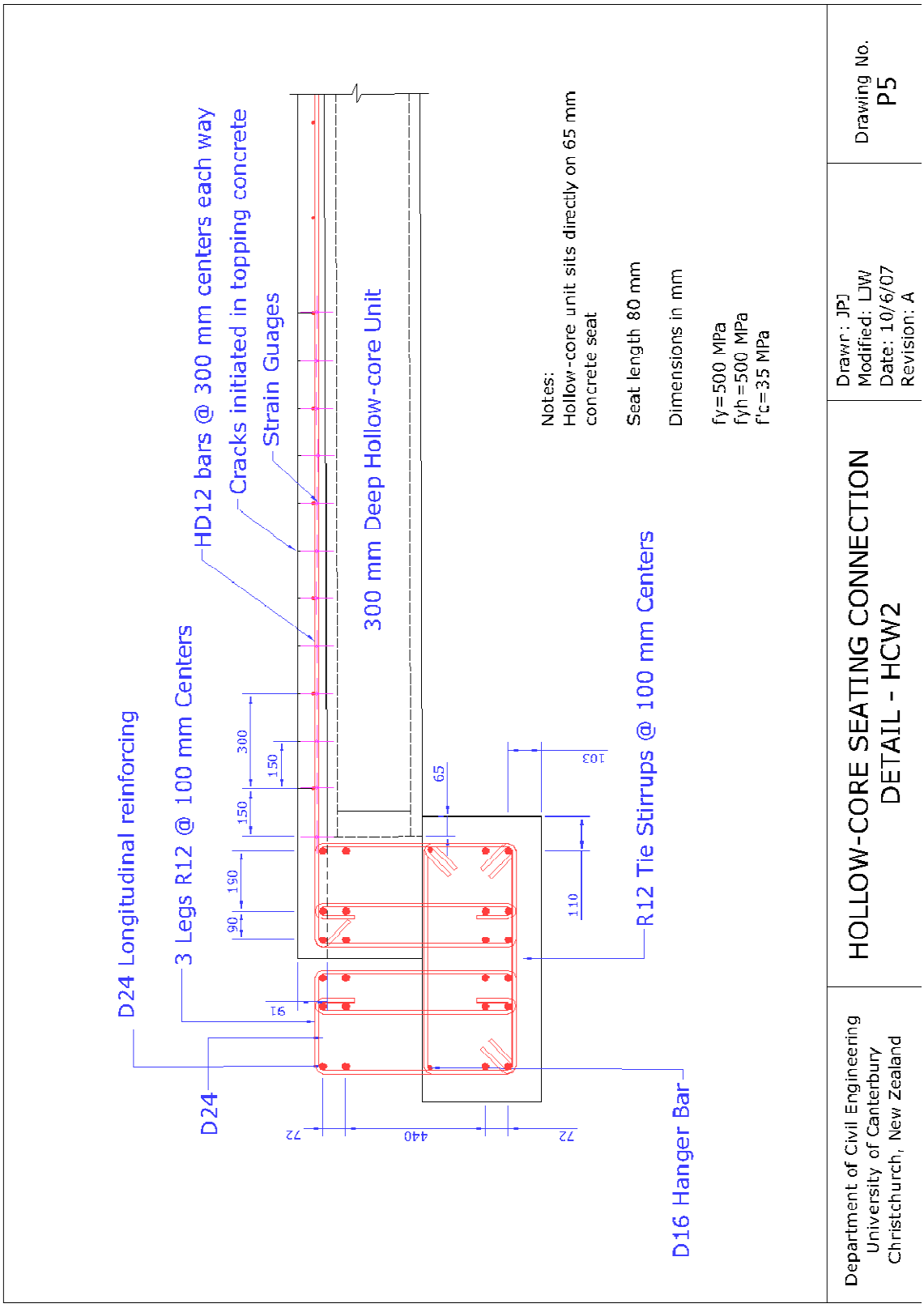

Figure C-5 Connection detail HCW2

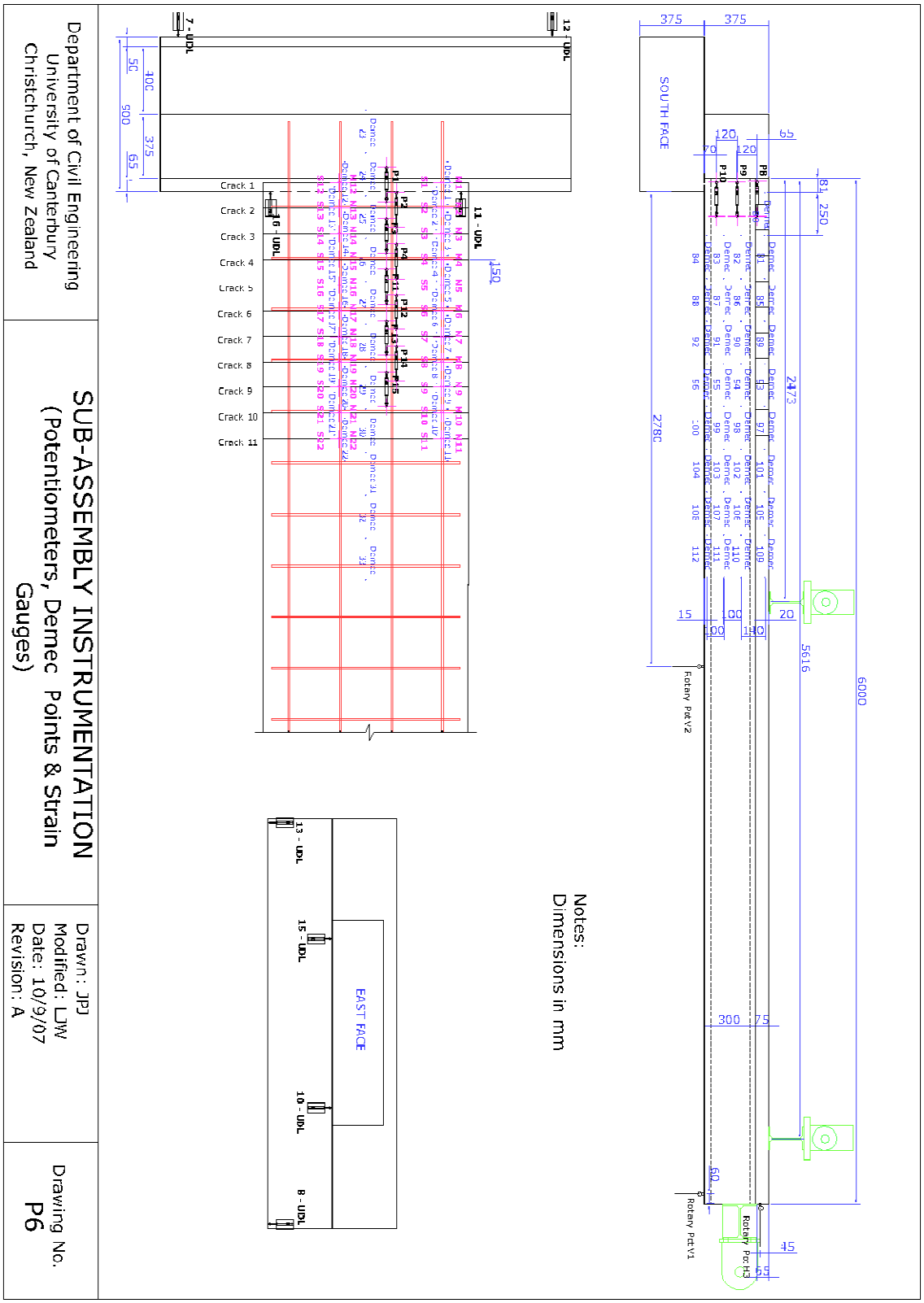

Figure C-6 Sub-assembly setup HCW2

C 2 Specimen Construction Photographic Log

Figure C-7 End of hollow-core unit showing core plugs to stop concrete from entering the voids

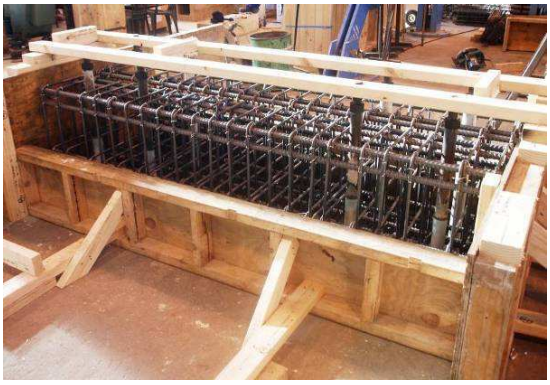

Figure C-8 Steel reinforcement and formwork ready to cast lower half of support beams

Figure C-9 Half beam cast and seat ready to place hollow-core unit

Figure C-10 End of unit - UC to attach horizontal actuator

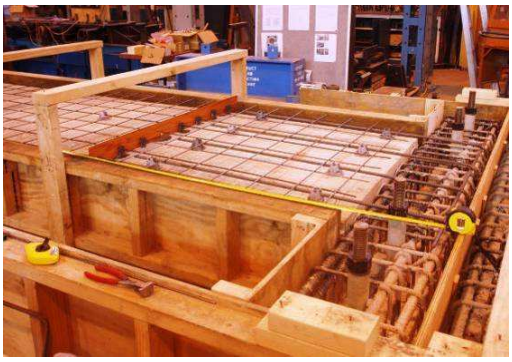

Figure C-11 Starter bars and mesh in HCW1

Figure C-12 Mild steel reinforcement and crack initiators HCW2

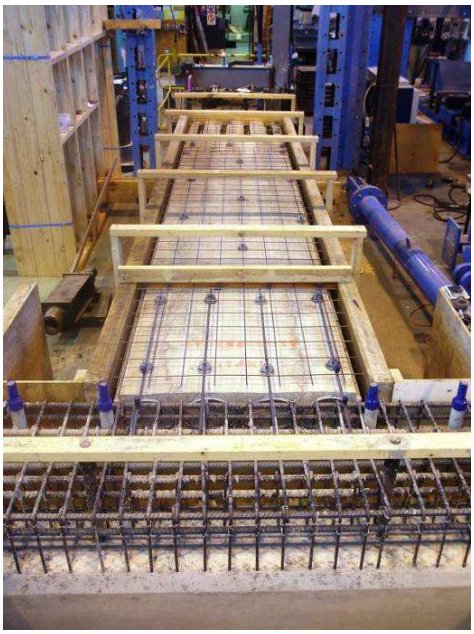

Figure C-13 HCW1 ready for placement of insitu topping concrete

Figure C-14 HCW2 ready for placement of insitu topping concrete

Figure C-15 HCW1 ready for testing

Figure C-16 HCW2 ready for testing

Figure C-17 Actuator V1 and actuator H3 connections

Figure C-18 Steel beams clamped around test unit to attach actuator V2

C 3 Instrumentation Photographs

Figure C-19 Couplers welded to starter bars in HCW1 to attach potentiometers over interface

Figure C-20 Strain gauge attached to reinforcement crossing beam-floor interface, HCW2

Figure C-21 Potentiometers at soffit of hollow-core unit

Figure C-22 Steel reinforcement crossing beam-floor interface, HCW2

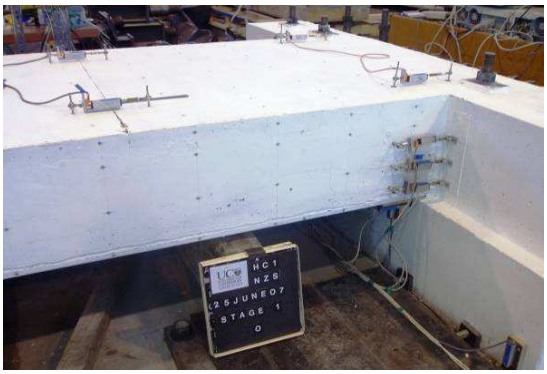

Figure C-23 Potentiometers crossing beam-floor interface and initiated crack, HCW1

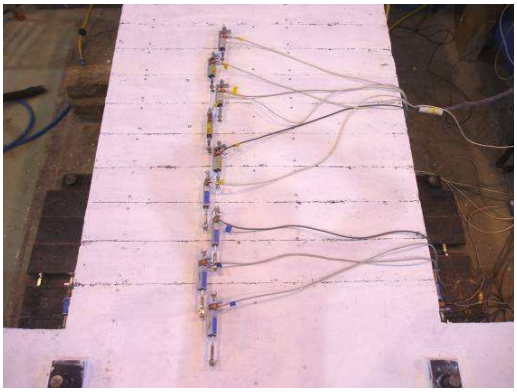

Figure C-24 Potentiometers spanning cracks initiated in topping of HCW2

Figure C-25 Rotary potentiometer under actuator V2 measuring vertical displacement

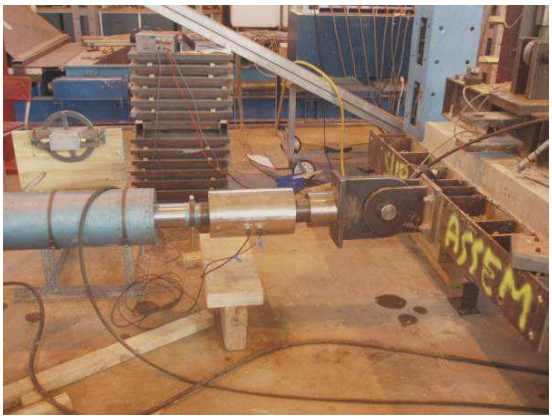

Figure C-26 Rotary potentiometer beside actuator H3 measuring horizontal movement

C 4 Dycore Unit Cross-Section

Both experimental test specimens were constructed using 300 mm deep *Dycore* hollow-core units. Figure C-27 compares the section dimensions specified by product literature to the measured section dimensions. The main difference was that the prestressing strands were closer to the soffit than specified. The top and bottom flanges were also thicker than specified, resulting in the total section being 315 mm deep rather than 300 mm.

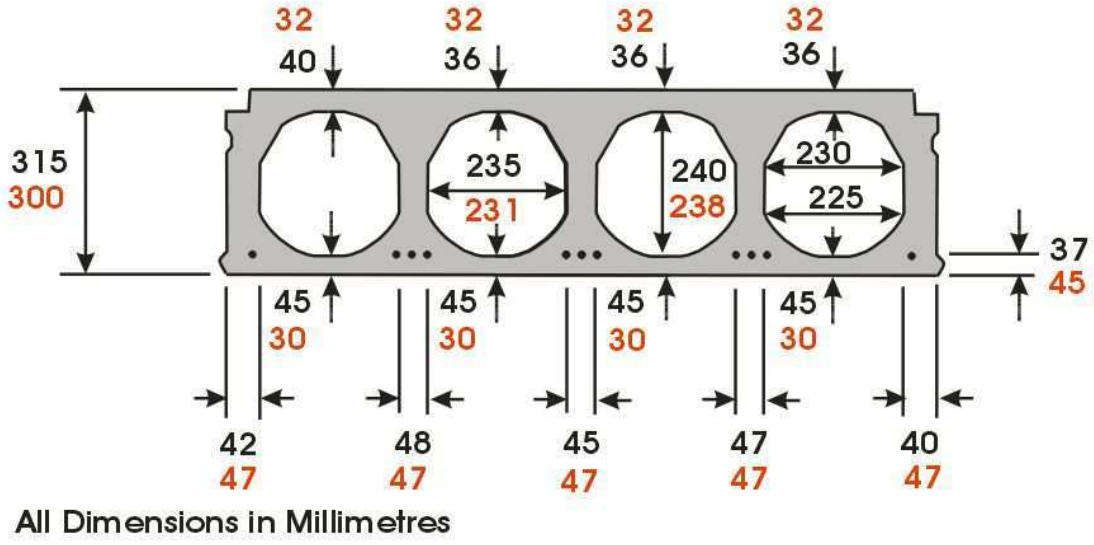

Figure C-27 Dycore hollow-core unit cross-section, red dimensions specified by manufacturer, black dimensions measured from units tested

C 5 Material Testing

C 5.1 Insitu Concrete

The compressive strength of insitu concrete, used for the support beams and floor topping, was measured from 100 mm diameter by 200 mm deep cylinders in standard compressive tests. Table C-1 gives the average compressive strengths from three cylinders, for each of the three different batches of concrete used and at three different times. HC1 Test day was 34 days after casting and HC2 test day was 19 days after casting.

Table C-1 Measured compressive strength of insitu concrete

	f'_c (MPa)		
	28 Day	**HC1 Test Day**	**HC2 Test Day**
Base Block Beam	25.80	26.48	29.52
Topping HCW1	25.73	32.46	-
Topping HCW2	25.76	-	34.09

C 5.2 Hollow-core Concrete

Compressive and tensile strengths of the hollow-core unit concrete were measured from drilled concrete cores. Because of the hollow-core unit geometry, cores were drilled parallel to the horizontal surface rather than perpendicular. The tests were performed on dry specimens with a diameter of 69.3 mm and had an aspect ratio of between 1.97 and 2.04 (average length of 139.0 mm). These aspect ratios are between the limits where no correction factors are required, as given by the American Concrete Institute (ACI) (American Concrete Institute. and ACI Committee 301. 1996). The maximum aggregate size in the specimens was 13 mm. The age of the specimens was unknown but assumed to be between 1.5 and 2.0 years. Cores used to find the compressive strength were capped at both ends.

Compressive tests were performed in accordance with the New Zealand standard for determining the strength in compression of drilled concrete cores (Standards New Zealand. 1986). Six tests were performed from each hollow-core unit with the average compressive strength and standard deviation shown in Table C-2. No correction has been made to account for the strengths coming from core samples rather than standard test specimens.

Table C-2 Compressive strength of hollow-core units

	f'_c (MPa)	Std. deviation (MPa)
HCW1	87.6	5.0
HCW2	84.8	6.3

The tensile strength of the hollow-core unit concrete was gained from standard splitting tests for drilled concrete cores, in accordance with the ACI standards (American Concrete Institute. and ACI Committee 301. 1996). The direct tensile strength, f_t, and the modulus of rupture, f_r, (flexural tensile strength) were then calculated from the splitting test strength, $f_{ct,sp}$, in accordance with the New Zealand Concrete Standard (Standards New Zealand. 2006). Table C-3 shows the tensile strength of concrete for the two hollow-core specimens. The direct tensile strength is taken as 90 % of the splitting test values. The modulus of rupture was obtained by the multiplying the direct tensile strength by a factor, K_t, which varies with member depth. A K_t value of 1.33 was assumed here, this corresponds with a member depth of 300 mm. The splitting tests were performed on cores taken parallel with the horizontal surface; therefore, it is possible the tensile stress applied during the splitting test was in the direction of casting. When the tensile stress acts in the direction of casting it can be 10 % to 30 % lower then strengths recorded from tensile stress acting perpendicular to casting.

Table C-3 Tensile strength of hollow-core units

	$f_{ct,sp}$ (MPa)	f_t (MPa)	f_r (MPa)
HCW1	6.9	6.2	8.8
HCW2	7.6	6.9	9.7

C 5.3 Mander Stress-strain Curve for Concrete

The stress-strain relationship used for the concrete was assumed to be that derived by Mander (1982). This is given by Equation C-1.

$$f = \frac{f'_{cc} x r}{r - 1 + x^r} \qquad \textbf{Equation C-1}$$

Where f is the compressive stress in the concrete, f'_{cc} is the maximum compressive stress for the confined concrete, this occurs at a strain of ε_{cc}. Equation C-2 gives r, where E_c is the

elastic modulus and E_{sec} the secant modulus. Equation C-3 gives x, this is the ratio of the strain, ε, corresponding to f , by ε_{cc}.

$$r = \frac{E_c}{(E_c - E_{sec})}$$ **Equation C-2**

$$x = \frac{\varepsilon}{\varepsilon_{cc}}$$ **Equation C-3**

The strain ε_{cc} can be found from Equation C-4. Where f'c is the cylinder strength of the concrete. For unconfined concrete f'_{cc} is equal to f'_c. However, in this research ε_{cc} is taken as Equation C-5, this is an average value derived empirically from experimental data (Fenwick R., personal communication, 2007).

$$\varepsilon_{cc} = 0.002\,(1 + 5\,(\frac{f'_{cc}}{f'_c} - 1))$$ **Equation C-4**

$$\varepsilon_{cc} = 0.00145 + 0.00001875\ f'_c$$ **Equation C-5**

The concrete in the hollow-core units was assumed to be unconfined. For test HCW1 the cylinder strength was measured as 87.6 MPa and the elastic modulus taken as that given by Equation C-6 (Standards New Zealand 2006).

$$3320\sqrt{f'_c} + 6900$$ **Equation C-6**

From the above equations, a stress-strain relationship can be plotted. Figure C-28 shows the stress-strain relationship used for strength predictions of HCW1. A similar curve was used for strength prediction of HCW2.

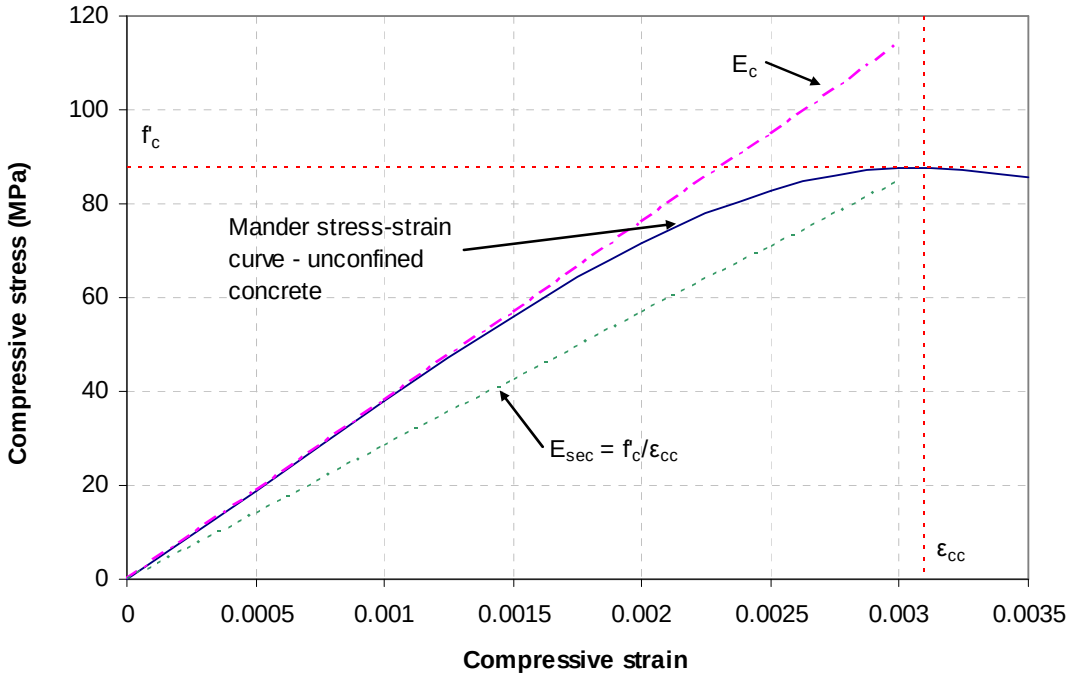

Figure C-28 Compressive stress-strain relationship used for hollow-core concrete

C 5.4 Stress-Strain Relationship of Grade 500 Steel

Grade 500, 12 mm diameter, deformed steel bars (HD12) were used in both test specimens. The stress-strain relationship for this steel was found using a standard monotonic tensile test. Three bars were tested and the results are shown plotted in Figure C-29.

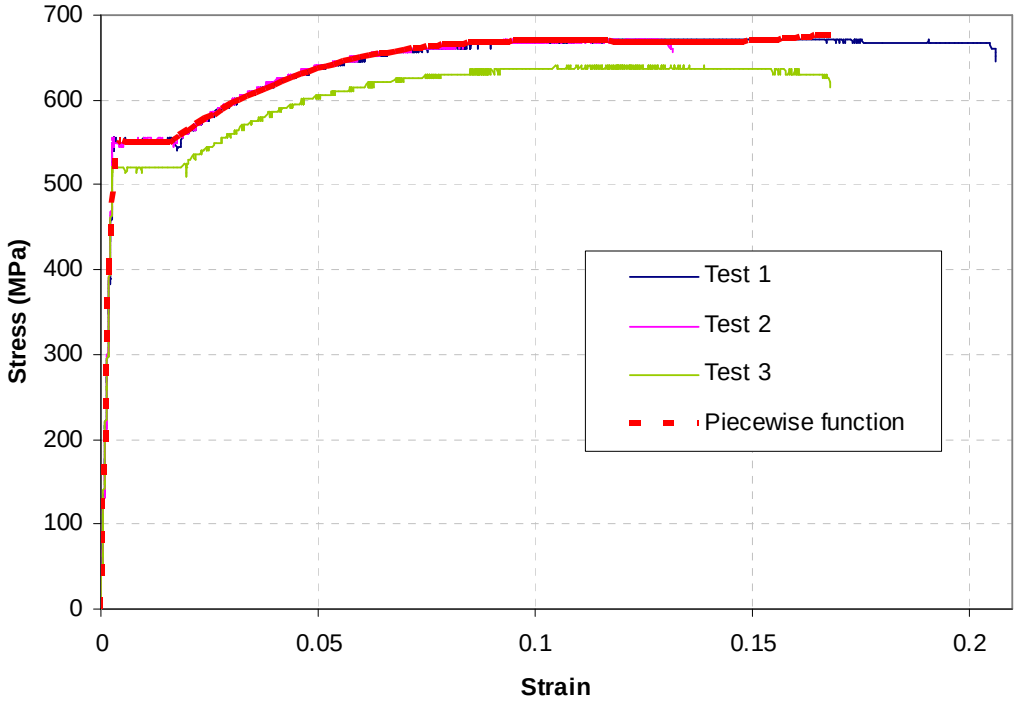

Figure C-29 Stress-strain relationship observed for HD12 steel reinforcement

The bar specimens used for Test 1 and 2 had very similar stress-strain characteristics; however, the specimen used in Test 3 exhibited lower yield and ultimate stress values. For strength predictions the stress-strain relationship was approximated by the piecewise function given in Equation C-7, this is shown in red in Figure C-29.

$$\begin{cases} \varepsilon \le \varepsilon_y & \varepsilon E_s \\ \varepsilon_y < \varepsilon \le \varepsilon_h & f_y \\ \varepsilon_h < \varepsilon \le \varepsilon_u & 113494\varepsilon^3 - 41710\varepsilon^2 + 4785\varepsilon + 484 \\ \varepsilon_u < \varepsilon & 0 \end{cases} \qquad \textbf{Equation C-7}$$

Where E_s is the elastic modulus and taken as 200 000 MPa. The other parameters were found from the test data and are given in Table C-4.

Table C-4 Key points taken from stress-strain relationship of HD12 bars

Yield Stress	**f_y (MPa)**	550
Yield Strain	**ε_y**	0.0028
Strain Hardening Stress	**f_h (MPa)**	550
Strain Hardening Strain	**ε_h**	0.016232
Ultimate Stress	**f_u (MPa)**	677.32
Ultimate Strain	**ε_u**	0.169

C 5.5 Stress-Strain Relationship for Mesh Reinforcement

In test specimen HCW1, 665 mesh reinforcement was used in the insitu topping concrete. The stress-strain relationship for this mesh was found using a standard monotonic tensile test. Three bars were tested and the results are shown plotted in Figure C-29.

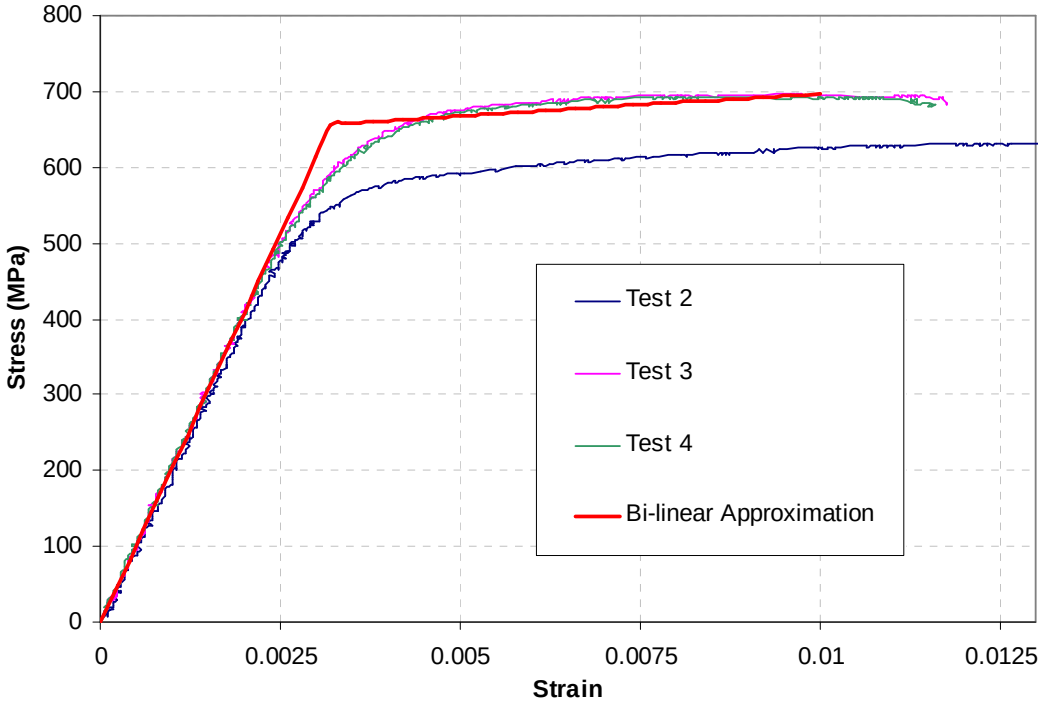

Figure C-30 Stress-strain relationship observed for HRC 665 mesh reinforcement

Four pieces of wire mesh were tested; however, data from the first test was rejected as the displacement measuring devise was not attached to the specimen correctly. Of the other three tests, tests 3 and 4 correlate well, however test 2 has a lower yield point and a higher ductility. In the strength calculations a bi-linear relationship was used to approximate the stress-strain curve. The bi-linear relationship used represent the stress-strain relationship exhibited by tests

3 and 4 is shown in red in Figure C-30. The piecewise function which gives this curve is given by Equation C-8.

$$\begin{cases} \varepsilon \le \varepsilon_{ym} & \varepsilon E_m \\ \varepsilon_{ym} < \varepsilon \le \varepsilon_{um} & ((f_{um} - f_{ym}) / (\varepsilon_{um} - \varepsilon_{ym}))(\varepsilon - \varepsilon_{ym}) \\ \varepsilon_{um} < \varepsilon & 0 \end{cases}$$

Equation C-8

Where E_m is the elastic modulus and taken as 200 000 MPa. The other parameters were found from the test data and are given in Table C-5. The yield point was taken as the point a line with a slope of E_m and off-set at zero stress of 0.01 strain, crossed the lines of measured stress-strain relationship.

Table C-5 Key points taken for approximation of stress-strain relationship for mesh reinforcement

Yield Stress	**f_{ym} (MPa)**	656
Yield Strain	**ε_{ym}**	0.0032
Ultimate Stress	**f_{um} (MPa)**	697.00
Ultimate Strain	**ε_{um}**	0.010

C 6 Assumed Self-Weight

Figure C-31 shows the components of the sub-assembly test set-up that contributed to the specimen self-weight. The steel beams, which connected the actuators to the specimen, are included in the self-weight. The weight of the concrete in the cores at the East end used to connect Actuator H3 to the hollow-core floor also contributed.

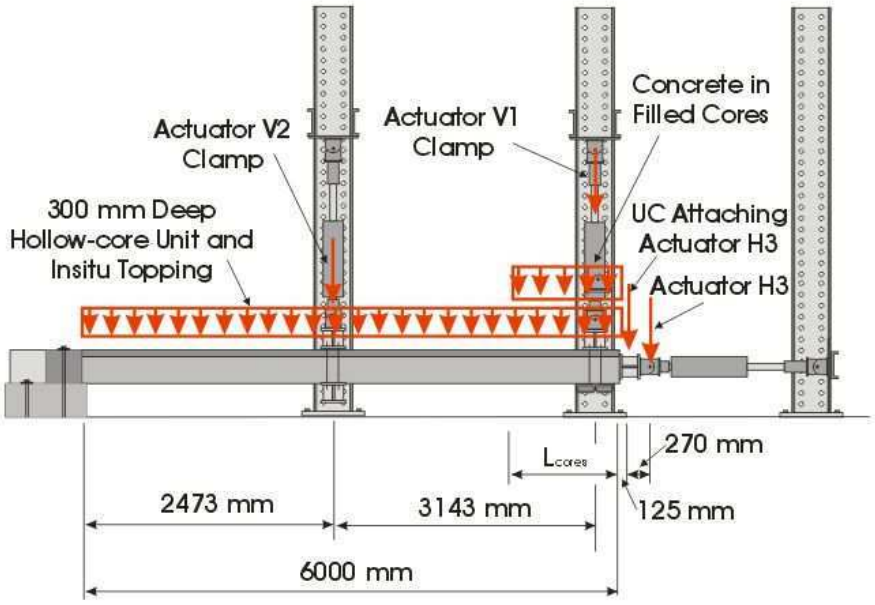

Figure C-31 Components of self-weight along test specimen

Table C-6 presents three sets of magnitudes for the different self-weight components. Column two of this table is the self-weight along the specimen originally calculated from a weight given by the manufacture for the hollow-core unit and weights approximated from measured geometry and the density of concrete and steel. The length that concrete entered the cores at the East end of the specimen was not measured and had to be assumed. The initial self-weight approximation was used when deriving the loads in Actuators 1 and 2 to create the desired bending moment profiles in the loading protocols. During testing, it became apparent that the original prediction for self-weight was too light and revisions were made to the predicted self-weight to improve its accuracy. These revised self-weights were used to calculate the actions induced in the specimen during testing presented in the results Chapters (8 and 9). These are shown in the third and forth columns of Table C-6. The revised weights were calculated assuming that the length that insitu concrete entered the cores at the East end was further than initially assumed and that the weight of the hollow-core unit and topping concrete was more.

Table C-6 Components of self-weight used in bending moment calculations

Parts of floor	Weights		
	Initial Approximation	Used for HCW1	Used for HCW2
Hollow-core unit and insitu topping	5.823 kN/m	6.25 kN/m	6.80 kN/m
Steel beams connecting Actuator V2	0.787 kN	0.787 kN	0. 787 kN
Steel beams connecting Actuator V2	0.787 kN	0.787 kN	0. 787 kN
Steel beam connecting Actuator H3	0.31 kN	0.31 kN	0.31 kN
Half of Actuator H3	1.74 kN	1.74 kN	1.74 kN
Concrete in filled cores	4.185 kN/m	4.185 kN/m	4.185 kN/m
Length of cores filled with concrete	1.0 m	1.3 m	1.5 m

Throughout the construction of specimen HCW2, the support beam at the West end and actuator V1 at the East end supported it. The load carried by actuator V1 was recorded throughout the construction process. It is assumed that before the insitu concrete hardens, the member acted as a simply supported member, as shown at the bottom of Figure C-32. As the topping concrete shrinks it can create some fixity at the support, this reduces the load in Actuator V1. If the connection at the support became fully fixed the bending moment profile will resemble that shown as a propped cantilever in Figure C-32.

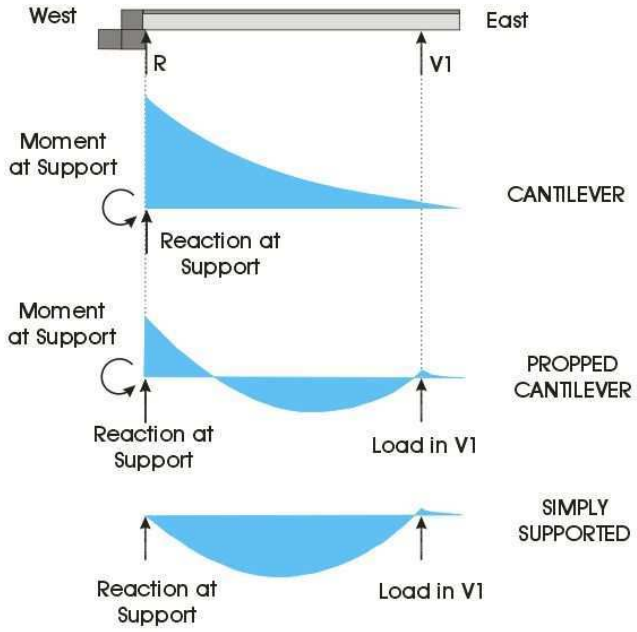

Figure C-32 Difference in bending moment diagram depending on if support connection is fixed or pinned

Table C-7 shows the theoretical difference in moments at the support beam and load in Actuator V1, if different support conditions are assumed, for the three different self-weight predictions. Over the construction period of test HCW2, the load in Actuator V1 varied between 29.8 kNm and 31.5 kNm. Comparing these to the values of load in Actuator V1 in Table C-7 it appears the self-weight may even be higher than that used for the results calculations of specimen HCW2. However, even a small moment capacity at the support beam, or movement of Actuator V1 could lead change the load recorded, so there is still some uncertainty in the self-weight value.

Table C-7 Actions induced by self-weights

	Initial Approximation	Used for HCW1	Used for HCW2
Moment at support if cantilever	147 kNm	161 kNm	174 kNm
Moment at support if propped by V1	23.2 kNm	25.2 kNm	27.8 kNm
Load in V1 if propped cantilever	21.4 kN	23.5 kN	25.4 kN
Load in V1 if simply supported	25.5 kN	27.9 kN	30.4 kN

C 7 References

American Concrete Institute., and ACI Committee 301. (1996). *Standard specifications for structural concrete ACI 301-96 : with selected ACI and ASTM references*, American Concrete Institute, Farmington Hills, Mich.

Mander, J. B. (1982). "Seismic Design of Bridge Piers." *Research Report 84-2*, University of Canterbury, Christchurch, New Zealand.

Standards New Zealand. (2006). *Concrete structures standard, NZS3101, Parts 1 & 2*, Standards New Zealand, Wellington, New Zealand.

Standards New Zealand. (1986). *Methods of test for concrete - Tests relating to fresh concrete*, Standards New Zealand, Wellington [N.Z.].

Appendix D Experimental Results: HCW1

D 1 Testing Photographic Log: HCW1

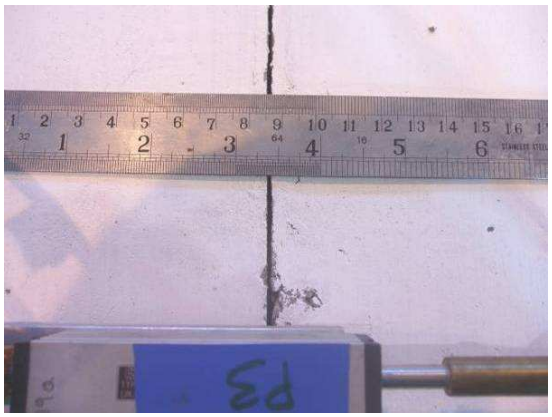

Figure D-1 Width of initiated crack at start of test

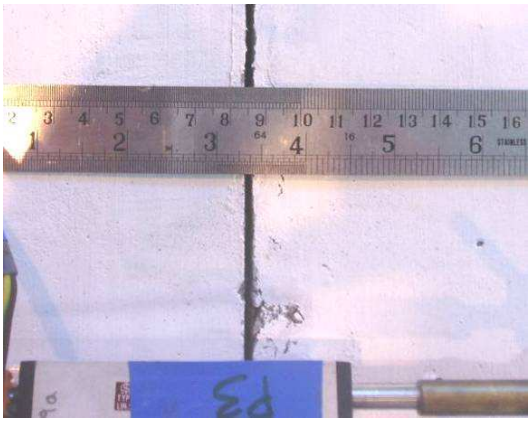

Figure D-2 Width of initiated crack at the end of Stage One – Increment 16

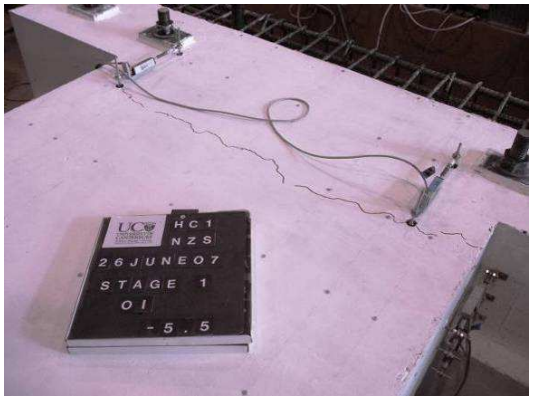

Figure D-3 Increment 2 – First crack in topping concrete, 100 mm from interface

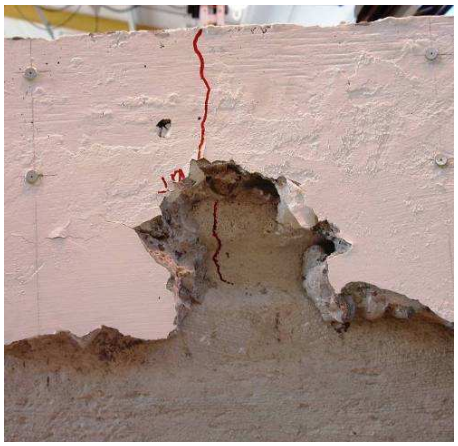

Figure D-4 Post test – Insitu concrete removed from side of unit and crack at 530 mm from interface seen

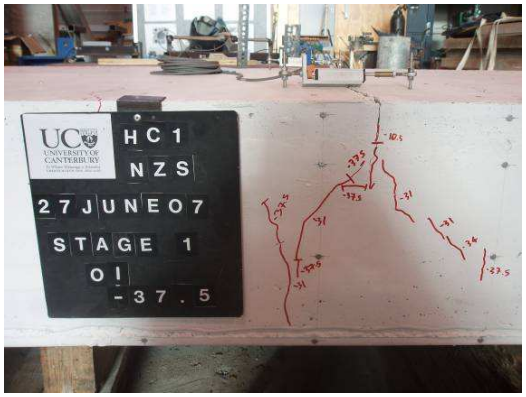

(a) Crack at the end of the starter bars – North side

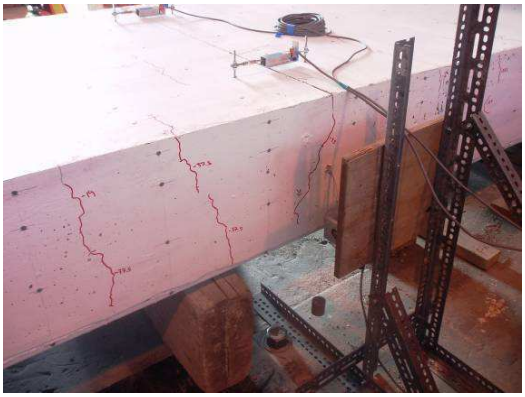

(b) Crack at the end of the starter bars – South side

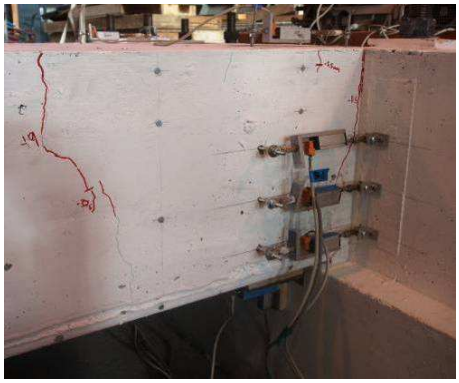

(c) Crack at beam-floor interface – North side

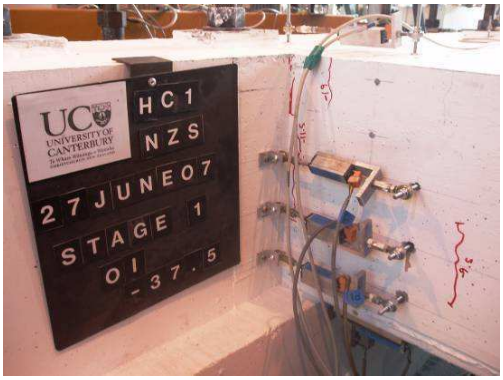

(d) Crack at beam-floor interface – South side

Figure D-5 Test unit HCW1 at the end of Stage One – Increment 16

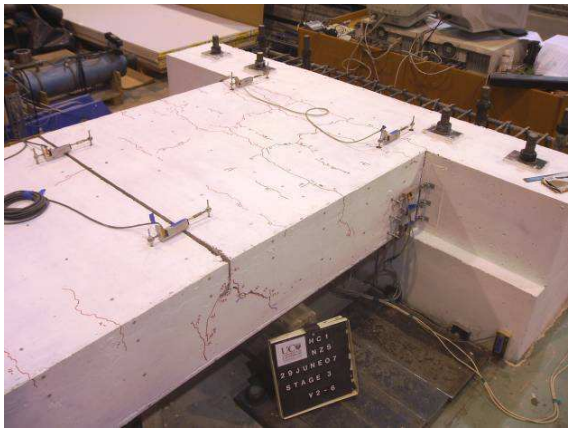

(a) Cracking in topping concrete at the end of testing

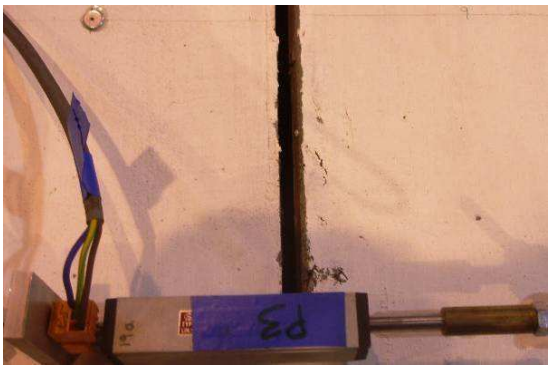

(b) Initiated crack at failure

(c) Crack at beam-floor interface – North side

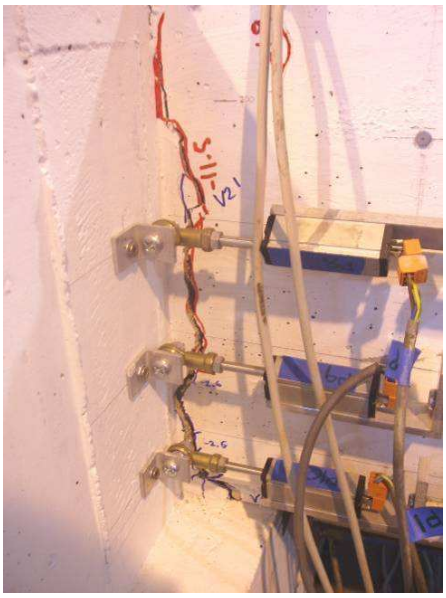

(d) Crack at beam-floor interface – South side

Figure D-6 Test unit HCW1 at the end of testing – Increment 66

D 2 Loads and Displacements of Actuators at Key Increments: HCW1

Table D-1 shows the data recorded at key points during HCW1 test, generally these coincided with when readings were taken from Demec points. For actuators V1 and V2 a negative load is vertically up and negative displacements are down from the initial position where the floor unit was level. For actuator H3 a negative load is pulling the floor horizontally away from its support and this corresponds to a positive displacement. Increment 66 was immediately after the specimen had failed. Increment 67 was after the specimen had been left for two days.

Table D-1 Loads and Displacements of Actuators during test HCW1

Stage	Increment	Load in actuators (kN)			Displacement at actuators (mm)		
		V1	V2	H3	V1	V2	H3
Stage One - Lowering actuator V1	0	-26.74	0.00	0.00	0.00	0.00	0.00
	1	-24.27	0.00	0.00	-1.75	0.00	0.00
	2	-19.78	0.00	0.00	-5.34	0.00	0.00
	3	-17.87	0.00	0.00	-7.32	0.00	0.00
	4	-14.38	0.00	0.00	-11.29	0.00	0.00
	4.1	-18.99	0.00	0.00	-11.29	0.00	0.00
	5	-13.82	0.00	0.00	-20.59	0.00	0.00
	5.1	-17.30	0.00	0.00	-20.59	0.00	0.00
	6	-14.61	0.00	0.00	-24.79	0.00	0.00
	7	-13.26	0.00	0.00	-27.76	0.00	0.00
	7.1	-19.89	0.00	0.00	-28.60	0.00	0.00
	8	-18.54	0.00	0.00	-31.73	0.00	0.00
	9	-18.65	0.00	0.00	-34.78	0.00	0.00
	10	-18.54	0.00	0.00	-35.62	-18.04	0.12
	11	-18.65	0.00	0.00	-35.62	-18.04	0.12
	12	-18.54	0.00	0.00	-35.62	-18.04	0.12
	13	-18.31	0.00	0.00	-36.16	-18.10	0.12
	14	-18.20	0.00	0.00	-36.61	-18.15	0.12
	15	-18.20	0.00	0.00	-36.69	-18.18	0.12
	16	-18.20	0.00	0.00	-37.15	-18.24	0.12

Table D-1 continued

Stage	Increment	Load in actuators (kN)			Displacement at actuators (mm)		
		V1	V2	H3	V1	V2	H3
Reducing Moments	17	-18.43	0.00	0.00	-37.15	-18.21	0.233
	18	-18.31	0.00	0.00	-37.15	-18.24	0.233
	19	-19.44	0.00	0.00	-36.16	-18.15	0.698
	20	-20.22	0.00	0.00	-34.71	-17.99	0.698
	21	-21.12	0.00	0.00	-33.10	-17.85	0.698
	22	-22.70	0.00	0.00	-30.13	-17.55	0.582
	23	-22.92	0.00	0.00	-29.21	-17.44	0.582
	24	-23.03	0.00	0.00	-28.76	-17.41	0.233
Applying Axial Load	25	-22.92	0.00	-70.62	-28.76	-17.41	0.349
	26	-23.03	0.00	-92.15	-28.68	-17.44	0.466
	27	-23.15	0.00	-106.20	-28.68	-17.44	0.698
	28	-23.15	0.00	-58.10	-28.68	-17.47	1.048
	29	-23.26	0.00	-58.10	-28.68	-17.44	1.164
	30	-22.92	0.00	-61.10	-29.29	-17.63	1.164
	31	-22.92	0.00	-60.60	-29.29	-17.63	1.164
	32	-22.92	0.00	-123.20	-29.29	-17.69	1.630
	33	-22.47	0.00	-170.80	-29.21	-17.69	2.095
	34	-22.58	0.00	-198.80	-29.21	-17.69	2.561
	35	-22.58	0.00	-219.90	-29.29	-17.74	2.910
	36	-22.70	0.00	-234.90	-29.29	-17.74	3.143
	37	-22.70	0.00	-255.90	-29.29	-17.74	3.376
	38	-22.70	0.00	-271.50	-29.29	-17.80	3.609
	39	-22.92	0.00	-273.00	-29.14	-17.77	3.725

Table D-1 continued

Stage	Increment	Load in actuators (kN)			Displacement at actuators (mm)		
		V1	V2	H3	V1	V2	H3
Increasing Moment with Axial Load	40	-12.13	-16.46	-216.90	-29.21	-17.36	4.42
	41	-12.36	-16.01	-215.90	-29.21	-17.36	4.54
	42	-36.74	41.08	-221.90	-29.67	-17.99	4.19
	43	-25.73	13.43	-219.40	-29.06	-17.69	4.31
	44	-16.52	-7.61	-213.40	-28.53	-17.36	4.54
	45	-17.64	-7.84	-158.80	-28.53	-17.38	4.31
	46	-13.48	-18.25	-158.30	-28.07	-17.25	4.31
	47	-11.91	-21.38	-153.80	-28.45	-17.25	4.31
	48	-12.81	-15.11	-219.40	-28.38	-17.22	4.77
	49	-10.45	-21.05	-204.80	-28.22	-17.11	4.77
	50	-7.98	-27.31	-199.80	-27.99	-16.94	4.89
	51	-7.87	-27.65	-181.80	-28.45	-16.94	5.01
	52	-9.89	-27.65	-147.70	-28.60	-17.00	4.54
	53	-9.66	-22.84	-202.80	-28.60	-16.97	5.01
	54	-12.81	-13.32	-229.40	-28.68	-16.86	5.70
	55	-14.05	-9.18	-238.90	-28.68	-16.81	5.94
	56	-14.72	-7.84	-227.90	-29.06	-16.81	6.17
	57	-10.22	-19.37	-215.40	-28.53	-16.39	6.40
	58	-6.85	-27.87	-198.80	-28.22	-16.01	6.75
	59	-7.42	-26.98	-197.30	-28.22	-16.01	6.87
	60	-8.32	-25.41	-192.80	-28.30	-16.01	6.99
	61	-7.42	-27.09	-193.30	-28.68	-16.01	6.99
	62	-7.42	-27.09	-192.30	-28.91	-16.01	6.99
	63	-11.12	-17.35	-209.90	-28.83	-15.90	7.45
	64	-14.38	-13.55	-171.30	-28.99	-15.79	7.68
	65	-14.27	-13.10	-181.30	-28.91	-15.79	7.68
	66	-23.15	0.00	-133.70	-28.83	-15.49	9.54
	67	-16.29	-24.18	-53.09	-29.21	-16.01	12.92

D 3 Uncertainty Associated with Bending Moment Calculation: Stage One

During Stage One of the HCW1 test, the bending moments induced at different locations along the test unit were calculated from self-weight of the test unit and the load recorded in

the actuator V1. A range of ± 16.8 kNm was given as the potential uncertainty of the calculated bending moment. This uncertainty arises from a combination of the uncertainties of the self-weight of the specimen and of the load in actuator V1. The magnitude of uncertainty changes along the length of the specimen and is greatest at the beam-floor interface. This is because at this location, the lever-arm to the force in actuator V1 is greatest and therefore any change in the load V1 is magnified as the lever-arm grows.

It can be assumed that the original self-weight calculated for the specimen is a lower bound and that the weight predicted for specimen HCW2 is an upper bound (see Table C-6). Comparing the bending moments created at the beam-floor interface, the effect these changes have on the calculated bending moment can be observed. In this case, the bending moment produced by the self-weight used for specimen HCW1 was 161 kNm, compared to 147 kNm and 174 kNm (see Table C-7). The bending moment at the interface from the self-weight is therefore 161 ± 14 kNm.

The load measured at actuator V1 also has some uncertainty. The load recorded could be ± 0.5 kN. This small uncertainty has a marked effect on the bending moment near the beam-floor interface because of the long lever arm over which it acts. A change in the load in actuator V1 of 0.5 kN results in a change in moment at the beam floor interface of 2.8 kNm. The bending moment at the beam-floor interface from the load in actuator V1 is V1*5.616 ± 2.8 kNm. The total bending moment at the beam-floor interface has an uncertainty of 14 + 2.8 = 16.8 kNm.

Appendix E Experimental Results: HCW2

E 1 Testing Photographic Log: HCW2

(a) Stage One – Wellington up

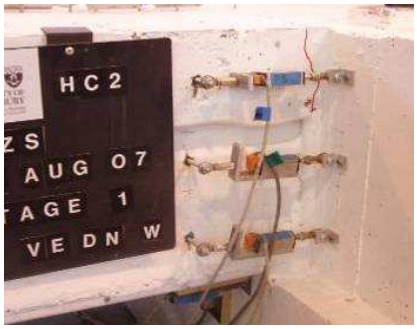

(b) Stage One – Wellington down

(c) Stage Two – Wellington up

(d) Stage Two – Wellington down

(e) Stage Three – Wellington up

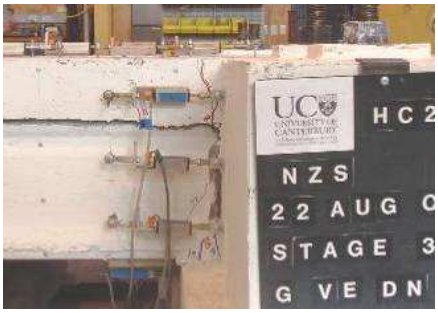

(f) Stage Three – Wellington down

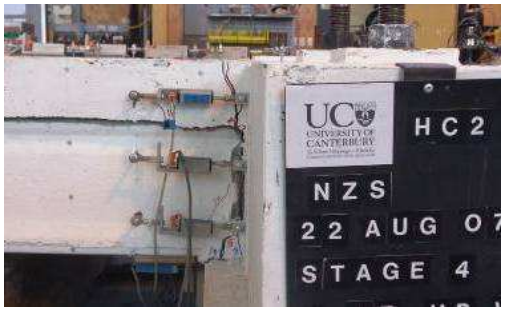

(g) Stage Four – Wellington up

(h) Stage Four – Wellington down

Figure E-1 Crack at beam-floor interface on North side of test unit during planned loading of HCW2 test

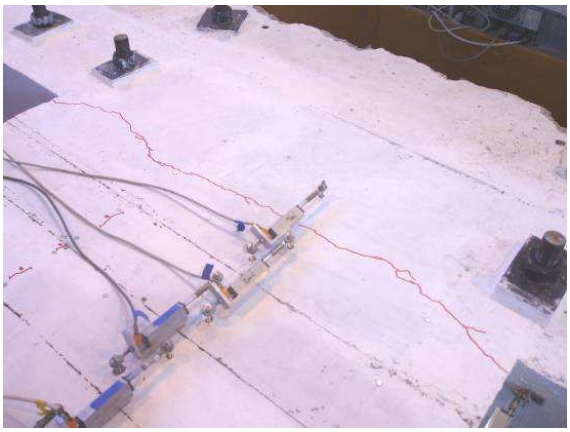

(a) Stage One – Wellington down

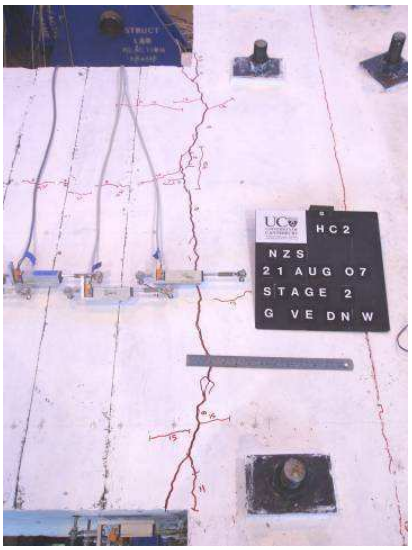

(b) Stage Two – Wellington down

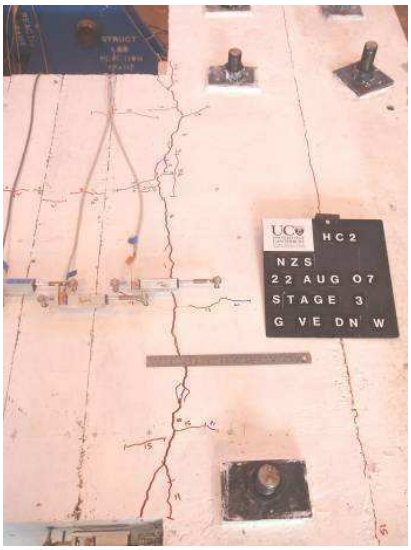

(c) Stage Three – Wellington down

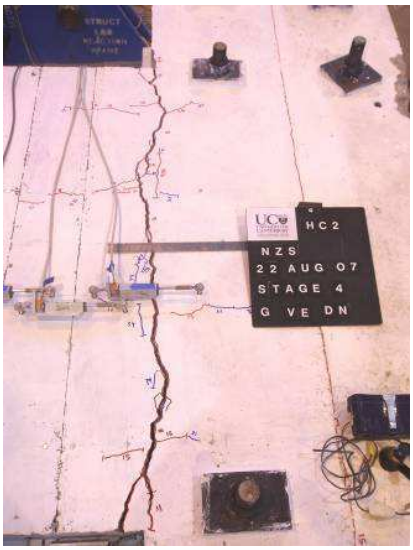

(d) Stage Four – Extended loading down

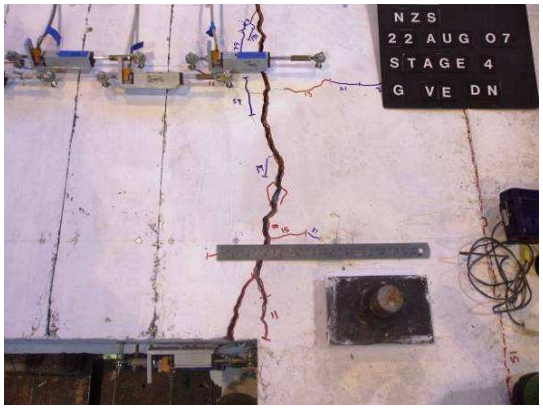

(e) Stage Four – Extended loading down – steel is visible down crack by ruler

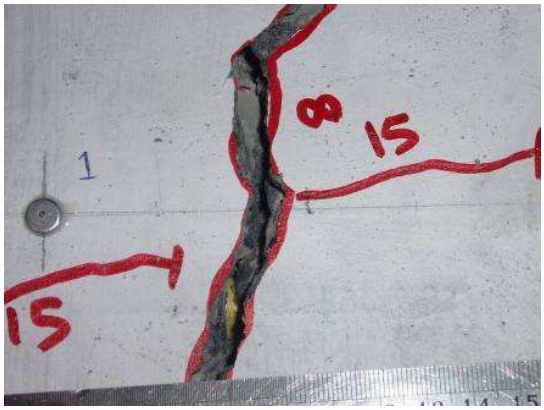

(f) Stage Four – Extended loading down – can see steel crossing crack (yellow)

Figure E-2 Crack at beam-floor interface on top surface of test unit during HCW2 test

(a) Stage Two - Wellington up - Deflected shape of test unit

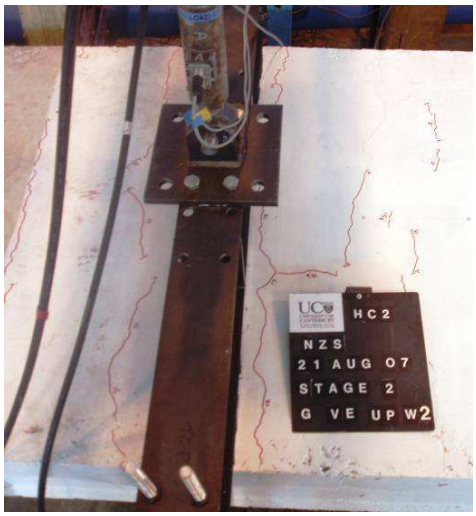

(b) Stage Two – Wellington up – Cracking in topping concrete near actuator V2

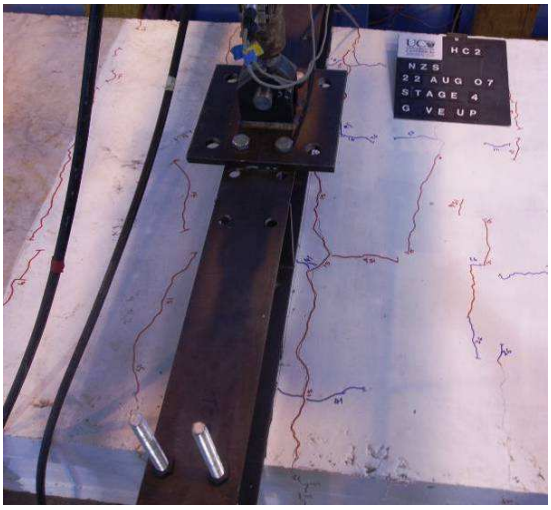

(c) Stage Four – Extended up - Cracking in topping concrete, flexural crack in unit at actuator V2 position

(d) Stage Four – Extended up – Minor spalling of seat

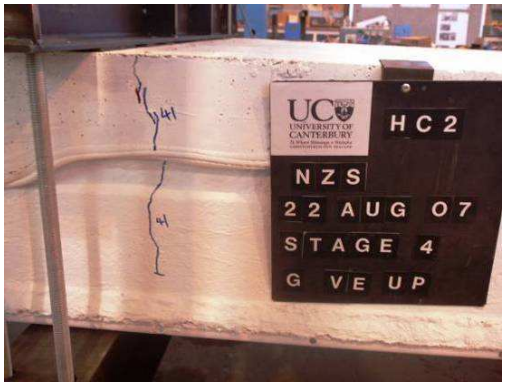

(e) Stage Four – Extended up – Flexural crack at actuator V2

Figure E-3 Visual performance indicators during test HCW2

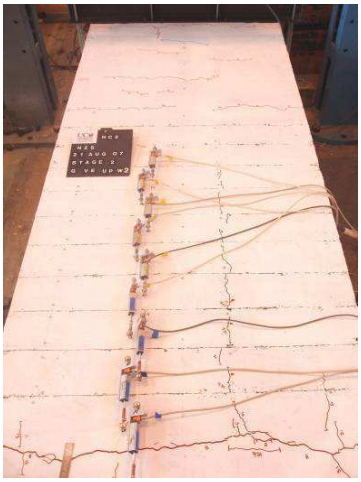

(a) Stage Two – Wellington up

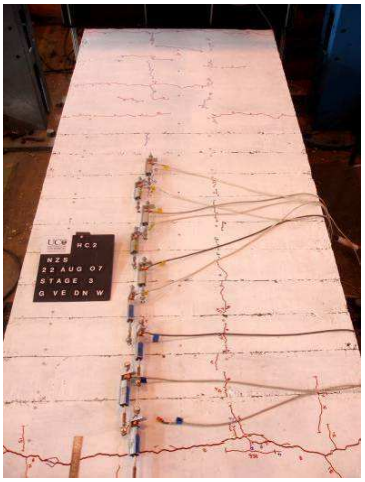

(b) Stage Three – Wellington down

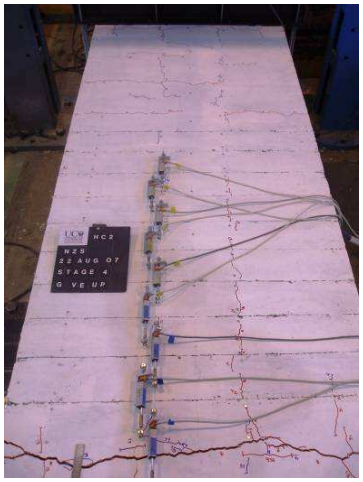

(c) Stage Four – Extended loading up

Figure E-4 Cracks in topping concrete during test HCW2 – Those marked in red formed during Stages One and Two, those in blue during Stages Three and Four

Figure E-5 Deflected shape of test unit during Phase Two of loading

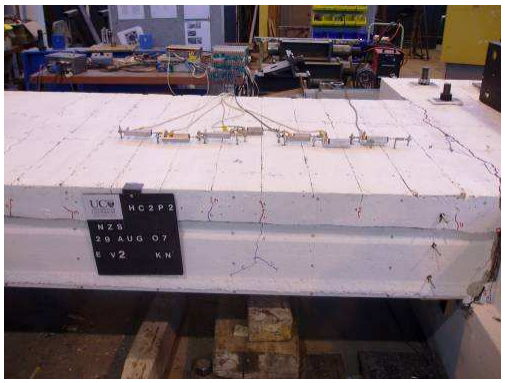

(a) Crack B - North

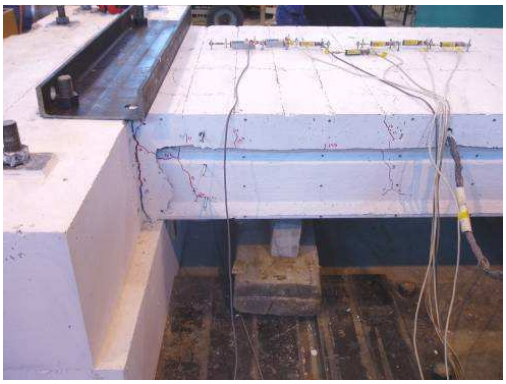

(b) Crack B - South

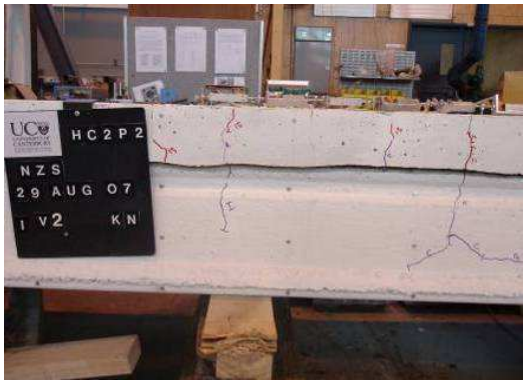

(c) Crack I - North

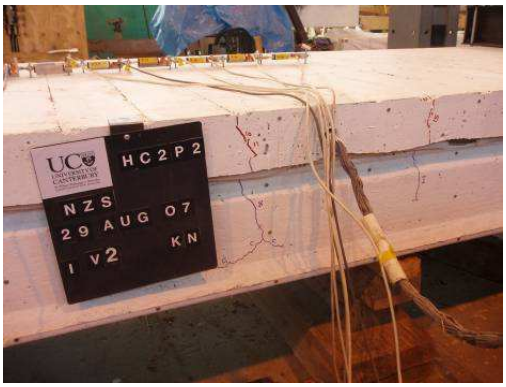

(d) Crack I - South

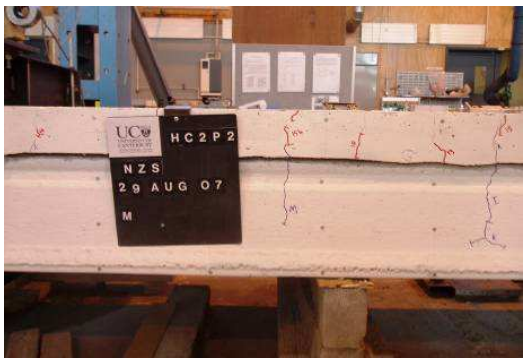

(e) Crack M - North

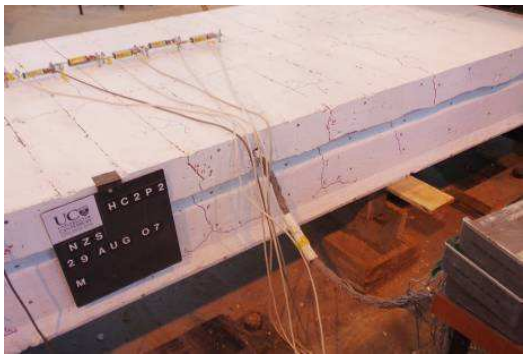

(f) Crack M - South

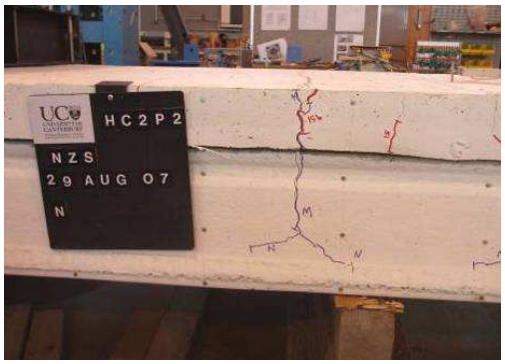

(g) Crack M at load N - North

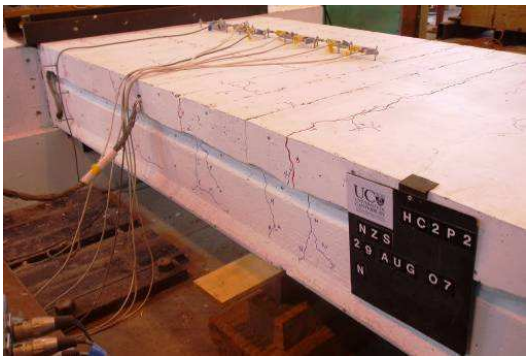

(h) Crack N - South

Figure E-6 Flexural cracks induced in test unit HCW2 during Phase Two of loading

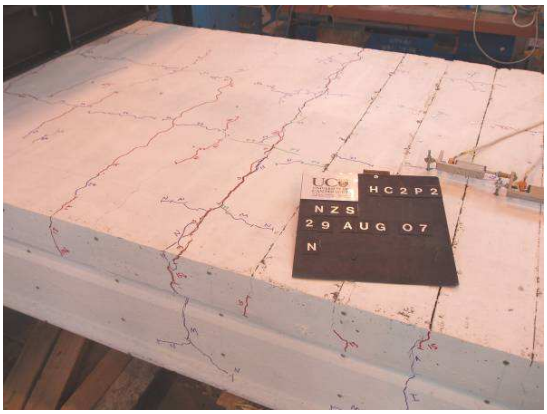

Figure E-7 Flexural crack induced 150 mm past the extent of crack initiators during Phase Two

Figure E-8 Spalling of seat during Phase Two

E 2 Loads and Displacement of Actuators at Key Points in Test HCW2

Table E-1 shows the data recorded at key points during test HCW2, these coincide with the bending moment profiles shown in Section 9. At the beginning of each stage, the floor unit was level. Column two shows the equivalent loading applied at each increment, G stands for gravity load equivalent to that of a 12 m span floor. VE stands for vertical earthquake actions either up or down (dn), these are scaled for either Christchurch (C) or Wellington (W). For actuators V1 and V2 a negative load is vertically up and negative displacements are down from the initial position where the floor unit was level. For actuator H3 a negative load is pulling the floor horizontally away from its support and this corresponds to a positive displacement.

Table E-1 Loads and Displacements of Actuators during test HCW2

Stage	Loading	Load in actuators (kN)			Displacement at actuators (mm)		
		V1	V2	H3	V1	V2	H3
Stage One - M at interface 0.5*M_y	Start of day	-25.06	0.45	-12.02	-0.02	0.00	-0.06
	G	-34.72	27.09	0.00	-0.43	-0.76	0.06
	G + VE up C	-20.90	6.94	0.00	-5.43	-1.95	-0.25
	G	-38.09	42.87	0.00	-2.23	-1.61	-0.20
	G + VE dn C	-51.46	70.30	0.00	0.61	-1.19	-0.03
	G	-35.17	40.97	0.00	-3.86	-2.17	-0.28
	G + VE up W	-12.13	-19.70	0.00	-7.65	-2.25	-0.48
	G	-38.09	41.08	0.00	-3.16	-1.91	-0.28
	G + VE dn W	-62.02	96.16	0.00	-2.54	-3.30	-0.22
	G	-39.77	39.29	0.00	-4.77	-2.93	-0.31
Stage Two - M at interface M_y	G	-30.45	30.34	0.00	-11.94	-5.67	-0.73
	G + VE up C	-11.91	-2.02	0.00	-28.27	-11.82	-1.43
	G	-31.91	30.11	0.00	-19.50	-9.22	-1.23
	G + VE dn C	-42.58	63.36	0.00	-21.48	-10.85	-1.34
	G	-31.80	32.91	0.00	-21.61	-10.27	-1.34
	G + VE up W	-1.80	-29.55	0.00	-32.49	-12.96	-1.70
	G + VE up W	0.79	-31.12	0.00	-43.34	-18.31	-2.10
	G	-28.43	28.88	0.00	-39.98	-18.13	-1.98
	G + VE dn W	-52.47	87.42	0.00	-43.34	-22.73	-2.12
	G	-32.13	32.91	0.00	-43.34	-21.60	-2.29
Stage Three - Axial load approximately 132 kN	Start	-30.45	0.00	0.00	-0.09	-0.30	-0.92
	with axial	-33.48	-0.11	131.70	-1.16	-0.44	-2.32
	G	-55.06	48.13	149.20	-2.97	-2.71	-2.40
	G + VE up C	-40.22	14.44	144.70	-2.07	-1.39	-2.60
	G	-54.61	47.46	145.70	-2.93	-2.75	-2.51
	G + VE dn C	-69.89	81.94	146.70	-4.27	-4.58	-2.60
	G	-54.94	46.90	144.20	-3.41	-3.28	-2.63
	G + VE up W	-26.85	-14.55	139.20	-1.41	-0.12	-2.88
	G	-55.17	48.47	142.70	-3.32	-3.01	-2.68
	G + VE dn W	-81.46	109.40	144.20	-5.56	-6.13	-2.54
	G	-54.83	46.57	142.20	-3.77	-3.58	-2.63

Table E1 cont.

Stage	Loading	Load in actuators (kN)			Displacement at actuators (mm)		
		V1	V2	H3	V1	V2	H3
Stage Four - Axial load approximately 264 kN	With axial	-36.18	-0.11	267.40	-0.11	0.34	-4.83
	With axial	-36.18	0.00	267.90	-0.11	0.36	-5.14
	G	-53.93	40.75	262.90	-1.39	-1.47	-5.17
	G + VE dn C	-67.08	70.63	258.90	-2.50	-3.16	-5.20
	G	-53.82	39.18	257.40	-1.59	-1.81	-5.25
	G + VE up W	-26.97	-19.59	260.40	0.48	1.29	-5.56
	G	-52.92	39.18	261.90	-1.29	-1.35	-5.48
	G + VE dn W	-79.66	98.51	267.40	-3.41	-4.58	-5.53
	G	-54.49	39.85	261.90	-1.70	-2.05	-5.78
	extended up	-27.86	-17.57	271.00	0.45	2.83	-6.59
	extended up	-19.55	-35.71	271.50	0.93	6.03	-8.63
	extended dn	-105.65	153.00	285.00	-5.88	-7.48	-8.52
Phase Two - Extended loading inducing flexural cracks	Beginning	-36.18	-0.11	267.40	-0.11	0.34	-4.83
	A	-36.18	0.00	267.90	-0.11	0.36	-5.14
	Ab	-53.93	40.75	262.90	-1.39	-1.47	-5.17
	B	-67.08	70.63	258.90	-2.50	-3.16	-5.20
	Bb	-53.82	39.18	257.40	-1.59	-1.81	-5.25
	C	-26.97	-19.59	260.40	0.48	1.29	-5.56
	D	-52.92	39.18	261.90	-1.29	-1.35	-5.48
	E	-79.66	98.51	267.40	-3.41	-4.58	-5.53
	F	-54.49	39.85	261.90	-1.70	-2.05	-5.78
	G	-27.86	-17.57	271.00	0.45	2.83	-6.59
	H	-19.55	-35.71	271.50	0.93	6.03	-8.63
	I	-105.65	153.00	285.00	-5.88	-7.48	-8.52
	Ib	-36.18	-0.11	267.40	-0.11	0.34	-4.83
	J	-36.18	0.00	267.90	-0.11	0.36	-5.14
	K	-53.93	40.75	262.90	-1.39	-1.47	-5.17
	L	-67.08	70.63	258.90	-2.50	-3.16	-5.20
	M	-53.82	39.18	257.40	-1.59	-1.81	-5.25
	N	-26.97	-19.59	260.40	0.48	1.29	-5.56
	O	-52.92	39.18	261.90	-1.29	-1.35	-5.48
	P	-79.66	98.51	267.40	-3.41	-4.58	-5.53

Appendix F Discussion

F 1 Calculating the expected Strain Profiles at Increment 16

The strain profile at seven locations along the test specimen, 250 mm apart were calculated at increment 16 of the test. To find these, first the bending moment along the section at increment 16 was found. Using the load in actuator V1 from Table D-1 and the self-weight of the specimen from Section C6, these are found and given in Table F-1.

Table F-1 Bending moments along test specimen at Increment 16

Distance from Beam-floor Interface (mm)	250	500	750	1000	1250	1500	1750
Bending Moment (kNm)	52.0	45.5	39.4	33.6	28.3	23.4	18.8

The predicted strain profile was found for each bending moment using equilibrium and strain compatibility relationships. Plane sections are assumed to remain plane. Material properties and section geometry from the experiment were used, these are given in Section 7.2. Other assumptions used in the flexural analysis, such as development lengths for prestressing and starter bars, are given in Section 5.4. The predicted height of neutral axis and strain at the soffit for the moments at sections given above are shown in Table F-2.

Table F-2 Predicted height of neutral axis and strain at soffit for sections along test specimen at Increment 16

Distance from Beam-floor Interface (mm)	250	500	750	1000	1250	1500	1750
Height of Neutral Axis above Soffit (mm)	83.9	115.3	107.2	89.4	98.1	108.0	119.4
Strain at Soffit	0.0004	0.0005	0.0006	0.0007	0.0007	0.0006	0.0006

When comparing these profiles with the measured strain values during the test it must be recalled that when the initial Demec readings were taken (at the beginning of the test) the specimen already had strains induced in it due to the prestressing and dead load. To find these the bending moments along the section at the beginning of the test were found, these are given in Table F-3. From these the predicted height of neutral axis and strain a soffit for sections along the test specimen at the beginning of the test were found (see Table F-4).

Table F-3 Bending moments along the test specimen at the beginning of the test

Distance from Beam-floor Interface (mm)	250	500	750	1000	1250	1500	1750
Bending Moment (kNm)	-6.2	-1.8	2.2	5.8	9.0	11.8	14.2

Table F-4 Predicted height of neutral axis and strain a soffit for sections along the test specimen at the beginning of the test

Distance from Beam-floor Interface (mm)	250	500	750	1000	1250	1500	1750
Height of Neutral Axis above Soffit (mm)	176.8	208.0	209.7	213.7	226.7	237.2	245.5
Strain at Soffit	0.0002	0.0004	0.0004	0.0004	0.0004	0.0004	0.0004

Table F-5 shows the data for the change-in-strains profiles between the start of the test and increment 16.

Table F-5 Predicted height of the zero change-in-strain and change-in-strain a soffit for sections along the test specimen between the beginning of the test and increment 16

Distance from Beam-floor Interface (mm)	250	500	750	1000	1250	1500	1750
Height of Neutral Axis above Soffit (mm)	39.5	41.5	39.4	38.4	41.1	43.7	46.2
Strain at Soffit	0.0002	0.0002	0.0002	0.0003	0.0002	0.0002	0.0002

F 2 Shear Stress Analysis

Table F-6 shows the properties used in the analyses described in Chapter 11.

Table F-6 Geometric and material properties used in the analysis of shear stresses

Hollow-core unit	300 mm deep dycore unit
Depth of insitu topping	75 mm
Compressive strength of hollow-core concrete	45 MPa
Compressive strength of insitu topping concrete	30 MPa
Stress-strain relationship of concrete	Mander (see Appendix C 5.3)
Type of longitudinal steel reinforcement in topping	12 mm diameter deformed bars
Yield strength of steel reinforcement	500 MPa
Ultimate strength of steel reinforcement	700 MPa
Stress-strain relationship of steel	Bi-linear (see Appendix C 5.4)
Total area of prestressing in external webs	150 mm^2
Total area of prestressing in internal webs	900 mm^2
Height of prestressing above soffit	37 mm
Stress in prestress in external webs (after losses)	-773 MPa
Stress in prestress in internal webs (after losses)	-1128 MPa